**Naval Research Laboratory**
Washington, DC 20375-5320

NRL/MR/6170--99-8353

# Studies on the Application of Plasma Arc Technology to Destruction of Shipboard Waste

BRUCE D. SARTWELL
*Surface Chemistry Branch*
*Chemistry Division*

EUGENE E. NOLTING
*Naval Surface Warfare Center, Carderock Division*
*West Bethesda, Maryland*

STEVEN H. PETERSON
DAVID A. COUNTS
ROY RICHARD
EUGENE KEATING
*GeoCenters, Incorporated*

JOHN L. GIULIANI
*Radiation Hydrodynamics Branch*
*Plasma Physics Division*

JAMES W. FLEMING
*Navy Technology Center for Safety and Survivability*
*Chemistry Division*

JOHN H. CALLAHAN
*Chemical Dynamics and Diagnostics Branch*
*Chemistry Division*



April 5, 1999

# REPORT DOCUMENTATION PAGE

*Form Approved*
*OMB No. 0704-0188*



| 1. AGENCY USE ONLY (*Leave Blank*) | 2. REPORT DATE | 3. REPORT TYPE AND DATES COVERED |
|---|---|---|
| | April 5, 1999 | Final |

4. TITLE AND SUBTITLE

Studies on the Application of Plasma Arc Technology to Destruction of Shipboard Waste

5. FUNDING NUMBERS

6. AUTHOR(S)

Bruce D. Sartwell, Eugene E. Nolting,[1] Steven H. Peterson,[2] David A. Counts,[3] Roy Richard,[4] Eugene Keating,[1] John L. Giuliani,[5] James W. Fleming,[6] and John H. Callahan[7]

7. PERFORMING ORGANIZATION NAME(S) AND ADDRESS(ES)

Naval Research Laboratory
Washington, DC 20375-5320

8. PERFORMING ORGANIZATION REPORT NUMBER

NRL/MR/6170--99-8353

9. SPONSORING/MONITORING AGENCY NAME(S) AND ADDRESS(ES)

10. SPONSORING/MONITORING AGENCY REPORT NUMBER

11. SUPPLEMENTARY NOTES

[1]Naval Surface Warfare Center, Carderock Division, West Bethesda, MD
[2]GeoCenters, Inc., Lanham, MD
[3]GeoCenters, Inc., Ft. Washington, MD
[4]GeoCenters, Inc., Newton Upper Falls, MA
[5]Radiation Hydrodynamics Branch, Plasma Physics Division
[6]Navy Technology Center for Safety and Survivability, Chemistry Division
[7]Chemical Dynamics and Diagnostics Branch, Chemistry Division

12a. DISTRIBUTION/AVAILABILITY STATEMENT

Approved for public release; distribution unlimited.

12b. DISTRIBUTION CODE

13. ABSTRACT (*Maximum 200 words*)

This report provides a background which discusses the waste generation on Navy ships, regulatory and congressional requirements related to Navy shipboard waste, thermal treatment of Navy waste, and how plasma arc technology is applied to waste treatment. It provides a description of the development of the plasma arc research facility at NRL and the experimental and theoretical modeling that was conducted at NRL from 1995 to 1998. These include modeling and experiments conducted on the voltage/current relationships for plasma torches, optical emission studies of both transferred arc and non-transferred arc torches, plasma torch chemistry, slag formation from Navy solid waste, molten slag motion under pitch and roll, and radiation heat transfer from a non-transferred plasma torch to a cold metal wall. Finally, this report provides a discussion of future work and provides appendices with detailed calculations and data.

14. SUBJECT TERMS

Thermal plasma
Plasma arc
Waste treatment
Shipboard waste
Remediation

15. NUMBER OF PAGES

157

16. PRICE CODE

| 17. SECURITY CLASSIFICATION OF REPORT | 18. SECURITY CLASSIFICATION OF THIS PAGE | 19. SECURITY CLASSIFICATION OF ABSTRACT | 20. LIMITATION OF ABSTRACT |
|---|---|---|---|
| UNCLASSIFIED | UNCLASSIFIED | UNCLASSIFIED | UL |

NSN 7540-01-280-5500

Standard Form 298 (Rev. 2-89)
Prescribed by ANSI Std 239-18
298-102

# TABLE OF CONTENTS

# STUDIES ON THE APPLICATION OF PLASMA ARC TECHNOLOGY TO DESTRUCTION OF SHIPBOARD WASTE

## 1.0 Background

### 1.1 Waste Generation On Navy Ships

At sea, U.S. Navy warships operate as individual, isolated communities which must receive their sustenance through underway replenishment either by air or from other ships. The materials transported to the ships, ranging from food to ammunition, are containerized to minimize their volume for ease of transport and storage. As individual communities, Navy ships generate their own waste which is approximately equivalent to standard municipal solid waste (i.e., trash), liquid waste (e.g., sewage, sink drains), or specific types of hazardous waste. Figure 1.1 is an illustration of the many types of waste that can be generated onboard Navy ships. Solid waste almost always occupies significantly more volume than the materials from which it is derived and, therefore, the use of the same underway replenishment mechanisms that provided the ship's sustenance are not practical for removing its untreated solid waste. In addition, there is the problem that much of the solid waste is contaminated with food, so even short-term storage results in decomposition that leads to odor and vermin, thereby reducing the quality of life onboard ships. Therefore, historically, the solution to the generation of solid waste onboard ships was to discharge it into the sea.

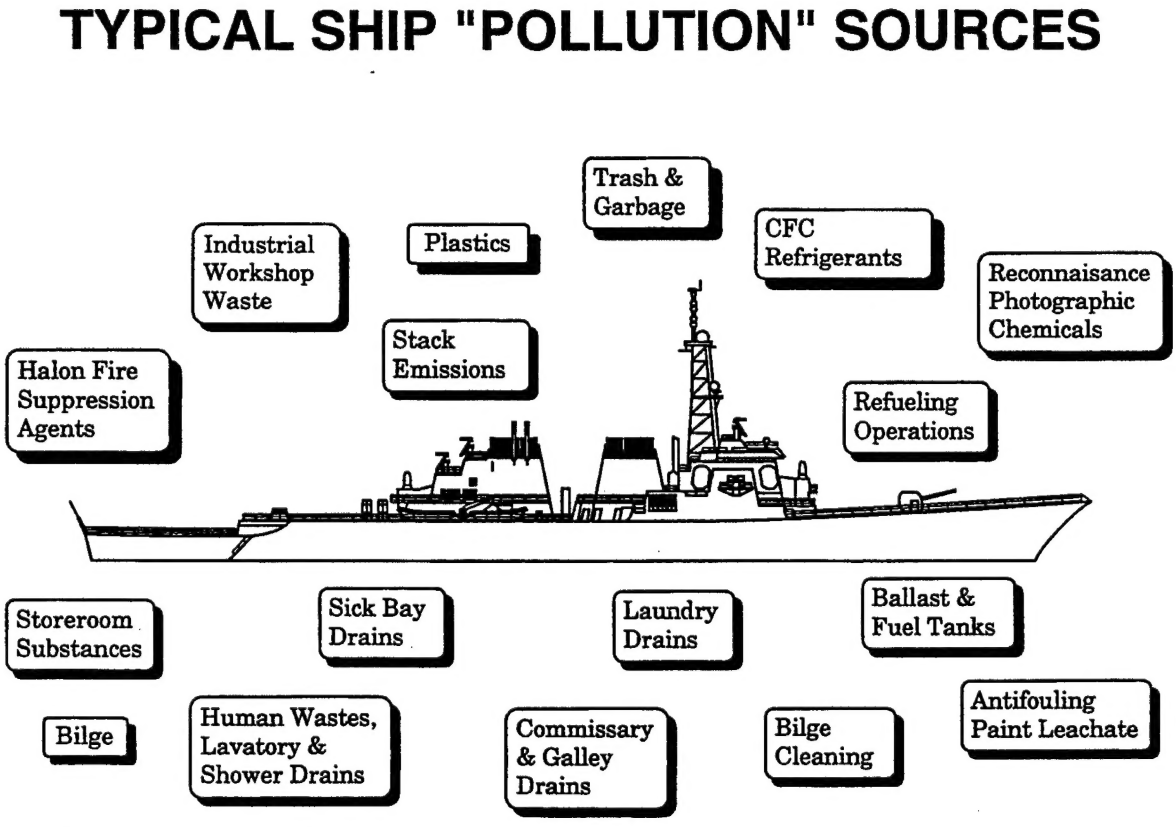


**Figure 1.1 Illustration of the many different sources of pollution effluents from typical Navy ships.**

Manuscript approved March 1, 1999.

The amount of Navy solid waste (NSW) and Navy liquid waste (NLW) generated onboard Navy ships is substantial as indicated in Tables 1.1 and 1.2, respectively. The quantities presented for NSW are based on studies conducted in the early 1990's and published in the "U.S. Navy Shipboard Solid and Plastics Waste Management Program Plan (The Green Book)" [1.1] . The compositional constituency of NSW, indicated in Table 1.3, was found to have strong similarities to municipal solid waste (MSW) as indicated in Table 1.4. Also, the NSW generation rate of 3.06 lb/person/day is comparable to the 4.2 lb/person/day reported for MSW. These earlier studies found that NSW was extremely heterogeneous and highly variable in composition both spatially and temporally.

**Table 1.1 Solid Waste Generation Rates and Total Waste Generated Per Week on Different Types of Navy Ships**

| Ship Class & Crew Complement / Waste Generation Rate | Destroyer 303 | Large Amphib 3,151 | Carrier 6,286 | Amphib RG 5,490 | CVN Joint Task Group 9,106 |
|---|---|---|---|---|---|
| Paper & Cardboard | | | | | |
| lb / man / day: 1.11 | 2,354 | 24,483 | 48,842 | 42,657 | 70,754 |
| $ft^3$ / man / day: 0.185 | 392 | 4,081 | 8,140 | 7,110 | 11,792 |
| Food | | | | | |
| lb / man / day: 1.21 | 2,566 | 26,689 | 53,242 | 46,500 | 77,128 |
| $ft^3$ / man / day: 0.027 | 57 | 596 | 1,188 | 1,038 | 1,721 |
| Metal | | | | | |
| lb / man / day: 0.41 | 870 | 9,043 | 18,041 | 15,756 | 26,134 |
| $ft^3$ / man / day: 0.043 | 91 | 948 | 1,892 | 1,652 | 2,741 |
| Glass | | | | | |
| lb / man / day: 0.13 | 276 | 2,867 | 5,720 | 4,996 | 8,286 |
| $ft^3$ / man / day: 0.007 | 14 | 150 | 299 | 261 | 433 |
| Plastics | | | | | |
| lb / man / day: 0.20 | 424 | 4,411 | 8,800 | 7,686 | 12,748 |
| $ft^3$ / man / day: 0.15 | 318 | 3,309 | 6,600 | 5,765 | 9,561 |
| Total weight lb 3.06 | 6,490 | 67,494 | 134,646 | 117,596 | 195,051 |
| Total Cubic Feet 0.41 | 873 | 9,083 | 18,120 | 15,825 | 26,249 |

**Table 1.2 Liquid Waste Generation Rates for Several Navy Ship Types (figures are expressed in thousands of gallons per day)**

| Ship Class | Approx. Complement | Mission Duration | Bilge Water | Oily Waste | Graywater | Blackwater |
|---|---|---|---|---|---|---|
| DDG963 | 350 | 30 days | 5 | 0.05 | 11 | 1* |
| CV 67 | 6,000 | 60 days | 50 | 0.5 | 180 | 180 |
| AD 41 | 2,100 | 30 days | 8 | 0.075 | 16 | 16 |

* = vacuum collected.

**Table 1.3 Navy Solid Waste Generation Rates and Compositional Constituency of Waste**

| Average Generation Rates | | |
|---|---|---|
| **Waste Stream Constituents** | **lb/man/day** | **%, by Weight** |
| Paper/Cardboard | 1.11 | 35.35 |
| Food | 1.21 | 40.76 |
| Metal | 0.41 | 13.06 |
| Glass | 0.13 | 4.14 |
| Plastic* | 0.21 | 6.69 |
| Total | 3.06 | 100.0 |

* Note: Plastics will not be incinerated, but treated, using the Plastics Waste Processor.

**Table 1.4 Typical Municipal Solid Waste (MSW) By Composition**

| Component | Average Content (% By Weight) | BTU/LB (Dry) |
|---|---|---|
| Food Waste | 33.5 | 6,528 |
| Paper, Cardboard | 33.5 | 7,500 |
| Plastics | 9.2 | 14,000 |
| Ferrous metal | 7.8 | 300 |
| Glass | 5.8 | 250 |
| Leather and Rubber | 4.8 | 13,000 |
| Textiles and Rags | 3.7 | 7,652 |
| Stones and Ceramics | 1.5 | 652 |
| Nonferrous metal (mainly aluminum) | 0.2 | 13,000 |

Moisture: Varies from 10 66% by weight
10% increase in moisture will reduce heating value of waste by 717 Btu/lb
Heating value of waste = 6968 - 71.7 X
(X is the moisture content, weight %)

A more recent study conducted onboard the USS John C. Stennis (CVN74) from 18-31 October 1997 indicated that either the earlier studies over-estimated the amount of solid waste generated on large Navy ships, or else the actual generation rates have decreased over the past few years. Figure 1.2 shows that the generation rate for pulpables was only 1.19 lbs/person-day as opposed to the "design rate" (i.e., rate from earlier studies) of 2.32 lbs/person-day, and Figure 1.3 shows that the generation rate for metal and glass was only 0.22 lbs/person-day as opposed to the "design rate" of 0.54 lbs/person-day. There are, of course, potential explanations for the discrepancies such as the Stennis survey was taken during predeployment, there was particular attention to waste management by the ship's command, etc.

- Food/Cardboard/Paper
- 76,972 lbs
- 5,498 lbs/day
- lbs/person-day
  - » Observed - 1.19
  - » Design - 2.32
- ft^3/person-day
  - » Observed - 0.18
  - » Design - 0.22

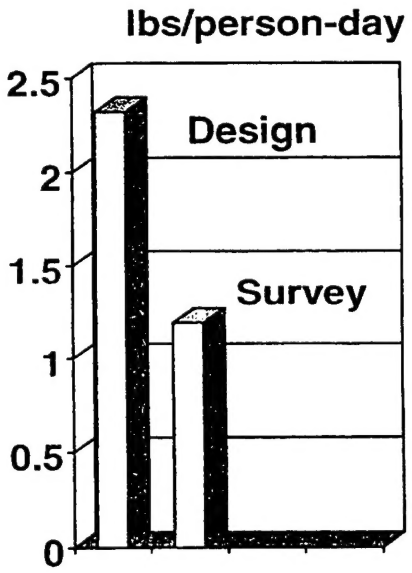


**Figure 1.2 Waste generation rates for pulpables from survey conducted on USS John C. Stennis in 1997 compared to design rates specified from previous studies.**

- 14,350 lbs
- 1025 lbs/day
- lbs/person-day
  - » Observed - 0.22
  - » Design - 0.54
- ft^3/person-day
  - » Observed - 0.03
  - » Design - 0.05
- 116 lbs/day - Al Cans

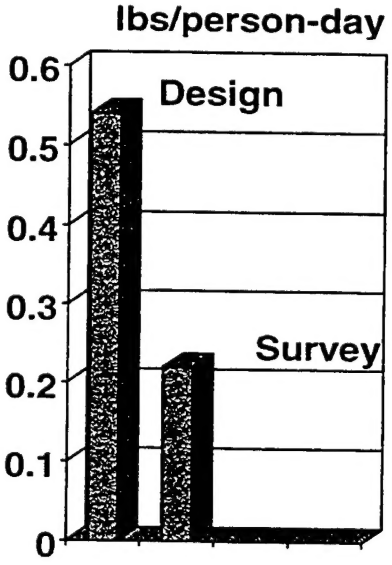


**Figure 1.3 Waste generation rates for metals and glass from survey conducted on USS John C. Stennis in 1997 compared to design rates specified from previous studies.**

## 1.2 Regulatory and Congressional Requirements Related to Navy Shipboard Waste

The issue of offboard discharge of waste from all types of ships was first addressed in the 1970's with the establishment of the International Convention for the Prevention of Pollution from Ships (1973) and its 1978 Marine Pollution Protocol, collectively known as MARPOL 73/78. Annexes I, IV, and V cover disposal of oil, sewage, and garbage, respectively. Regulation 5 of Annex V requires that commercial shipping meet a zero non-food solid waste discharge requirement in specified bodies of water, designated Special Areas. At this time, the Special Areas in effect are the Baltic Sea, the North Sea and Antarctic waters south of 60 degrees latitude. Other Special Areas specified are the Mediterranean Sea, the Black Sea, the Persian Gulf, the Red Sea, the Caribbean Region, and the Gulf of Mexico. These latter areas will not be placed into effect until adequate shore facilities for waste handling are available.

Although MARPOL explicitly excludes public vessels, including warships, Congress required the Navy to comply with the provisions of Annex V by the enactment of the Marine Plastic Pollution Research and Control Act of 1987. This law would have banned by 31 December 1993 the overboard discharge of plastics waste anywhere at sea and of non-food solid waste in the designated Special Areas. The National Defense Authorization Act (NDAA) of Fiscal Year 1994 extended the Navy surface ship compliance with Annex V to 31 December 1998 for plastics waste and to 31 December 2000 for non-plastics waste. The law also required the Navy to submit to Congress by 30 November 1996 its plan for compliance. The report generated by the Navy in response to this requirement provided information derived from Navy and independent studies of waste processing technologies, ship impacts, costs, and environmental effects associated with shipboard storage and/or processing of solid wastes. The Report concluded that no technology currently exists which would enable the Navy to satisfy the Annex V solid waste discharge restrictions with acceptable mission and cost impacts. Without the development of an alternative technology, meeting the non-food zero discharge requirement would require long-term storage and transfer of the solid waste material back to shore, requiring activities that would significantly increase the fleet's operational costs. In addition, the storage of waste has important negative mission impacts in areas of damage control, shipboard quality of life, as well as health and safety.

The 1996 Report to Congress determined that in the near term the discharge of pulped or shredded non-plastic solid waste is the only practicable, mission-compatible, and affordable solution for Fleet trash management in the Special Areas. The Report also concluded that plasma arc pyrolysis represented the most promising advanced technological approach to achieving full compliance with Annex V for surface ships, and stated that the Navy would continue to explore the feasibility of plasma arc technology for processing a variety of shipboard wastes. Congress agreed with the Navy's findings and subsequently modified the law in the NDAA of Fiscal Year 1997 which allowed the Navy to discharge the following non-plastic, non-floating garbage in Special Areas: a slurry of seawater, paper, cardboard, and food beyond 3 nautical miles; and shredded and bagged metal and glass beyond 12 nautical miles. In response to these legislative requirements, the Navy is currently installing plastics processors, pulpers, and metal/glass shredders onto virtually all ships. The plastics processors provide for shredding, heating, and compacting of the plastics into disks that can be stored onboard. All of the other waste is converted into a form for discharge as specified in the FY1997 NDAA.

The 1997 law also expressed the "Sense of Congress" that "it should be an objective of the Navy to achieve full compliance with Annex V as part of the Navy's development of ships that are environmentally sound." This Congressional direction indicates that the Navy must continue to investigate potential approaches for eventually eliminating the discharge of non-food solid waste in the Special Areas.

## 1.3 Thermal Treatment of Navy Waste

Prior to MARPOL Annex V, warships used incinerators for the destruction of classified messages with the larger warships also burning some limited amounts of paper trash. These non-fuel-fired incinerators require manual, batch feeding and also require manipulation of the burning waste throughout the entire incineration process. At the beginning of the post-MARPOL Annex V period, some efforts were made to try and utilize the currently installed incinerators on the larger platforms to process cardboard and paper wastes, wood, textiles, and oily rags. These units were found to have insufficient capacity and proved to be unsuitable even for processing only the paper and cardboard fraction of NSW.

Efficient processing of waste at sea via any thermal destruction incineration device must be characterized by an ability to achieve complete combustion of the burnable fraction of the waste. Destruction must also occur in a manner that does not contribute further to airborne pollution. Practical waste treatment technologies must provide destruction and removal efficiencies (DRE) of organic compounds at a level greater than 99.99%. Incomplete combustion of organics leading to emission of toxic compounds represents the principal problem associated with any thermal destruction device.

For the application of any thermal destruction method to the treatment of NSW onboard a ship during operations, the principal considerations are: (1) the overall volume of space that the unit occupies and its weight, (2) impact of preprocessing of the waste on ship's operations and size of preprocessing equipment, (3) the ability to reduce as large a fraction of the waste as possible to a benign gaseous state for discharge, and (4) the ability to reduce the volume of the residual waste that cannot be gasified to an absolute minimum. Item 1 is self-evident because of the lack of available space on warships. Item 2 is significant because it is desired that no additional manpower be required for operation of the thermal treatment system. Item 3 relates to the combustion of organic material or vaporization of certain inorganic materials. Table 1.5 indicates the elemental composition and heating values for the different components of NSW. The heating values were obtained by inputting the elemental concentrations into the spreadsheet given in Reference 1.2. For a more detailed discussion on the methodology of Chang, Boie, and DuLong in determining heating values, the reader is referred to that reference. Because of the high heating values of most components of NSW, it is believed that the vast majority can be combusted and emitted as gases. Item 4 relates principally to the metal and glass but also includes the small inorganic component of paper and food products. In the future, the Navy would like to build "zero-discharge" ships which would not require the discharge of any solid waste at sea. Therefore, the solid residue that is extracted from the thermal destruction system will have to be retained onboard. Because of limited storage space on warships, this requires that the residue occupy a minimum volume.

## Table 1.5 Representative Analysis and Heating Values of NSW Components

| | | | | | | | | | | | | Estimated HHV (Btu per Pound) | | |
|---|---|---|---|---|---|---|---|---|---|---|---|---|---|---|
| **Feed Name** | **As-Fired lb** | **%C** | **%$H_2$** | **%$O_2$** | **%$N_2$** | **%S** | **% Cl** | **% Ash** | **% Moisture** | **Dry Basis Total %** | **Input HHV Btu per Dry Pound** | **by Chang** | **by Boie** | **by DuLong** |
| Food | 1.21 | 44.9900 | 6.4300 | 28.7600 | 3.3000 | 0.5200 | 0.0000 | 16.0000 | 72.0000 | 100.0000 | 6269.3 | 9473.2 | 8151.8 | 7429.7 |
| Paper | 0.75 | 43.4100 | 5.8200 | 44.3200 | 0.2500 | 0.2000 | 0.0000 | 6.0000 | 10.2400 | 100.0000 | 7377.6 | 7868.7 | 8565.9 | 6822.1 |
| Metals | 0.41 | 4.4704 | 0.5990 | 4.3005 | 0.0501 | 0.0098 | 0.0000 | 90.5702 | 2.0000 | 100.0000 | 72.2 | 1389.6 | 88.5 | 71.9 |
| Cardboard | 0.36 | 43.7300 | 5.700 | 44.9300 | 0.0900 | 0.2100 | 0.0000 | 5.3400 | 5.2000 | 100.0000 | 6803.7 | 7788.8 | 8616.5 | 6803.7 |
| Glass | 0.13 | 0.5299 | 0.0707 | 0.3621 | 0.0300 | 0.0000 | 0.0000 | 99.0073 | 2.0000 | 100.0000 | 1.0 | 152.5 | 1.1 | 1.0 |
| Total | 2.86 | | | | | | | | | | | | | |
| Total Mass (lb) | | 0.61 | 0.08 | 0.57 | 0.01 | 0.00 | 0.0000 | 0.61 | 1.03 | 100.0000 | 9,564.6 | 11,928.3 | 11,664.6 | 10,569.5 |
| Total lb Mols | | 0.05 | 0.04 | 0.02 | 0.00 | 0.00 | 0.0000 | 0.61 | 0.06 | 100.0000 | Total Btu Input | Estimated Total Heat Input Total Btu | | |

As far back as 1989 the Navy conducted a comprehensive survey of thermal destruction technologies for shipboard solid waste with the purpose of identifying and evaluating the most promising ones based on shipboard constraints. These are itemized in Table 1.6. Although the study was conducted almost ten years ago, the general conclusions regarding the various technologies are still valid. Of the four general categories of technologies, only plasma arc possesses the capability of satisfying all four of the considerations listed above. The others have one or more of the following drawbacks: (1) inability to process most inorganic materials, (2) require excessive space for a given throughput of material, and (3) require large off-gas treatment systems to ensure clean emissions.

A recent assessment of the Navy's waste treatment and disposal problem was conducted by the National Research Council's (NRC) Naval Studies Board (NSB) [1.3]. Their report included a recommendation that the Navy investigate technologies and methodologies that would lead to an integrated system that could treat all of a ship's waste streams. They also acknowledged the potential advantages of newer thermal treatment technologies, such as plasma arc, while at the same time recognizing that there exist technology gaps that must be overcome prior to their successful implementation.

As a result of the Congressional mandate in the 1997 NDAA and the conclusions reached in the 1996 Navy Report to Congress, the Navy is now moving to design, construct, and test a pre-prototype plasma arc waste destruction system (PAWDS) capable of treating a broad spectrum of NSW.

## 1.4 Plasma Arc Technology Applied to Waste Treatment

Plasma is considered to represent the fourth state of matter, together with solids, liquids, and gases which represent the three other states. A plasma can be described as a gas to which a specific amount of energy has been added to separate the gas component molecules (or atoms in the case of inert gases) into a collection of ions, electrons, charge-neutral gas molecules or atoms, and other species in varying degrees of excitation (such as free radicals). Depending on the amount of energy added, the resulting plasma can be characterized as thermal or nonthermal.

In a thermal plasma, enough energy is introduced so the plasma constituents are in thermal equilibrium, i.e., the ions and electrons are, on average, at the same temperature. An electrical arc is one example of a thermal plasma, a manifestation of which is a lightning bolt bridging the gap between a storm cloud and the earth. The temperature of the electrons and ions in thermal plasmas is generally between 0.5 and 1.5 electron volts (eV), with 1 eV associated with a gas temperature of 11,600 K. To generate an electrical arc, all that is required are two electrically conducting bodies at different electrical potentials in relative proximity, with a gaseous medium between the bodies at or near atmospheric pressure. Instantaneous electrical discharges are encountered in real life fairly often such as lightning mentioned above or just the discharge encountered between one's hand and a doorknob when the relative humidity is very low and the human body picks up a static electrical charge. Sustaining a thermal plasma requires a power supply that can provide continuous current while maintaining the voltage difference between the electrically conducting electrodes. A significant amount of heat is generated with continuous plasma arcs or electrical discharges because of the finite resistance of the plasma.

**Table 1.6 Thermal Destruction Technologies**

| Technology | Nominal Operational Temperature | Application/ Destruction Characteristics | Primary Gas Products | Solid Products | Waste Volume Reduction | Remarks |
|---|---|---|---|---|---|---|
| Incineration<br>• Starved Air<br>• Excess Air | 900°C<br>1650°F | Solids & Liquids by Exothermic Combustion | $CO_2$, $H_2O$, $N_2$<br>Some:<br>• Hydrocarbons<br>• $NO_X$<br>• $SO_X$ | Particulates (Flyash)<br>• Ash<br>• Metal<br>• Glass | High | Low Energy Input<br>Available Units Generally Produce Excessive Air Emissions and Hazardous Ash |
| Wet Air Oxidation | 316°C<br>600°F | Liquids by Low-Temperature Pressurized Oxidation | $CO_2$, $H_2O$<br>Hydrocarbons | Particulate<br>• Char<br>• Inorganics | Moderate | Moderate Energy Input<br>Incomplete Conversion of Organics<br>Fairly easy to design, build and control |
| Super Critical Water Oxidation | 374°C<br>705°F | Liquids by Medium Temperature<br>High Pressure | $CO_2$, $H_2O$, | Particulates & Salts | Maximum | Moderate Energy Input (Depends on Waste Stream)<br>Can Produce Complete Oxidation of Organics |
| Plasma Arc<br>• Pyrolysis<br>• Incineration | >2000°C<br>>3630°F | Solids & Liquids by Very High Temperature/ Gasification Reactions | $CO_2$, $H_2O$, $N_2$ | Inert Maximum Density Slag | Maximum | Very High Energy Input<br>Air Emissions Control is easier than with conventional Incineration. Ash can be vitrified, making it inert. |

For example, the resistance of a 10-cm-long, 100 kW plasma arc is approximately 1 ohm. (Additional information related to this is provided in Section 3). If sufficient current is forced to pass through the plasma, then there is resistive heating in the same manner as when excess current is forced through a copper wire conductor. Because the conductor is a gas, it cannot "melt" and therefore extremely high temperatures can be achieved. The thermal temperature inside a high-power plasma arc is generally between 6000 and 20,000 degrees C.

A nonthermal plasma is one in which the mean electron energy, or temperature, is considerably higher than that of the bulk-gas molecules or atoms. Because energy is added to the electrons instead of the ions and background gas molecules, the electrons can attain energies of from 1-10 eV, while the background gas remains at ambient temperature. This nonthermal condition can be created at both atmospheric or subatmospheric pressure. A naturally occurring nonthermal plasma is the Aurora Borealis and there are numerous example of artificial nonthermal plasmas such as fluorescent lights. In these cases light is generated with very little heat.

In terms of waste treatment, nonthermal plasmas have been used for destruction of certain types of toxic or hazardous gases, where the ions, electrons, free radicals, and radiation in the plasma cause chemical reactions to occur that break down the molecules. If the proper conditions are maintained in the plasma, the atoms from the decomposed toxic gas molecules can combine with other atoms/molecules to produce benign species that can be exhausted. There have been examples where nonthermal plasmas have been used to destroy emissions from diesel engines. However, for the treatment of waste such as MSW or NSW, which consists of a wide variety of inorganic and organic materials, the heat from a thermal plasma is required. There are numerous examples of the design and construction of thermal plasma waste treatment systems [1.4-1.10], but that is beyond the scope of this report. Although with thermal plasmas there exist the ions, electrons, free radicals, and radiation as with nonthermal plasmas, in each case the thermal plasma has only been used as a heat source to melt and vitrify inorganic materials and to pyrolyze and (usually) combust organic materials. The effects of the plasma constituents on the chemical reactions, while undoubtedly present, have not actually been utilized in a controlled manner to assist in the destruction of the materials being treated. This remains a potentially fruitful area for research. Some of the optical emission studies presented in Section 4 of this report provide insight in that area.

The device that is generally used to generate a thermal plasma in a controlled reactor is the plasma torch which, in its most simplistic configuration, is nothing more than a cylinder containing one or two water-cooled electrodes. There are two principal categories of water-cooled direct current plasma torches, and they are classified by their operating modes. These are transferred arc and non-transferred arc which are illustrated in Figure 1.4. The transferred arc design contains only one electrode in the torch, with the material being processed as the other electrode. These types of torches form the heart of plasma-arc melters which have been used for decades for the industrial-scale refining of metals. For waste treatment, these types of torches would only be used if a substantial percentage of the waste was inorganic material that would not volatize. If the waste is non-conducting at room temperature (e.g., contaminated soil), then generally an electrical conductor such as a graphite liner or sacrificial metal is used with the

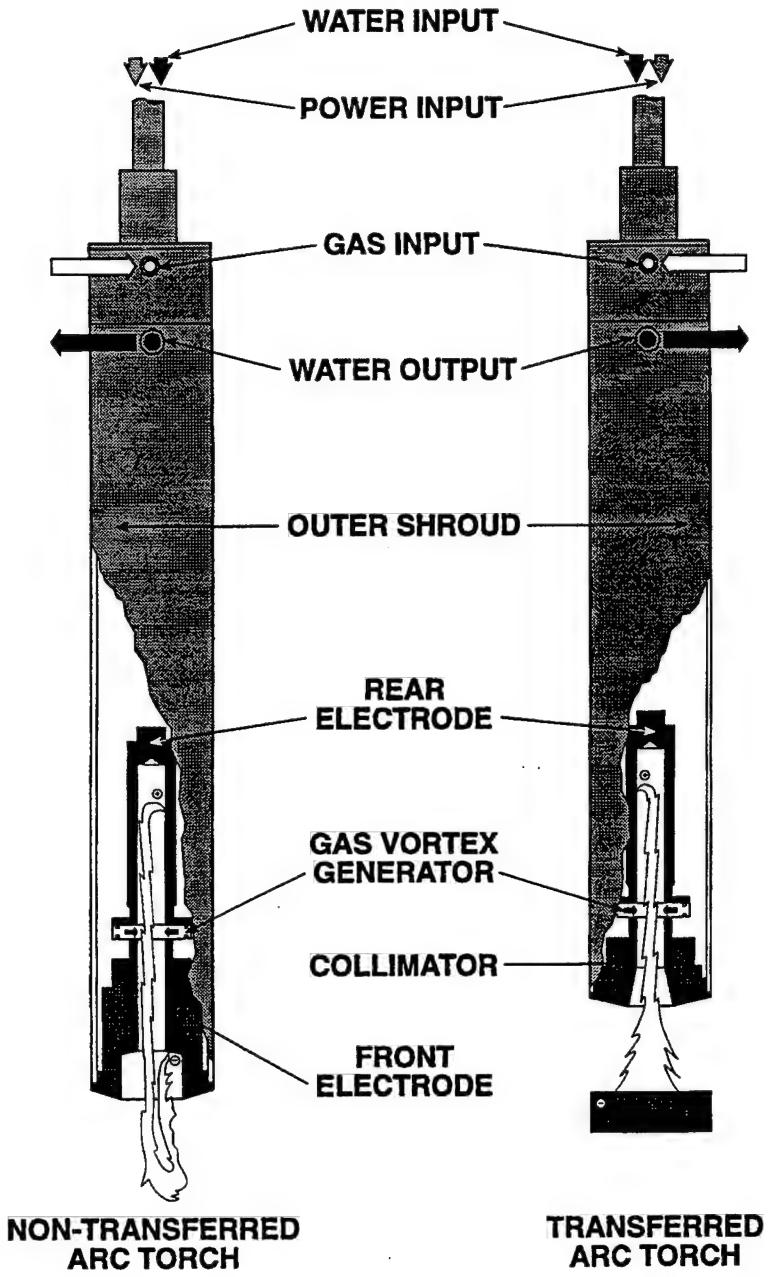


**Figure 1.4 Illustration of the two different types of plasma arc torches**

material, with the arc initially established between the torch and the conductor. The heat generated by the plasma then melts the waste material, generating a molten pool, which becomes electrically conducting. Then the plasma is allowed to transfer directly to the waste which accelerates the vitrification process because heating is caused not only by radiation from the plasma but also from the electron current passing directly into the waste material. If the inorganic material being treated contains sufficient glass formers, such as soil or sand, then a slag is formed which, when cooled, will encapsulate heavy metals. Slag formed in this manner

generally passes all leaching tests, including the standard EPA Toxicity Characteristic Leaching Procedure (TCLP) test. Therefore, it is expected that this product would remain stable for geologically long periods of time, indicating that it could be disposed of in standard landfills. There is also the possibility that there would be commercial uses for the vitrified slag such as roadbed aggregate.

The non-transferred arc plasma torch has both electrodes inside the torch; therefore the energy is dissipated in the gas phase as opposed to the transferred arc torch where some of the energy is dissipated by resistance heating of the condensed phase (i.e., the material being treated). Even though both electrodes are inside the torch body, the plasma extends beyond the end of the torch because of the high gas flow through the torch. These types of torches are most appropriate for treating organic wastes, especially if they are in liquid form. In this case, there is no molten slag pool formed and the heat from the plasma is used to pyrolyze the organic constituents. Usually, oxygen is introduced into the processing chamber either as a pure gas, as air, or as steam, in order to oxidize the carbon. If the system is operated in a pure pyrolysis mode, then large quantities of carbon black are produced which can contaminate the chamber and interfere with operation. In general, when treating organic materials, the goal is to convert as much of the materials to a gaseous state and produce as little solid residue as possible. Quite often a secondary treatment chamber is required in order to ensure complete oxidation of the carbon to carbon dioxide. In this case, the principle constituents exiting the primary processing chamber are CO and $H_2$, and the principle constituents exiting the secondary processing chamber are $CO_2$ and $H_2O$.

There are several advantages in using plasma arc systems for the treatment of waste materials over conventional fuel-fired incinerators. The first is obviously the higher temperatures and higher energy fluxes of the plasma. The maximum heat flux for an oxygen-fuel flame is about 0.3 $kW/cm^2$ whereas the energy flux for a DC transferred arc is about 16 $kW/cm^2$ [1.11]. The higher flux for plasma arc devices is due to the higher temperatures, the higher gas velocities at the nozzle of the torch, and higher thermal conductivities of the plasma gases. For transferred arcs there is the additional heat flux from the electron transfer in the area of the anode arc root attachment in the material being treated. The second advantage is that the total gas volume required to sustain a plasma arc is considerably less than what is required for a fuel-fired burner. It has been estimated that for a given throughput of material, the total gas volume required for a plasma arc system is only 10% of that for a fuel-fired burner system. This means that the off-gas handling system can be significantly smaller for a plasma arc system. A third advantage is that the plasma energy can be provided to a system with independent control of the oxygen concentration (i.e., oxidizing, reducing, or inert gas environments, independent of the reactor temperature). This is a distinct advantage over combustion systems where the available energy flux and the oxygen concentration are not independent of the temperature. Also, it is possible to operate with high-energy fluxes with highly reducing systems or highly inert systems, although certainly the cost of the gases used will be a factor in making such decisions. In considering waste treatment onboard ships, for nuclear-powered ships such as most aircraft carriers, there is sufficient excess electrical generating capacity to operate a plasma arc system; therefore, no additional generating capacity is required. However, for a fuel-fired incinerator there would be the requirement for onboard storage of the liquid fuel, which would add to the total volume required for the system.

Because the commercial applications of plasma arc technology have generally been in the metals processing industry, when companies or organizations started designing systems for waste treatment, they used the same basic design that involved the formation of a slag bed inside a primary processing chamber that contained one or more plasma torches. Because of the applicability of thermal plasmas to destroying many different types of wastes, the basic philosophy was to have a system that would be capable of feeding and treating mixtures of inorganic and organic materials. Although there have been many different designs for plasma arc waste treatment systems, they have all had basically the same components. One example is the system manufactured by Retech, Inc. of Ukiah, California that was tested in the early 1990's by the EPA under the Superfund Innovative Technology Evaluation (SITE) Program [1.12]. The evaluation was conducted at the Department of Energy's Component Development and Integration Facility in Butte, Montana. The purpose was to determine the applicability of plasma arc technology as a treatment method for soils contaminated with organic and/or inorganic compounds. Figure 1.5 is a schematic of that system, which had the following as its principal components:

(1) feeder to introduce the soil in a continuous, controlled manner into the processing chamber
(2) primary processing chamber with an oxygen lance
(3) plasma torch in the primary processing chamber operating in the transferred mode, to provide heat to the soil
(4) secondary chamber to complete oxidation of the organic materials
(5) fuel-fired afterburner to provide heat for oxidation in the secondary chamber
(6) slag collection chamber
(7) exhaust gas treatment system.

The exhaust gas treatment system consisted of the following:

(1) quench tank
(2) jet scrubber
(3) packed-bed scrubber
(4) demister
(5) stack blower (induced draft fan) which provided for a slightly negative pressure inside the entire system

Most plasma arc systems that are intended to treat both organic and inorganic materials have all of these components in various configurations. The Retech systems utilize a rotating hearth inside the primary processing chamber (a design that is designated plasma arc centrifugal treatment, or PACT) which, according to the company, provides for better mixing of the slag when it is heated by the plasma torch. There are other designs that utilize a fixed hearth with one or more taps for extracting the molten slag. In the PACT systems, the centrifugal force keeps most of the molten slag against the side walls of the hearth. When sufficient slag has been produced, the rotation is slowed which allows the slag to flow through an orifice in the center of the chamber and into the slag collection chamber located below the primary chamber. Organic materials that were contained in the soil volatize in the primary chamber and oxygen is introduced to partially combust the carbon, with the gas, consisting of principally CO and $H_2$, passing through the orifice into the secondary chamber where air is introduced to complete the oxidation. Gas and slag temperatures in the primary chamber are generally in the range of 1200-1500 degrees C, with gas temperatures in the secondary chamber also in the same range. In

order to prevent the possible formation of dioxins and furans the gas emitted from the secondary chamber is quenched to below 200 degrees C. The remainder of the exhaust gas treatment system is intended to remove particulates and halogens (principally chlorine) from the gas stream so that more than 99.9% of what is emitted to the atmosphere is $CO_2$ and $H_2O$.

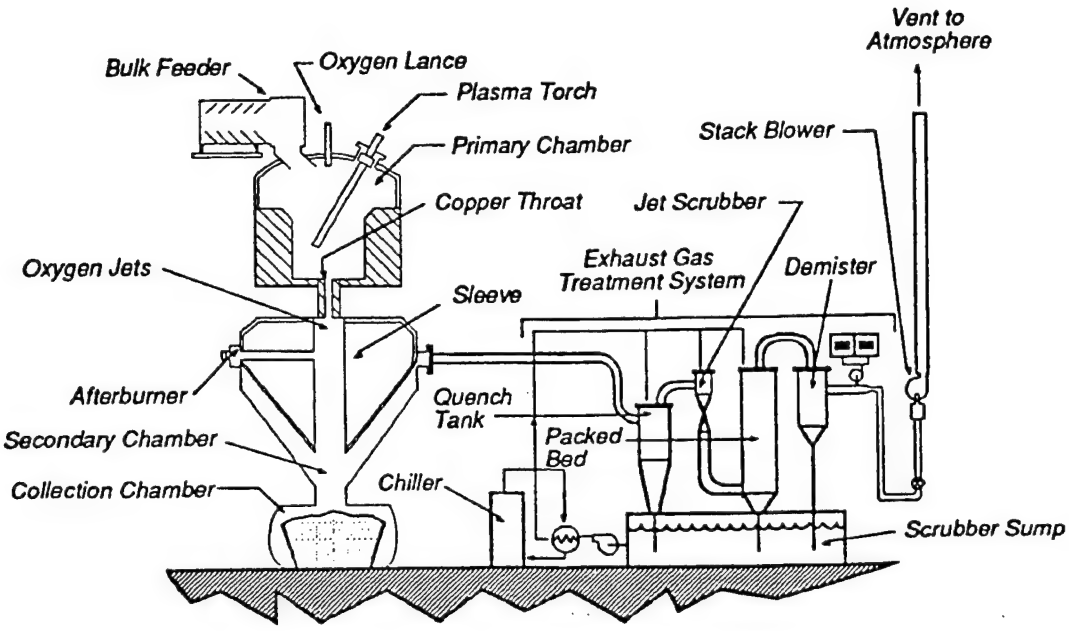


**Figure 1.5 Schematic of the plasma arc system used for the treatment of soils contaminated with organic and inorganic toxic compounds at the Department of Energy Component Development and Integration Facility in Butte, Montana**

The basic Retech system is shown more as a flow diagram in figure 1.6. In this case, the diameter of the primary processing chamber is 5 feet and the overall average throughput of the system is about 450 pounds per hour for inorganic material, although the throughput will be less for organic material depending on the heat content. Because of the size of the primary and secondary chambers and the required exhaust gas treatment components, this system occupies an overall footprint of approximately 1500 square feet, with a maximum height of 30 feet. Such a system, and other plasma arc systems with comparable throughputs, are clearly too large for incorporation into Navy warships, including aircraft carriers. The development of a shipboard plasma arc waste destruction system (PAWDS) will require a new paradigm in which the philosophy of design will have to be drastically altered. For land-based systems, not only is size generally not a consideration, but also the applications are targeted towards treatment of hazardous and remediation wastes containing toxic chemicals. Because of current inexpensive availability of landfills, treatment of MSW with thermal-plasma-based systems is not considered to be economically viable in the United States at present. However, on Navy ships, it is precisely MSW-type waste that must be treated and in systems that are severely restricted in size and weight. Because the vast majority of NSW is organic, there is no necessity for designing systems containing slag beds. It is apparent that the optimum design will involve separating the organic and inorganic components of NSW and designing compact plasma arc systems to address each, with the only commonality between systems related to treatment of exhaust gases.

## 1.5 Overview of Report

This report describes basic and applied research that were conducted at the Naval Research Laboratory from 1995 to 1998 with the overarching objective of addressing technological issues related to the application of plasma arc technology to the destruction of waste generated onboard Navy ships. In order to accomplish that objective, a plasma arc research facility was established in the Surface Chemistry Branch at NRL. Section 2 describes the origins of the NRL research program and the establishment of the facility, including the acquisition of the original plasma arc system and subsequent modifications and additions that were made to the system which were necessary for conducting the experimental studies. Section 3 describes work that was done to determine the characteristics of the plasma torch in the NRL system and Section 4 presents results of optical emission studies on various thermal plasmas produced in the NRL system. Section 5 presents both experimental and modeling results related to the chemical reactions that occur in the presence of a thermal plasma and Section 6 presents results related to the formation of slag produced by the interaction of thermal plasma arcs with inorganic material. Because plasma arc systems placed onboard ships could be subjected to pitch and roll, Section 7 presents the results of a modeling study on the motion of molten slag under those conditions.

As mentioned at the end of Section 1.3, the Navy is now proceeding with a development project to design, construct, and test a prototype plasma arc waste destruction system (PAWDS) capable of treating most NSW generated onboard ships. This project had initially been scheduled to begin in Fiscal Year 1997 and then Fiscal Year 1998, but in each case it was postponed due to fiscal constraints. A limited amount of work was conducted in those years, however, especially related to the development of conceptual designs for a shipboard system. Section 8 of this report presents results of heat transfer studies which would be crucial to implementation of one of the conceptual designs for treatment of the organic fraction of NSW.

Finally, Section 9 briefly describes the initiation in Fiscal Year 1999 of the formal Navy Advanced Technology Demonstration Project on development of the prototype shipboard system.

## 1.6 References


1.1 "U.S. Navy Shipboard Solid and Plastics Waste Management Program Plan (The Green Book)," Naval Sea Systems Command, NAVSEA 05V Environmental Engineering Group, April 1993

1.2 W. R. Niessen, "Combustion and Incineration Processes," 2nd edition, Marcel Dekker, New York, NY 1995

1.3 Naval Studies Board, "Shipboard Pollution Control, U.S. Navy Compliance with MARPOL Annex V," National Academy Press, Washington, DC, 1996

1.4 "Plasma Arc Technology. Current Practices for Waste Treatment: An Information Exchange," Conference Proceedings. Published by Concurrent Technologies Corporation, Johnstown, PA, 1996

1.5 A. D. Donaldson et al., "A Review of Plasma Destruction of Hazardous Mixed Waste," ASME Heat Transfer Division, Vol. 161, p. 41, 1991

1.6 R. A. Hamilton, J. K. Whittle, and J. Trescott, "DC Plasma Arc Melter Technology for Waste Vitrification," Proceedings of the International Symposium on Environmental Technologies: Plasma Systems and Applications, Vol. I, pp 67-76, Georgia Tech Research Corporation, 1995

1.7 R. C. Eschenbach, M. P. Schlienger, and R. E. Haun, "Swirl Flow Transferred Plasma Arc for Vitrification of Waste, Metal Recovery and Special Metal Refining," Ibid., Vol. I, pp. 251-260

1.8 G. Mescavage and K. Filius, "Plasma Arc Technology Development for Application to Demilitarization of Pyrotechnic Ordnance," Ibid., Vol. II, pp. 597-608

1.9 J. W. Sears et al., "The Plasma Centrifugal Furnace: A Method for Stabilization and Decomposition of Toxic and Radioactive Wastes," Waste Management, Vol. 10, p. 165, 1992

1.10 K. McKinley and E. Brown, "Application of Plasma Technology for the Treatment of Mixed Wastes," Proceedings of the 1997 International Conference on Incineration and Thermal Treatment Technologies, pp. 105-110, publ. by University of California at Irvine Office of Environmental Health and Safety, 1997

1.11 R. Eschenbach, Retech, Inc., private communication, 1996

1.12 R. Haun, R. Eschenbach, D. Battleson, C. Alsberg, and T. Jackson, "SITE Test Results With the PCF-6," Proceedings of the 1992 International Conference on Incineration, pp. 126-133, publ. by University of California at Irvine Office of Environmental Health and Safety, 1992

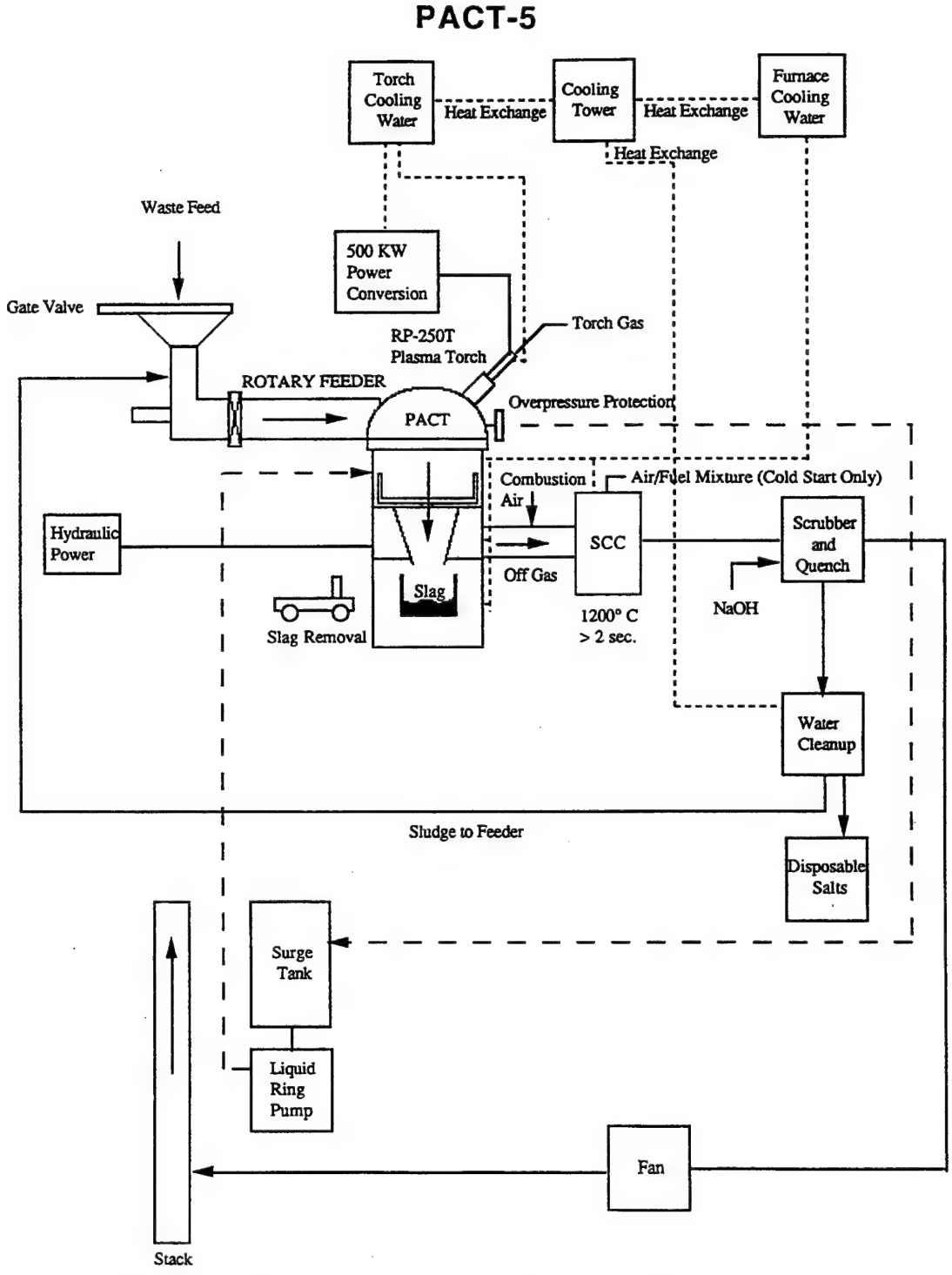


**Figure 1.6 Schematic of the Retech PACT 5 plasma arc system**

## 2.0 Establishment of NRL Plasma Arc Facility

### 2.1 Background

In the early 1990's the Naval Surface Warfare Center, Carderock Division (NSWC-CD), issued a contract to General Atomics to determine if it was feasible to design a complete plasma arc system that could be incorporated onto Navy warships to treat solid waste. That study did establish the feasibility for such a system, but it was clear that there were still significant technological challenges associated with utilizing plasma arc technology on ships. Also in the early 1990's the Office of Naval Research through the Naval Sea Systems Command funded an applied research program at the University of Maryland Combustion Laboratory to compare several techniques for the thermal destruction of solid wastes that would be viewed as applicable for shipboard use. These included plasma arc pyrolysis, fluidized bed pyrolysis, and electric pyrolysis. The evaluation was based on the performance capabilities of each technology and its ability to meet the Navy's unique requirements regarding size, weight, shock and vibration resistance, materials of construction, reliability, and maintainability. The limitations, advantages, and disadvantages of each thermal destruction technology were considered. The evaluation showed that high temperature pyrolysis using a plasma arc torch had the most potential for successful development for destruction of solid wastes onboard ships. Using a low-power plasma torch, the University of Maryland conducted a number of experimental studies related to thermal destruction of cellulose materials.

In 1993 the Office of Naval Research established a Special Research Option designated the Environmentally Sound Ships Program. This was a large, integrated program that was intended to address Navy priorities in the areas of waste disposal and cleaning processes associated with ship operations. The Naval Research Laboratory was assigned management for a portion of the program which was concerned with specific types of waste, including graywater, blackwater, oily waste, and bilge water. The basic and applied research to be funded under this program was expected to lead to new products and processes for "management to compliance" of these types of shipboard waste. Some of the areas supported under the NRL program were: (1) short-lived photo-cleavable detergents as replacement for the current non-dischargeable detergents, (2) electrified microheterogeneous catalysis reactor employing zeolite to process oxidatively resistant organic wastes, (3) high-flow-rate bioreactor incorporating tangential filtration using recyclable microbeads, and (4) utilization of semipermeable and selective membranes to de-water large waste streams or to adsorb specific species. Also included in the NRL program was a project on plasma arc thermal conversion of shipboard aqueous wastes. It was decided to concentrate on aqueous wastes because of the ongoing efforts related to solid waste at NSWC-CD and the University of Maryland. The objective of the NRL project was to determine, understand, and control the mechanisms of discrete physical and chemical decomposition of surrogate shipboard-generated black-, gray-, and bilgewater using plasma arc pyrolysis.

Critical to the NRL project was the establishment of a plasma arc research facility in the Surface Chemistry Branch. It was necessary that such a facility contain a DC plasma torch capable of operating at power levels of at least 100 kW and which could be operated in either the transferred or non-transferred mode. It was also necessary that the plasma torch be housed in a

water-cooled chamber of sufficient size to permit the treatment of different types of materials and which contained a significant number of viewports for visual and spectroscopic observations of the plasma and for other types of diagnostic instrumentation. As a result, in early 1994 NRL issued a solicitation for a complete plasma arc system, with only Retech, Inc. responding. A contract was issued to Retech for construction and delivery of the system in October 1994. In the Summer of 1995 NSWC-CD first proposed the major project for development of a prototype PAWDS as mentioned in Section 1.5. Since that time, NRL has closely collaborated with NSWC-CD and the work conducted at NRL has been directed towards technological issues associated with the treatment of both solid and liquid wastes.

## 2.2 Development and Description of NRL Plasma Arc Facility

Figure 2.1 is a top view of the entire system as provided by Retech and Figure 2.2 is a side view of just the processing chamber containing the plasma torch. The water-cooled processing chamber is 30 inches inside diameter by 30 inches long and is mounted horizontally on freestanding legs. The outer wall is 3/8-inch-thick mild steel separated by plug-welded standoffs to a 3/8-inch-thick mild steel inner wall. The ½-inch passage between the walls allows for optimum cooling water flow and maintains the outer wall at or near room temperature during operation. The DC plasma torch is mounted vertically on the top of the chamber and consists primarily of a hollow electrode, a gas injection ring, and an exit nozzle, similar to what was illustrated in Figure 1.4. The plasma torch, designated as the RP-75N/T, has a nominal rating of

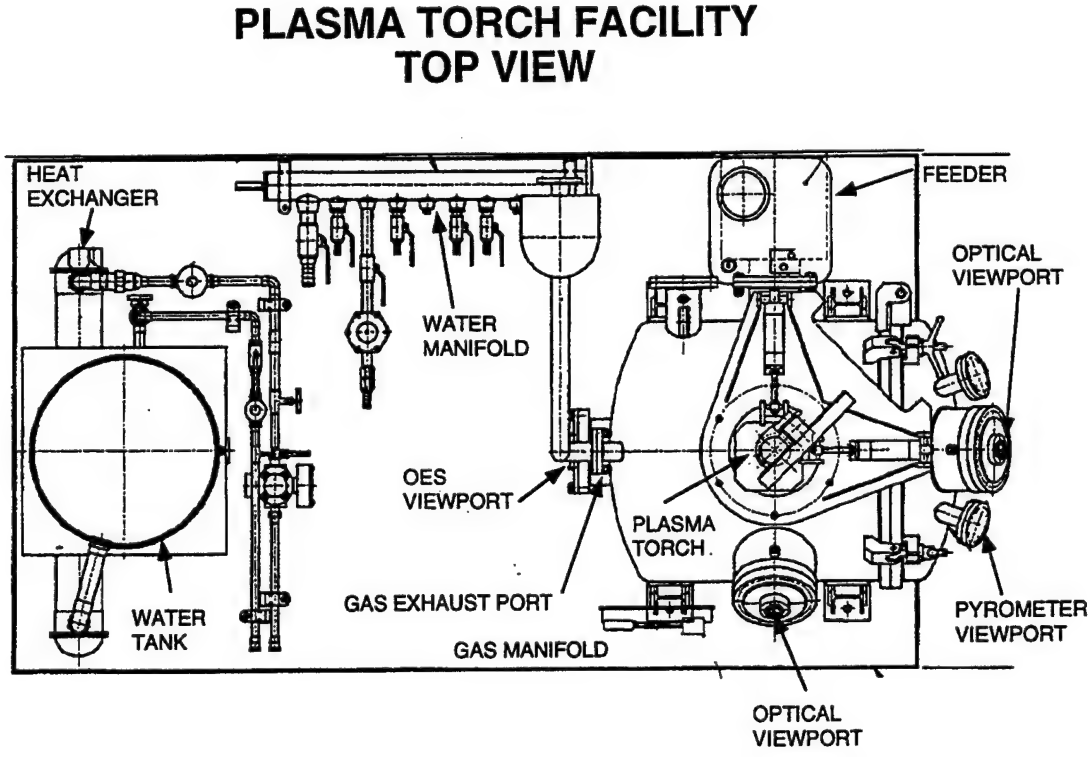


**Figure 2.1 Top view of complete plasma arc system as provided to the Naval Research Laboratory by Retech, Inc.**

150 kW but is capable of being operated from 50 to 180 kW in either the transferred or non-transferred mode. Conversion of the torch from one mode to the other requires changing the electrical ground path and the nozzle assembly, identified in Figure 1.4 as the collimator or front electrode. The torch is mounted on a vacuum ball joint to allow X-Y movement in all horizontal directions (from vertical to a 15 degree angle) within the perimeter of the crucible (described below). The movement is accomplished by the use of two hydraulic cylinders mounted to the stationary steel

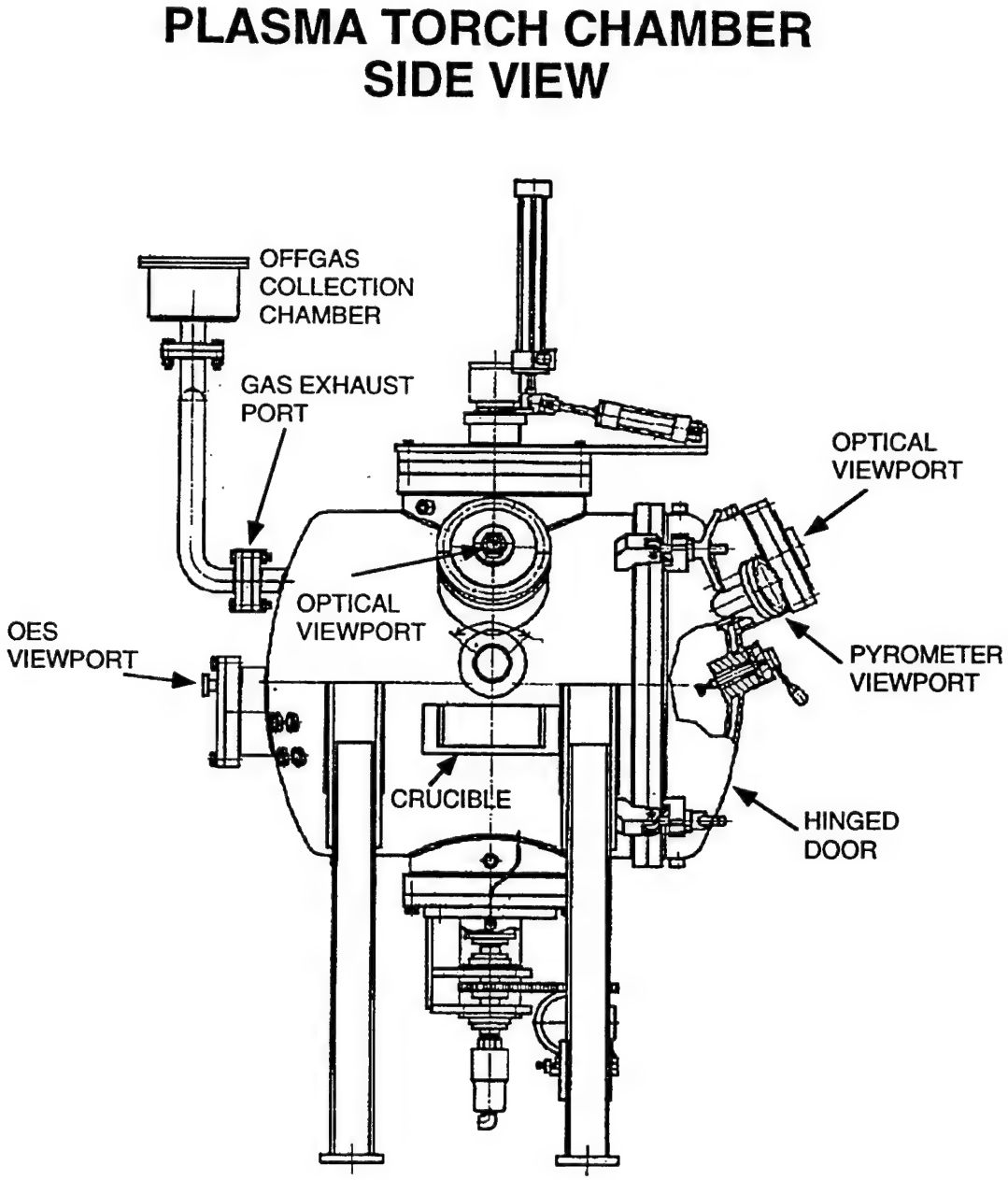


**Figure 2.2 Side view of the plasma arc chamber provided to the Naval Research Laboratory by Retech, Inc.**

frame attached to the main chamber flange. Vertical, or Z-direction, positioning of the torch is accomplished by a 14-inch-stroke hydraulic cylinder which is parallel to the axis of the torch. Cooling to the chamber walls is provided by city water whereas deionized water, stored in the water tank shown in Figure 2.1, is used for cooling of the plasma torch. A gas manifold allows for the introduction of different gases into the plasma torch. A standard practice is to initiate the plasma using helium gas, with the flow changed over to the working gas, normally nitrogen or air, after 1-2 minutes. The offgas collection chamber was connected to the fume hood system of the Chemistry Building which was able to maintain the chamber at slightly less than atmospheric pressure.

Inside the chamber and located below the plasma torch is a rotating ceramic crucible. This was initially 12 inches outside diameter, 10 inches inside diameter, and 4 inches deep, but was later replaced by a crucible 18 inches outside diameter, 16 inches inside diameter, and 4 inches deep. The position of the crucible is illustrated in Figure 2.2. The crucible is mounted onto a city-water-cooled, variable-speed rotating copper table which is electrically grounded. The smaller crucible contains a graphite liner to which the plasma arc can be transferred when the torch is operated in that mode. For operating in the transferred mode using the larger crucible, copper metal is placed in the center which serves as the initial arc attachment point. As indicated in Figures 2.1 and 2.2, the chamber contains a number of ports which have been utilized as optical viewports or for various diagnostic instrumentation. On one port is a two-color Ircon optical pyrometer which has been used to measure the temperature of the molten slag inside the crucible. A fiber optic cable is mounted onto another viewport and connected to an Oriel spectrometer for the optical emission studies. A more detailed description of the optical emission spectroscopy system is provided in Section 4. A Super-VHS video camera is mounted on one of the optical viewports. Figure 2.3 is a simplified, not-to-scale illustration of the chamber showing the positioning of the various components.

A significant number of modifications and additions were made to the plasma arc facility in order to conduct the various experiments discussed in this report as well as provide maximum flexibility in terms of the types of materials that could be treated in the system. The first group of significant modifications involved adding (1) a feeder that would permit continuous introduction of solid material into the crucible, (2) a liquids feeder, (3) thermocouples in various parts of the system, and (4) continuous emissions monitors to determine the composition of selected gases in the exhaust. The initial ram feeder for solid materials provided with the system consisted of a half-cylinder approximately 8 inches long and 4 inches in diameter that could be retracted into a load-lock chamber where it could be filled with material. The cylindrical feeder could then be introduced into the chamber with the end extending over the edge of the crucible. A plunger then would push all of the material in the feeder into the crucible. This batch-type of feeding was acceptable if all of the material was inorganic but was not acceptable for material with a substantial organic fraction because of the large amount of gas generated when the material dropped into the hot crucible. In order to provide for continuous feed of any type of solid material at variable rates based on the organic/inorganic fraction of material, a loss-in-weight vibratory feeder was acquired and installed in the room above the plasma arc system. Six-inch-diameter steel piping was then run from the vibratory feeder through one of the ports on the chamber, with the end of the "chute" extending over the edge of the crucible. This is shown

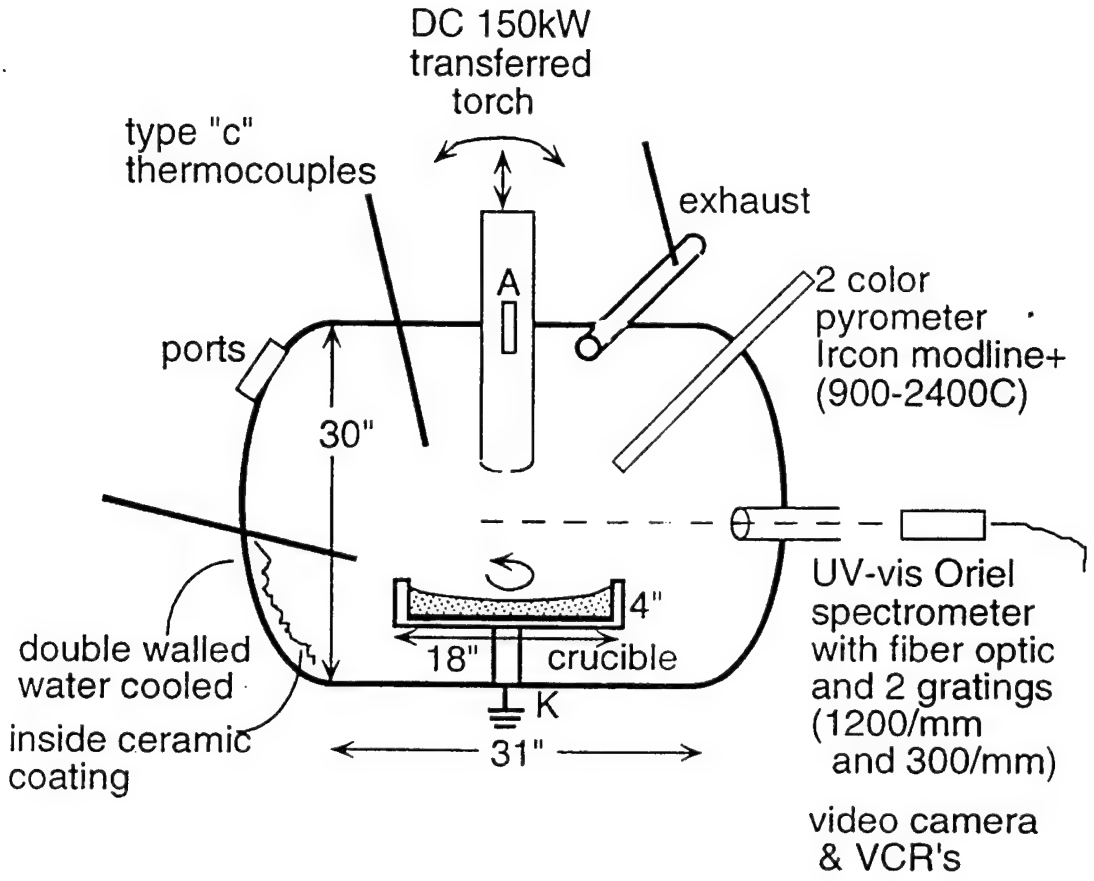


**Figure 2.3 Illustration of the various components and their relative positioning in the plasma arc chamber.**

schematically in Figure 2.4 with the door to the chamber removed. The draw of gases though the exhaust line induced by the fume hood system prevented gases from escaping through the chute. A liquid feed system was also added to the facility which consists of a holding container, a slurry pump, and a water-cooled, double-walled feed line that passes through one of the ports on the chamber and extends over the edge of the crucible in the vicinity of the nozzle of the plasma torch. The slurry pump has a variable speed motor and any Teflon-compatible liquids can be pumped into the chamber at a rate that is variable from approximately 0.2 to 1.0 liters per minute (approximately equivalent to 0.4 to 2.0 pounds per minute). In addition, a number of C-type thermocouples were placed in the chamber and the gas exhaust line as illustrated in Figures 2.4 and 2.5 in order to be able to measure gas temperatures throughout the system

Although the exhaust gases from the chamber were not treated in any manner but were introduced into the fume hood system of the Chemistry Building, it was still important to be able to determine the composition of the exhaust gases, so an atmospheric-pressure-sampling residual gas analyzer (RGA) and several continuous emissions monitors (CEM) were acquired and sampling ports were installed in the gas exhaust line. The RGA consists of a Balzers Prisma

Quadrupole Mass Spectrometer (QMS) and a differential pumping system that could extract gases from the exhaust line at atmospheric pressure, pass them through several collimators and into a small vacuum-pumped antechamber at a pressure of less than $10^{-5}$ Torr. The QMS can determine relative concentrations of gases with molecular weights ranging from 1 to 300. The CEMs consist of the following:

- Thermo Environmental Inc. Model 51 Total Hydrocarbon Analyzer
- Thermo Environmental Inc. Model 48C Gas Filter Correlation Carbon Monoxide Analyzer
- Thermo Environmental Inc. Model 42C High Level Chemiluminescence NO-$NO_2$ Analyzer
- Thermo Environmental Inc. Model 15C Gas Filter Correlation HCl Analyzer
- Panametrics TMO2D Oxygen Analyzer

Prior to being introduced into any of the CEMs, the gases pass through a Perma Pure Inc. GASS-II sample conditioning system which heats and dries the gases to a dew point of minus 25 degrees C at 25 standard liters per minute flow rate. The following is a description of each of the CEMs.

- The total hydrocarbon analyzer continuously analyzes the gases using a flame ionization detector and has the capability for internal calibration. It has a detection range of 0.1 to 10,000 parts-per-million (for propane), a repeatability of 2% of reading, and analog or RS-232 outputs.
- The carbon monoxide analyzer is a microprocessor-based non-dispersive infrared analyzer and has the capability for internal calibration. It has a detection range of 0.1 to 10,000 parts-per-million and analog or RS-232 outputs. The analyzer is designated by the EPA as a reference method for the measurement of ambient concentrations of CO pursuant with the requirements defined in 40 CFR53.
- The $NO_x$ analyzer is a microprocessor-based chemiluminescence instrument. It is internally calibrated and uses zero-grade air for the ozonator feed. It has a detection range of 0.050 to 10,000 parts-per-million, a response time that is adjustable from 1 to 200 seconds, and analog or RS-232 outputs.
- The HCl analyzer is a microprocessor-based non-dispersive infrared analyzer and has the capability for internal calibration. It has a detection range of 0.2 to 5000 parts-per-million, a response time of 120 seconds, and analog or RS-232 outputs.
- The oxygen analyzer is a microprocessor-based thermo-paramagnetic analyzer and has the capability for internal calibration. It has a detection range from 0 to 30 volume percent, an accuracy of plus-or-minus 1%, and analog or RS-232 outputs.

A significant number of studies were conducted with the system in the configuration illustrated in Figures 2.4 and 2.5. However, it became clear that in order to be able to treat a wide variety of materials and to be able to ultimately support the development of a prototype shipboard system, the NRL plasma arc system required an exhaust gas treatment system. Therefore, in late 1997 a gas quench and venturi scrubber system were acquired, with installation completed in the Spring of 1998. The final configuration of the system is shown in Figures 2.6 and 2.7. The previous gas exhaust line was converted to an input line for providing either air or oxygen for combustion of organic material. The port on which the ram feeder had been mounted

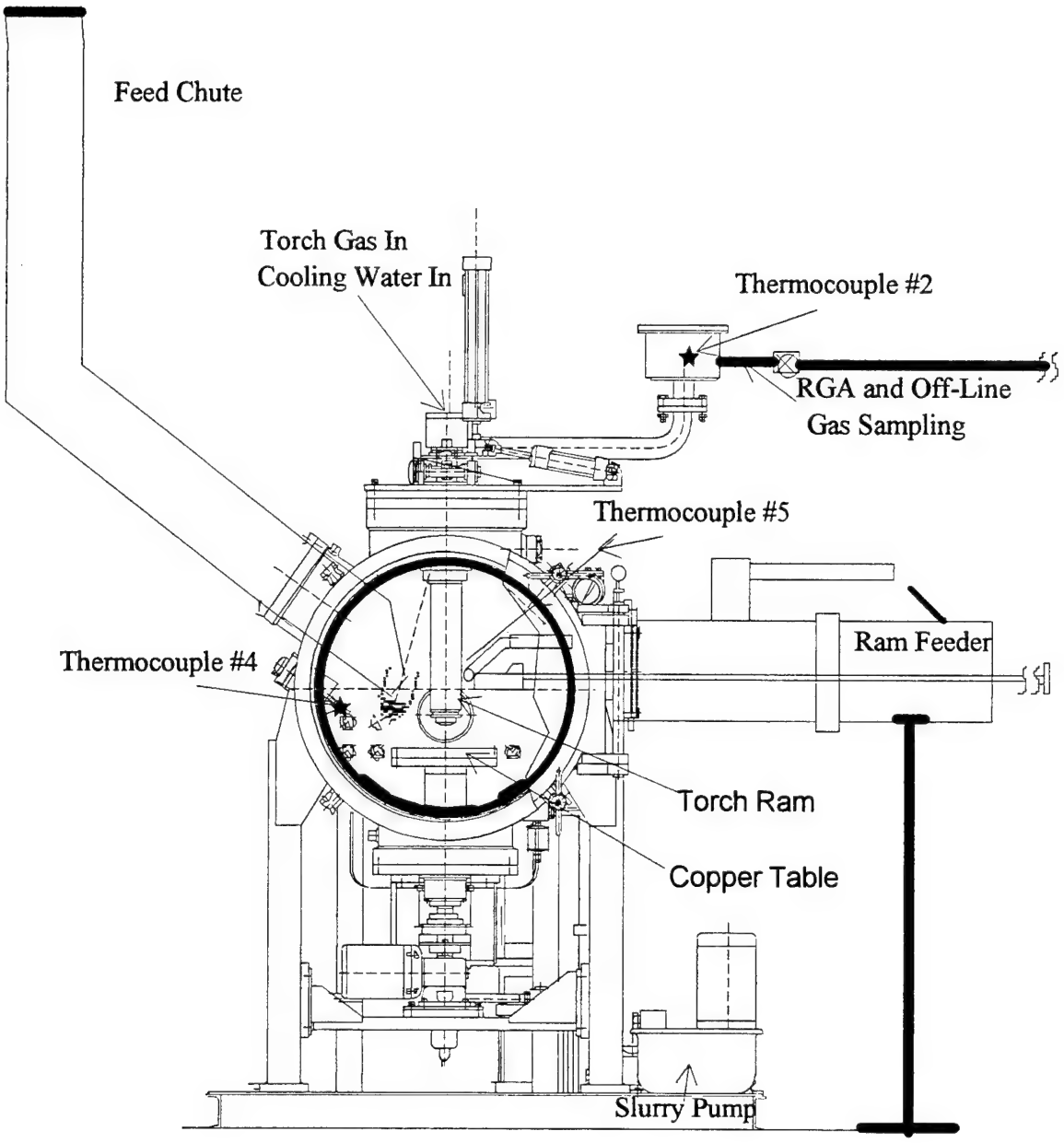


**Figure 2.4 Side view of plasma arc chamber (with chamber door removed) showing location of feed chute, ram feeder, exhaust gas sampling line, and several thermocouples**

was converted to an exhaust gas line. The first part of the line contains two water spray quench nozzles to cool the exhaust gas from approximately 1000 degrees C to less than 200 degrees C to ensure that there would be no formation of dioxins or furans in the exhaust. Then the gas passes

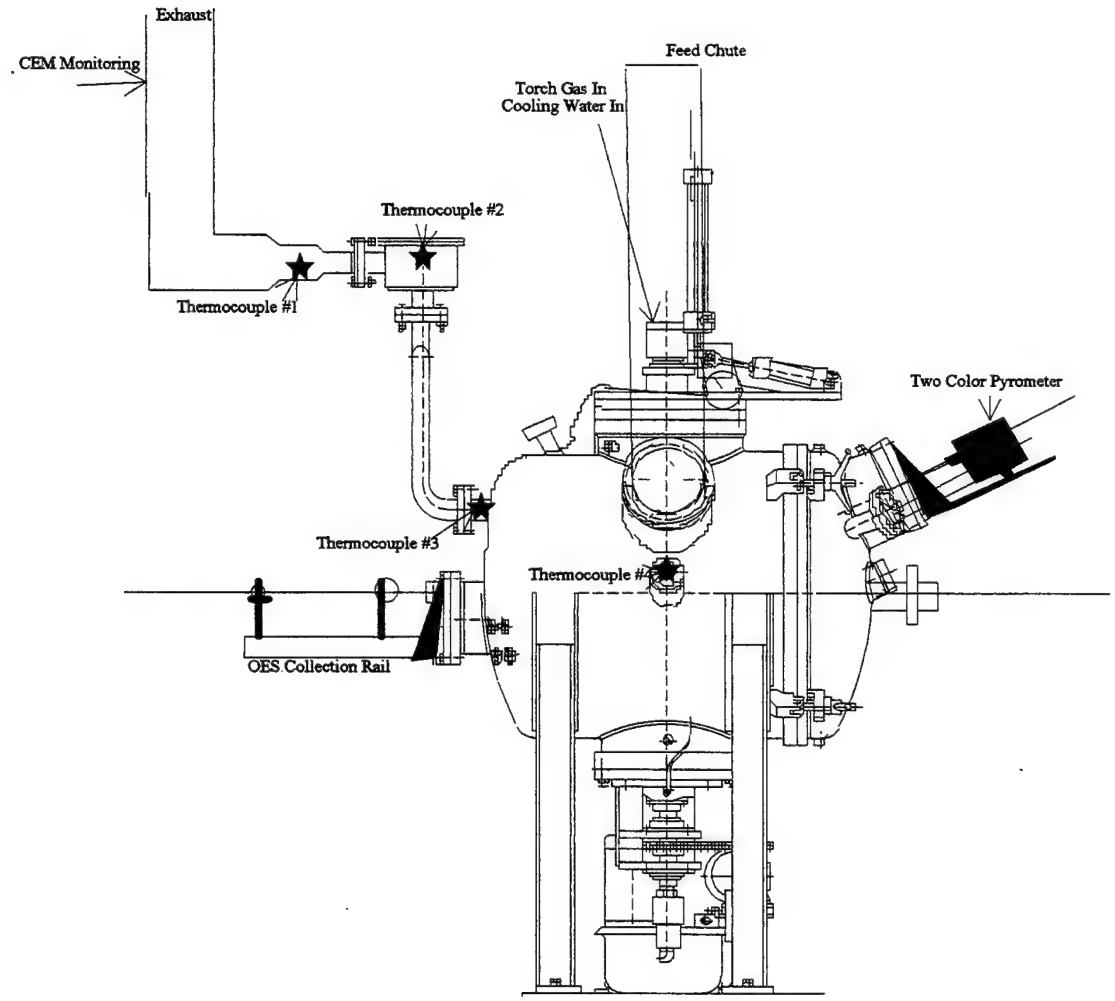


**Figure 2.5 Side view of plasma arc chamber (from viewpoint of feed chute) showing location of thermocouples**

through a scrubber for removal of particulates. The scrubber consists of a venturi eductor and a gas-and-water separator unit and is capable of treating 1000 actual cubic feet per minute of gas. The water flow into the scrubber is 72 gallons per minute at a pressure of 60 pounds per square inch. Finally, the gas passes through a 250 standard cubic feet per minute induction blower that maintains a slight negative pressure (ranging from 1-4 inches of mercury) in the chamber. The thermocouples were reconfigured so that gas temperature can be monitored starting from inside the chamber through the input to the induction blower. Thermocouple locations are indicated in

Figures 2.6 and 2.7. The high-temperature thermocouples, designated numbers 1 through 4 are C-type thermocouples embedded in zirconia. The low-temperature thermocouples, designated numbers 5 through 8, and located after the water quench, are K-type. The input and output temperatures of the coolant water provided to the chamber, chamber door, rotating table, and plasma torch are also monitored using K-type thermocouples.

Two independent data acquisition (DAQ) systems are used to collect the plasma system calorimetry, gas temperature, and CEM data. Both DAQ systems use programs written locally using National Instrument's LabVIEW version 5.0.1. Both systems record the data, along with a time-stamp, as spreadsheet files for data analysis. Data analysis is initially conducted using Microcal Origin 5.0. The two DAQ systems are designated as plasma chamber and CEM and are described in detail below.

Plasma chamber DAQ – The plasma chamber DAQ system uses an IBM Aptiva with a 133MHz Pentium processor. Temperature data from the chamber, exhaust gas, and cooling-water thermocouples, and plasma torch power supply voltage and amperage values are collected using a National Instruments (NI) AT-MIO-64E-3 analog to digital card interfaced with an NI SCXI-1303 module. The water flow meters are Omega model FTB-4065 and FTB-4607H pulsed meters which output an NPN signal whose frequency is proportional to the flow rate. The flow meter signal is collected using a NI PC-TIO-10 digital timing card, interfaced using a NI SC-2072. The flow meter signals and the water temperature signals are combined to give the calorimetry for the main processing chamber, the chamber door, the rotating table, and the plasma torch electrode and cap. The torch current and voltage signals are 0 – 10V proportional output signals.

CEM DAQ – The CEM DAQ system uses an IBM clone PC with a 486DX5/133 processor. The NOx, HCl, total hydrocarbon, and CO analyzers give a 0 – 10 Volt proportional output signal which are collected using an Analog Devices 6B12 modules. The oxygen analyzer gives a milliVolt range proportional output signal that is collected using an Analog Devices 6B11 module. The data are interfaced with the computer using an Analog Devices 6B backplane via an RS-485 protocol serial line to the computer.

The complete NRL plasma arc facility is shown in Figure 2.8. It has recently been used for the treatment of various types of liquid materials including diesel fuel and vegetable oil. The results of those studies will be presented in future reports.

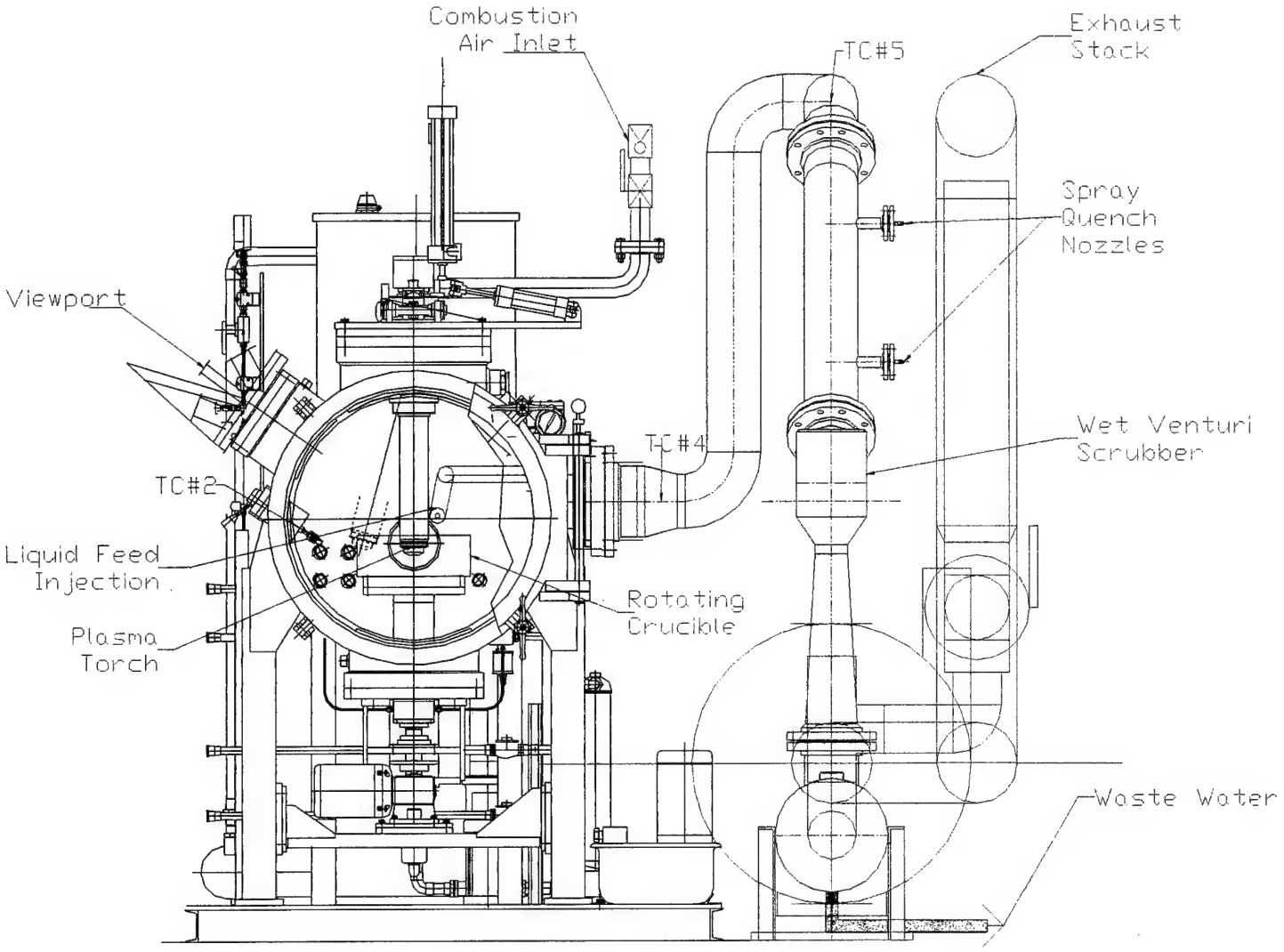


**Figure 2.6 Schematic of the NRL plasma arc system in final operating configuration showing spray quench and wet venturi scrubber.**

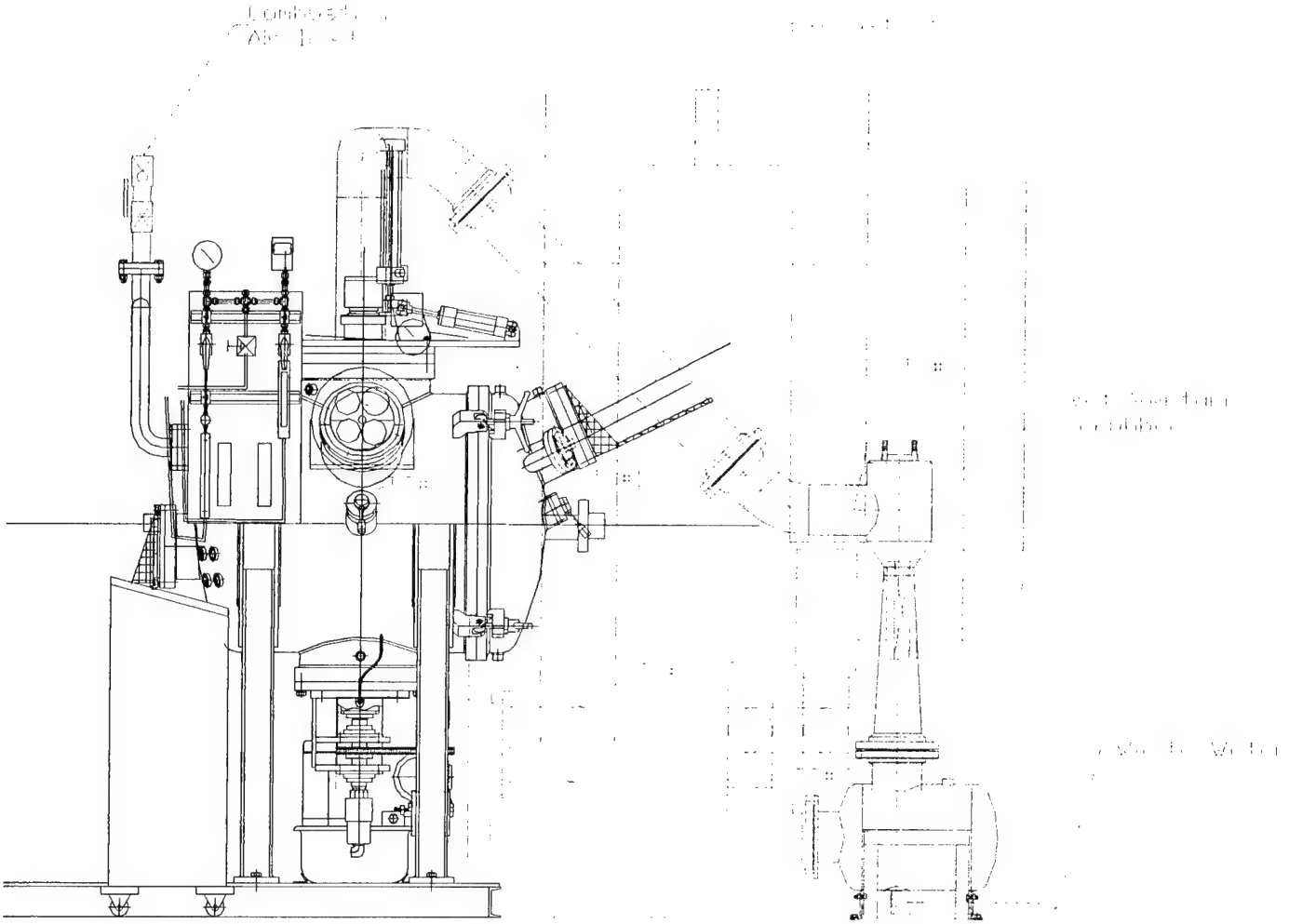

**Figure 2.7 Schematic of NRL plasma arc system in final configuration.**

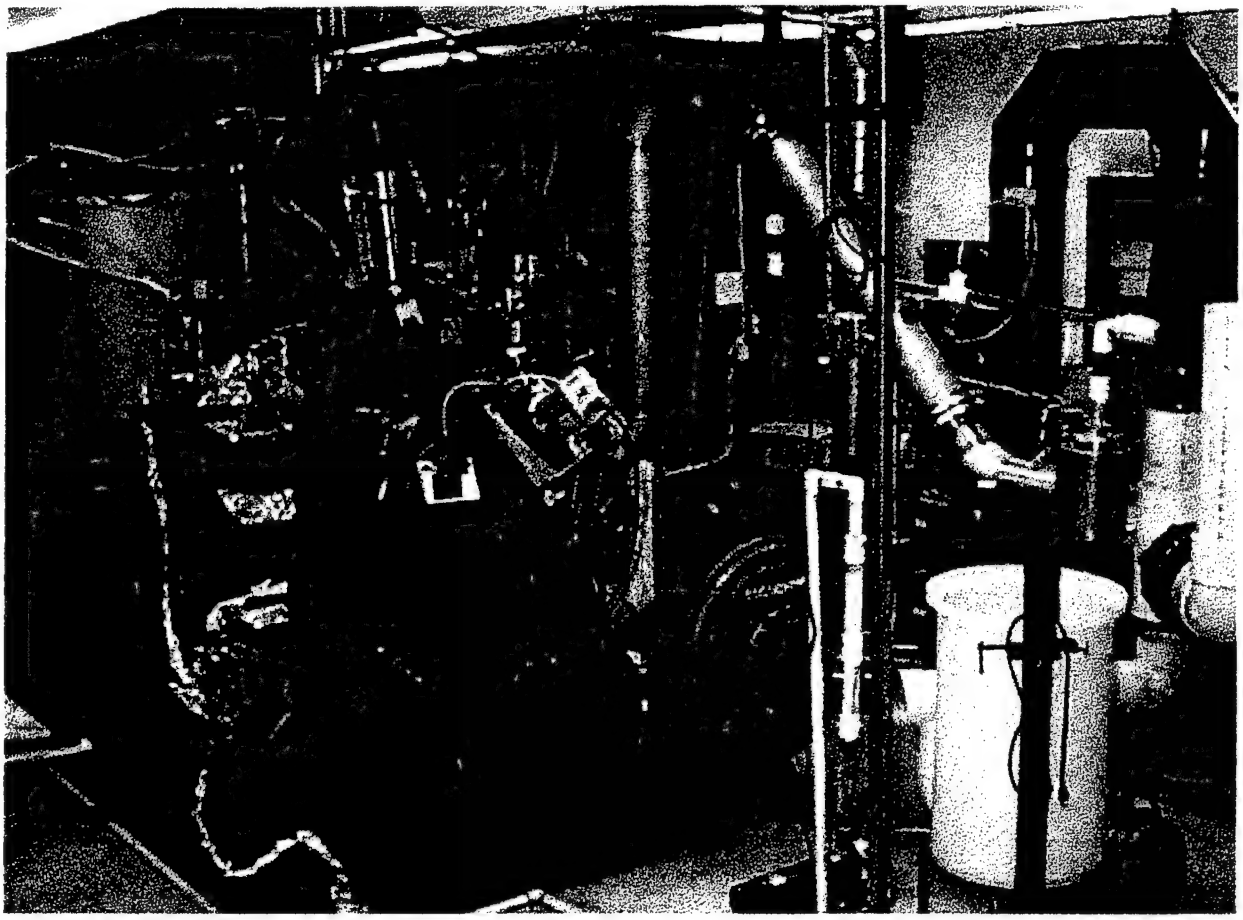

**Figure 2.8 Photograph of NRL plasma arc system**

## 3.0 Measurement of Voltage/Current Relationships for Plasma Torch

### 3.1 Experimental Results

A key operating parameter for plasma arc torches is the torch power which is the product of the current in the arc and the voltage across the arc. The torch in the NRL system is a Retech RP-75N/T which utilizes a constant current power supply and which can be operated in both non-transferred and transferred operating modes. The arc voltage is determined by several factors and a mathematical discussion is presented below. The two dominant variables of the arc voltage are the length of the arc and the conductivity of the plasma gas. In non-transferred mode, the arc length is essentially constant for a given torch geometry and plasma gas. However, in transferred mode, the arc length is an independent variable. In order to establish the operating characteristics of the RP-75N/T in transferred mode, several experiments were conducted to determine the functional relationship between the length of the plasma arc and the arc voltage for the system.

The data for the transferred arc experiments are presented below as arc voltage as a function of arc length. The measured arc length is the distance from the torch exit to the conducting plate on the rotating table as shown in Figure 3.1. There is a small additional length inside the torch to the arc attachment point. As shown in the analysis below, the slope of the voltage curve gives the average electric field in the plasma arc. The RP-75N/T configuration prohibits the torch from having a zero arc length; however important parameters are the slope of the arc length versus arc voltage curve and the time dependent behavior of the transferred arc.

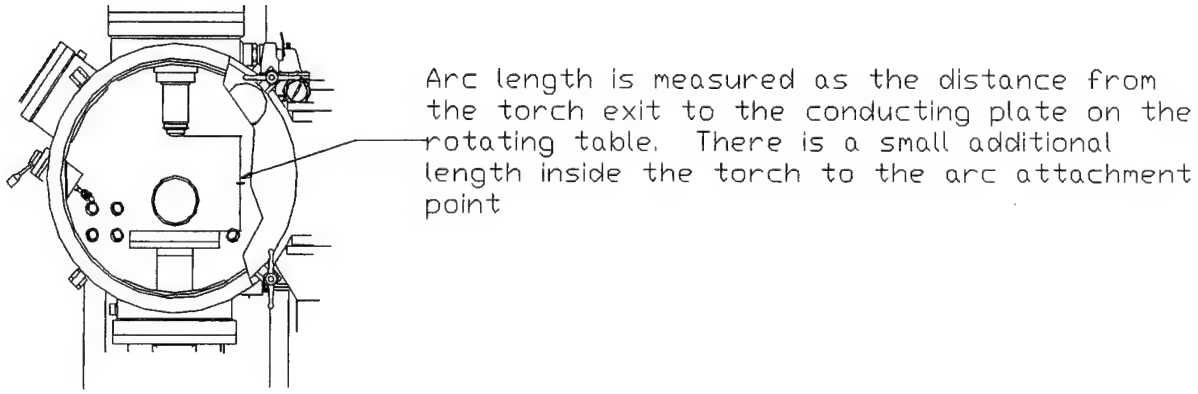


**Figure 3.1 Inside of NRL Plasma Arc Chamber Showing How Arc Length is Determined**

The discussion of arc voltage as a function of arc length can be expressed mathematically as follows [3.1 – 3.3]:

$$\mathbf{J} = \sigma\mathbf{E} \tag{3.1}$$

Where:

$\mathbf{J}$ = Current density
$\mathbf{E}$ = Electric Field
$\sigma = (e^2 n_e)/(m_e \nu_{en})$ = DC conductivity of the plasma
$e$ = Fundamental charge, ($1.9 \times 10^{-19}$ Coulombs)
$n_e$ = Number of electrons
$m_e$ = Mass of electrons
$\nu_{en}$ = Collision frequency of electrons with neutrals.

Assuming uniform current density and conductivity the total current, I, at any height in the arc column is:

$$I = \pi R^2 \mathbf{J} = \pi R^2 \sigma \mathbf{E} \tag{3.2}$$

Where:

R = Radius of the arc column

The axial electric field is:

$$\mathbf{E} = -\partial V/\partial z \approx -V_{arc}/l \tag{3.3}$$

Where:

$V_{arc}$ = arc voltage
$l$ = arc length

Combining equations 3.2 and 3.3 gives the effective resistance of the arc.

$$V_{arc} = (l/\pi R^2 \sigma) I \tag{3.4}$$

Where:

$$l/\pi R^2 \sigma = \text{Resistance of the arc with } \sigma \text{ dependent on gas properties} \tag{3.5}$$

The total voltage in a transferred arc is the sum of the voltage drop in the arc (as calculated above), the anode fall voltage, and the cathode fall voltage:

$$V_{total} = V_{arc} + V_{anode} + V_{cathode} \quad (3.6)$$

For the configuration at NRL, the arc voltage is varied and the anode and cathode fall voltages are assumed to be constant.

As seen in equation 3.4, the arc voltage is dependent upon the conductivity of the plasma gas and the arc length. Several experiments were conducted and the data are presented below. In these experiments the torch system was operated in transferred mode with constant plasma gas conditions while the arc length was varied. The voltage was read from either analog meters or a data acquisition system.

The first transferred arc experiment was conducted using helium at 255 Amps, nitrogen at 340 Amps, nitrogen at 255 Amps, and argon at 420 Amps. The empty crucible was 1-foot in diameter with a graphite annulus for arc initiation. The results, shown in Figure 3.2, are consistent with equation 3.4. The arc voltage varies linearly with arc length; however, various plasma gases with different conductivities produce a shift between the curves. Not surprisingly, changing the current from 340 Amps to 255 Amps for nitrogen causes only a small change in the arc length versus arc voltage curves.

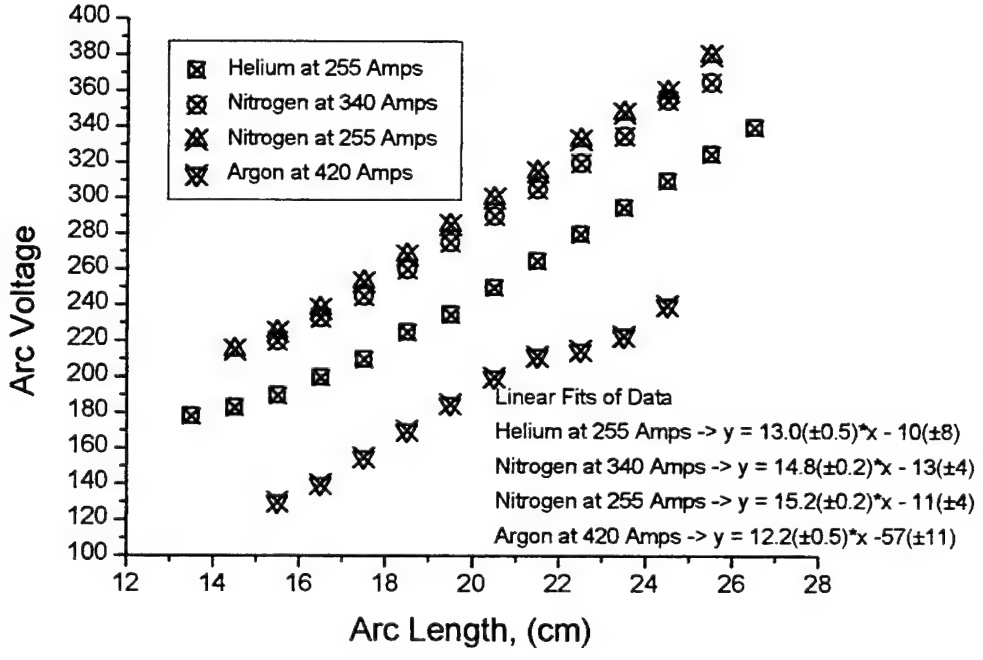


**Figure 3.2 Arc Voltage Versus Arc Length Data: Experiment 1**

The second experiment monitoring arc voltage as a function of arc length was conducted in conjunction with optical emission spectroscopy (OES). The crucible was 1-1/2 foot diameter with no graphite liner, and was filled with a mixture of copper and sand. Polystyrene petri dishes were fed into the system and gas samples collected; after the final feed the voltage vs. arc-length data were collected in conjunction with the OES. The plasma gas was nitrogen at 90.0±0.1 slpm and the arc current was 350 Amps. The results are presented in Figure 3.3. What is significant is that at the longer and shorter arc lengths there is a flattening of the arc voltage.

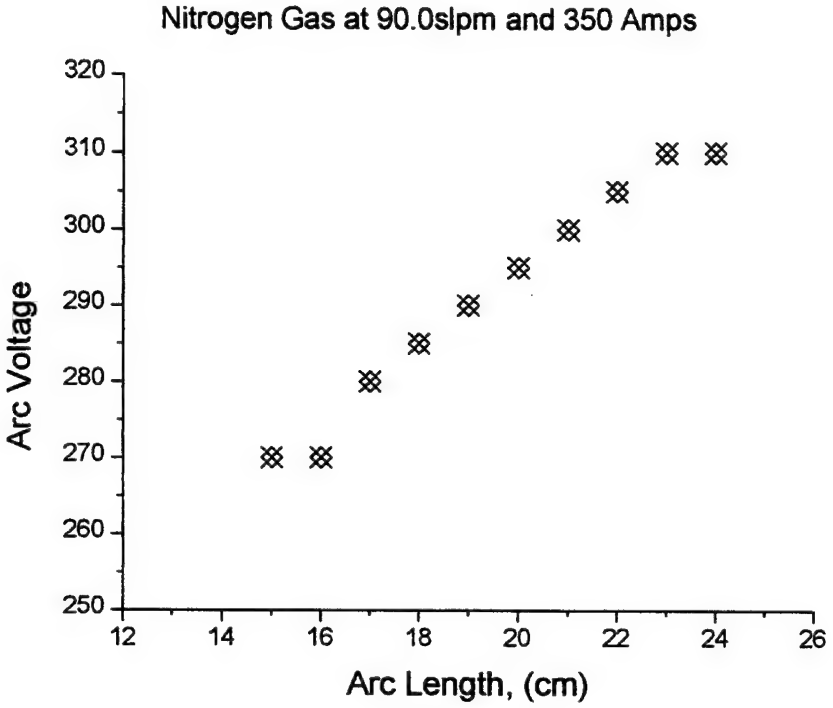


**Figure 3.3: Arc Voltage Versus Arc Length Data: Experiment 2**

While the data show linear behavior in the center, the arc voltage at the extremes (15cm, 16cm, 23cm and 24cm) is constant. For Experiments 1 and 2 the voltage was read from the analog display on the power supply. Due to a desire to better understand the constant arc voltage at the extremes, a better method of determining arc voltage was required.

Voltage data collection was improved by installation of a Fluke 8506A digital multi-meter, giving the capability to calibrate the voltage reading and therefore record the arc voltage more accurately. The next experiments were conducted using the 1-1/2 foot diameter crucible filled with a mixture of surrogate Naval Shipboard Waste. During Experiment 3 the plasma gas was nitrogen at 90.0±0.1 slpm and the arc current was 350 Amps. During Experiment 4 the plasma gas was air at 129 slpm and the arc current was 350 Amps. The results are presented in Figures 3.4 and 3.5.

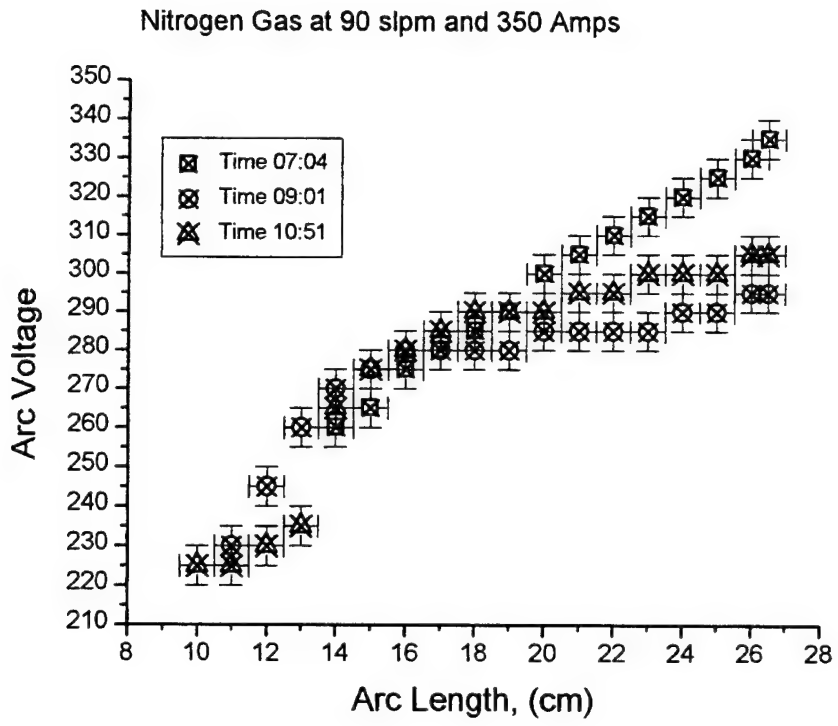


**Figure 3.4 Arc Voltage Versus Arc Length Data: Experiment 3**

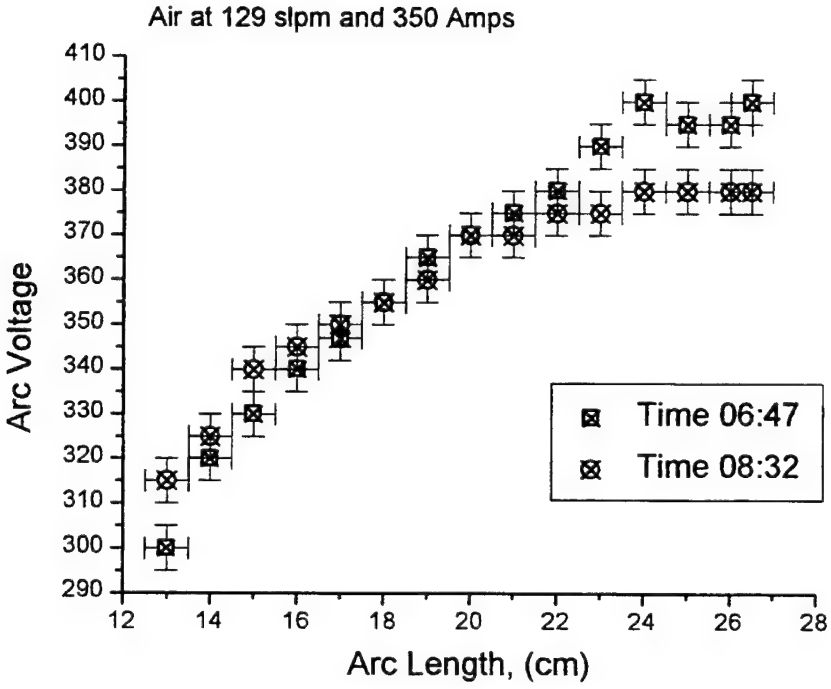


**Figure 3.5 Arc Voltage Versus Arc Length Data: Experiment 4**

Both sets of data show that there is a shift in the relationship between arc voltage and arc length at different times. For nitrogen there is a shift at 20 cm and for air there is a shift at 22 cm. This behavior can be explained with the help of optical emission spectroscopy. In figures 3.6 and 3.7 two spectra are shown, the first from a 15cm arc length and the second from a 24.8cm arc length.

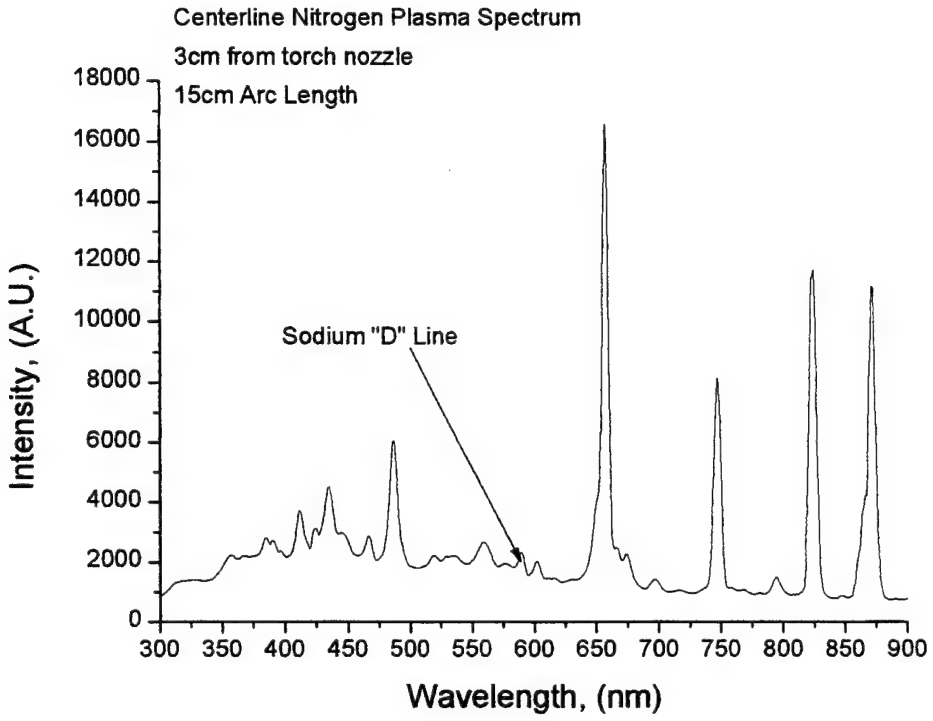


**Figure 3.6 15-cm Arc Length Plasma Optical Emission Spectrum**

For the longer arc, sodium emission is observed. The sodium arises from the evaporation of slag material containing glass. Because sodium has a lower ionization potential than the working gas, more electrons are liberated in the arc gas and the electrical conductivity increases. At a fixed current this means that the electric field decreases. As seen in equation 3.3, the electric field in the arc is given by the slope of the voltage versus arc length curve. Thus for long arcs, ($l \approx 25$cm), the vaporized sodium gets entrained in the plasma arc, but for short arcs, ($l \approx 15$cm), there is less mixing of the sodium into the arc plasma.

To ensure that the change in conductivity of the plasma gas was responsible for the time dependent change in the arc voltage, Experiments 5, 6, and 7 were conducted with no crucible, only a graphite base plate and enough copper to initiate the arc. Nitrogen was the plasma gas, but the gas flow and current were varied along with rotation of the table. Some of the data are presented in Figures 3.8 through 3.10

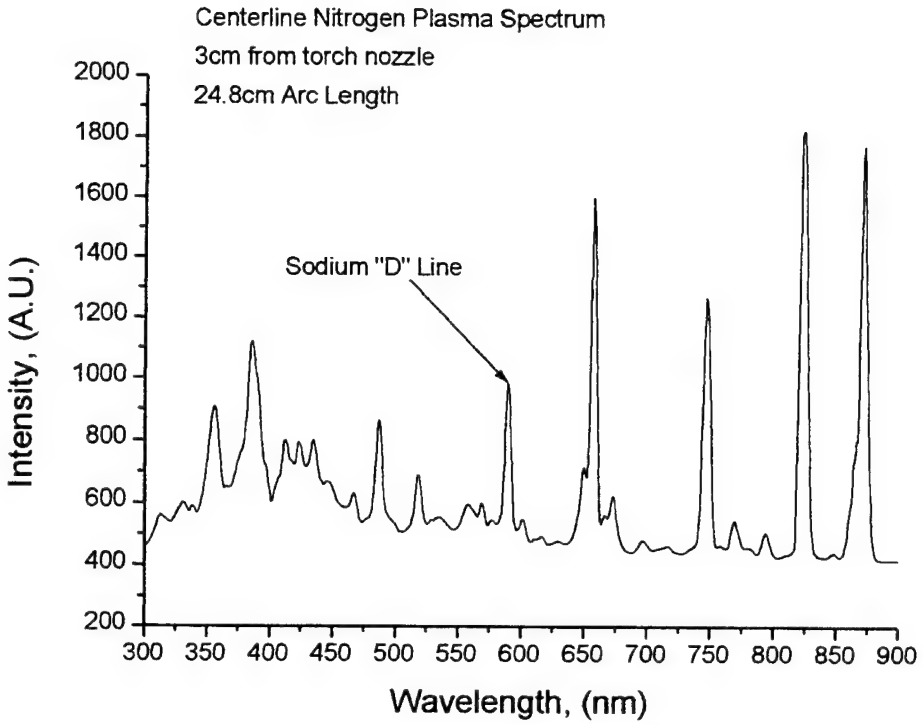


**Figure 3.7 24.8-cm Arc Length Plasma Optical Emission Spectra**

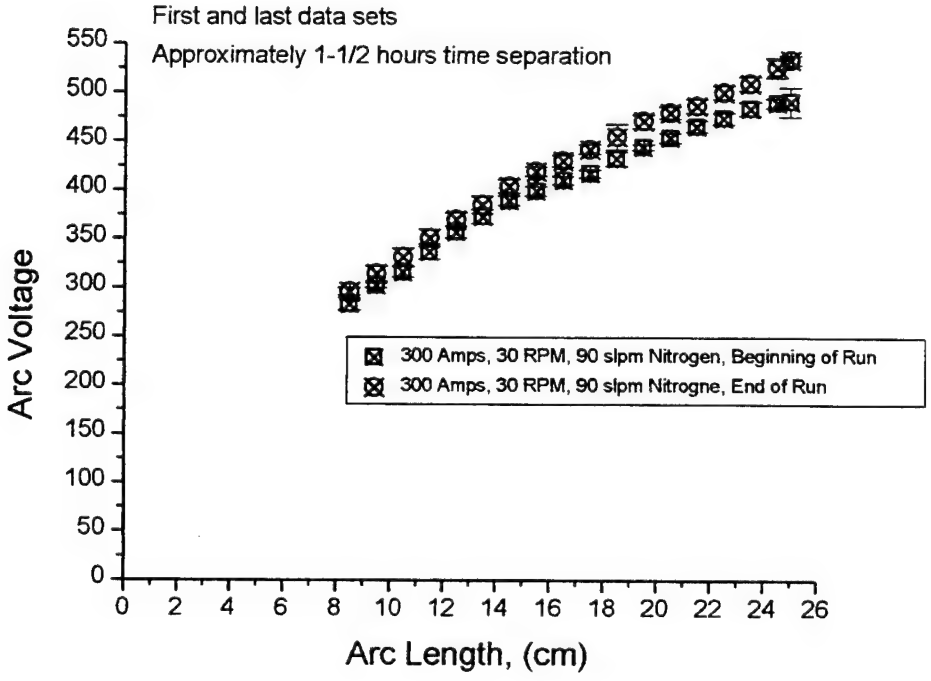


**Figure 3.8 Arc Voltage Versus Arc Length Data: Experiment 5**

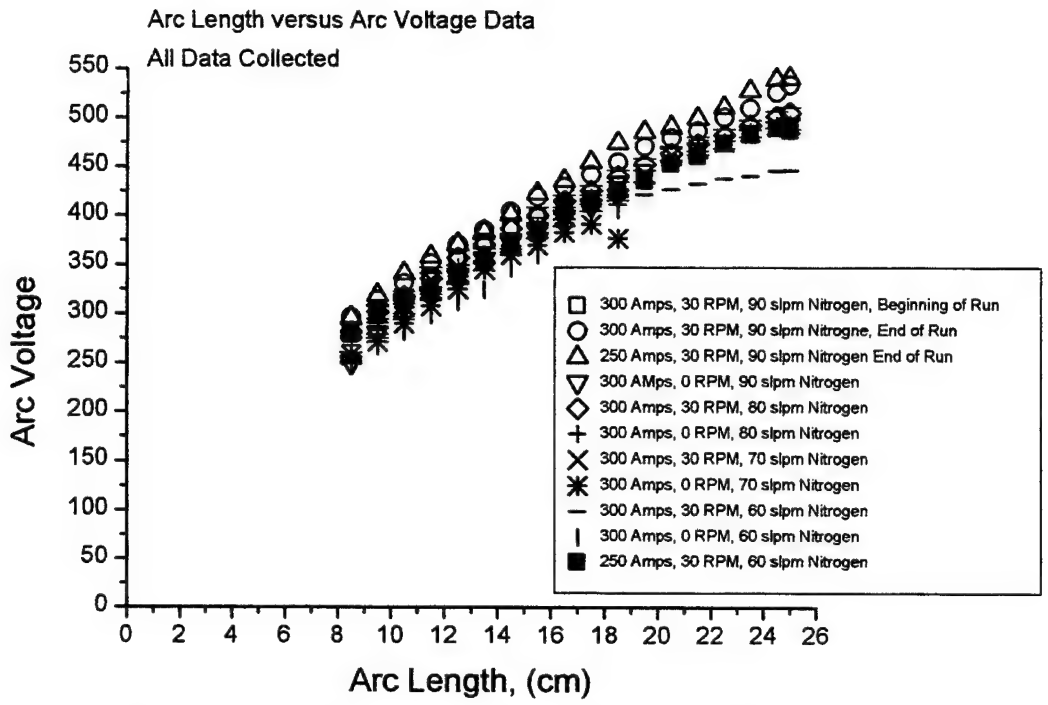


**Figure 3.9 Arc Voltage Versus Arc Length Data: Experiment 6**

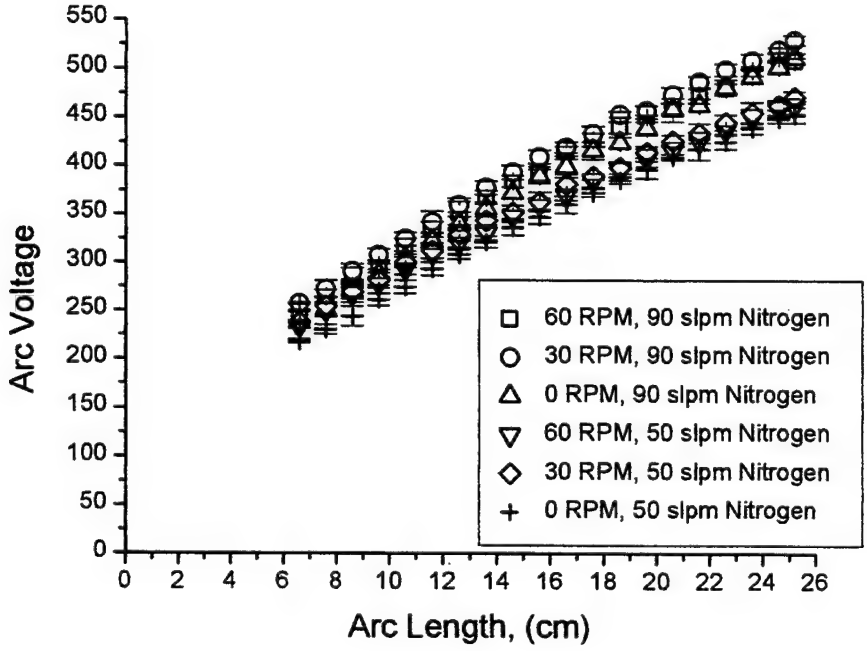


**Figure 3.10 Arc Voltage Versus Arc Length Data: Experiment 7**

Figure 3.8 shows that without the low ionization material becoming entrained in the plasma gas, thereby changing the conductivity, the arc voltage versus arc length is fairly constant over time. Figures 3.9 and 3.10 show that the rotation of the table has almost no effect on the arc voltage. However, changing the plasma gas flow rate, which changes the conductivity, does have an impact on the arc voltage versus arc length.

## 3.2 References


3.1 H. K. Choi and W.H. Gauvin, Operating Characteristics and Energy Distribution in Transferred Plasma Arc Systems. Plasma Chemistry and Plasma Processing, Vol. 2, No. 4, Pages 361 - 386, 1982

3.2 W. H. Gauvin, Some Characteristics of Transferred-Arc Plasmas. Plasma Chemistry and Plasma Processing, Vol. 9, No. 1, Pages 65S - 84S, 1989 (Supplement)

3.3 Yuri P. Raizer, Gas Discharge Physics. 2nd Ed., New York: Springer-Verlag, 1997

## 4.0 Optical Emission Studies of the Plasma Torch

### 4.1 Introduction

Although plasma arc technology is fairly well understood the successful application of plasma torches in novel systems requires testing, evaluation, and understanding of potential designs. This is indicated by the recent development of a number of simulation models for efficiency and design scaling of high current devices [4.1-4.4]. In the Plasma Arc Waste Destruction System (PAWDS) for shipboard waste treatment one has a unique design tradeoff between efficiency and size, the latter quantity being of little concern in land based systems but of primary concern on board seafaring vessels. An essential engineering component in the tradeoff issue is the power balance of the system. For a given electrical power input to the plasma how much is transferred to the anode, to the cathode, to chamber walls by radiation, to the crucible containing slag by conduction and ohmic heating, to the ambient gas in the chamber by mixing with the arc gas, and finally how much is carried off by the exhaust gases. Experimental investigations on the power balance have been performed on several high current torch systems [4.5,4.6]. Parisi and Gauvin [4.6] found that heat transfer by radiation is the main mechanism of energy transfer to a surrounding enclosure for a long transferred arc of argon or nitrogen. Since the radiated power is a strong function of the arc gas temperature (the power being proportional to the fourth power of temperature if the plasma was a blackbody emitter), an essential parameter characterizing a plasma arc is its temperature. If local thermodynamic equilibrium (LTE) is assumed, then a knowledge of the input gas constituents, chamber pressure $p$, and measured arc gas temperature $T_g$ is sufficient to determine the plasma conditions. In particular, the composition of the heated gas, including the electron density $n_e$ is specified by $T_g$ and $p$.

This section discusses the use of optical emission spectroscopy (OES) to characterize the plasma in both the non-transferred and transferred arc configuration of the NRL torch system. The temperature measurement is a starting point for the analysis of the power balance relation in the system. First, spatially resolved, broadband optical measurements of emission lines from atomic hydrogen in the plasma are used to estimate the electron temperature [$T_e(r)$] profile across the arc. The arc plasma is assumed to be radially symmetric and $r$ is the radial coordinate within the arc. The analyzed results indicate that the core of the arc is close to LTE with a central temperature of 6,200K in the non-transferred mode and ~15,000K in the transferred mode. However, in the outer periphery of the arc, called the mantle, conditions are far from equilibrium. Photo-absorption of the radiation emitted from the core plays a significant role in determining the internal energy of the gas in the mantle. A second set of experiments was conducted to measure $n_e$ through Stark broadening, This information can also be used to investigate the equilibrium condition. Limited spectral data suggest that $n_e$ is ~800 times larger than one would expect from the LTE assumption ($n_e \simeq 10^{14}$ $cm^{-3}$) using the above temperature at atmospheric pressure. The conclusion of non-equilibrium conditions would appear to be quite unusual given the classic work of Maecker [4.7,4.8]. We note, however, that other recent observations also indicate a significant departure from LTE [4.9] in arcs. A third set of experiments for optical emission studies consisted of broadband surveys taken during treatment of standard waste slags with a transferred arc. The spectra demonstrated a clear

entrainment process of the vapor from heated waste slag into the core of the arc which affects the conductivity of the plasma.

## 4.2 OES Analysis of the Non-Transferred Arc

The spectroscopic setup for the NRL torch system is depicted in Figure 4.1. During the observations the torch is kept is the vertical position and translated along the $z$-axis which intercepts the center of the crucible. Emission from the arc passes through a narrow collimator port at the rear of the chamber which is sealed with a sapphire window. A pinhole behind the window and lens system combine to form an image of the arc with parallel rays subject to a factor of four de-magnification. An optical fiber matched to the lens system and mounted on a translatable stage detects the image. The visible emission from the arc is about a centimeter in diameter and the fiber is stepped so that a spectrum is acquired every 0.2 cm in the $y$-direction across the arc. The spatial resolution is $\sim$0.1 cm at the position of the arc. Three centimeters of the arc along the vertical $z$-direction are accessible at the fiber optic plane. Two gratings can be used in the spectrometer, but only results from the low resolution (300 lines/mm) covering the entire optical domain will be discussed here. Each spectrum is corrected for the wavelength dependent response function of the optical system.

A sample spectrum is presented in Figure 4.2. The operating conditions are 333 Volts, 375 Amps, 125 kW, 100 slpm (standard liters per minute) of $N_2$, with a $H_2$ seeding of 5 slpm. The system is in the non-transferred mode and the spectrum is taken at the center of the arc ($y = 0$), 1 cm down from the torch nozzle. Several prominent atomic emission complexes from neutral nitrogen (NI) are noted. Each feature is actually a combination of three to five individual lines decaying to the $^4$P term level. The spectral resolution is insufficient to resolve the individual lines. The complex with upper levels in the $^4$S term will be denoted by N1; with upper levels in the $^4$P term by N2; and with upper levels in the $^4$D term by N3. These complexes are noted in Figure 4.2. An energy level diagram for neutral nitrogen is shown in Figure 4.3(a) where the three lines comprising the N1 complex are called out. Molecular emission from $N_2$ is negligible or at most weak throughout the visible arc. The hydrogen emission lines $H_\alpha$ and $H_\beta$ are also noted in Figure 4.2 and the corresponding hydrogen energy level diagram is given in Figure 4.3(b). These hydrogen features are individual lines and can be used to estimate the electron temperature $T_e$ in the arc. The closer the emission line ratio $H_\alpha/H_\beta$ is to unity, the higher $T_e$ is.

Spectra were taken at 15 positions across the arc in the $y$-direction and at 1, 2, and 4 cm down from the torch nozzle in $z$, all at the same operating conditions mentioned above. The procedure was duplicated to get a second set of data. Emission line intensities are measured from each spectrum after subtracting the continuum background and the ratios $H_\alpha/H_\beta$, N1/N2, and N3/N2 are obtained. All the data sets are combined to enhance the signal-to-noise ratio. The resulting observed emission ratios are presented in Figure 4.4(a) for nitrogen and Figure 4.4(b) for hydrogen. Note that the nitrogen ratios show little dependence on the $y$-position, while the $H_\alpha/H_\beta$ ratio displays a dip in the center of the arc, corresponding to a high temperature, and a leveling off in the mantle of the arc.

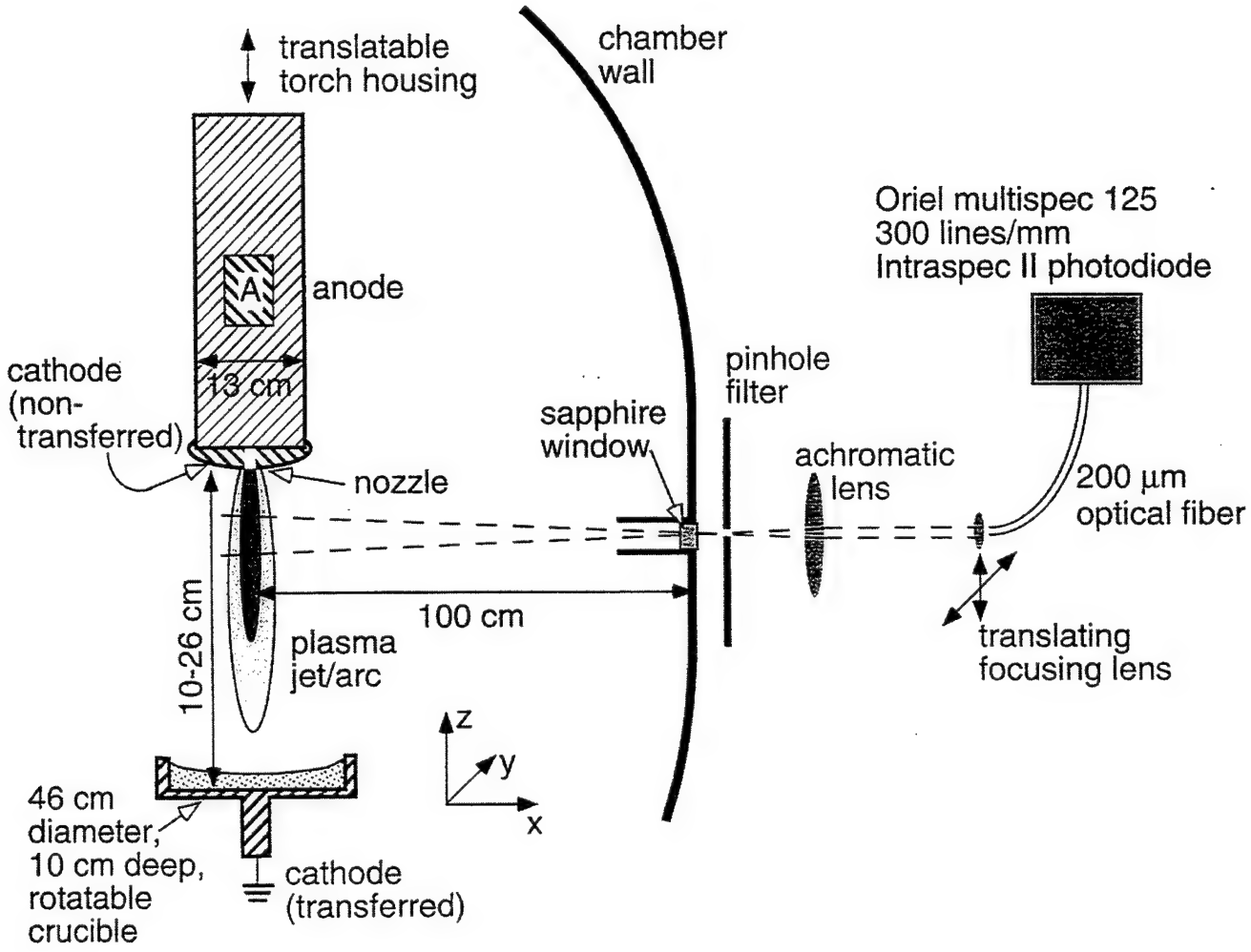


**Figure 4.1 Schematic drawing of the NRL torch chamber and spectroscopic arrangement. The coordinate origin is located at the bottom center of the crucible.**

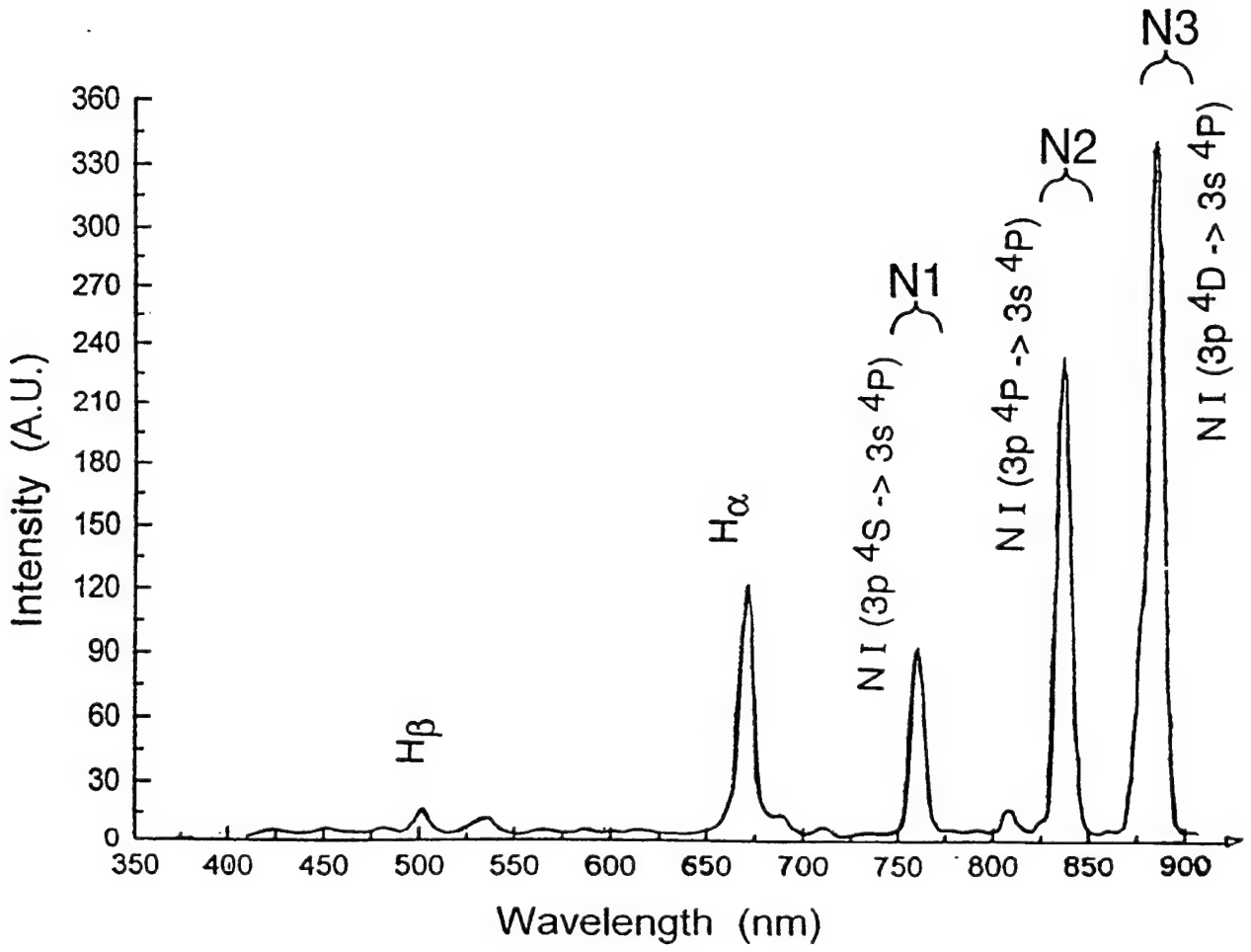


**Figure 4.2 Sample optical spectrum of the plasma arc in the non-transferred mode taken at the center of the arc ($y = 0$), 1 cm down from the torch nozzle. Each emission feature from neutral nitrogen (NI), denoted as N1, N2, and N3, is actually a complex of lines as described in the text. Two of the Balmer lines from hydrogen, $H_\alpha$ and $H_\beta$, are also noted. The operating conditions are 333 Volts, 375 Amps, 125 kW, 100 slpm (standard liters per minute) of $N_2$, with a $H_2$ seeding of 5 slpm.**

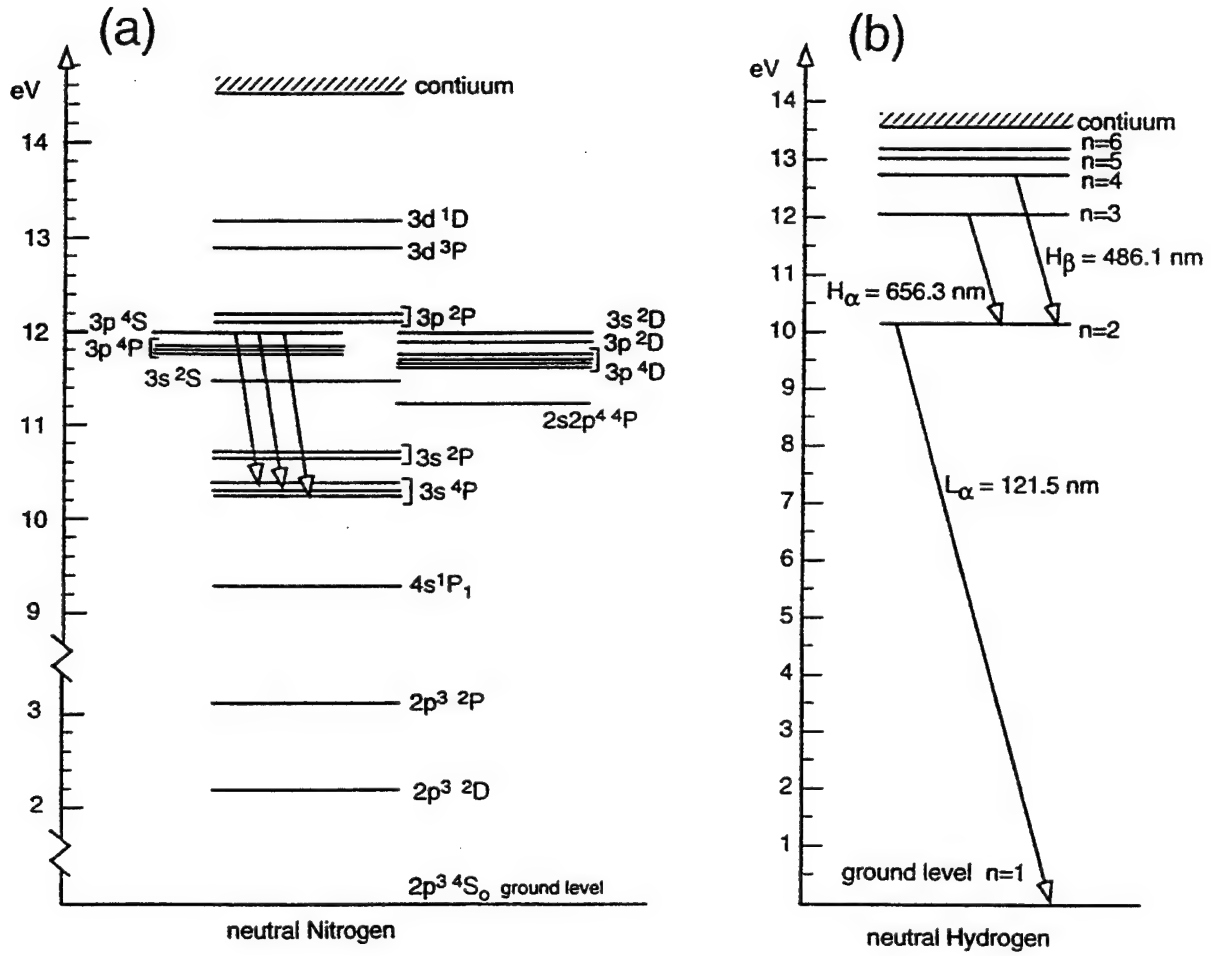


**Figure 4.3 Energy level diagrams for neutral nitrogen (a) and hydrogen (b). 1 eV corresponds to 11,650K or 1,240 nm.**

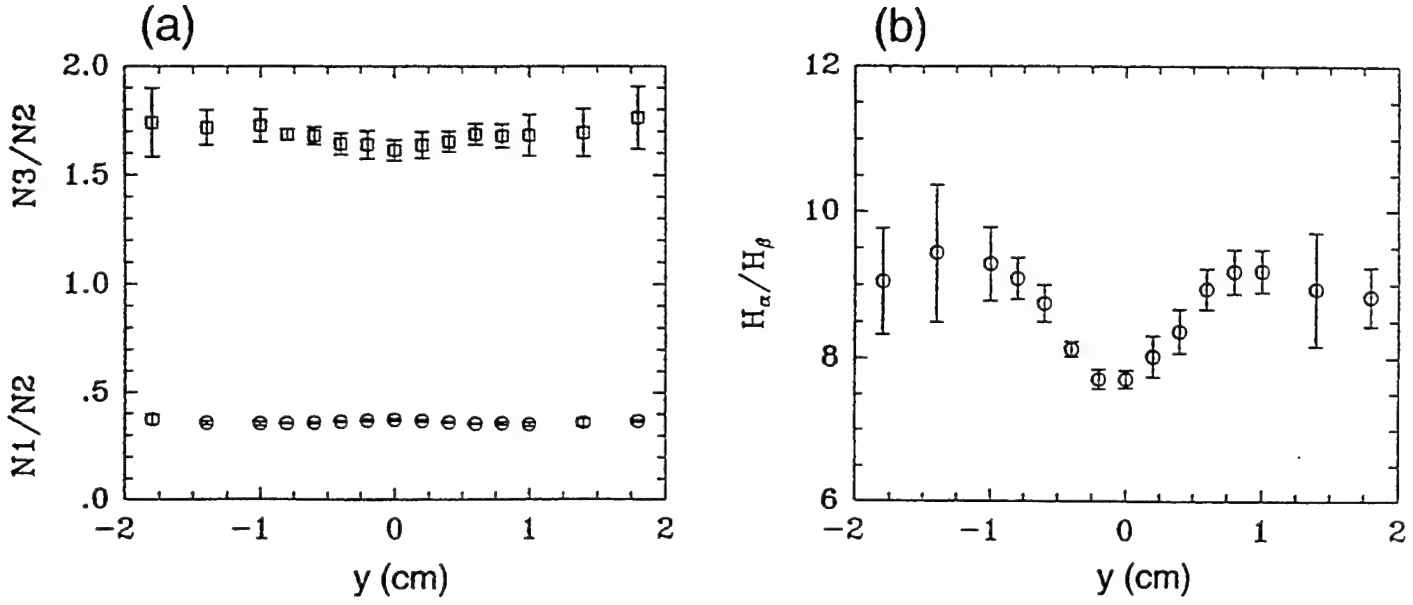


**Figure 4.4 Observed ratios of emission features from nitrogen (a) and hydrogen (b) as a function of $y$-position across the arc. The error bars denote one sigma standard deviations of six measurements at each position.**

The data are analyzed according to the following procedure. A Gaussian temperature profile $T_g(r)$ for the gas is assumed in the arc, peaking at the center and decaying to the periphery. The ambient gas temperature in the chamber is measured with thermocouples to be ~1,600K. For a fixed pressure of 1 atmosphere, an equilibrium calculation is performed for an $N_2$-$H_2$ mixture corresponding to the input flow conditions. An example temperature profile and composition calculation is shown in Figure 4.5. Using the results for atomic nitrogen and hydrogen, two different models for the excited state populations are employed. For the first model, the excited states are assumed to be in LTE with the ionization and Boltzmann statistics readily providing the populations of the excited states. The second model employs collisional radiative equilibrium (CRE) to calculate excited state populations [4.10-4.12]. The levels included in the calculation of the population dynamics for nitrogen are those shown in Figure 4.3 for the neutral atom as well as 19 levels for the $N^+$ ion. For hydrogen, five levels of the neutral atom are followed and one level for $H^+$. The processes included in the CRE model are shown schematically in Figure 4.6(a). They include electron collisional excitation and de-excitation, photo-absorption and radiative decay, electron collisional ionization and three-body recombination, photo-ionization and radiative recombination. If the photo-processes are neglected, the collisional rates reproduce LTE conditions because the rates are detailed balanced. The arc plasma is modeled with twenty radial zones to evaluate the populations. It should be noted that the photo-excitation processes can be non-local, i.e., the self-consistent radiation transfer calculation is coupled to the level rate equations such that emission in one zone can propagate and subsequently be absorbed in another zone. Based on the population results at different radii from either the LTE case or the CRE case, a post-process, radiative transfer calculation along a line in the $x$-direction at 15 impact parameters spread in the $y$-direction is performed to produce the synthetic spectra. A schematic of the transport geometry used to produce the synthetic spectra is shown in Figure 4.6(b).

Let us begin with the LTE case and consider the ratios for the nitrogen features. In LTE ratios of emission line intensities are a function of $T_g$ alone and the predicted N1/N2 and N3/N2 ratios are shown as the solid lines in Figure 4.7. As noted above, the observed ratios from Figure 4.4(a) are weakly dependent upon the $y$ impact parameter and hence only the average value for each ratio is marked at the right side of Figure 4.7. The observed N3/N2 ratio indicates a high arc temperature ($T_g > 10,000$K), while the N1/N2 ratio indicates the opposite ($T_g \sim 2000$K). This is the first indication that a simple LTE model for the high powered arc at NRL is not fully consistent with the data. The points in Figure 4.7 labeled "model" will be described below.

Next consider the $H_\alpha/H_\beta$ data and the model calculations. Figure 4.8 displays the hydrogen data from Figure 4.4 along with the best fit results from the LTE and CRE models. The temperature profile adopted for this best fit is determined by matching the synthetic spectra to the core of the arc ($y \sim 0$) with the excited state populations determined by the LTE condition. The profile $T_g(r)$ is the one shown in Figure 4.5. The $H_\alpha/H_\beta$ ratio in LTE decreases at high temperatures because the populations of the $n = 3$ and $n = 4$ states of hydrogen become nearly equal, while the ratio increases at low temperatures due the predominant population of H($n = 3$) over that of H($n = 4$). The same temperature profile is then used in the CRE model to calculate excited state populations and synthetic spectra. Both the LTE and CRE models are consistent with an equilibrium plasma in

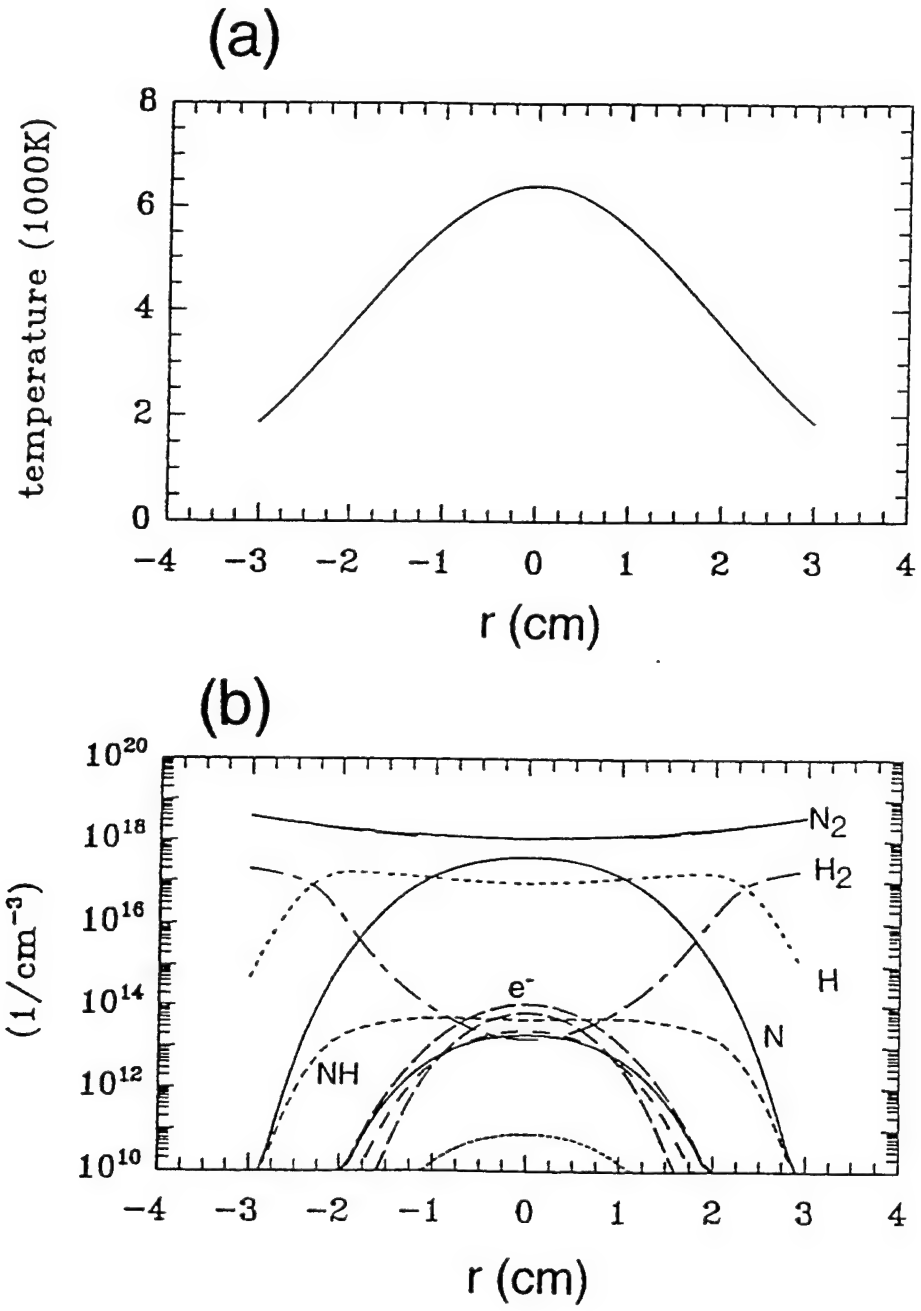


**Figure 4.5 An assumed temperature profile (a) and the corresponding equilibrium densities of the dominant species (b) at one atmosphere along a diameter of the model arc. $r$ is the radial coordinate centered on the arc.**

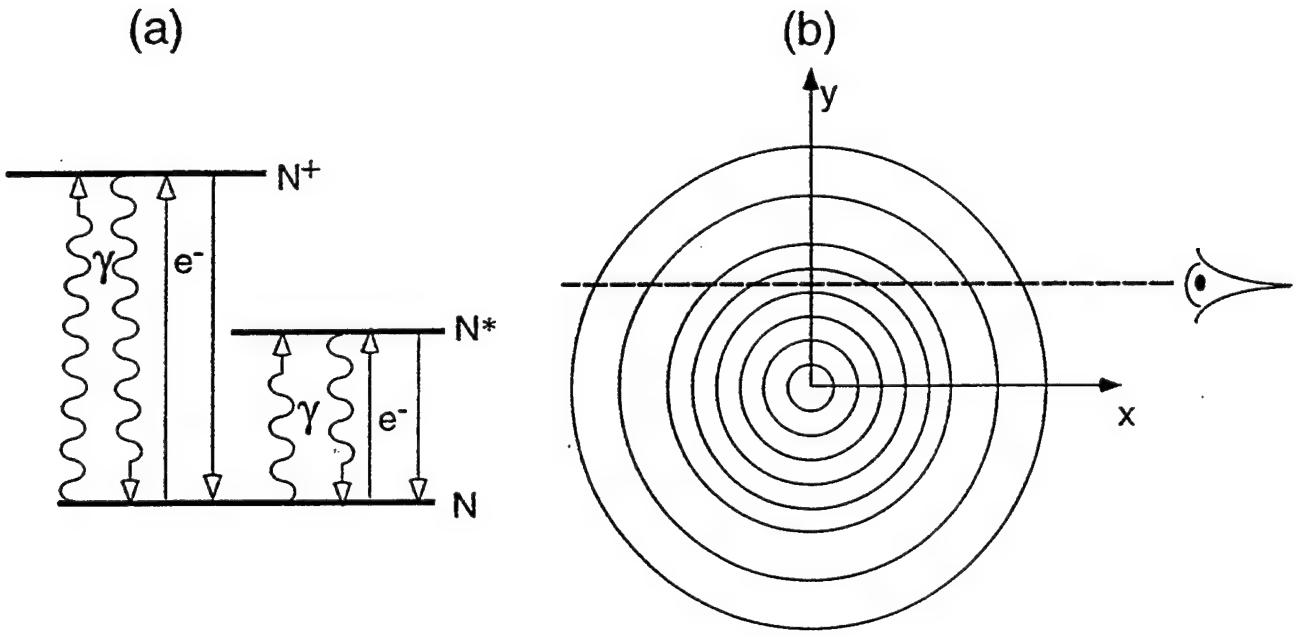


**Figure 4.6 (a) A schematic of the atomic processes included in the collisional radiative equilibrium model to calculate the excited level populations of the atomic species giving rise to the emission lines. (b) The geometry used to calculate the synthetic spectra from the model arc. The circles represent spatial zones used to numerically calculate the level populations and radiation transport. The impact parameter for calculating the synthetic spectra is measured along the $y$-direction.**

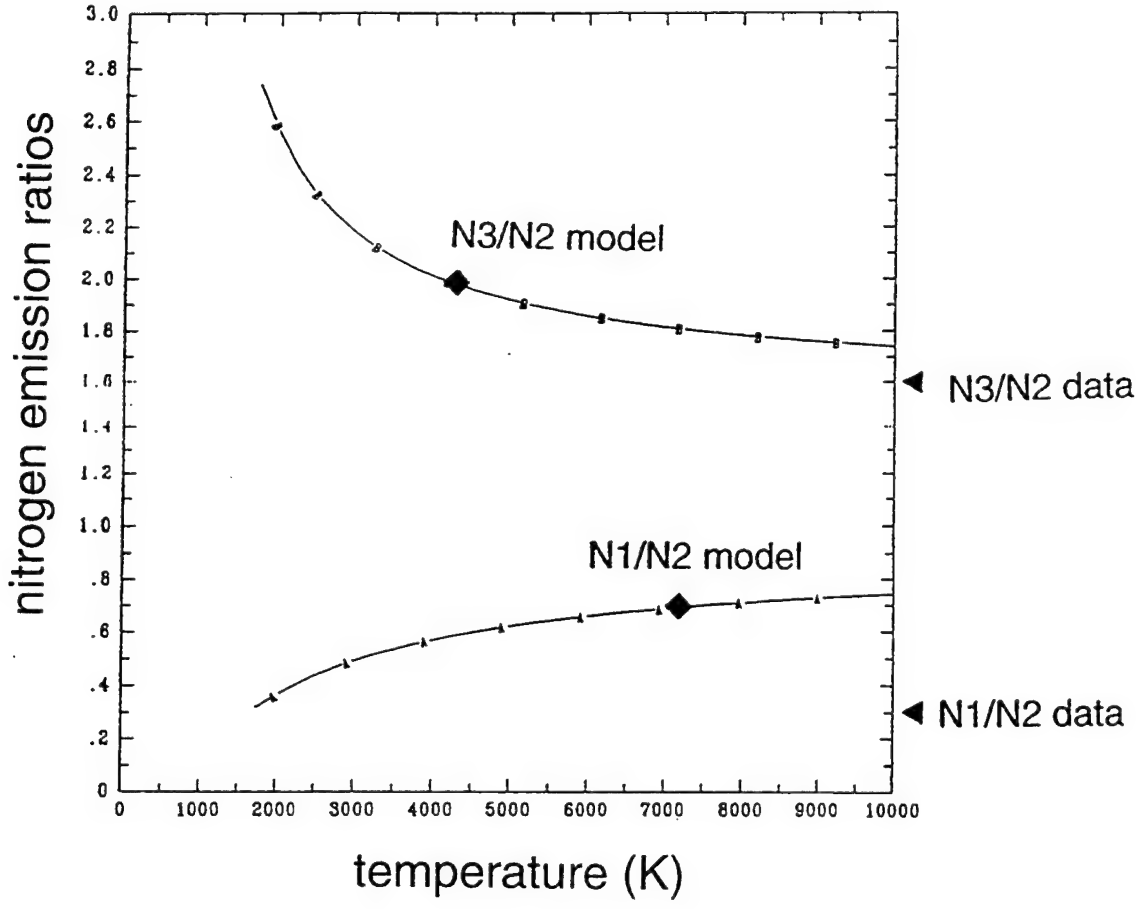


**Figure 4.7** The solid lines are the calculated ratios for the N1/N2 and N3/N2 emission features of nitrogen assuming LTE conditions. The data from Figure 4.4 are marked on the right side. The model ratios arise from the CRE calculation described in the text.

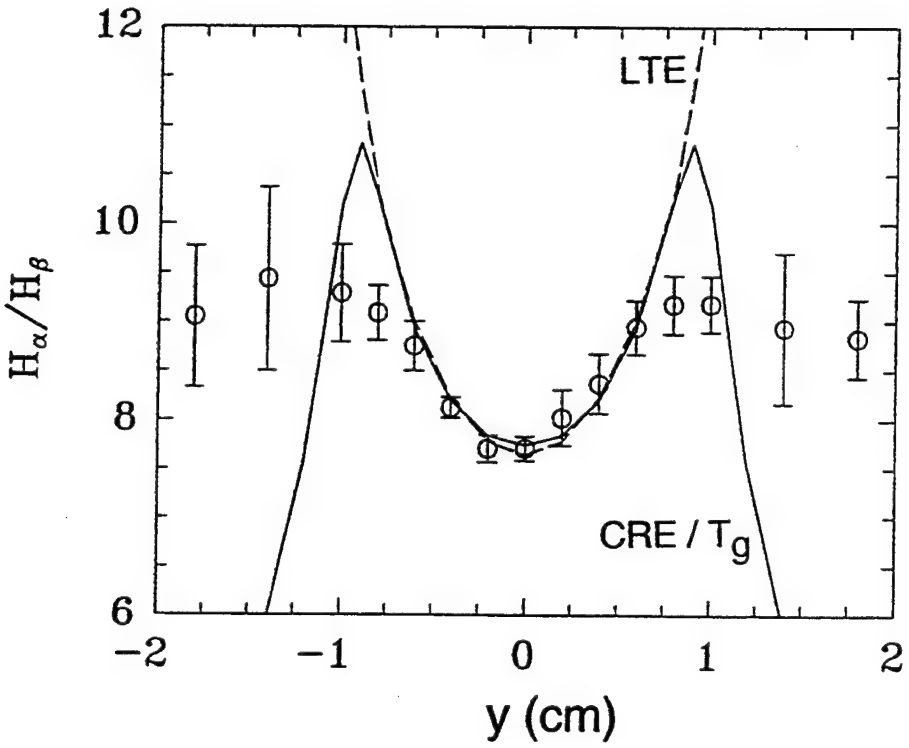


**Figure 4.8 The $H_\alpha/H_\beta$ emission ratio as predicted from synthetic spectra using the LTE and CRE conditions to determine the excited state populations. The CRE model is a single temperature model. Both models predict a core temperature for the non-transferred arc of 6,200K, but the results in the arc mantle differ significantly from the data of Figure 4.4.**

the core of the arc at a temperature of 6,200K. However, in the mantle of the arc, beyond $\mid y \mid > 0.8$ cm, the two models diverge dramatically from each other, as well as from the data. In the LTE case, the predicted $H_\alpha/H_\beta$ ratio continues to rise in the arc periphery due to the decreasing $T_g(r)$. In the CRE case, the turnover in the ratio reflects a photo-absorption effect. The $L_\alpha$ ($n = 1 \rightarrow 2$), $L_\beta$ ($n = 1 \rightarrow 3$), and $L_\gamma$ ($n = 1 \rightarrow 4$) photons emitted from the hot core of the arc are absorbed in the cooler mantle and enhance the excited state populations of $n = 2, 3$ and 4 over what they are in LTE. The first Lyman photon ($L_\alpha$) is depicted in Figure 4.3(b). Furthermore, in the mantle the mean free path of a $L_\alpha$ photon is smaller than that of a $L_\beta$ photon, which in turn is smaller than that of a $L_\gamma$ photon. As a consequence the spectrum hardens, i.e., the low energy photons are removed leaving a more energetic spectrum. At the photon flux propagates into the periphery of the arc the $H(n = 4)$ population becomes anomalously high compared to $H(n = 3)$. This leads to a decrease in the $H_\alpha$ emission compared to that of $H_\beta$. To verify that the effect is caused by the inclusion of photo-processes in the CRE model, such processes were turned off in the CRE calculation and the resulting curve for the $H_\alpha/H_\beta$ ratio followed that found for the LTE case.

The fact that the data matches neither the LTE nor the CRE in the mantle of the arc suggests that the temperature profile in the periphery needs to be revised. One solution found to reproduce the data consists of a two temperature model. The gas temperature $T_g(r)$, which controls the density through the uniform pressure assumption, remains the same as above, but the electron temperature $T_e(r)$ is nearly uniform throughout the arc. The two temperature profiles are shown in Figure 4.9(a), along with the calculated populations of the atomic constituents in the arc from the model (b), and the comparison between the predicted $H_\alpha/H_\beta$ emission ratio and the data (c). Note that the peak electron density is $1 \times 10^{14}$ cm$^{-3}$, which is similar to the LTE peak value of Figure 4.5(b). The match to the hydrogen line ratio is quite good for this model and indicates that there is a significant departure from thermal ($T_g \neq T_e$) as well as from excitation equilibrium (non-Boltzmann) in the arc mantle.

Synthetic spectra were also calculated for nitrogen with the CRE model using the above two temperature distribution. The predicted results for the emission ratios are ~2 for N3/N2 and ~0.7 for N1/N2. These points are labeled as "model" in Figure 4.7. The thermal non-equilibrium of the model is reflected in the fact that the two predicted ratios are not vertically aligned on the two LTE curves. The N3/N2 ratio predicts a low temperature (~4000K), while the N1/N2 ratio predicts a higher temperature (~7000K). This is opposite to the trend indicated by the observed data and continued research on nitrogen excitation mechanisms is warranted to obtain consistency with the hydrogen results.

To further investigate the plasma arc conditions a high resolution 2 meter monochrometer was fielded to measure Stark broadening of the $H_\beta$ line. This broadening is related to the electron density in the line forming region. Figure 4.10 displays the measured $H_\beta$ profile for the operating conditions of 300 Amps, 333 Volts, 90 slpm of $N_2$, and 4.5 slpm of $H_2$. The data are taken on the arc centerline, 2 cm below the torch nozzle. The instrumental broadening was checked with a hydrogen lamp to be only ~3 Angstroms. Using standard Stark broadened profiles for the analysis [4.13] and assuming a uniform plasma, the data, which presents a 38 Angstroms FWHM, indicate an electron density of $8 \times 10^{16}$ cm$^{-3}$. This is a surprising 800 times larger than the electron density of Figure 4.9(c) calculated with the best fit two-temperature CRE model. The interpreted high

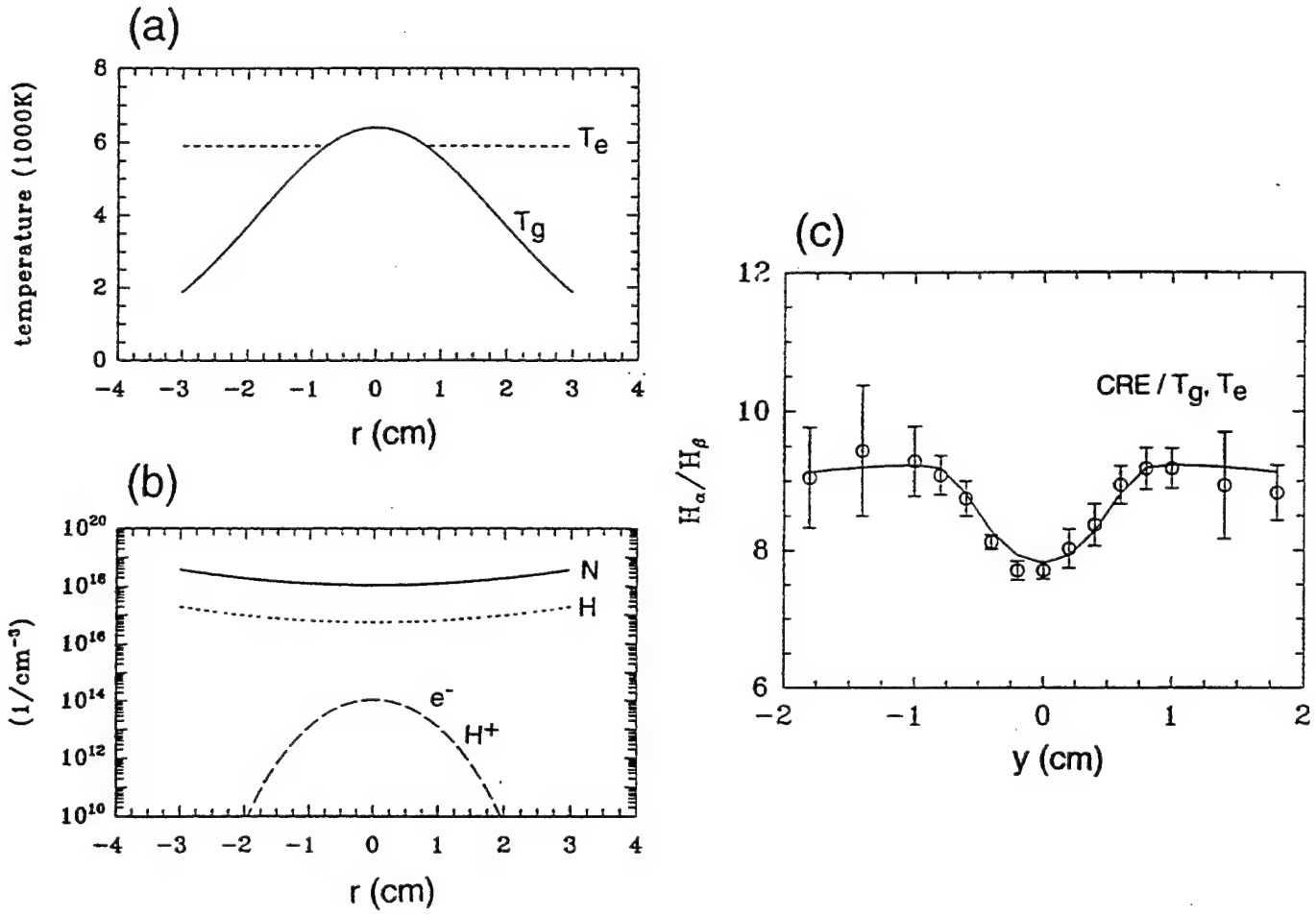


**Figure 4.9 (a) The assumed gas $T_g$ and electron $T_e$ temperature profiles used for the two temperature CRE model. (b) The calculated densities of the atomic arc constituents from the model. (c) The resulting $H_\alpha/H_\beta$ emission ratio from the synthetic spectra from the two temperature model.**

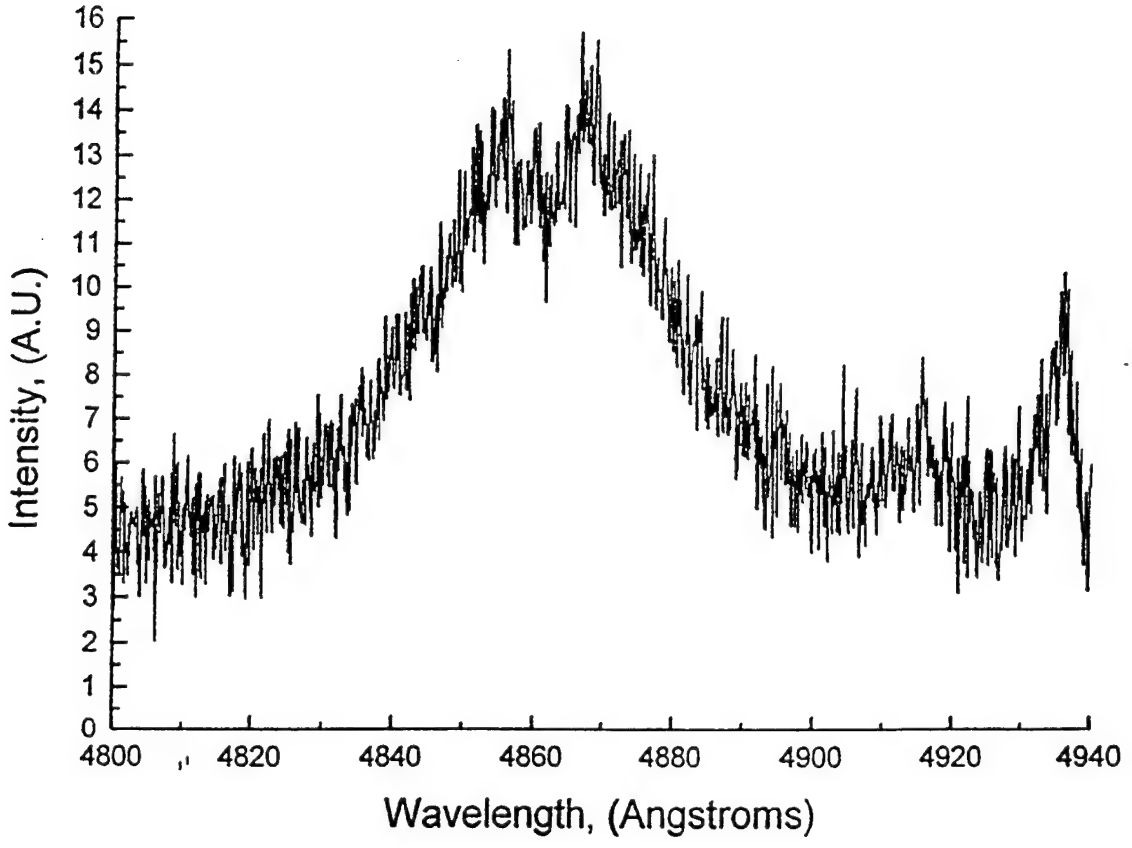


**Figure 4.10 Measured Stark broadened profile for the $H_\beta$ line at 300 Amps and 333 Volts in the non-transferred mode. The data is taken on the arc centerline, 2 cm below the torch nozzle.**

electron density is likely to be somewhat of an overestimate since the presence of known gradients in the plasma can effect the emergent profile from which the density is inferred. A proper analysis would involve creating a synthetic profile based on the multi-frequency transport for a Stark broadened line. This calculation is more complex than the transport method used in the above CRE model which assumed a simpler Voigt emission profile.

Chen, et al., [4.9] used hydrogen Stark broadening to measure electron densities in a non-transferred Argon-Helium-Hydrogen arc jet. Their temperature profile was determined from absolute intensity measurements of an Argon emission line and the neighboring continuum. The densities inferred from Stark broadening, both in the arc mantle as well as downstream of the nozzle exit, were found to be several times larger than the corresponding LTE electron densities based on the measured temperature profile. The Stark broadened profiles were analyzed in the same manner as discussed above without performing a detailed radiation transfer calculation for the broadened line in the presence of plasma gradients. Chen, et al., suggest that the excess $n_e$ is due to a population of high energy electrons (a few eV) diffusing out from the hot core of the arc near the nozzle exit orifice. Departures from equilibrium have also been observed in a transferred free burning, atmospheric pressure, arc plasma. Cram, et al., [4.14] computed excited level populations using the LTE assumption with a model temperature profile against the populations from a CRE model for a pure Argon arc. The results were compared with spectroscopic observations of the 4p excited state. They found that the observed density of the 4p level in the mantle of the arc is twelve orders of magnitude larger than the LTE predictions, and even two orders of magnitude above their CRE results. At the same time, Rayleigh scattering measurements of the total number density of Argon atoms agreed with the LTE estimates. They interpreted their result of excess excited state argon as due to the absorption in the arc periphery of resonant UV radiation from the arc core.

## 4.3 OES Analysis of the Transferred Arc

Spectroscopic analysis has also been performed on the NRL torch in the transferred mode. The conditions are: 300 Volts, 330 Amps, 90 slpm of $N_2$, and 4.1 slpm of $H_2$. The spectroscopic set-up is the same as described above. The additional parameter for transferred arcs is the height above the bottom of the crucible, which is the cathode in the reverse polarity configuration of the Retech torch at NRL. Spectra were taken at various heights ranging from 10 to 26 cm. We present the analysis for the 15 cm torch height. The analysis follows the same procedure as described for the non-transferred arcs except a single temperature CRE model is used to calculate the excited state populations. According to the classical Elenbaas-Heller relation [4.15], the temperature profile of a transferred arc is parabolic outside of a central core with high electrical conductivity. Five such temperature profiles are considered for discussion and displayed in Figure 4.11(a). For each temperature profile the population distributions are calculated and the predicted $H_\alpha/H_\beta$ ratio is determined by performing the radiation transport as indicated in Figure 4.6(b). The resulting ratios are presented in Figure 4.11(b) for each temperature profile. Temperature profile A with a central value of 12,000K is too cold, as the predicted $H_\alpha/H_\beta$ ratios lie entirely above the observed values throughout the arc. Likewise profile C with a central of 18,000K is too hot since the predicted ratios lie below the observations. The central temperature which leads to a match with the data from the arc core is 15,000K, as indicated by profile B. This central temperature for the transferred arc is nearly three times higher than found for the non-transferred arc. However, in the mantle of

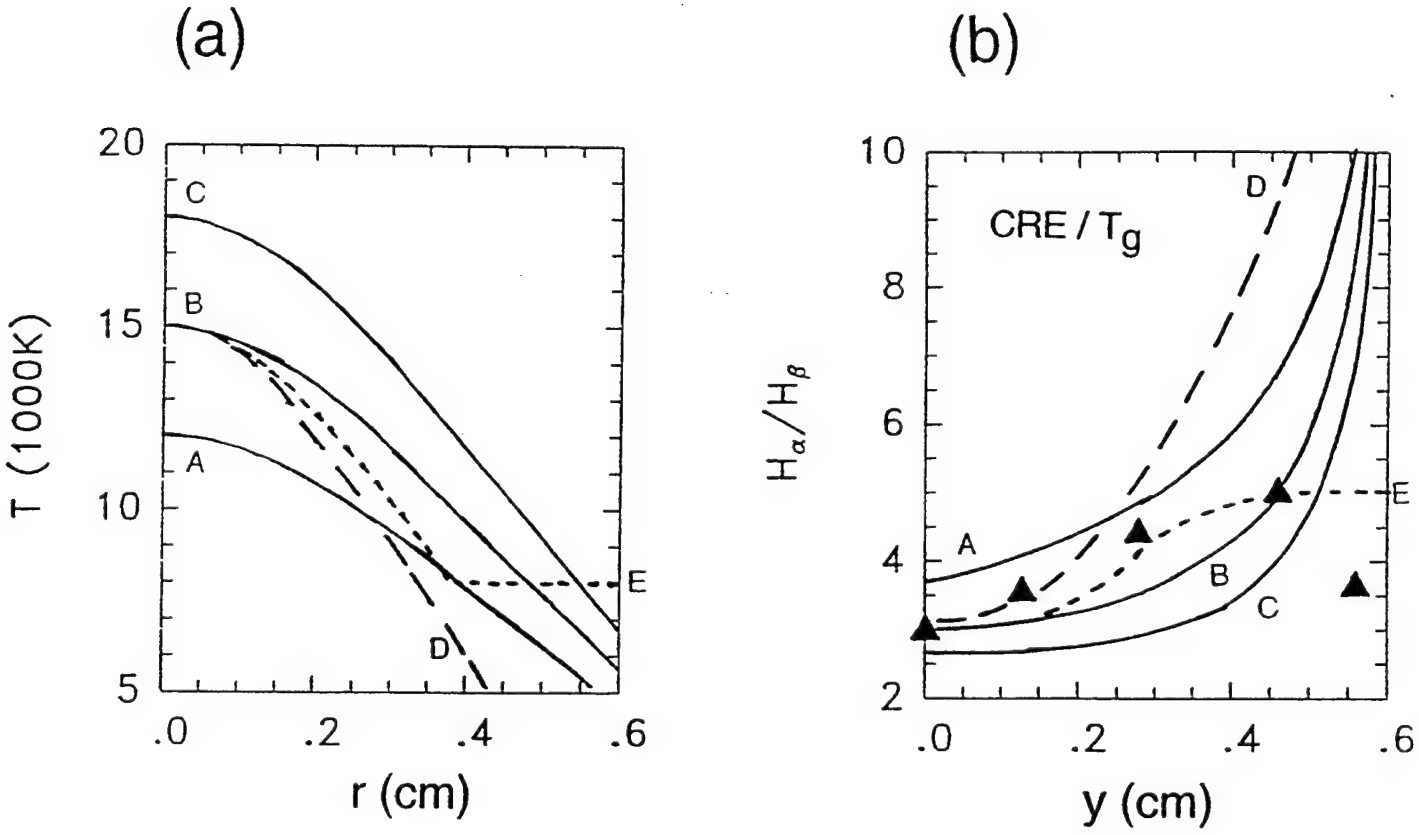


**Figure 4.11 (a) Various temperature profiles assumed for the plasma arc in transferred mode. (b) The predicted $H_\alpha/H_\beta$ ratios from the CRE model for each of the assumed temperature profiles. Data are denoted by the solid triangles. Profile E is the best fit giving an arc core temperature of 15,000K. Torch conditions are 300 Volts and 330 Amps, 90 slpm of $N_2$, 4.1 slpm of $H_2$, and a torch height of 15 cm above the bottom of the crucible.**

the arc all three profiles predict $H_\alpha/H_\beta$ ratios which far exceed the outermost data value at the 0.55 cm $y$-position. Profile D shows the effect of a rapid falloff in the temperature which is again a poor fit to the data in the mantle. In order to approximately match the data it is necessary to assume a temperature plateau in the arc periphery, as shown by profile E. As with the non-transferred arcs, the spectroscopic interpretation of the data suggests that non-equilibrium processes elevate the excitation temperature in the mantle of the arc compared to the classical parabolic solution.

Figure 4.12 displays the calculated atomic synthetic spectrum over the UV-vis-IR range for the transferred arc plasma corresponding to the conditions in the previous paragraph. The $H_\alpha$ and $H_\beta$ emission lines are marked for orientation of the reader. Note the significant UV emission arising from the resonance lines of atomic nitrogen and the Lyman series of hydrogen. Integrating over the wavelength we find that the total radiated power per centimeter of arc length is ~3.5 kW/cm. Given that the torch height is 15 cm, the total radiated power comprises 53% of the input power, 99 kW. For comparison the Planck emission from a 15,000K blackbody of 1 cm diameter is shown as the dotted line. Note that the emission lines around 1000 nm are very optically thick, as they touch the blackbody limit, however, the energetic part of the spectrum is far below a blackbody emitter. The effective gray body emissivity for this plasma is estimated to $3.8 \times 10^{-4}$ from the ratio of the calculated radiated power to that from the blackbody at the central temperature.

The transferred arc mode is typically used in Retech PACT systems for vitrification of solid wastes. Similar experiments were performed with the NRL torch system using a nominal waste slag consisting of iron, sand, soda glass, aluminum, titanium-oxide, aluminum silicate di-hydride, calcium carbonate, and calcium phosphate. An analysis of some of these runs revealed an interesting change in the electrical characteristics of the arc in conjunction with material entrainment from the slag vapor. Figure 4.13 presents data for the arc voltage as a function of height for two experiments, one using air as the working gas, the other nitrogen. For each experiment the voltage data was taken early in the run at about 15 minutes, and once more at about two hours. The electric field $\mathcal{E}$ in the arc is $d\mathcal{V}/dz$, where $\mathcal{V}$ is the measured voltage and $z$ is the distance along the arc. Note that for both working gases $\mathcal{E}$ decreases in time for long arcs as the slag is vitrified, but remains constant for the shorter arcs. The explanation for this is found in the spectroscopic survey data. Figure 4.14(a) shows the spectra for a long arc (24.8 cm) observed through the centerline 3 cm below the torch nozzle and taken two hours into the slag vitrification. The strong sodium D-lines at 589.0 and 589.6 nm are shown as a single feature due to the low resolution. The sodium arises from the soda glass in the slag and is easily transformed into the vapor phase (boiling point of 1156K at one atmosphere). The presence of the neutral sodium emission in the spectra of the long arc indicates that sodium is mixing into the arc. Since sodium has a low ionization potential (5.1 eV), it will readily ionize in the arc and enhance the free electron density in the plasma. This in turn raises the electrical conductivity of the plasma, $\sigma$, which is proportional to $n_e$. According to Ohm's law, the current density in the arc $\mathcal{J}$ is related to the electric field through $\mathcal{J} = \sigma\mathcal{E}$. For a constant arc current and diameter, an increase in $\sigma$ during vitrification due to sodium entrainment, leads to a decrease in the electric field as shown by the voltage vs height data in Figure 4.13. However, for short arcs, say less than 15 cm, sodium does not appear to be entrained into the arc according to the spectra in Figure 4.14(b). This implies that the electrical conductivity does not increase with time and the electric field remains constant, as indicated by the constancy of $\mathcal{V}$ vs $z$ in Figure 4.13 for $z \leq 15$ cm.

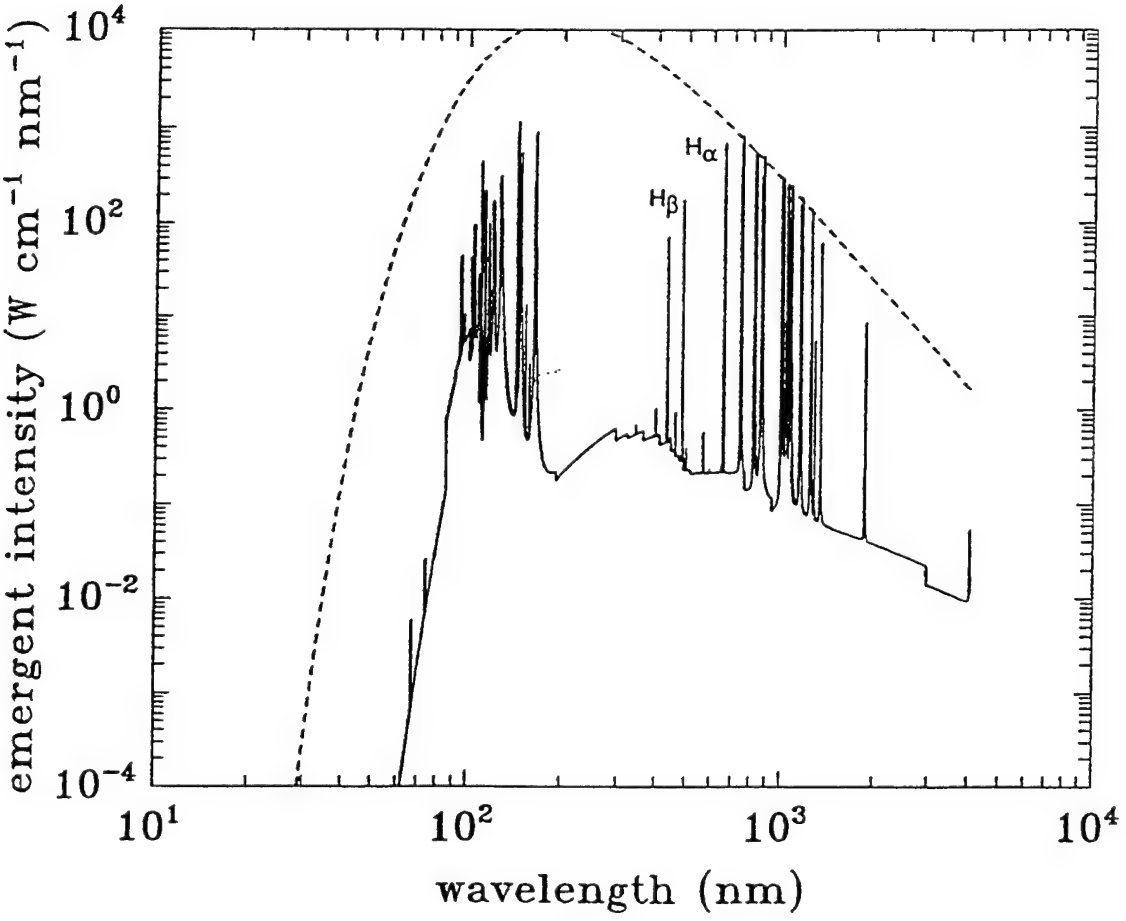


**Figure 4.12 Synthetic emergent spectrum over the entire UV-vis-IR range based on the CRE calculations for the conditions stated in the text. The Planck spectrum at the central temperature of 15,000K is shown as a dotted line. The effective gray body emissivity is** $3.8 \times 10^{-4}$.

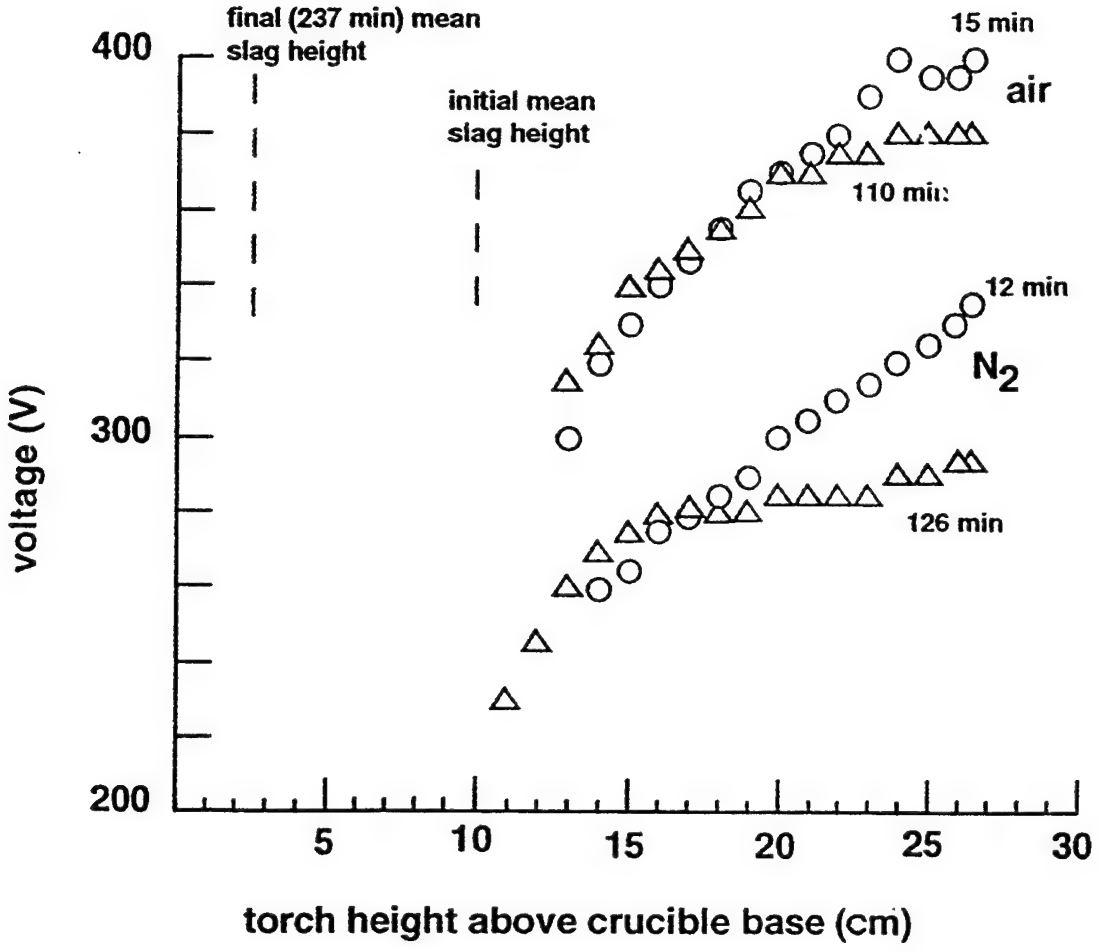


Figure 4.13 Voltage data for the transferred arc mode as a function of height for two experiments with different working gases. For each experiment the data was taken both early and late in the run. A change in the electrical characteristics of the arc (volts/cm) during the run is clearly seen.

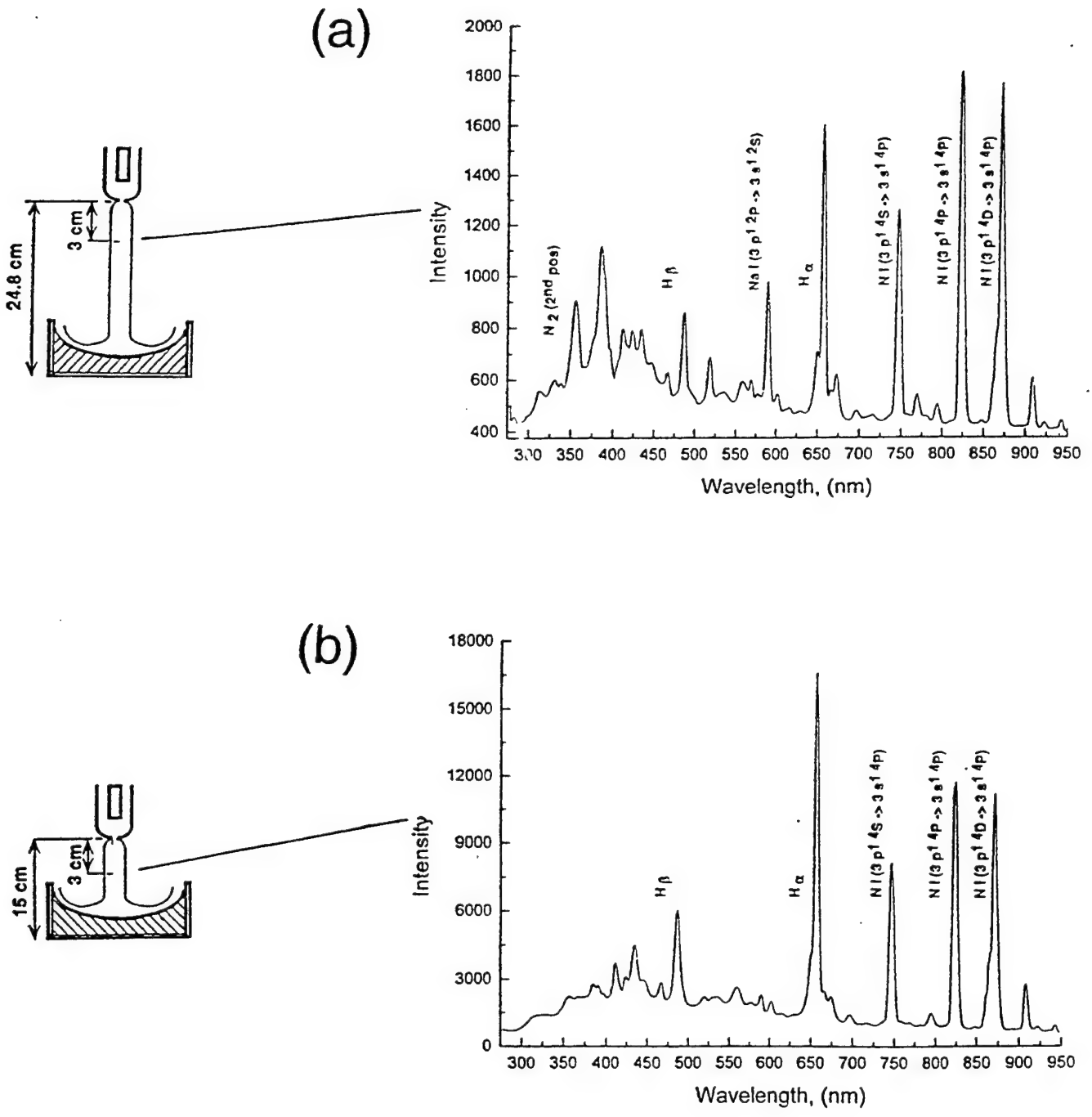


**Figure 4.14 (a) Spectra obtained through the center of a long arc after two hours of nominal slag vitrification. (b) Similar spectra except for a short arc. The strong Na D-line emission is present in the long arc but not in the short one, indicating vapor entrainment in the former.**

The entrainment of sodium into the core of a long arc indicates the presence of a toroidal convection cell which surrounds the plasma jet from the torch. This flow pattern is generated by the combination of downward flow from the torch, confinement by the chamber walls, and an exhaust port near the top of the chamber. Cao, et al. [4.4] present two dimensional numerical simulations of the flow streamlines for such a convection cell. In their geometry the exit nozzle of the torch is at the top of the chamber and the lower surface, which the plasma jet impacts, has the same diameter as the chamber. The convection cell is predicted to extend from the chamber top down to the lower surface for both short and long arcs. Although their calculations did not include evaporation, it is clear that if volatile material from the slag is caught up in the cell and the cell is next to the plasma jet, then the material can diffuse into the arc core. The geometry of the NRL chamber is slightly different: the exit nozzle of the torch is well below the chamber top and a crucible about half the diameter of the chamber contains the slag. It is conjectured that in the NRL chamber the stagnation pressure from the arc flow against the crucible pushes the bottom of the convection cell upward. For short arcs ($< 15$ cm), the bottom of the cell lies above the torch nozzle and the evaporated gases are isolated from the plasma jet. For long arcs, part of the cell is in contact with the plasma jet and entrainment ensues. This conjecture on the convection cell size could be tested by spectroscopic analysis of the arc for significant.y different flow rates.

## 4.4 Summary

Optical spectroscopy was performed on both the non-transferred and transferred arc configurations of the NRL plasma torch. The data, in the form of emission line ratios, was analyzed using two different plasma models: LTE and CRE. The latter accounts for such processes as photo-excitation/ionization, and radiative decay/recombination. It was found that the core of the arc several centimeters below the torch nozzle exit is close to LTE, with a central temperature of 6,200K for the non-transferred and ~15,000K for transferred arc. For both arcs, however, the data indicate that the periphery of the arc is far from thermal and excitation equilibrium. The CRE model with the photo-processes was able to match the data if a high temperature plateau was assumed for the periphery.

Initial measurements of the Stark broadened $H_\beta$ line in the non-transferred arc imply an electron density ~800 times larger than the best fit model predicts. This discrepancy needs further research, but possibly suggests that electrons from the hotter plasma formed near the cathode inside the torch body are diffusing out into the plasma jet.

For the power balance in the transferred arcs, the models predict that ~50% of the power input appears as plasma radiation. This is consistent with calorimetry measurements of the chamber cooling water which imply that 45% of the power input to the torch is absorbed by the chamber walls without slag and 65% with slag. The increase in the latter case results from re-emission by the hot slag surface. The effective gray body emissivity for the transferred nitrogen arc with a 5% hydrogen admixture is $\sim 3.8 \times 10^{-4}$. The electrical characteristics of the transferred arc were found to change in time as a slag load was processed. Based on spectroscopic studies, easily volatized material with low ionization potentials become entrained in the arc and raise the electrical conductivity of the plasma. It is possible that this phenomena, which is readily detected by a drop in the voltage of long arcs, could be used as a diagnostic of the processed state of the slag.

Finally, it is noted that a plasma arc torch is more than just a heat source in waste treatment, which after all could be accomplished with standard combustion. The presence of free electrons and non-equilibrium conditions in the arc region alter the chemistry in the chamber and can enhance the breakdown of ambient or vaporized gases. The subsequent chemical products in the exhaust line is sensitive to the arc temperature and electron density. This suggests the potential for control of the exhaust composition beyond conventional combustion and a consequent minimization of the design requirements on a secondary combustion chamber.

## 4.5 References


4.1 S. Paik, G. Hawkes and H.D. Nguyen, "Effect of Working Gases on Thermal Plasma Waste Treatment", *Plasma Chemistry and Plasma Processing*, Vol.**15**, pp.677-692, 1995.

4.2 S. Paik and H.D. Nguyen, "Numerical Modeling of Multiphase Plasma/Soil Flow and Heat Transfer in an Electric Arc Furnace", *International Journal of Heat and Mass Transfer*, Vol.**38**, pp.1161-1171, 1995.

4.3 J.J. Gonzalez, A. Gleizes, S. Vacquie and P. Brunelot, "Modeling of the Cathode Jet of a High-Power Transferred Arc", *Plasma Chemistry and Plasma Processing*, Vol.**13**, pp.237-271, 1993.

4.4 M. Cao, P. Prouix, M.I. Boulos and J. Mostaghimi, "Mathematical Modeling of High-Power Transferred Arcs", *Journal of Applied Physics*, Vol.**76**, pp.7757-7767, 1994.

4.5 A. Bokhari and M. Boulos, "Energy Balance for a DC Plasma Torch", *Canadian Journal of Chemical Engineering*, Vol.**58**, pp.171-176, 1980.

4.6 P.J. Parisi and W.H. Gauvin, "Heat Transfer from a Transferred-Arc Plasma to a Cylindrical Enclosure", *Plasma Chemistry and Plasma Processing*, Vol.**11**, pp.57-79, 1991.

4.7 H. Maecker, "Theory of Thermal Plasma and Application to Observed Phenomena", in *Discharge and Plasma Physics*, pp.245-265, ed. S.C. Haydon, (Univ. of New England:Armidale), 1964.

4.8 H. Maecker, "Arc Measurements and Results", in *Discharge and Plasma Physics*, pp.266-288, ed. S.C. Haydon, (Univ. of New England:Armidale), 1964.

4.9 W.L.T. Chen, J. Heberlein and E. Pfender, "Diagnostics of a Thermal Plasma Jet by Optical Emission Spectroscopy and Enthalpy Probe Measurements", *Plasma Chemistry and Plasma Processing*, Vol.**14**, pp.317-332, 1994.

4.10 D. Duston, R.W. Clark, J. Davis and J.P. Apruzese, "Radiation Energetics of a Laser-Produced Plasma", *Physical Review, A*, Vol.**27**, pp.1441-1460, 1983.

4.11 J.P. Apruzese, J. Davis, D. Duston and R.W. Clark, "Influence of Lyman-series Fine-Structure Opacity on the K-Shell Spectrum and Level Populations of Low-to-Medium-Z Plasmas", *Physical Review, A*, Vol.**29**, pp.246-253, 1984.

4.12 R.W. Clark, J. Davis, J.P. Apruzese and J.L. Giuliani, "A Probabilistic Model for Continuum Transport in Dense, Optically Thick Plasma", *Journal of Quantitative Spectroscopy and Radiative Transfer*, Vol.**53**, pp.307-302, 1995.

4.13 H. R. Griem, *Plasma Spectroscopy*, (McGraw-Hill: New York), 1964.

4.14 L.E. Cram, L. Poladian and G. Roumeliotis, "Departures from Equilibrium in a Free-Burning Argon Arc", *Journal of Physics D: Applied Physics*, Vol.**21**, pp.418-425, 1988.

4.15 Y.P. Raizer, *Gas Discharge Physics*, (Springer-Verlag: Berlin), p.277 (1991).

## 5.0 Experimental Measurements and Modeling of Plasma Torch Chemistry

### 5.1 Introduction and Background

In designing and testing a plasma arc reactor system for destruction of shipboard solid waste, it is important to determine what gas should be used in the torch and for the reactions required to assure that the waste is converted to gaseous products to the maximum practical extent. Initial tests showed that purely thermal destruction in the absence of an oxidizer (i.e. pyrolysis with a nitrogen torch) would produce large amounts of soot, which would not be practical for a shipboard reactor. Experiments and thermodynamic models help clarify the desired chemistry and led to recommendations for torch gas and operating conditions. The experiments were conducted using the NRL plasma torch reactor; these early tests provided essential information about the waste destruction process that was incorporated into the PAWDS conceptual design. Thermodynamic models of plasma arc torches and induced waste destruction chemistry helped to define the effects expected of different candidate torch gases and to predict the characteristics of the products. This report describes the early destruction experiments and the thermodynamic modeling carried out in 1995 and 1996.

### 5.2 Experimental Studies

Initial pyrolysis studies were performed using the NRL plasma torch system described in Section 2.0,with a nitrogen transferred arc torch. Various materials were processed, with gas grab samples collected for analysis by gas chromatography/mass spectrometry (GC-MS) with the intent to observe the extent of destruction of the feed material.

#### 5.2.1 Procedure

Air samples were initially screened using a Varian 3400 gas chromatograph equipped with thermal conductivity and flame ionization detectors. Samples were injected onto a Porapak N packed column using a gas sampling valve with a 1 milliliter sampling loop. The column was ramped from 50 to 150 °C. A gas standard containing methane, ethane, ethylene and acetylene was used to quantitate the amount of these gases present in the sample. A benzene standard was used to estimate the benzene concentration in the sample in order to estimate the dilution ratio needed to employ GC/MS analysis.

The air samples were analyzed by gas chromatography/mass spectrometry on a Finnigan ITS-40 ion trap mass spectrometer system equipped with a Tekmar Aerotrap 6000 thermal desorption/cryogenic trapping and focussing unit. Air samples were passed onto the cryogenic trap at known flow rates (controlled by flow controllers) for specified periods of time (and thus a known volume). The cryogenic trap consisted of a bed of glass beads held at -150 °C. Once the trapping period passed, a section (cryofocussing region) of the GC column at its head was cooled to -150 °C and the glass bead trap was heated to 250 °C, transferring and trapping the organic compounds at the head of the column. The rest of the column was held at –10 °C during this time. After the cryotrap had been desorbed for the specified period, the cryofocussing region was heated to 250 °C in less than one minute and the compounds were desorbed onto the column. The column was held at -10 °C for 2 minutes, and the temperature of the column was

then increased at 8 °C/minute until it reached a temperature of 200 °C, where it was then held for the duration of the run. During this period, the ion trap mass spectrometer scanned from 35-350 amu at a scan rate of approximately 4 scans per second. Spectra were then averaged together and presented once every second. Data were stored for later analysis. The mass spectrometer was periodically tuned using a standard autocalibration procedure that employed perfluorotributylamine (PFTBA) as a calibrant.

5.2.2 Results

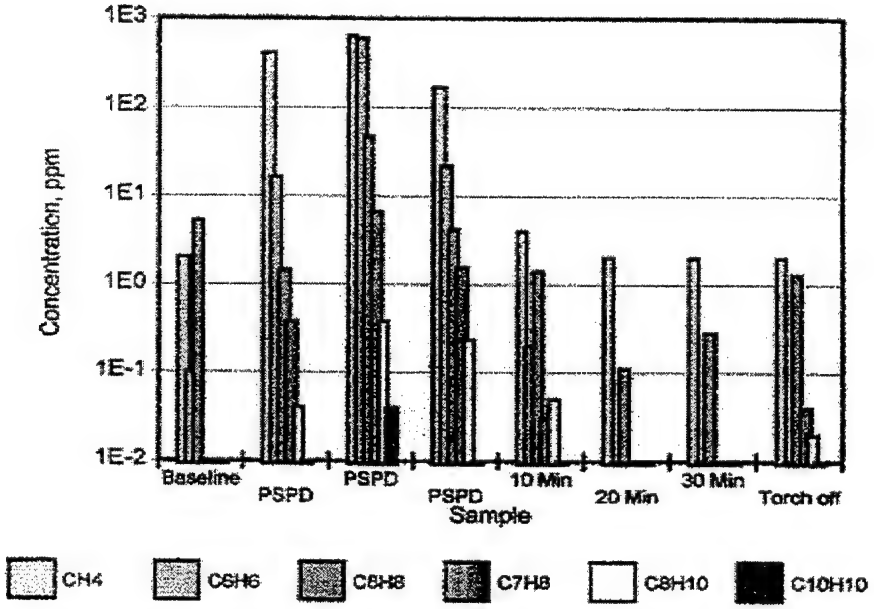


**Figure 5.1 Pyrolysis products of polystyrene petri dishes (PSPD) heated with a nitrogen transferred arc torch.**

An early experiment was pyrolysis of some sets of polystyrene petri dishes (PSPD), introduced in batches weighing approximately 64 grams. Samples were collected before the first set was fed, at various times after feeds, and then for a period of time at the end of the run, including after the torch was extinguished. The results of the GC-MS analyses of these samples are shown in figure 5.1. The initial background material was probably residual gas from earlier experiments; the reactor is large and difficult to clean out but the low part per million background was acceptable. When polystyrene was fed in, destruction was very rapid as the material was dropped into the hot crucible. Almost immediately the inside of the reactor becomes black due to soot formation. The gases exiting the reactor cooled as they traveled through the exhaust line, and at the sampling point the temperature was typically about 100° C. Evidence of the destruction efficiency is the high concentration of methane observed, although there was also some benzene present, which was probably due to incomplete destruction of the styrene.

Another experiment examined the destruction of high-density polyethylene (HDPE) by a $N_2$ torch. The GC-MS results for these samples are shown in Figure 5.2. In this case, the major products observed by GC were methane, acetylene and ethylene, and with some ethane detected after sample feeding was terminated. For the samples collected right after feeds, the methane, acetylene and ethylene make up nearly all of the products. Some benzene is observed in Figure 5.2, even though there should be no ring structures in the polyethylene; it may have been left from earlier experiments and "hidden out" somewhere in the reactor, although it did increase in conjunction with the HDPE feeds. It is encouraging to note that the long carbon backbone of the polyethylene is mainly broken down into $C_1$ and $C_2$ species.

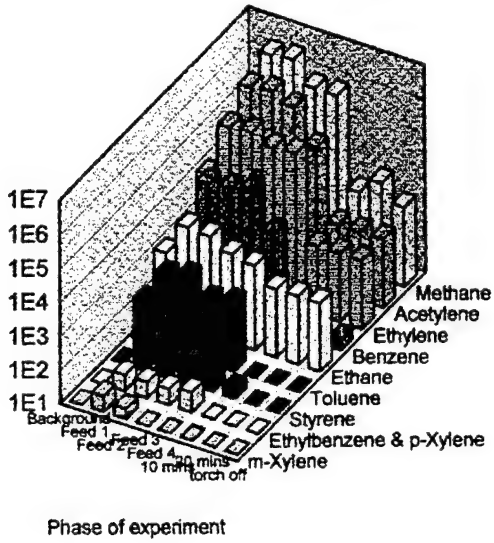


**Figure 5.2 Pyrolysis products from thermal destruction of high-density polyethylene heated with a nitrogen transferred arc torch. The bottom axis represents sample times: background before the first feed, four sets of HDPE feeds, residual gases at 10 and 30 minutes after the last feed, and then after the torch was extinguished. Concentrations are in ppb.**

Galley waste was collected from the USS Wasp, an amphibious troop transport ship, in August, 1995. The waste collected and subsequently processed consisted of paper plates, food scraps, cans, bottles and food wastes in the cans and bottles, and also included some water. An interesting item was a whole orange. When it was dropped in on the slag surface it appeared to just sit there and turn black, then back to orange as it heated up to incandescence. It lasted for several minutes before it collapsed; apparently the water in the pulp kept the internal temperature no higher than 100 °C until all the water had evaporated. Only then did the bulk of the orange pyrolyze, although it was probably ablating at the surface. On the other hand, glass bottles were melted and incorporated into the molten slag in a few seconds, and the cans also melted quickly.

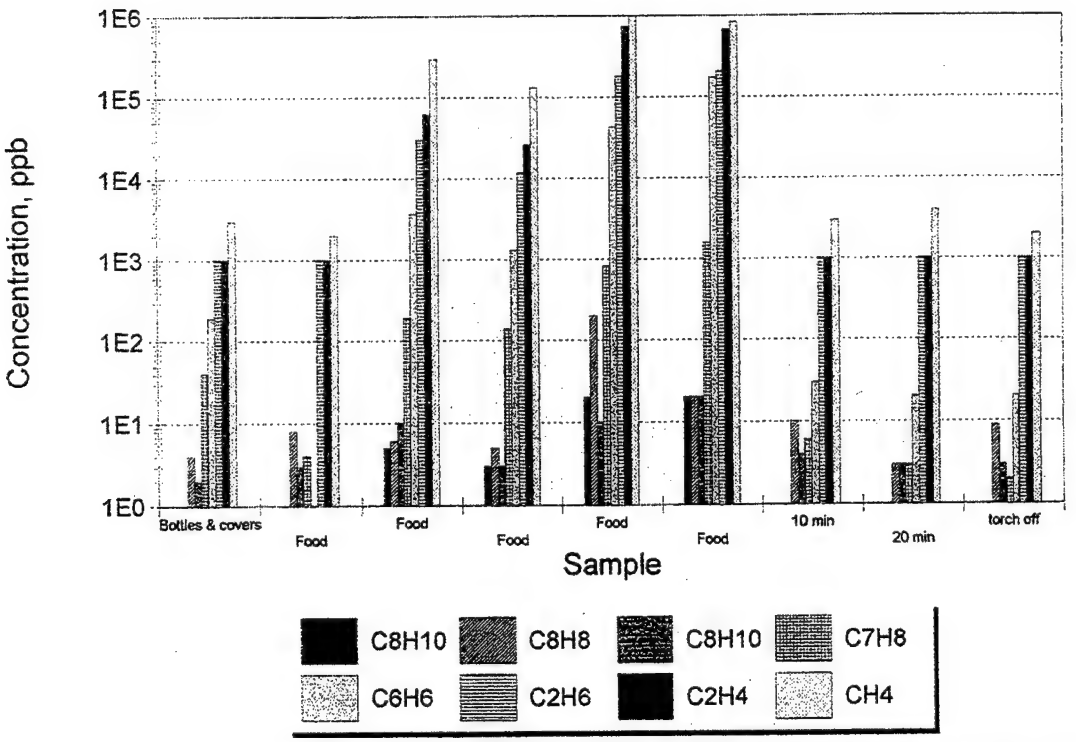


**Figure 5.3 Pyrolysis products from thermal destruction of USS Wasp galley waste with a nitrogen transferred arc torch. Samples at 10 and 20 minutes were after the last feed.**

The analytical results for a number of samples are shown in figure 5.3. Depending on the detailed composition of each feed, different amounts of gases were formed. It is encouraging that the gas products were mainly methane, ethylene and ethane, showing good destruction of the wastes, which in this case included a lot of paper and had water in some of the feeds. There should also have been CO, $CO_2$ and $H_2$ formed, but the GC did not detect these. Methane, ethane and ethylene make up the vast majority of the compounds detected. It is important to understand that the GC would have detected most complex volatile and semivolatile organic compounds if they were present at a significant concentration.

## 5.3 Thermodynamic Calculations for Characterization of Torch Gas

Land-based Plasma arc torches most frequently utilize Argon as the working gas. In the PAWDS configuration, alternative torch gases will probably be required other than Argon in the at-sea application of plasma energy. In the shipboard environment, possible torch gases were limited to those that are readily available, such as air and steam, or those that can be easily generated, such as nitrogen and oxygen. Six torch gases were considered in this brief torch gas study and included Argon, nitrogen, oxygen, air, enriched air, and steam. Torch gas characteristics were investigated and compared over the temperature range of 3000 to 6000 K. Theoretical predictions for the ideal thermal characteristics of these plasma torch gases were based on fundamental thermochemical analysis. All calculations in this effort were made using the STANJAN PC computer software[5.1]. The program obtains the Thermochemical State for a chemically reactive system consisting of one or more phases. The method of element potentials

is used to determine the Equilibrium State of minimum mixture Gibbs function, subject to an atom population constraint. All required thermodynamic data are based on JANAF Tables[5.2].

Two types of computer runs are possible with the STANJAN code. First a frozen composition run can set the moles of reactant state and hence the atom population. This execution will also calculate the sums of the individual species enthalpy (h), internal energy (u), specific volume (v), and entropy (s) of each reactant phase. Secondly a product run can be executed to determine the equilibrium composition of a mixture specified by choices of extensive property pairs. The extensive properties can be values obtained from reactant runs. STANJAN calculates total moles (N) and mixture molecular weight (MW) for both reactant and product cases.

The STANJAN computer software was utilized to predict both the reactant torch feed gas and the gaseous equilibrium product composition, mixture specific volume and mixture enthalpy for one atmospheric pressure torch gas conditions over the specified temperature range. Note that equilibrium predictions strongly depend on the species considered to be present. Constituents considered to possibly exist in the gaseous product state included the following: Ar, H, HO, $H_2$, $H_2O$, N, NO, $NO_2$, O, and/or $O_2$.

In the analysis 1 kg mole of torch gas @ STP $\rightarrow$ equilibrium dissociated gas products @ $T_2$
A reactant total enthalpy $H_{react}$ can be determined as

$H_{react}$ <kJ> = $h_{react}$ <kJ/kg react.> x $MW_{react}$<kg react./kg mole react.> x $N_{react}$<kg moles react.>

A product total enthalpy $H_{prod}$ can likewise be determined using mixture properties as

$H_{prod}$ <kJ> = $h_{prod}$ <kJ/kg prod mixt.> x $MW_{prod}$<kg prod mixt./kg mole mixt.> x $N_{prod}$<kg moles mixt.>

But since this $H_{prod}$ is based on 1 kg mole of reactant then one can also write $H_{prod}$ <kJ/kgmole react.> and

$H_{prod}$<kJ/kg react.> = $H_{prod}$ <kJ/kgmole react.>/ $MW_{react}$<kg react./kg mole react.>

Plasma torch power can now be expressed in terms of $H_{react}$ and $H_{prod}$ as

P<kW> = $m_{react}$<kg react./sec> x ($H_{react}$<kJ/kg react.> - $H_{prod}$<kJ/kg react.>)

Mass flow rate predictions for the six selected gases were estimated by specifying torch power and providing STANJAN predictions for torch gas equilibrium dissociated products as a function of temperature. Mass flow rates were obtained for torch powers that ranged from 50 to 500 kW and torch gas temperatures over the temperature range of 3000 to 6000 K. Figure 5.4 illustrates the results of these calculations for the case of a 150 kW torch power. Appendix A provides a more detailed summary of these calculations.

An inspection of Figure 5.4 reveals that in order to deliver the same torch power at higher operating torch gas temperatures, a lower gas mass flow rate is required. Furthermore, an inspection of Figure 5.4 reveals that at any given operating temperature and specific torch power, the highest mass flow rate required is with argon while the lowest is with steam. This result is not surprising since the enthalpy of the torch gases depends on the specific heats of the constituents and water vapor has the highest specific heat at any given temperature. Furthermore, in terms of delivered enthalpy per unit mass of gas flowing, equilibrium products of dissociated oxygen is seen to deliver more enthalpy per mass than equilibrium products of pure dissociated nitrogen at high temperatures. The benefits of oxygen delivery are also seen in the air curve as compared to that of nitrogen. Enriched air (for the purposes of this analysis arbitrarily set at 50% oxygen and 50% nitrogen by volume) further shows a reduction in required gas flow rate over that of air.

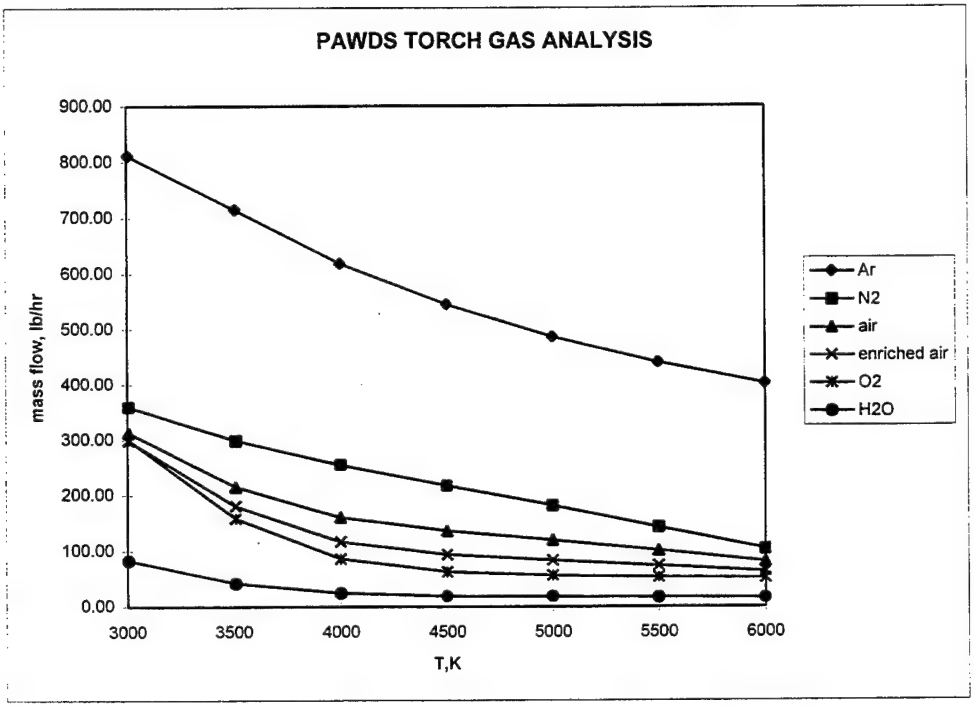


**Figure 5.4 Torch Gas Mass Flow Rate vs. Operating Temperature for 150kW Torch for Various Torch Gases**

Actual torch conditions are such that gas conditions are not at chemical equilibrium. In addition, the analysis did not consider or include the free electron gas contributions present in portions of the plume of an actual plasma torch flow. These real gas conditions in an actual torch flow at high temperatures can be neglected in first order considerations of torch flow analysis. These effects will have a great impact on torch-induced chemistry. These preliminary results indicate that in order to deliver the same enthalpy fluxes, the amount of working gas needed for the non-argon torches are of the same order of magnitude and in most instances significantly less. However, important torch issues not considered include chemical reaction kinetics, electrode interactions with torch gases, etc. The potential kinetic benefits of oxygen

enrichment of an air torch or the presence of water in a waste stream that would provide active radical species such as O atoms as well as hydrogen H and hydroxyl OH radical enrichment are worth further investigation. These torch calculations provide a basis of evidence and support further study of the interaction of torch gas chemistry and pyrolytic destruction of NSW.

## 5.4 Thermodynamic Calculations for Torch-Induced NSW Chemistry

In the shipboard environment, possible torch gases are limited to those that are readily available, such as air and steam, or those that can be easily generated, such as nitrogen and oxygen. Thermodynamic models were evaluated, using the NASA code CET93 [5.3], based on the waste composition of Table 1.4, to aid in further identification of the most desirable torch gas. An initial PAWDS unit "straw man" design considered the possibility of pyrolysis of the waste, followed by combustion of the gaseous pyrolysis products in a secondary combustion chamber (SCC). However, problems with this approach include soot formation and poor energy efficiency since the effect is to require maximum torch energy for pyrolysis, and then maximum heat removal in the SCC and for cooling of the stack gases to provide an acceptable infrared signature. The CET93 models predict the gases formed at various temperatures for each of the possible torch gases, as well as the gross slag composition. Experience has shown that at high enough temperatures the predictions are quite accurate for major components of the gas products. Conceptually, as the products cool, the reaction rates decrease and at some temperature the kinetics become slow compared to the cooling rate and that composition gets "frozen in" for the gas emissions. The main criteria for evaluating the models were the following:

- No soot formation at a wall with an assumed temperature of 1000 K, to assure complete destruction of the organic fraction of the waste.
- Minimization of the volume of gases produced, because of the severe size constraint.

Because of considerations about the lifetime and service of refractory materials that may be used to line the reaction chamber, 1800 K was selected as the temperature for comparing gas volumes. However, soot formation is only predicted at temperatures of 1000 K and lower, and this temperature may be representative of wall temperature in a reactor, so 1000 K was used for soot and slag predictions. Figure 5.5 shows the predictions of soot formation for the various torch gas candidates, and figure 5.6 shows the predicted volumes of gas products.

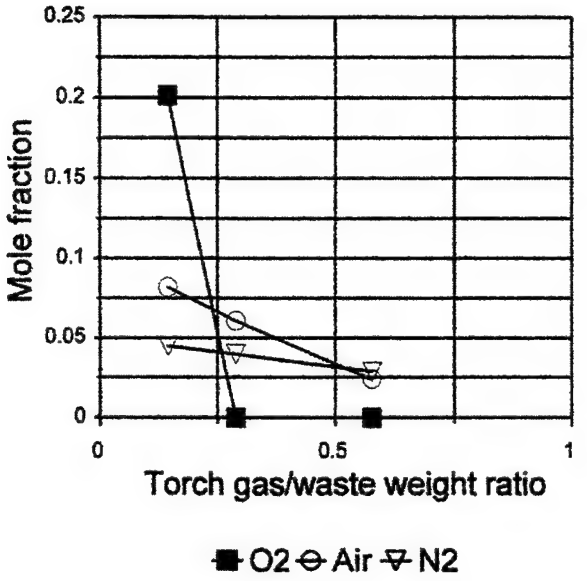


**Figure 5.5 Soot formation at a 1000 K wall occurs at a minimum torch gas to waste weight ratio for oxygen, followed by air and nitrogen.**

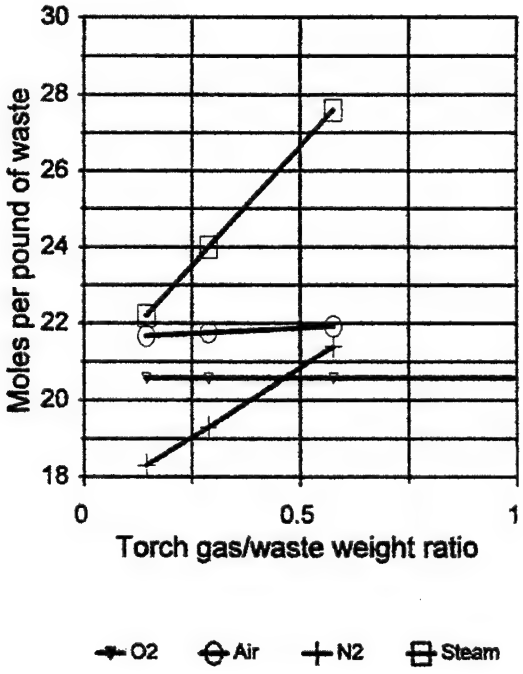


**Figure 5.6 Gaseous products produced by destruction of NSW with plasma torch gases.**

The results of the models indicate that oxygen would be the most attractive torch gas from the point of view of the destruction chemistry. $O_2$ is reactive and can convert C from the waste

into CO to avoid soot formation. Air and steam can also provide oxygen to the system, but both give a larger amount of gaseous products. Air is effective because it contains $O_2$, but the volume of product gases is larger because of the large $N_2$ fraction. No soot formation was predicted with any of the steam models, due to reaction of steam with carbon by the classic town gas mechanism to form CO and $H_2$. However, the $H_2$ released causes the gas volume to be greater than that for an oxygen torch, and will require additional combustion air in the secondary chamber. For the nitrogen torch, soot formed at all gas/waste ratios considered. Extrapolation of the soot mole fraction to zero gives an estimate of 1.36 lbs. of torch gas per pound of waste to give no soot at 1000 K, compared with $O_2$ which eliminates soot at <0.3 lbs of gas/lb of waste. Extrapolation of the gas production in figure 5.6 then predicts that the gas produced would be 27 moles, which would be significantly more than for the other candidate torch gases.

The result of the modeling effort for torch gas selection is that oxygen is the best choice for minimizing gas volume. Nitrogen is not reactive enough to prevent soot formation; air suffers from being 80% $N_2$, so the amount needed to prevent soot formation is larger than for $O_2$, and the inert $N_2$ fraction just represents a heat sink for torch energy. Steam looks like the second choice, but at the small steam to waste ratio, the hydrogen released when the organics extract oxygen from the water increases the gas volume. Oxygen gives the least amount of gas products at the minimum required to prevent soot formation, and has the additional attractive feature that the amount of gas product is essentially independent of the ratio of oxygen to waste, because any additional oxygen just converts CO to $CO_2$. This seems to be a significant advantage when the variable nature of trash is considered; the organic content can be expected to vary as material is fed into the reactor. Oxygen as torch gas should provide better accommodation to the variation without introducing as much variation in the gas stream to be handled downstream in the system. Compared to $N_2$, the oxidizing torch gases also have the attractive feature that combustion of some of the organic material releases energy in the primary reaction chamber, providing energy for pyrolysis of more waste while reducing the torch energy required.

It is possible to estimate NOx production under different torch conditions. From the model of waste processed with air, figure 5.7, significant amounts of NOx may be produced, if the system is allowed to equilibrate at high temperature. For the other possible torch gases, it is unlikely that both nitrogen and oxygen will be mixed at the high temperatures that give such copious NOx production. However, in the eductor configuration (described in Section 8.0), it is expected that NOx will "reburn" with the CO and $H_2$ products, and that the equilibrated temperature will be under 2000 K at the secondary combustor exit.

From this modeling exercise, we conclude that the torch gas most favored for shipboard destruction of Navy solid waste is oxygen. However, including oxygen generating capability in the PAWDS design could significantly impact the amount of equipment needed, but it would present the following benefits:

- conversion of organic matter to volatile compounds at the lowest gas volume,
- provides a gas with good heating value to the SCC if minimum $0_2$/waste ratio is used,
- is more predictable in the amount of gas product formed when waste composition varies,
- minimize NOx formation.

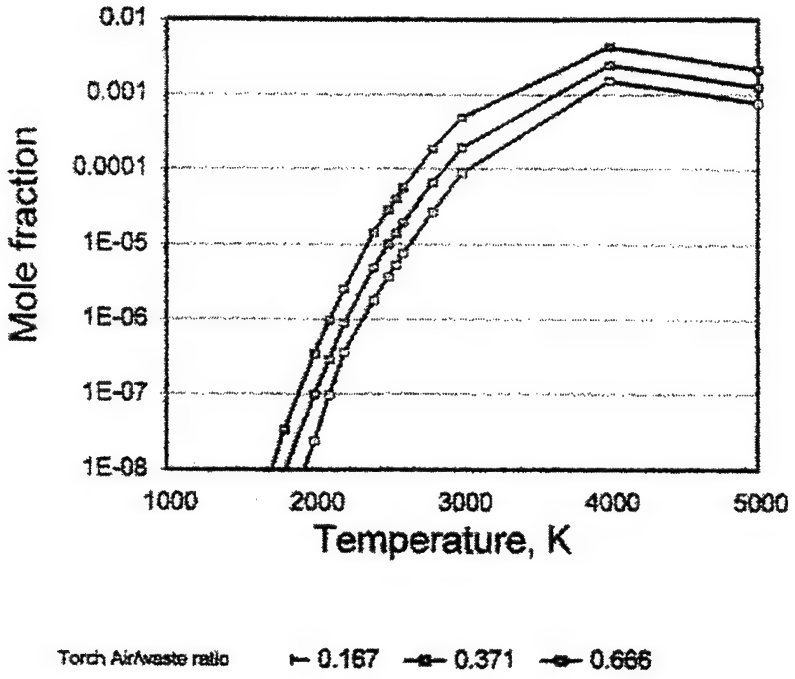


**Figure 5.7 Predicted NOx formation during plasma torch destruction of NSW using air as the working torch gas.**

Steam would be the next best candidate, and steam is easy to generate on board ships. However, steam works as an oxidizer by producing $H_2$, which adds to the volume of gas products, and will require a larger SCC and more combustion air in the SCC. Given the practical problems associated with oxygen and steam, air seems an acceptable working gas.

The models provide preliminary estimates of the gas composition and the slag composition. These are shown in figures 5.8 and 5.9. For the concentrations, major gases means those that are at least 1 ppm for one of the torch gas/waste ratios. However, only the few highest concentration gases need to be considered for such properties as the overall gas volume or its heating value. It is now evident why the volume of gases is constant as $O_2$ is varied: at low oxygen CO and $H_2$ have the highest mole fractions, but as $O_2$ is increased these decrease and $CO_2$ and $H_2O$ increase. It is also observed that the model predicts that at 1800 K there can be some carryover of volatile iron species expected.

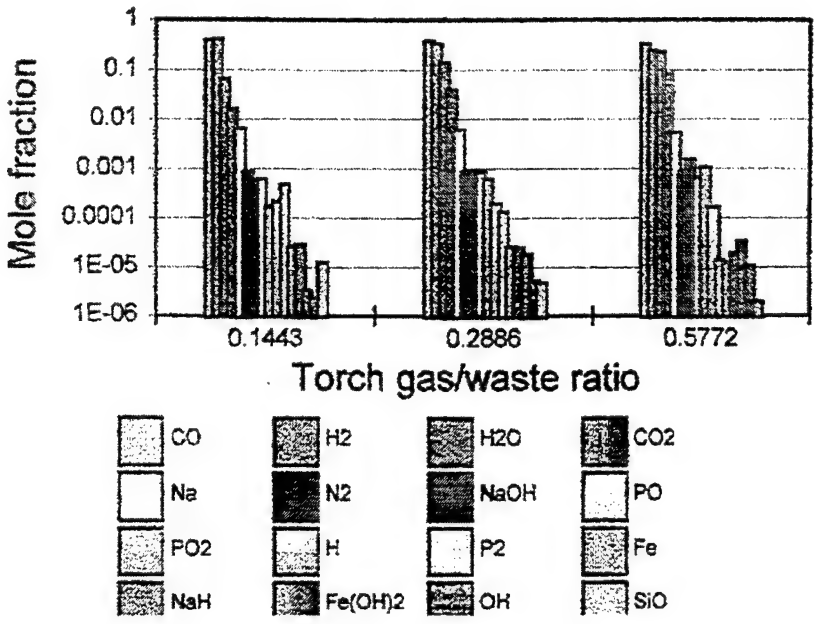


**Figure 5.8 Destruction of NSW with a plasma torch under oxidizing conditions gives these predicted gaseous products. This prediction is for oxygen as the torch gas, but air gives similar results except for a much greater amount of $N_2$ and more NOx.**

The predicted slag composition is shown in figure 5.9. For completeness, it should be noted that it was necessary to exclude mixed aluminum silicates from the models to get convergence, so the species shown may interact. However, the main purpose of this

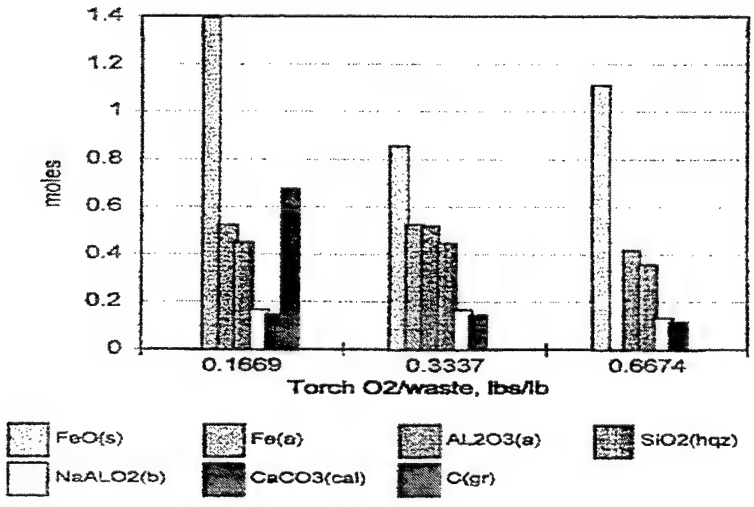


**Figure 5.9 Predicted slag products from destruction of NSW with a plasma arc torch with oxygen as the working gas. Use of air would give similar results.**

modeling exercise was to assess the gases; the slag is mainly shown to predict the completeness of capture of the inorganics. The conditions shown are all oxygen poor (which is required in the eductor design of Section 8.0 to minimize heat load). At the lowest torch gas to waste ratio, graphite soot is still predicted, and the iron is metallic. It is likely that operating under such conditions would produce a two-phase slag with a dense, low viscosity metal phase underneath a viscous but less dense glassy molten glass layer that would lead to problems of slag behavior as the ship pitches and rolls. A higher degree of oxidation would be preferred to get a single-phase slag.

## 5.5 Discussion

Some qualitative observations based on this work important to the design of the ATD PAWDS unit, and ultimately for the Navy shipboard waste management program.

- These early experiments were all conducted using a transferred arc with nitrogen as the working gas and have demonstrated that it is rather easy to extinguish the arc when high organic-content feed is introduced. It seems very likely that a non-transferred arc (NTA) may be more robust and better able to withstand the blast of gases that results when organic feed is put in the reactor, and it may be that NTA is better able to assure destruction reactions in the gas phase.
- Thermochemical characteristics for alternative torch gases to Argon were analytically compared over a wide range of operating conditions including nitrogen, oxygen, air, enriched air and steam. This work included both preliminary torch characteristics as well as torch induced NSW destruction chemistry studies.
- A nitrogen torch was shown both experimentally and analytically to not be viable for processing of organic wastes, because the carbon needs something to react with to generate volatile species. Air would work, but will generate high levels of NOx under torch conditions, and it also gives a higher off gas volume because of the $N_2$ component.
- The modeling work suggests that $O_2$ and steam are better candidates with oxygen preferred for minimum gas evolution. However, the need for oxygen generating equipment must be weighed against the reduced gas production.
- Air enrichment offers some attractive benefits that merit some further investigations.

The materials challenges associated with this project are daunting. The SiC[1] crucibles that are the standard equipment provided by Retech have shown a strong tendency to crack and fall apart due to thermal cycling; they crack on the first use and continue to crack with each cycle. The use of a graphite lining reduces this problem, but processing of wet materials that generate steam has destroyed the graphite when it was tried. Graphite will not be useful if the torch gas is oxidizing.

[1] The crucibles are "Buffalo Patch 41 1 ", 67% SiC, 21.2% $Si0_2$, 8.6% $A1_20_3$, 1.6% $Fe_2O_3$, other 1.6%. They have steel reinforcement; differential expansion causes the cracking.

These experiments and models showed the need to improve our analytical capabilities through the addition of a residual gas analyzer and some continuous emission monitors. The results were key information that led the PAWDS design effort away from the conventional mode of processing material in a plasma torch reactor by forming a pool of molten slag and dumping waste onto the slag for destruction and reaction chemistry to occur.

## 5.6 References


5.1 Stanjan Chemical Equilibrium Solver, V. 3.89, IBM-PC ©, Wm. C. Reynolds, Stanford University, 1987.

5.1 JANAF Thermochemical Tables, 2nd Edition, NSRDS-NBS 37, 1971.

5.3 CET93/PC is available from Cosmic, The University of Georgia, 382 East Broad St., Athens, GA 30602-4272. It calculates the thermodynamic equilibrium state of a chemical system by free energy minimization, based on a library of thermodynamic properties.

## 6.0 Slag Formation from Navy Solid Waste

### 6.1 Introduction

One option for shipboard waste processing is to oxidize the inorganic material to form a vitreous slag which will not leach metals and therefore will pass the EPA toxicity characteristic leach procedure (TCLP) test. However, the constraints imposed on the shipboard system raise some questions about the ability to fully oxidize the metals. Oxidizing is most attractive if the slag can be rapidly cooled by pouring it into water, causing it to shatter. The resulting slurry could be discharged overboard, eliminating any need to store it on board the ship. If, however, such discharge would still violate the MARPOL prohibition on discharge of solid waste, then oxidation only increases the weight and volume of the waste that must be stored. For shipboard waste processing, there is a need to minimize the processing time, but there is a question about the efficiency of oxygen transport to react with metal once a metal oxide layer forms on the surface of the melted material. Finally, an issue that arose in testing is that melting and oxidizing iron and aluminum together creates the possibility of a thermite reaction and its effect on the crucible containing the materials. A slag oxidation study was undertaken to address these issues, using the NRL plasma arc system.

### 6.2 Solid waste stream

Navy shipboard waste was described in Table 1.3, and amounts to about 1.4 kg per person per day, which is quite similar to generation rates of conventional municipal solid waste in quantity and composition. About 0.25 kg consists of iron and aluminum cans and bottles, with a lesser amount of non-pulpable food waste such as bones, and the inorganic filler from paper. These form the basis of the slag handling aspect of shipboard waste processing

The initial concept for a shipboard plasma reactor that was considered was based on conventional plasma reactor designs such as that described in Section 1.4. In such a reactor a substantial inventory of molten slag is maintained, which serves as a thermal reservoir to distribute the heat from the torch. Material added to the reactor typically sits on the slag surface or sinks into the hot slag, depending on the relative densities. Heat from the slag then pyrolyzes organic material in the feed, and melts the noncombustible material. If sufficient oxygen is available, the organic vapors will burn and the metals will be oxidized. It was thought that such an approach would permit treatment of shipboard waste with minimal pretreatment. The early experiments using the NRL system as well as a demonstration burn of simulated NSW conducted using the plasma arc system located at MSE, Inc. in Butte, MT identified some problems with this approach for shipboard applications.

- The effective processing temperature was only that of the melt, which lost the major advantage of the high temperature of the plasma torch. Organic matter fed into the reactor could persist for minutes, especially if wet. For example, an orange and a jar of honey each lasted several minutes sitting on hot slag. The destruction process seemed to be heat transfer limited under such conditions, and heat conduction into the material was balanced by heat loss from steam formation, until the water evaporated. Only then did the interior temperature of the material rise above the boiling point of water.

- When aluminum was added to hot iron oxide, a thermite reaction could occur. If it does, the reaction is extremely exothermic. The thermal shock can cause cracking and erosion of crucible materials.

Several conceptual design studies were performed resulting in an additional understanding of the slag problem in the shipboard environment. A major concern was the effect of ship motion on the molten slag. A PAWDS is required to be operational with up to 15° of pitch and roll. This means that it will be necessary to process waste in deteriorating conditions until the limit is reached. It will then be necessary to shut down to maintain reactor integrity and personnel safety while even worse sea conditions persist. As a result of these considerations, an alternative concept was developed which will be demonstrated under the ATD Program. It permits rapid startup and shutdown, and provides rapid cooling of slag to a safe temperature.

6.3 Slag formation studies

Small-scale laboratory slag modeling experiments were conducted at NSWC-CD facilities to determine the melting behavior of nominal composition slags as well as slags resulting from various waste stream excursions such as "No Steel", "No Glass", "No Paper", or "No Aluminum" [6.1,6.2]. These excursions were selected because of the inevitable variations in the composition of the waste stream.

The melting experiments were performed using shredded (3x3 mm squares) steel and aluminum cans, crushed bottle glass, calcium carbonate and/or kaolin to simulate minerals in the paper, and calcium carbonate and phosphoric acid to simulate the mineral part of bones in food. The 30 to 40g batches contained in dense 100 ml 99.8% alumina crucibles were processed in oxidizing atmosphere (air) furnace at 1400-1500°C with different heating rates (from 2 to10°C/min) and holding times (up to 2 hours).

Figure 6.1 shows photographs of slag (in sectioned alumina crucibles) resulting from heat treatment of the wastes at 1400°C for 2 hours with 3°C/Min heating rate. The figure indicates that "Nominal", "No Aluminum", and "No Glass" excursions formed molten slag. Compared to that, slag resulting from the "No Paper" and "No Steel" excursions were not fully molten. The melting behavior of the slag was found to be well correlated with the $Fe_2O_3$ /CaO weight ratio in the various slag compositions (Table 6.1). All slag that melted during the experiments had similar ratio values in the range 3.4 to 3.9. Significant deviations from this value in the "No Paper", and "No Steel" cases resulted only in partial melting.

**Table 6.1 Calculated chemical compositions of oxidized slags formed from NSW chemistry variations.**

| Chemical Compounds | Oxide Content in Various Slags (weight %) | | | | |
|---|---|---|---|---|---|
| | Nominal | Excursions in Nominal Slag | | | |
| | | No Paper | No Steel | No Al | No Glass |
| $Fe_2O_3$ | 46.52 | 50.34 | 0 | 62.80 | 54.81 |
| $Al_2O_3$ | 26.13 | 29.39 | 48.71 | 0.28 | 30.54 |
| $SiO_2$ | 11.15 | 12.54 | 20.77 | 15.05 | 0 |
| CaO | 13.51 | 2.70 | 25.18 | 18.24 | 13.98 |
| $P_2O_5$ | 0.57 | 0.64 | 1.06 | 0.76 | 0.67 |
| $Na_2O$ | 2.11 | 2.38 | 3.94 | 2.86 | 0 |
| $Fe_2O_3$ / CaO | 3.4 | 19.4 | 0 | 3.4 | 3.9 |

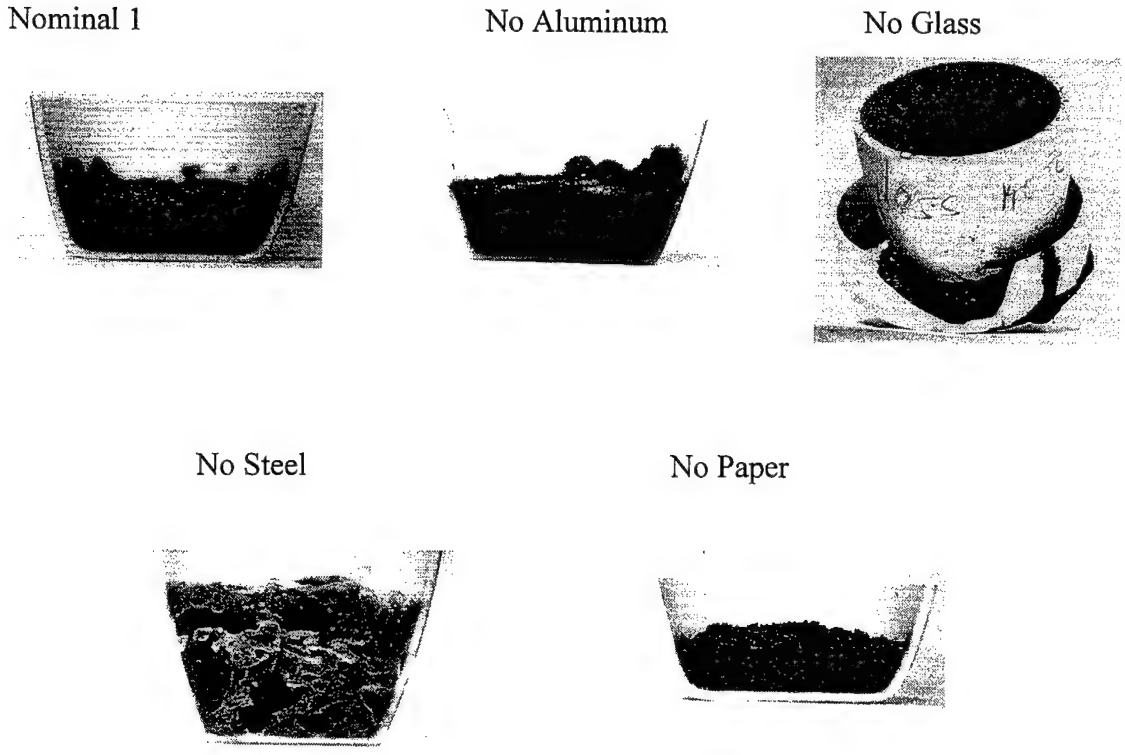


**Figure 6.1 Slag formed from variations of Navy Solid Waste, heated at 1400 °C in air for two hours (from references 6.1 and 6.2)**

The slag resulting from the "No Glass" excursion exhibited boiling and splashing, as well as cracking and partial melting of the crucible. This phenomenon is attributed to a severe thermite reaction, as a result of chemical interaction between iron oxide and aluminum during heating above 1200 °C. The heat generated by the reaction resulted in a rapid increase of temperature, probably in excess of 2050 °C (the melting temperature of alumina) leading to cracking (due to thermal shock.) and melting of the crucible and leaking of the slags. In a full-scale reactor this reaction could result in the catastrophic destruction of the system.

The results of thermogravimetric/differential thermal analysis (TGA/DTA) showed that the maximum rate of oxidation of steel occurs at a temperature lower than that of aluminum. This indicates that during processing of Navy wastes, steel will be oxidized before aluminum, creating favorable conditions for the occurrence of the thermite reaction. The occurrence of the thermite reaction was also observed during large-scale experiments conducted at NRL in an oxidizing atmosphere using the plasma torch in transferred arc mode. Figure 6.2 shows a section of a SiC crucible damaged by the high temperature of the thermite reaction. Melting occurred at the level of the surface of the molten material in the crucible.

**Figure 6.2 Section of SiC crucible attacked and melted due to thermite reaction**

The occurrence of the thermite reaction only in the "No Glass" excursion suggests the critical importance of the presence of a glass melt during waste processing for suppression of the reaction under oxidizing conditions. The protective effect of a glass melt is a result of physical separation of aluminum from iron oxides, as well as the low temperature oxidation of Al by the reduction of $SiO_2$ (from glass) which takes place below the thermite reaction ignition temperature. These results and techniques for suppression of the thermite reaction during processing of "No Glass" waste have been described in another paper[6.1].

The NRL plasma arc system was used to make larger batches of slag for characterization, and to observe the effects of more realistic conditions on slag formation. One issue is the ability to oxidize material with an air torch, and whether the oxygen capture efficiency changes with the extent of oxidation. For shipboard slag processing, oxidation affects potential ultimate disposal options. If slag can be fully oxidized to form a vitreous, nonleachable glass, then disposal at sea may be an option. However, if the ban on solid waste dumping means that not even a nonleachable slag can be dumped, then full oxidation is not required. A melt of metal and glass will need to have mechanical properties that allow it to be stored on board ship safely, and then it should be amenable to disposal ashore in a municipal waste facility or for recycling.

A series of slag formation experiments was conducted to determine how the efficiency of oxidation of the metals in NSW depends on experimental parameters [6.3]. The variables were torch current, torch gas flow rate and torch height. The transferred arc torch was operated on nitrogen while material was fed into the crucible onto the surface of the molten waste. After all feed was in the crucible, the torch was switched over to air, and the materials were "cooked" for 30 minutes. A final test was done with the torch using air for the whole feeding and oxidizing period, to achieve maximum oxidation under these test conditions. The feed materials were steel can stock, aluminum soda cans and glass bottles. The aluminum cans and bottles were collected from cafeteria waste at the NSWC-CD site, and therefore are representative of NSW. All the materials were prepared using a standard Navy shredder. For the metals, this process formed a very low-density springy material, so it took a considerable amount of feeding to get 7 kg of material into the crucible. The recipe for the test materials is given in Table 6.2

**Table 6.2 Chemical recipe for slag formation tests**

| For each experiment, 7 kg waste materials (metals + glass + paper filler + $Ca_3(PO_4)_2$ powder) are used | | |
|---|---|---|
| Material | Weight [grams] | wt % |
| Fe | 2888.2 | 41.26 |
| Al | 1540 | 22.0 |
| Glass | 1348.2 | 19.26 |
| $CaCO_3$ | 576.1 | 8.23 |
| Kaolin ($Al_2Si_2O_7 \cdot 2H_2O$) | 576.1 | 8.23 |
| $TiO_2$ | 60.9 | 0.87 |
| $Ca_3(PO_4)_2$ | 10.5 | 0.15 |
| Total | 7000 | 100 |

While the test runs were underway, gas composition in the exhaust line was monitored with a Balzers Quadstar 300 residual gas analyzer. Figure 6.3 shows a composite of all runs. Each run has three segments. Initially the torch gas was nitrogen as material was fed into the chamber and melted. During the second segment the torch was switched to air and the material in the crucible was oxidized. At the two flow levels, the oxygen that was supplied during 30

minutes was 34% of stoichiometric for the low flow experiments, and 49% for the high flow experiments.

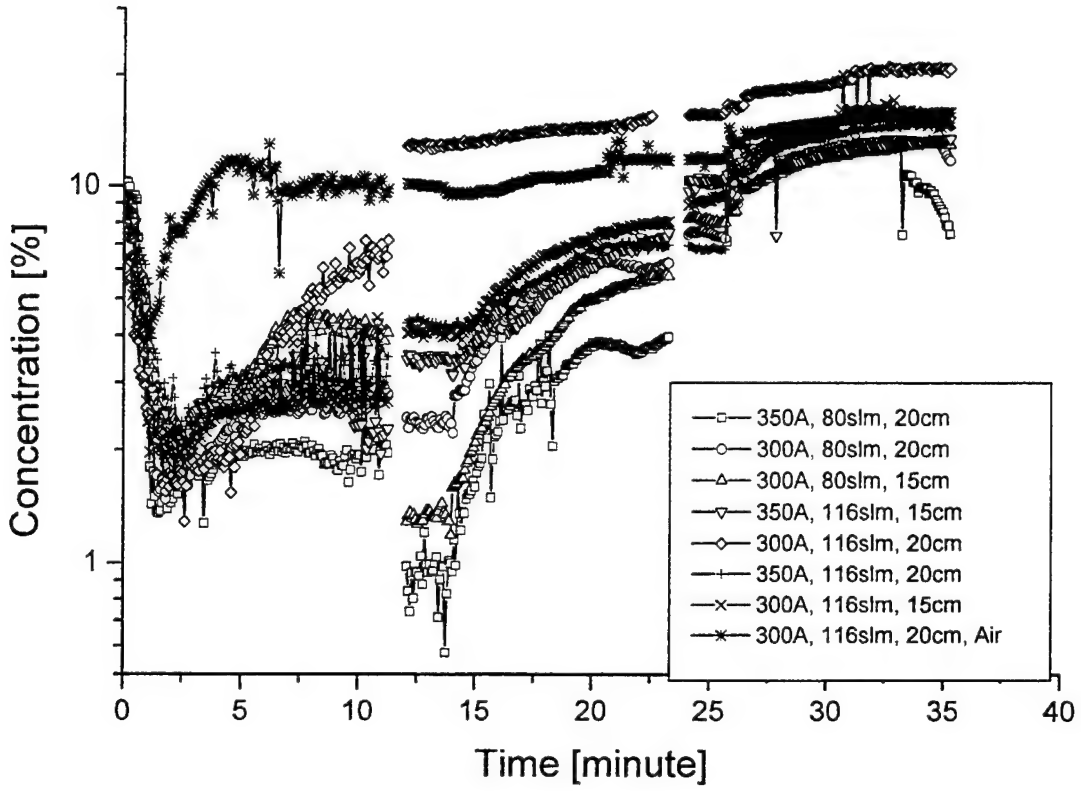


**Figure 6.3 Oxygen concentration in the reactor off-gas during slag oxidation experiments, showing variation in oxygen transport and capture as oxide layer builds up.**

The figure illustrates that when the torch was switched to air (at approximately 12 minutes on the x axis), oxygen consumption was at a maximum and then declined as oxide built up on the slag, shown by the increase of oxygen in the exhaust gas. After 30 minutes of oxidation the torch was turned off, but air continued to flow. The exhaust oxygen concentrations quickly stabilized at the values determined by the flows of air through the torch and the nitrogen flows used as purge gas to keep windows clear. It is clear that oxygen capture depends on the experimental conditions, with the following results:

- Greatest oxidation efficiency came at low airflow, high current and minimum torch height. These conditions maximize the plasma temperature.
- The run with the torch on air during feeding and melting as well as during the oxidizing exposure (the highest curve from 1-12 minutes in Figure 6.3) gave the greatest extent of oxidation, making a uniform, dense glassy slag.
- Small spherical deposits of elemental iron were dispersed through all the slags, indicating multiple small thermite reactions had occurred. Figure 6.4 shows a picture of the slag formed during the run with air for the whole duration, i.e. the most oxidized sample. Iron deposits are visible throughout the slag.

- Oxygen capture efficiency decreased as the extent of oxidation increased. Full oxidation would require a significant excess of oxygen, probably requiring an air lance.

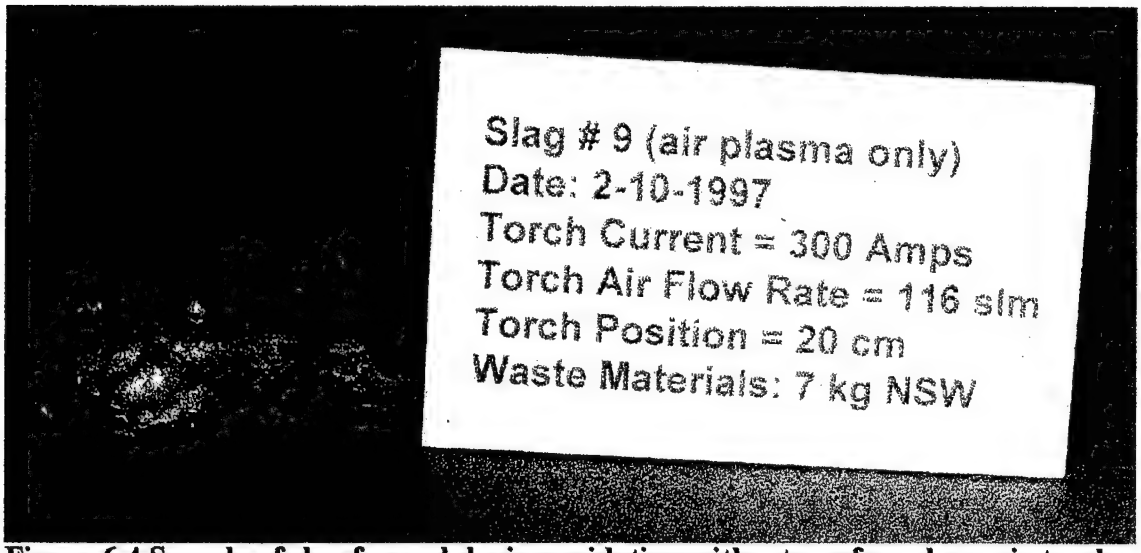


**Figure 6.4 Sample of slag formed during oxidation with a transferred arc air torch.**

Physical properties of slag are important for design of the shipboard reactor, and for storage of slag on ships due to deck load limits. Slag densities were determined by weighing and volume determination. Volumes were determined by immersing samples in water to determine displacement. These results are shown in Table 6.3. For planning purposes, a slag density of 3.2 +/- 0.3 g/cm$^3$ results, but full oxidation should make the density lower, and not oxidizing it will increase the density, depending on the actual mix of iron, aluminum and glass.

**Table 6.3 NSW oxidized slag densities**

| Torch current amps | Torch air flow rate slm | Torch position cm | Volume wrapped ml | Mass g | Packing density g/ml | Volume unwrapped ml | Mass g | Density g/ml |
|---|---|---|---|---|---|---|---|---|
| 300 | 80 | 15 | 75 | 211 | 2.813 | 73 | 210 | 2.877 |
| 350 | 80 | 15 | 60 | 196 | 3.267 | 52 | 195 | 3.75 |
| 300 | 116 | 15 | 51 | 121 | 2.373 | 38 | 120 | 3.158 |
| 350 | 116 | 15 | 42 | 129 | 3.071 | 42 | 129 | 3.071 |
| 300 | 80 | 20 | 41 | 99 | 2.415 | 32 | 98 | 3.063 |
| 350 | 80 | 20 | 43 | 86 | 2.000 | 30 | 85 | 2.833 |
| 300 | 116 | 20 | 61 | 162 | 2.656 | 50 | 161 | 3.220 |
| 350 | 116 | 20 | 41 | 115 | 2.805 | 34 | 114 | 3.353 |
| 300 | 116 | 20 | 30 | 72 | 2.400 | 25 | 72 | 2.880 |

The slag surface was monitored by an optical pyrometer as it was heated. Visual examination indicated that there is usually some bubbling, so we interpret the highest temperatures observed as the boiling temperature of the slag. Because the composition is constantly varying, the high temperature readings were rather noisy, so they were averaged over the time for one rotation of the crucible. When the torch was extinguished, the hot slag surface cooled and the cooling curve was recorded. When the slag surface froze, there was a change in the slope of the cooling curve so the freezing point could be determined. Results for these slag oxidation experiments are shown in Table 6.4.

**Table 6.4 Slag melting and boiling points for oxidized NSW slag**

| Date | Melting temp, °C | Boiling temp, °C |
|---|---|---|
| January 21 | 915 | 1700 |
| January 22 | 1200 | 1500 |
| January 23 | 1000 | 1500 |
| January 28 | 1000 | 1550 |
| January 29 | 1075 | 1525 |
| January 30 | 1100 | 1500 |
| January 31 | 1080 | 1500 |
| February 3 | 1130 | 1640 |
| February 4 | 1150 | 1750 |
| February 5 | 1200 | 1500 |
| February 6 | 1100 | 1400 |
| February 7 | 1200 | 1550 |
| February 11 | 1220 | 1650 |
| February 12 | 1130 | 1575 |
| February 13 | 1200 | 1575 |

The estimated accuracy of the freezing points is about 20 °C, and for the boiling point about 50 °C. Since these experiments all started with the same nominal composition, these results illustrate the range of variability due to extent of oxidation and probably due to incomplete mixing.

## 6.4 Conclusions

The results of slag formation studies of simulated Navy Solid Waste in laboratory oven conditions and under a plasma arc torch using air as the torch gas are reported. These studies show that the metals in NSW can be oxidized to form a glassy slag. However, complete oxidation under an air plasma torch is limited by slow oxygen transport through oxide on the surface. If oxidation is selected for the shipboard waste destruction strategy, additional oxygen will need to be supplied to get oxidation in the desired amount of time.

Oven experiments showed that variations in the basic NSW composition may result in slags with high melting points and in some cases there was no melting even at 1500 °C; however, in the plasma torch experiments failure to melt was never observed. With a transferred arc torch, conduction of the arc current through the material can heat to the melting point of all compositions that were tested.

The thermite reaction was identified as a problem in the oven studies, due to the oxidation of iron at a lower temperature than aluminum, followed by highly exothermic oxidation of the molten aluminum. The heat released by the thermite reaction caused melting of SiC crucible wall. However, in mixed NSW melted by a transferred arc air torch, only small pieces of iron were found distributed throughout the slag, indicating that small localized thermite reactions occurred. It is necessary to guard against a "worst case" scenario, in which a large amount of iron is oxidized in a crucible, followed by addition of aluminum. The current design of a metal and glass melter for shipboard waste has been selected to address this concern.

## 6.5 References


6.1 I. G. Talmy, J. A. Zaykoski, C. A. Martin, J. W. Cofield, S. Dallek, C. R. Wong, and E. E. Nolting. "Occurrence and Suppression of Thermite Reaction in Slags From Destruction of Navy Shipboard Wastes." Proceedings of 1997 International Conference on Incineration and Thermal Treatment Technologies, published by Office of Environmental, Health & Safety at the University of California, Irvine, pp. 621-625, 1997.

6.2 I. G. Talmy, J. A. Zaykoski, and C. A. Martin. Naval Surface Warfare Center Carderock Division Report No. NSWCCD-TR-1999/002, 1999.

6.3 Steven H. Peterson, David A. Counts, Qingyuan Han, Bruce D. Sartwell, Inna Talmy, James Zaykoski, and Curtis A. Martin. "Slag Formation From Navy Solid Waste With a Plasma Arc Torch Destruction System." Proceedings of 1997 International Conference on Incineration and Thermal Treatment Technologies, published by Office of Environmental, Health & Safety at the University of California, Irvine, pp. 101-104, 1997.

## 7.0 Modeling of Slag Motion Under Pitch and Roll

### 7.1 Theoretical and Experimental Measurements

The initial design concept for the shipboard plasma system was based on the conventional thermal plasma waste treatment systems that were being marketed and sold for land based usage. An example is the rotating crucible system described in Section 1.4 which utilizes a transferred arc plasma torch and which holds a large inventory of molten material, or slag, during processing. After starting the system and melting any initial waste material in the crucible, additional waste material is fed into the system and is thermally processed on the surface of the slag. A critical issue for this type of plasma processing is the motion of the molten material under shipboard conditions. Calculations were made and experiments were conducted using the NRL plasma arc system to examine this situation.

A set of initial assumptions and approximations for modeling the problem were: (1) the molten material in the crucible is considered to be a nearly incompressible fluid; (2) the fluid is Newtonian with respect to stress/strain relationship, (i.e. these two are linearly related); (3) there is a no-slip boundary condition; (4) the pressure at the surface is one atmosphere and pressure increases with depth in the fluid; (5) the velocity is purely azimuthal; (6) mass is conserved; (7) the rotation is occurring at the center of the moment of inertia of the ship; and (8) the rotation rate of the crucible is much greater than the pitch and roll rate.

Using the above approximations, a coordinate system and nomenclature were selected to model the problem. The crucible is assumed to be a right circular cylinder with radius $R_o$, rotating around the symmetry axis with angular velocity $\Omega$, (Omega). The origin of the coordinate system is at the base of the crucible, the z-axis is aligned with the rotation axis, and the azimuthal angle $\phi$ is also measured relative to the rotation axis. The tilt angle between **g**, (local gravitational unit vector), and the negative z-axis is denoted by the angle $\Theta$, (Theta), (when $\Theta = 0$, the rotation axis and gravity are parallel). Figure 7.1 illustrates this coordinate system.

Equation 7.1 relates the height of the material within the crucible as a function of radius, rotation rate, tilt angle, and tilt axis. A complete derivation of this equation is provided in reference 7.1.

$$z(r, \phi, \Theta, \Omega) = M/(\rho\pi R_o^2) + (r^2/R_o^2 - \tfrac{1}{2})(R_o^2\Omega^2)/(2g\cos\Theta) + r\tan\Theta\sin\phi \qquad (7.1)$$

There are three terms in the equation. The first is the result of filling up a right circular cylinder with liquid. The second is the result of rotating that liquid in the right circular cylinder and tilting it. Finally, the third term is related to the tilting of the crucible and having a plane of maximum displacement. Looking at the second and third terms, as the tilt angle approaches 90 degrees, the material will spill out and the solution breaks down. The $\sin\phi$ term means that there is a plane in the problem which gives the maximum and minimum displacement of the fluid. Analysis of the problem is concentrated in this plane.

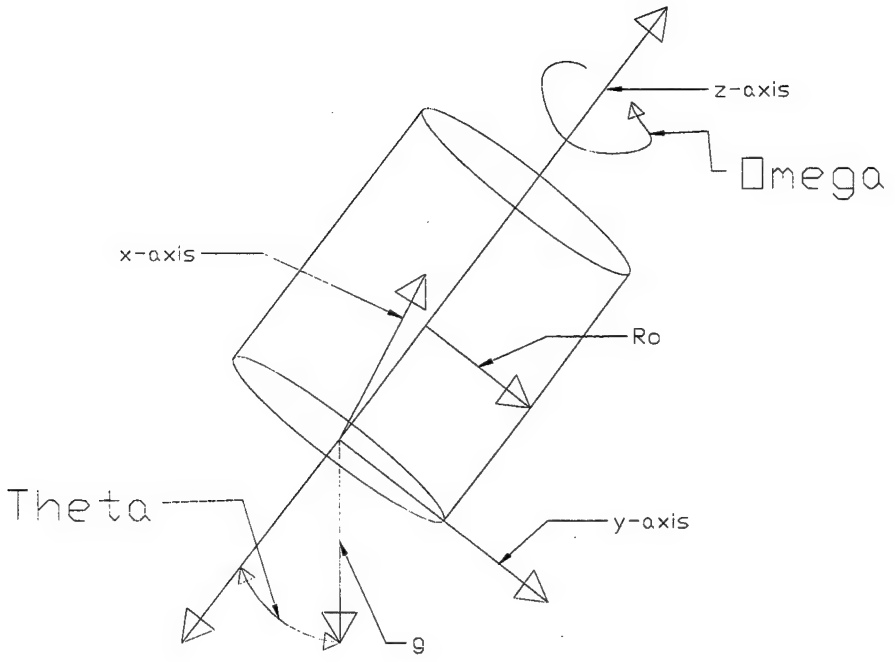


**Figure 7.1: Coordinate System and Nomenclature**

Case 1: No pitch and roll, no rotation. Equation 7.1 reduces to:

$$z(r,0,0,0) = z_o = M/(\rho\pi R_o^2) \tag{7.2}$$

where $z_o$ is the height of homogenous mass, M, of a fluid with a density, $\rho$, inside a right circular cylinder with radius, $R_o$.

Case 2: Dividing equation 7.1 by $z_o$ yields a dimensionless equation that gives the maximum displacement of the fluid:

$$z(r, \phi, \Theta, \Omega)/z_o = 1 + (R_o/z_o)(R_o\Omega^2)/(2g\cos\Theta)[(r/R_o)^2 - \tfrac{1}{2}] + (R_o/z_o)(r/R_o)\tan\Theta\sin\phi \tag{7.3}$$

A maximum of slag height will occur at $r = R_o$, (the outer diameter of the cylinder), and $\phi = \pi/2$. Putting these values into equation 7.3 and defining the result as a new function, $\zeta(\Theta,\Omega)$ yields:

$$z(R_o, \pi/2, \Theta, \Omega)/z_o = \zeta(\Theta,\Omega) = 1 + (\tfrac{1}{2})(R_o/z_o)[(R_o\Omega^2)/(2g\cos\Theta) + \tan\Theta] \tag{7.4}$$

The term $(R_o/z_o)$ is the aspect ratio of the problem. Using the following numerical values:

M = 100 kilograms
r = 3 grams per cubic centimeter, (an assumed density)
$R_o$ = 0.23 meters
then:
$z_o$ = 0.2 meters

Using the values above and equation 7.4, below is Table 7.1, listing $\zeta(\Theta,\Omega)$ for different rotation rates and pitch and roll angles (in radians, from zero to thirty degrees). The left column is $\Theta$ and the top row is $\Omega$ (in revolutions per minute), with the values of $\zeta(\Theta,\Omega)$ in the table.

**Table 7.1: Tabulated Theoretical Dimensionless Values For $z/z_o$**

| $\Theta$ in radians | $\Omega$ in revolutions per minute, (RPM) | | | | | | |
|---|---|---|---|---|---|---|---|
| | 7.5 | 15 | 30 | 45 | 60 | 90 | 120 |
| 0 | 1.004 | 1.017 | 1.067 | 1.118 | 1.266 | 1.599 | 2.065 |
| 0.1 | 1.119 | 1.132 | 1.182 | 1.234 | 1.383 | 1.718 | 2.186 |
| 0.2 | 1.237 | 1.250 | 1.301 | 1.354 | 1.505 | 1.845 | 2.320 |
| 0.3 | 1.360 | 1.373 | 1.425 | 1.480 | 1.634 | 1.983 | 2.471 |
| 0.4 | 1.491 | 1.504 | 1.558 | 1.615 | 1.775 | 2.137 | 2.643 |
| 0.5 | 1.633 | 1.647 | 1.704 | 1.763 | 1.932 | 2.311 | 2.842 |
| 0.52 | 1.669 | 1.683 | 1.741 | 1.801 | 1.971 | 2.356 | 2.894 |

Figure 7.2 summarizes the results from Table 7.1.

From Figure 7.2 it is easy to see the behavior that is predicted by the model: the greater the pitch and roll angle and/or the faster the rotation rate, the greater the molten slag maximum height, a result that was expected.

The model was tested by conducting experiments using the NRL plasma arc system. Since it was not possible to simulate pitch and roll, the comparison is to the non-pitch and roll case. The first result is presented graphically in Figure 7.3.

The first experimental test was conducted with sand and copper as the melt material and the torch was centered above the crucible. After the material cooled, the surface was mapped using a polar grid with one centimeter radial points. The points were then averaged resulting in a mean height, which was used to compare against the theory. There are two reasons for the extreme departure of the experiment from the theory: (1) The torch gas pushed the material away from the center, and (2) the material did not fully melt and changed the boundary from a right circular cylinder to a right circular paraboloid.

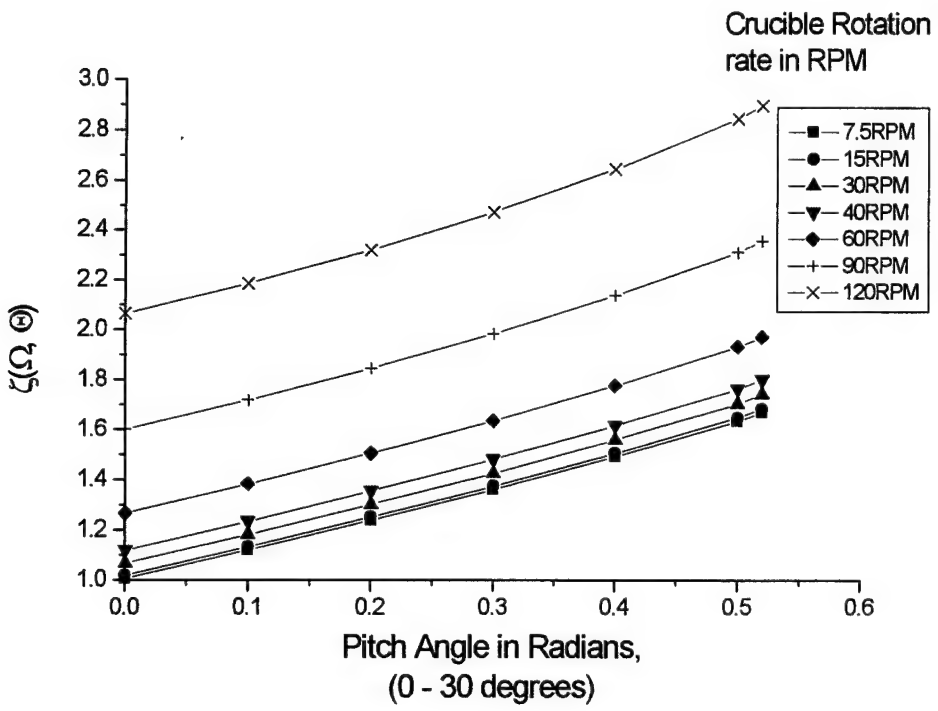


**Figure 7.2 Ratio of maximum height of slag at edge to height at rest as a function of pitch angle for several rotation rates**

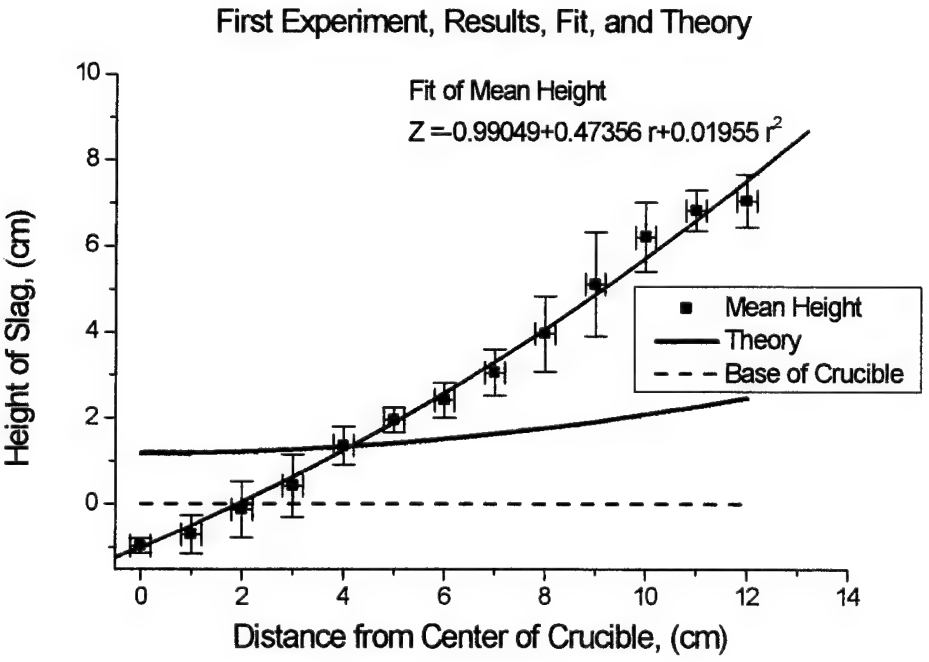


**Figure 7.3 Results of first experimental test of theory**

To test the theory against more suitable conditions a water filled glass vessel was rotated and video taped. The resulting surface was compared with the theory and the result is presented below in Figure 7.4.

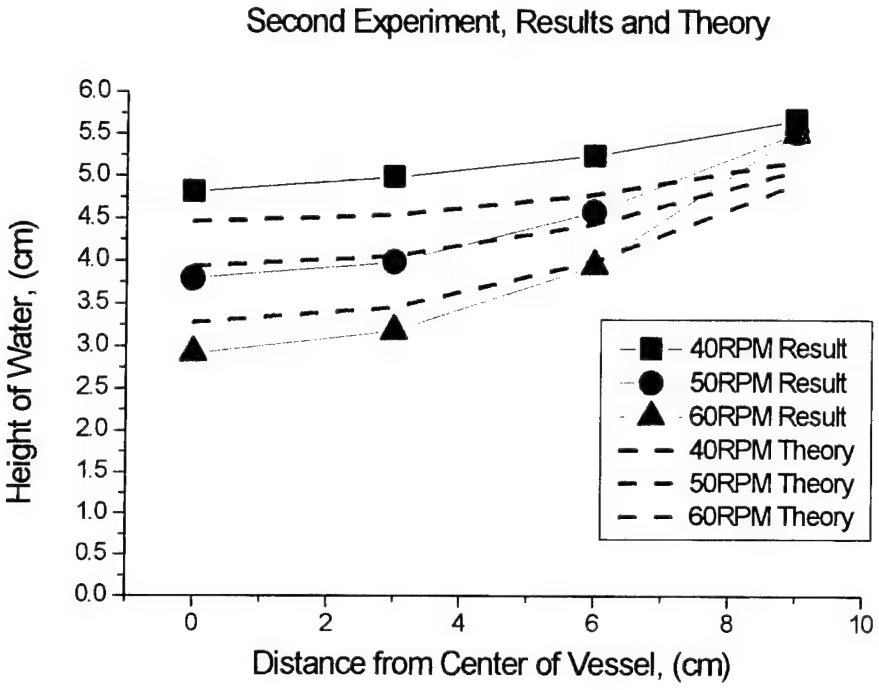


**Figure 7.4 Experimental test with water and glass vessel**

The second experimental results were much more encouraging. While the result showed the model was not perfect, the results of the model were at least qualitative enough to present a steady-state picture of how to expect the surface of a molten slag to deform under pitch and roll conditions.

Additional experiments were conducted at NRL and the results are shown in Figures 7.5 through 7.8. Each slag produced was mapped and compared with the model. One useful result was that from the mapping and comparisons with the model, one could determine the assumed uniform homogeneous density. Depending on the operating conditions, it was possible to produce either highly oxidized material or high metallic content material, and that would greatly affect the resulting density.

After conducting these tests it was realized that the utilization of a high slag content shipboard system would not be practical and it was moot to expend further efforts at improving the model to account for dynamic shipboard motion or to conduct further experimental efforts to support the model. However, if in the future the decision is made to pursue a high slag content system, a theoretical basis for additional modeling has been developed.

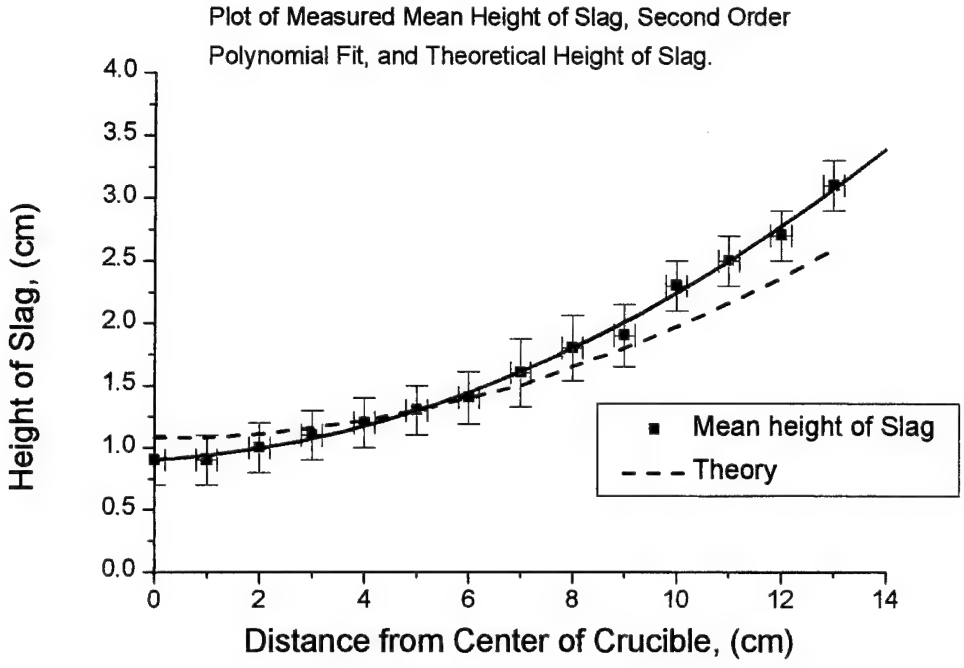


**Figure 7.5 Comparison of model with experimental results**

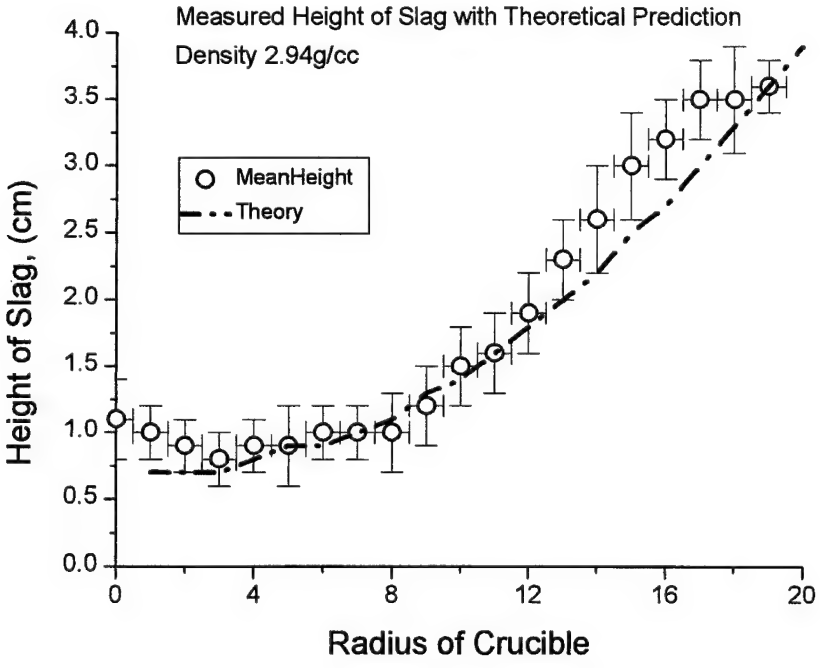


**Figure 7.6 Comparison of model with experimental results**

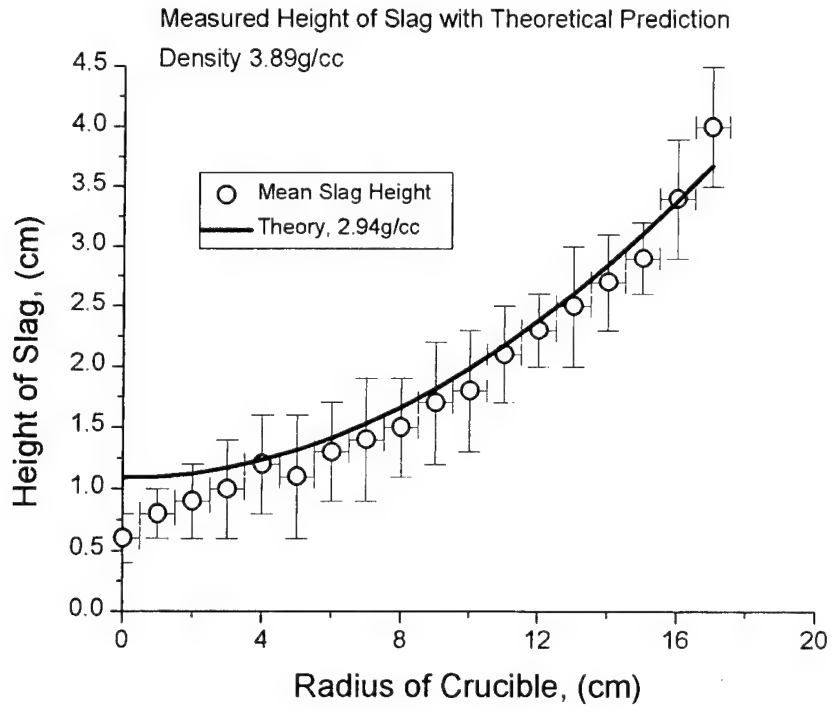


**Figure 7.7 Comparison of model with experimental results**

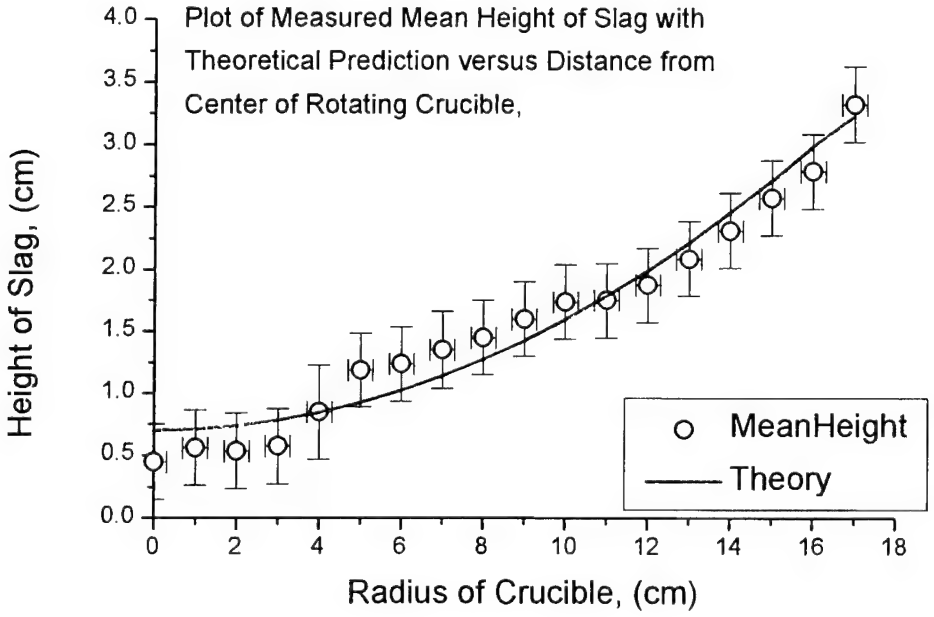


**Figure 7.8 Comparison of model with experimental results**

## 7.2 References

7.1 D. A. Counts, "Surface Deformation of Molten Slag Under Rotation and Shipboard Pitch and Roll: A Steady State Analysis", Dissertation, University of Maryland, College Park, MD, May 24, 1996

## 8.0 Radiation Heat Transfer Studies (Hot Tube Testing)

### 8.1 Background and Experimental Procedures

Based on all of the previous literature reviews, conceptual studies, and experimental studies conducted at NRL and elsewhere, it was determined that in order to meet the technical challenges of developing plasma arc technology for deployment on Navy ships, the fundamental design criteria used in the manufacture of existing land-based thermal treatment equipment must be changed. Since most conventional plasma arc waste treatment systems evolved from metallurgical processing systems, they have been designed to contain a molten slag bed that is generally maintained at a temperature of approximately 1500° C, with the gases in the primary processing chamber generally at about the same temperature. This means that the thermal destruction process occurs at these temperatures rather than at the actual plasma arc temperature of 4000-8000° C. Operation at these lower temperatures has two important consequences: (1) slower thermal destruction rates, and (2) less dissociation of complex organic molecules into their atomic constituents. A high thermal destruction rate is an important requirement in reducing overall system size.

To maximize the heating rate and thereby improve the thermal destruction rate, it is important to bring the waste material directly in contact with the high-temperature plasma arc and to maximize the waste material's surface-to-volume ratio. Increasing this ratio can be achieved by segregating it from the inorganic waste stream and pulverizing it into small particle sizes, which reduces the time required to raise the temperature of the material to that required for complete pyrolysis.

A second issue to be addressed is the standard use of thick refractory materials to insulate the chamber walls. This refractory material both increases size and weight (typically the refractory materials are a substantial portion of the weight of land-based systems). Another equally important drawback in the use of thick refractory materials is the heat-up and cool-down times which typically range from a few hours to as much as 18 hours. The approach taken to remove the requirement for most of the refractory materials is to use a cold-wall design which employs either water or air cooling to maintain the wall at survivable temperatures.

Figure 8.1 illustrates the design features of what is called a plasma-fired eductor (PFE) which incorporates most of the features described above. In the figure, particularized organic waste (typically 500 micrometers or less in diameter) is introduced in an annular flow around the plasma arc. Particles of this size occur naturally with the use of the standard Navy pulpers, which could be employed to pre-process and transport the organic waste as a slurry to the PAWDS unit. The transport of food waste by slurry is used in some cruise ship waste management systems.

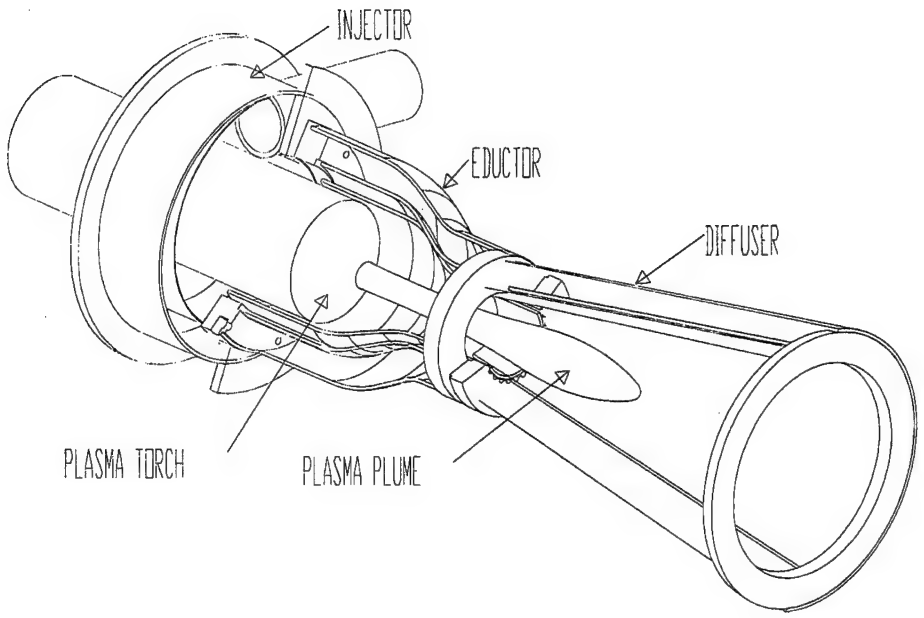


**Figure 8.1 Illustration of the plasma-fired eductor (PFE) designed for the treatment of the organic portion of shipboard waste**

Of critical concern related to the application of the PFE to treatment of the organic portion of NSW is the heat load on the inner walls. Although the testing of an actual eductor will not be performed until 1999, initial experiments were conducted as PFE proof-of-concept studies to examine heat-loading on the walls of a constant-diameter cylinder, designated the Hot Tube. This effort was intended to verify that the proposed PFE could be utilized to destroy the defined Navy shipboard organic waste stream. The actual PFE could then be used in a follow on effort for extensive testing of combustion efficiency, waste stream perturbations, geometry optimization, materials analysis and computational fluid dynamic (CFD) verification.

The purpose of the heat transfer experiments was to verify cooling and materials requirements for operation close to the non-transferred arc thermal plasma plume. Other researchers have investigated the radiation heat transfer from transferred arc plasmas [8.1]. Due to the novel nature of the geometry of the proposed PFE and the proximity of the wall to a non-transferred arc plasma plume, a separate set of experiments was conducted. The experimental apparatus was designed and fabricated for hot tests of materials and heat transfer utilizing the NRL plasma arc system. The primary objectives of the hot tube experiment were:

- Verify assumptions regarding convective and radiative heat transfer coefficients from the plasma plume
- Provide experimental verification of expected heat loss.

- Demonstrate the ability to maintain a 500° C temperature of the stainless steel liner without adverse effects.
- Demonstrate the utilization of copper wool insulation and calibrate the known thermal conductivity versus packing density for stainless steel wool to copper wool.
- Gain practical experience in water cooling a multi-layered composite tube in a plasma environment.
- Development of a water cooling system applicable to the experimental plasma eductor
- Preliminary verification of the heat transfer analysis and assumptions
- Demonstration of composite wall geometry

The experimental system was designed to operate in conjunction with the thermal plasma system at NRL. This required minimal alteration to the NRL system, most of which would be required for support of later eductor experiments. Figure 8.2 presents a two-view sectioned assembly drawing of the final hot tube design. The assembly is composed of a stainless steel inner liner [4] designed to float between two ceramic board end mounting plates [5] thereby accommodating the axial thermal expansion of the liner. The inner liner has a nominal inside diameter of 6 inches and is approximately 10 inches long. The end caps are attached to an aluminum brazement composed of the outer housing [2] and the cooling tubes [1]. Between the outer housing and the inner liner is an annular gap [3] which can be filled with various insulation materials.

The primary reason for performing hot tube experiments was to verify the heat transfer calculations and models for the PFE and demonstrate the ability to limit the heat loss to the stainless steel liner to a value low enough that PFE thermal efficiency would be acceptable. During the experiments, analysis of the hot tube performance was conducted in order to insure proper operation. The results of the calculations and models are summarized below.

Thermal expansion calculations for the inner liner and outer shell were performed to insure that sufficient clearance was provided in mounting the inner liner so that no excessive thermal stresses were induced in the liner or shell through interference. The result of those calculations indicated that the difference in shell and liner axial growth would be a maximum of .003 inches and that the radial clearance change would be .001 inches. The ceramic board end plates which constrain the inner sleeve relative to the shell were designed to accommodate up to .01 inches in axial growth of the inner liner thus avoiding any possible interference. The centering of the shell within the assembly is provided by the bronze wool insulation which is inherently compressible and could easily accommodate the change in radial clearance.

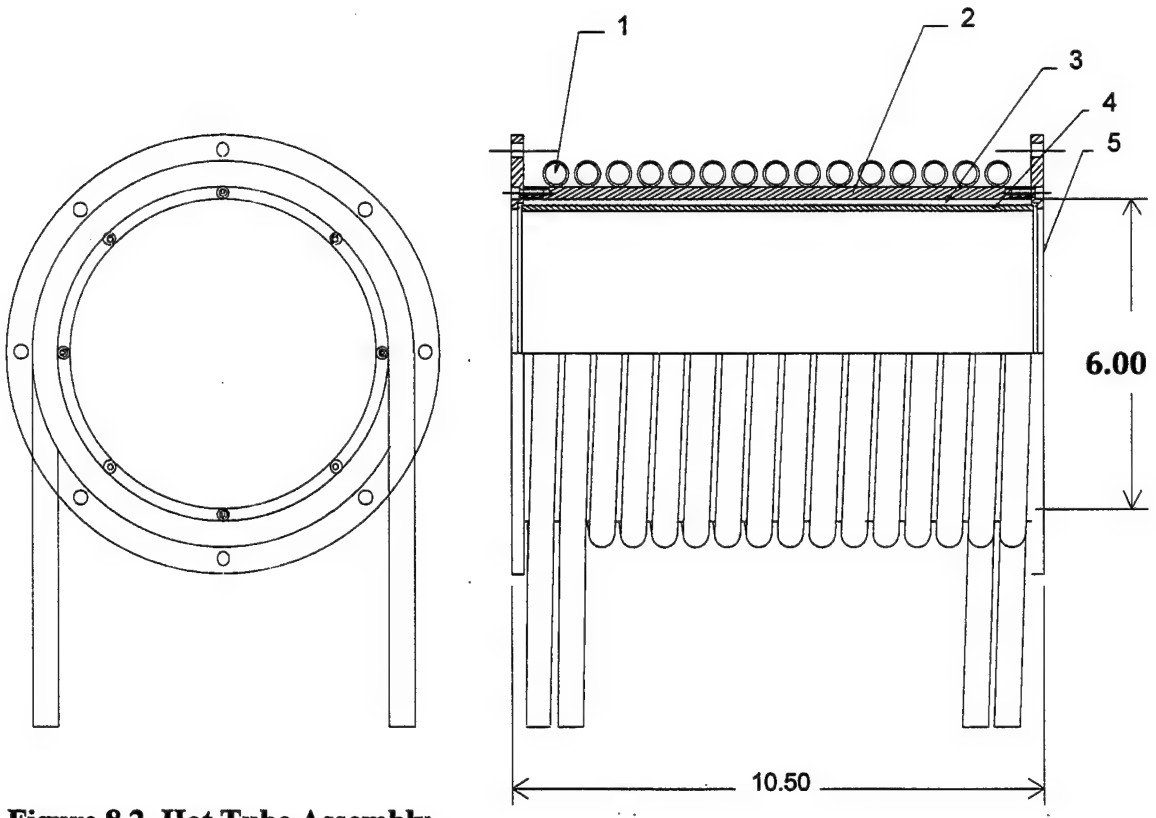


**Figure 8.2 Hot Tube Assembly**

An analysis of the heat transfer from the plasma torch to the wall was performed with emphasis on two primary concerns. First was to insure that the liner temperature did not exceed 900° C , which was the limiting temperature that was believed to be reasonable for the liner to meet its structural and erosion requirements. The value for the radiation heat transfer coefficient was obtained from consideration of flame radiation and the convective heat transfer coefficient was based on values from similar heating conditions. Given the thermal properties of the hot tube assembly and an assumed bulk plasma plume temperature of 2500K the required thermal conductivity of the insulation layer was calculated as:

$$k_{insulation} = 2.879 \text{ watt per meter per Kelvin} \qquad \{8.1\}$$

The required packing density of bronze wool in order to achieve this thermal conductivity was determined from empirical curves for the thermal conductivity of stainless steel wool versus packing density. The required packing density was calculated to be 25% or 84 gm per inch of liner tube. For experimental purposes three separate insulation zones were packed around the liner. The first four inches were packed at a density of 25%, the next three inches were packed at 19% and the final three inches were packed at 13%. Given the time constraint on hot tube experiments this variable packing allowed for investigating the effect of changing insulation without having to uninstall and repack the hot tube.

The hot tube was mounted into the plasma arc system in a vertical orientation along the axis of the plasma torch as shown in Figure 8.3. This configuration allowed the torch to be

positioned anywhere along the axis of the hot tube so that the desired section of the liner sleeve could be exposed to the plasma plume.

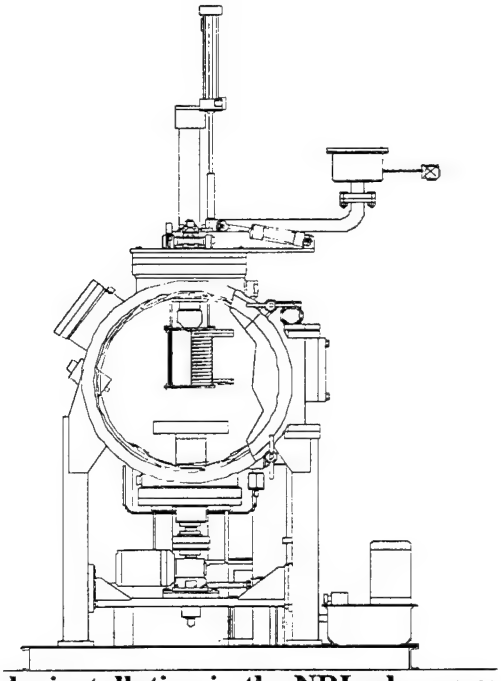

**Figure 8.3 Hot Tube installation in the NRL plasma arc system**

The hot tube was instrumented with a series of two groups of thermocouples, (one group of six and one group of seven) spaced fairly uniformly along the length of the hot tube, with the two groups being 180 degrees apart. The thermocouples were inserted through holes in the outer housing and pressed against the outer surface of the liner sleeve. Since the temperature drop across the sleeve was small and could be estimated for a known heat flux, the thermocouples gave a good indication of the inner surface temperature of the sleeves. Additional thermocouples were used to monitor the entrance and exit temperatures of the cooling water in the two cooling loops. After initial testing four thermocouples were added to monitor the temperature of the outer case at various locations along its length. In addition to the cooling loop temperatures the water flow rates in each of the two cooling loops were monitored. Once instrumented the entire hot tube assembly was insulated with ceramic insulation to minimize any heat gain from the chamber.

The cooling loop piping is illustrated in Figure 8.4. The loops were supplied with cold tap water through a pair of shut-off valves [1]. The water flow in each loop was monitored by flow transducers [3] and the flow rate were recorded by the data acquisition system. Maximum loop pressure was controlled by pressure relief valves [4] on the output side of each line. Flow control valves [5] were utilized on the output of each loop to establish the desired flow rate. The output from each loop was then piped to the laboratory sink.

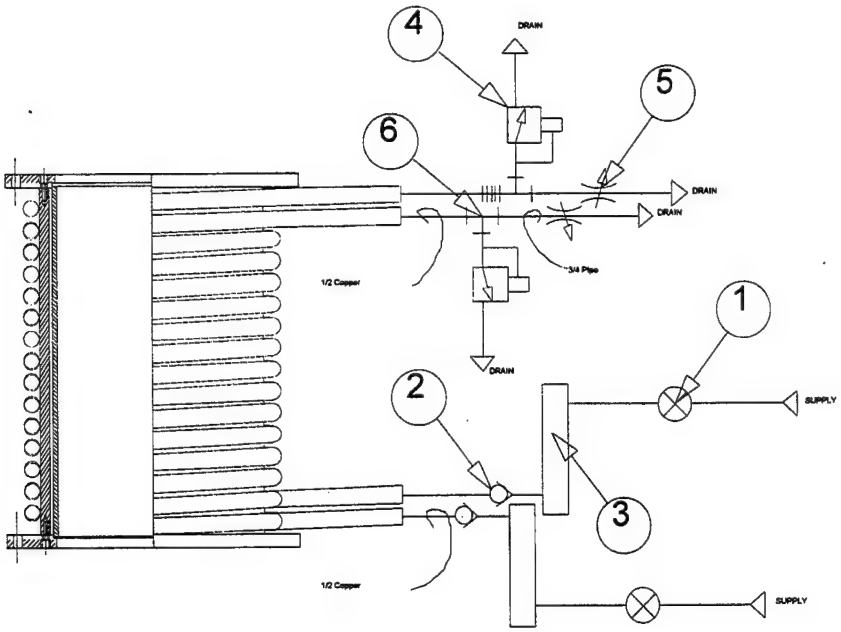


**Figure 8.4 Cooling Loops Piping**

The system went through start-up testing and debugging prior to experimental testing. The data acquisition and control system were exercised and calibration checks were conducted to validate flow and thermal measurements. Figure 8.5 presents a schematic layout of the primary thermocouple and flow transducers installed in the hot tube experimental setup.

Thermocouples 1 to 13 were located along two sides of the hot tube, 90° apart, extending through the outer shell and pressing against the inner liner. During the experimental testing, thermocouple 13's position was changed so that it was exposed inside the end of the hot tube in the gas flow and about 1 mm off the liner surface. Thermocouples IN-1 and IN-2 were in thermocouple wells attached to the cooling water feed lines to monitor inlet water temperature. Thermocouples OUT-1 and OUT-2 were in thermocouple wells attached to the cooling water drain lines to monitor outlet water temperature. Flow transducers were inserted in both the cooling water supply lines to monitor cooling water flow rate. The cooling water loops were connected in counterflow so one loop fed from the top of the hot tube and the other loop fed from the bottom.

Five experiments were conducted and the following is a brief summary of the test runs. All of the data from the five experiments is provided in appendix B.

Experiment Number One - short tests at 300 amps
Proof of principle test.
Experiment Number Two - 1205 Seconds, 300 Amps, 380 Volts
Torch approximately at the center of the hot tube

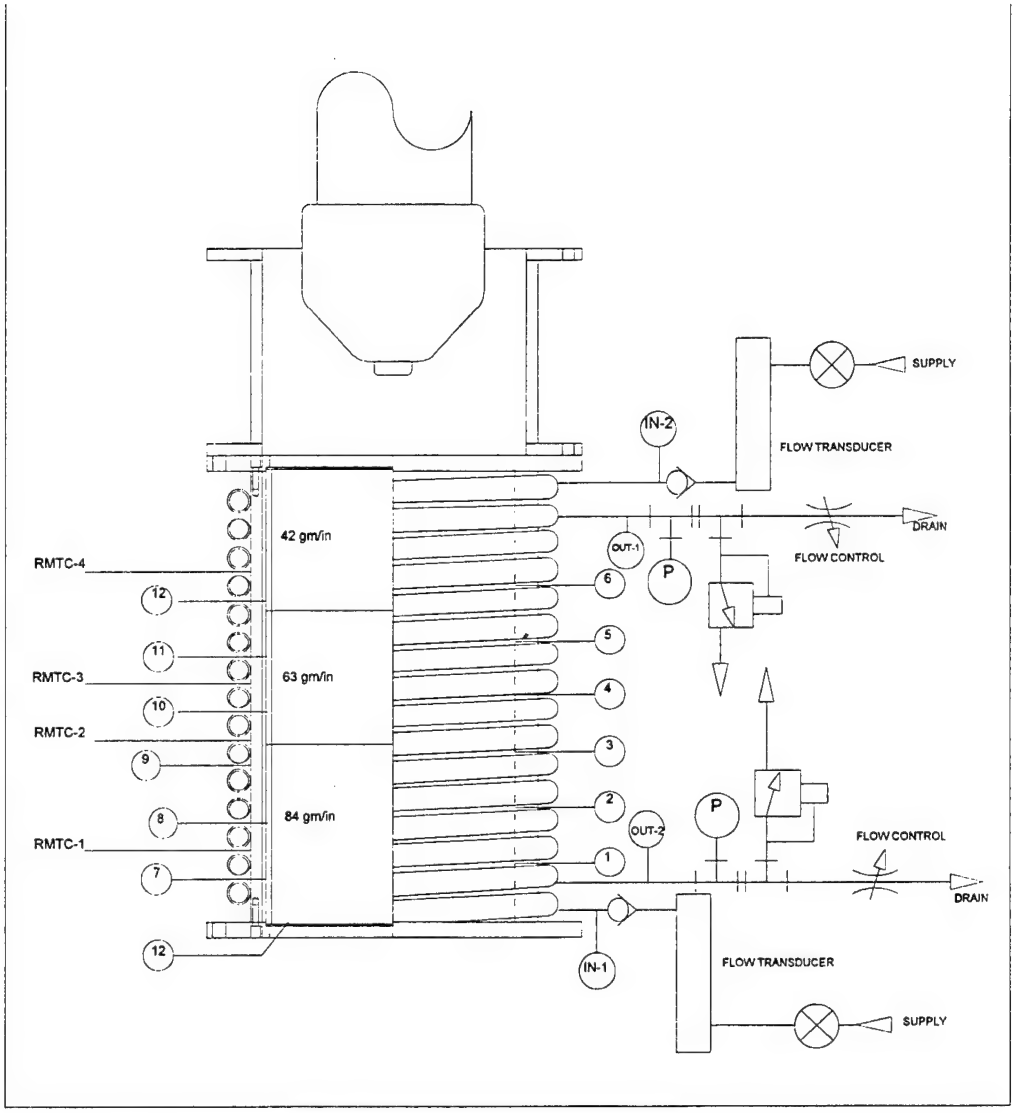


**Figure 8.5 Hot Tube Instrumentation.**

Experiment Number Three - 477 Seconds, 300 Amps 380 Volts
Torch approximately at the center of the hot tube, water flow adjusted
Experiment Number Four - 987 Seconds, 400 Amps, 320 Volts
Torch approximately at the center of the hot tube
Experiment Number Five - 868 Seconds, 400 Amps, 320 Volts
Torch fully retracted, maximum exposure of hot tube to plasma arc

## 8.2 Test Results

Initial start up operation was executed in a manner to insure that the system was operating as expected. The torch was operated for a short period (30 seconds) beginning in the

fully extended position and then automatically retracted up through the hot tube. The operation time was increased over three of four runs until it was established that the hot tube had sufficient cooling.

Figure 8.6 is a plot of the liner temperatures indicated by four of the twelve liner thermocouples for Experiment Four. This test illustrates the full temperature response range for the hot tube experiments. For this test the initial cooling water flow rate was set at approximately 1.5 GPM per cooling loop for the first four minutes and then reduced to .5 GPM per loop. At the ten minute mark the torch was shut down and the water flow rate increased to 2 GPM. Thermocouples 1 and 6, the upper and lower thermocouples on one side of the hot tube, are very similar in response as is the response of thermocouple 12, the upper thermocouple on the opposite side. However thermocouple 7, the bottom thermocouple on the same side as twelve, is somewhat different in character. The response of thermocouple 1 is indicative of a loss in good thermal contact with the liner wall after initial heating.

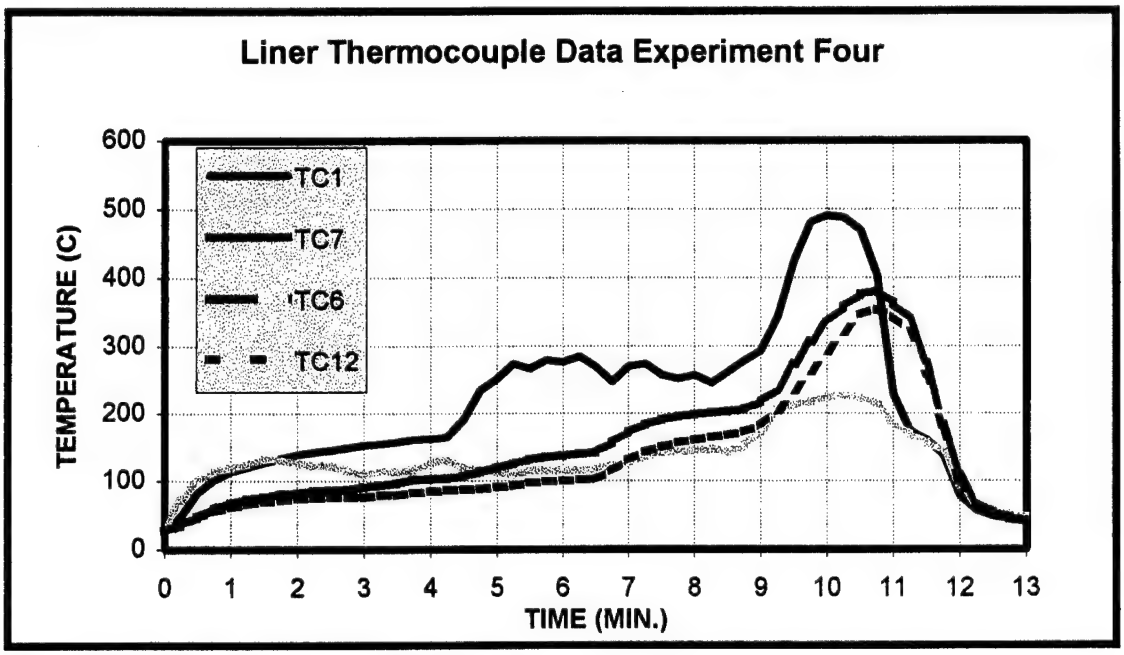


**Figure 8.6 Liner Thermocouple Data**

## 8.3 Conclusions

The hot tube experiment met all of its primary objectives. One primary concern for the eductor was operating a plasma torch in close proximity to a metal wall, keeping the wall sufficiently cool, while keeping the heat loss to the wall within reasonable limits. The approach of a composite wall with a stainless steel liner, metal wool insulation, and an outer water jacket worked well. The heat loss to the walls was higher than predicted, however the reason for this became obvious upon further research into the contact resistance for stainless steel versus copper bronze. The original estimates for the thermal conductivity of bronze wool were performed in accordance with the procedure recommended by Technetics, Inc. a producer of stainless steel wool. The only correction factor employed to change from one metal wool to another was to

correct for the change in the thermal conductivity of the materials. However, published data on the thermal contact resistance of stainless steel versus bronze indicates that there is as much as an order of magnitude better thermal conductivity between bronze surfaces than that for stainless on stainless. If these differences are taken into account the calculated values for heat loss agree quite well with the experimental results

## 8.4 References

8.1 Parisi, P. J., and W. H. Gauvin, Heat Transfer form a Transferred-Arc Plasma to a Cylindrical Enclosure, Plasma Chemistry and Plasma Processing, Volume 11, Number 1, Pages 57 - 78, 1991

## 9.0 Conclusions and Future Work

As mentioned in Section 1.5, in Fiscal Year 1999 a Navy Advanced Technology Demonstration (ATD) project was initiated with the overall objective of establishing thermal plasma arc as a superior technology for the thermal destruction of Navy Shipboard Solid Waste. This objective will be accomplished by designing and constructing a land-based test system demonstrating the following: (1) Full-scale operation; (2) 75 times or greater reduction in the solid waste volume; (3) At least 50 percent reduction in system size versus currently available commercial systems; (4) Minimization of manning levels and training requirements; and (5) Maximization of equipment shipboard compatibility.

The ATD program will build a full-scale plasma arc unit capable of processing one-half the Navy Shipboard Solid Waste generated by a typical Nimitz-class aircraft carrier. (The intent would be to ultimately install two units on a carrier). To reduce demonstration costs, the system will be land-based, but employ only technologies suitable and appropriate to a shipboard design. To the extent practicable, the PAWDS ATD unit will be configured for shipboard installation. The unit will be used to process both surrogate NSW and actual ship-generated waste material. A range of test samples, considered consistent with expected variability of NSW, will be processed to determine the PAWDS operational envelope.

Because previous studies, including those reported here, have determined the current land-based technology is insufficient to satisfy shipboard requirements, an entirely new technical approach is required. This approach has several innovative features. In the shipboard design, the solid waste is segregated into its organic and inorganic constituents. The segregation of constituents provides for relative constancy of the thermal destruction chemistry by minimizing the effects of waste stream variations. The segregation of the waste stream therefore simplifies the required control/sensor systems and reduces the need for continuous human supervision. In order to process the segregated waste constituents, the PAWDS design will consist of two integrated plasma processing units, one for the organic and one for the inorganic waste streams. These separate processing units will further allow optimization of overall system performance.

The approach employed by the organic processing unit will bring the organic waste material into direct contact with the plasma plume. This will be achieved by utilizing a plasma eductor design that employs an injector to distribute pulverized organic material into a flow stream around the ultra-high temperature plasma. Pulverizing the waste into finely divided particles decreases the thermal conduction times required to bring the waste to pyrolytic temperatures to a few milliseconds. The proposed organic processing design was illustrated in Figure 8.1. This design maximizes the destruction rate and minimizes the time needed to gasify the organic matter. The plasma eductor represents a significantly smaller primary processing chamber than currently used in commercial plasma systems which provides a volume reduction on the order of 100 times smaller than a commercial unit. Pyrolytic gases (CO and hydrogen) formed in the plasma eductor are transported into a secondary chamber for final combustion and formation of $CO_2$ and water vapor.

Both the eductor and secondary chamber use cold-wall designs, which provide further system size and weight reductions. In addition to size reductions, the cold-wall design greatly

reduces the start-up and cool-down times required for thermal chambers that are lined with refractory material. Rejected heat transmitted through the chamber walls can be used to assist in the drying of the organic waste prior to injection into the eductor. Eliminating the refractories also provides for a more robust mechanical system in regard to shock and vibration.

A separate plasma unit will be utilized to process the inorganic waste, primarily iron, aluminum, and glass. The purpose of this unit is to densify the inorganic waste, destroy biological contamination (food waste), gasify secondary organics (paper labels, etc.), process inorganic residue from the plasma-fired eductor, and provide a method to treat organic waste not conducive to pulverizing (e.g., oil and fuel filters, wood, etc.). A goal of this unit's design is to reduce the amount of molten material present at any given time during the processing period. The molten material is rapidly solidified into a thin disk. The thin-disk geometry will decrease the time required to reach a reasonable handling temperature. In addition, the size of the disk has been selected to be light enough to be moved manually. The ATD hardware will be configured to allow for both oxidation or non-oxidation of the inorganic material. The inorganic plasma unit is also connected to the secondary chamber in order to oxidize any pyrolytic gases formed during the treatment process.

In summary, the PAWDS represents a high-risk, high-payoff technology which will enable the Navy to meet the federal laws that prohibit the discharge of solid waste in "special areas" and which will help achieve the goal of an environmentally sound ship for the 21$^{st}$ century.

## 10.0 Acknowledgements

Some of the work reported here was performed under NRL Work Unit 61-5475 for the Office of Naval Research Environmentally Sound Ships Program, PE 0601153N. Dr. Harold Guard (ONR Code 331) was the Program Manager.

The remainder of the work reported here was performed under CDNSWC Work Unit Number 6340-300 for the Office of Naval Research Applied Research Program for Environmental Quality, PE 0602121N. Dr. Harold E. Guard (ONR Code 331) is the Program Manager and Mr. Alexander E. Lardis (CDNSWC Code 6301) is the Technical Manager.

# APPENDIX A

# ENERGY BALANCE AND

# DESIGN DATA FOR

# PAWDS TORCH GAS ANALYSIS

# DEFINITION OF SYMBOLS AND ABREVIATIONS

| | |
|---|---|
| DHt | torch specific enthalpy difference spreadsheet output variable |
| gal/min | torch gallons per minute flow rate spreadsheet out variable |
| H | torch outlet product hydrogen atom concentration spreadsheet input variable |
| HO | torch outlet product hydroxyl radical concentration spreadsheet input variable |
| H2 | torch outlet product diatomic hydrogen molecule concentration spreadsheet input variable |
| H2O | torch outlet product water molecule concentration spreadsheet input variable |
| Ht1 | torch inlet reactant molar specific enthalpy spreadsheet input variable |
| Ht2 | torch outlet product molar specific enthalpy spreadsheet output variable |
| Mtorch | torch mass flow rate spreadsheet out variable |
| MWt | torch outlet product mixture molecular weight spreadsheet output variable |
| N | torch outlet product nitrogen atom concentration spreadsheet input variable |
| N2 | torch outlet product diatomic nitrogen molecule concentration spreadsheet input variable |
| NO | torch outlet product nitric oxide concentration spreadsheet input variable |
| NO2 | torch outlet product nitrogen dioxide concentration spreadsheet input variable |
| Ntorch-tot | torch outlet total moles of product mixture spreadsheet output variable |
| O | torch outlet product oxygen atom concentration spreadsheet input variable |
| O2 | torch outlet product diatomic oxygen molecule concentration spreadsheet input variable |
| Power | torch power spreadsheet input variable |
| scfm | torch standard cubic feet per minute flow rate spreadsheet out variable |
| Ttorch | torch temperature spreadsheet input variable |

| | |
|---|---|
| *F* | torch temperature in degrees Fahrenheit |
| *K* | torch temperature in degrees Kelvin |
| *kg* | torch mass units in S.I. |
| *kgmole* | torch molar concentration units in S.I. |
| *kJ* | torch energy units in S.I. |
| *kW* | torch power units in S.I. |
| *lb* | torch mass units in |
| *sec* | torch time in seconds |
| *hr* | torch time in hours |

# 50 kW CASE

| | | | | | | | | |
|---|---|---|---|---|---|---|---|---|
| Power | **50** | *kW* | | | | | | |
| **Ttorch** | ***K*** | **3007** | **3510** | **4000** | **4500** | **5000** | **5500** | **6000** |
| | *F* | 4952.6 | 5858 | 6740 | 7640 | 8540 | 9440 | 10340 |
| | | | | | | | | |
| **O2 torch** | | | | | | | | |
| Ht1 | *kJ/kgO2* | 0 | 0 | 0 | 0 | 0 | 0 | 0 |
| O2 | *kgmole* | 1.122E-01 | 4.756E-01 | 1.189E+00 | 1.736E+00 | 1.922E+00 | 1.974E+00 | 1.990E+00 |
| O | *kgmole* | 9.439E-01 | 7.622E-01 | 4.055E-01 | 1.321E-01 | 3.886E-02 | 1.309E-02 | 5.166E-03 |
| Ntorch-tot | *kgmole* | 1.056E+00 | 1.238E+00 | 1.594E+00 | 1.868E+00 | 1.961E+00 | 1.987E+00 | 1.995E+00 |
| MWt | *kg/kgmole* | 30.299 | 25.851 | 20.069 | 17.131 | 16.317 | 16.105 | 16.041 |
| Ht2 | *kJ/kgprod* | 3966 | 7519 | 13910 | 18970 | 21150 | 22250 | 23070 |
| Ht2 | *kJ/kgO2* | 3.966E+03 | 7.519E+03 | 1.391E+04 | 1.897E+04 | 2.115E+04 | 2.225E+04 | 2.307E+04 |
| DHt | *kJ/kgO2* | 3.966E+03 | 7.519E+03 | 1.391E+04 | 1.897E+04 | 2.115E+04 | 2.225E+04 | 2.307E+04 |
| Mtorch | *kg O2/sec* | 1.261E-02 | 6.650E-03 | 3.595E-03 | 2.636E-03 | 2.364E-03 | 2.247E-03 | 2.167E-03 |
| | ***lb O2/hr*** | **100.06** | **52.78** | **28.53** | **20.92** | **18.76** | **17.84** | **17.20** |
| | | | | | | | | |
| **H2O torch** | | | | | | | | |
| Ht1 | *kJ/kgH2O* | -15860 | -15860 | -15860 | -15860 | -15860 | -15860 | -15860 |
| H | *kgmole* | 6.767E-02 | 4.085E-01 | 1.183E+00 | 1.726E+00 | 1.910E+00 | 1.966E+00 | 1.985E+00 |
| HO | *kgmole* | 1.081E-01 | 2.405E-01 | 2.066E-01 | 8.189E-02 | 2.798E-02 | 1.066E-02 | 4.656E-03 |
| H2 | *kgmole* | 1.582E-01 | 2.995E-01 | 2.362E-01 | 8.997E-02 | 3.034E-02 | 1.147E-02 | 4.990E-03 |
| H2O | *kgmole* | 7.539E-01 | 3.760E-01 | 6.922E-02 | 5.895E-03 | 5.286E-04 | 6.552E-05 | 1.114E-05 |
| O | *kgmole* | 2.846E-02 | 1.923E-01 | 5.892E-01 | 8.681E-01 | 9.586E-01 | 9.849E-01 | 9.936E-01 |
| O2 | *kgmole* | 5.475E-02 | 9.561E-02 | 6.753E-02 | 2.208E-02 | 6.459E-03 | 2.176E-03 | 8.596E-04 |
| Ntorch-tot | *kgmole* | 1.171E+00 | 1.612E+00 | 2.351E+00 | 2.794E+00 | 2.934E+00 | 2.976E+00 | 2.989E+00 |
| MWt | *kg/kgmole* | 1.538E+01 | 1.117E+01 | 7.662E+00 | 6.447E+00 | 6.140E+00 | 6.055E+00 | 6.026E+00 |
| Ht2 | *kJ/kgprod* | - 1.467E+03 | 1.239E+04 | 3.392E+04 | 4.729E+04 | 5.268E+04 | 5.552E+04 | 5.765E+04 |
| Ht2 | *kg/kgH2O* | - 1.468E+03 | 1.240E+04 | 3.395E+04 | 4.733E+04 | 5.273E+04 | 5.557E+04 | 5.770E+04 |
| DHt | *kJ/kgH2O* | 1.439E+04 | 2.826E+04 | 4.981E+04 | 6.319E+04 | 6.859E+04 | 7.143E+04 | 7.356E+04 |
| Mtorch | *kg H2O/sec* | 3.474E-03 | 1.769E-03 | 1.004E-03 | 7.913E-04 | 7.290E-04 | 7.000E-04 | 6.797E-04 |
| | ***lb H2O/hr*** | **27.57** | **14.04** | **7.97** | **6.28** | **5.79** | **5.56** | **5.39** |
| | | | | | | | | |
| **AIR torch** | | | | | | | | |
| Ht1 | *kJ/kgAIR* | -0.137 | -0.137 | -0.137 | -0.137 | -0.137 | -0.137 | -0.137 |
| N | *kgmole* | 5.806E-05 | 9.460E-04 | 7.838E-03 | 4.052E-02 | 1.502E-01 | 4.371E-01 | 1.054E+00 |
| NO | *kgmole* | 2.071E-01 | 2.693E-01 | 2.349E-01 | 1.615E-01 | 1.077E-01 | 7.359E-02 | 5.071E-02 |
| NO2 | *kgmole* | 9.312E-05 | 6.645E-05 | 2.612E-05 | 7.449E-06 | 2.231E-06 | 7.604E-07 | 2.824E-07 |
| N2 | *kgmole* | 3.656E+00 | 3.625E+00 | 3.639E+00 | 3.659E+00 | 3.631E+00 | 3.505E+00 | 3.208E+00 |
| O | *kgmole* | 2.200E-01 | 7.699E-01 | 1.426E+00 | 1.750E+00 | 1.867E+00 | 1.918E+00 | 1.946E+00 |
| O2 | *kgmole* | 7.864E-01 | 4.803E-01 | 1.697E-01 | 4.433E-02 | 1.247E-02 | 4.137E-03 | 1.575E-03 |
| Ntorch-tot | *kgmole* | 4.870E+00 | 5.145E+00 | 5.477E+00 | 5.655E+00 | 5.769E+00 | 5.938E+00 | 6.260E+00 |
| MWt | *kg/kgmole* | 2.820E+01 | 2.669E+01 | 2.508E+01 | 2.428E+01 | 2.381E+01 | 2.313E+01 | 2.194E+01 |
| Ht2 | *kJ/kgprod* | 3.800E+03 | 5.530E+03 | 7.424E+03 | 8.771E+03 | 1.002E+04 | 1.181E+04 | 1.476E+04 |
| Ht2 | *kg/kgAIR* | 3.800E+03 | 5.530E+03 | 7.424E+03 | 8.771E+03 | 1.002E+04 | 1.181E+04 | 1.476E+04 |

| | | | | | | | | |
|---|---|---|---|---|---|---|---|---|
| DHt | *kJ/kgAIR* | 3.800E+03 | 5.530E+03 | 7.424E+03 | 8.771E+03 | 1.002E+04 | 1.181E+04 | 1.476E+04 |
| Mtorch | *kg AIR/sec* | 1.316E-02 | 9.041E-03 | 6.735E-03 | 5.701E-03 | 4.990E-03 | 4.234E-03 | 3.388E-03 |
| | ***lb AIR/hr*** | **104.43** | **71.76** | **53.45** | **45.24** | **39.60** | **33.60** | **26.89** |
| Power | **50** | *kW* | | | | | | |
| **Ttorch** | *R* | **3000** | **3500** | **4000** | **4500** | **5000** | **5500** | **6000** |
| | ***F*** | 4940 | 5840 | 6740 | 7640 | 8540 | 9440 | 10340 |

**N2 torch**

| | | | | | | | | |
|---|---|---|---|---|---|---|---|---|
| Ht1 | *kJ/kgN2* | -1.36E-01 | -1.36E-01 | -1.36E-01 | -1.36E-01 | -1.36E-01 | -1.36E-01 | -1.36E-01 |
| N2 | *kgmole* | 1.000E+00 | 9.999E-01 | 9.991E-01 | 9.955E-01 | 9.836E-01 | 9.521E-01 | 8.832E-01 |
| N | *kgmole* | 1.376E-05 | 2.190E-04 | 1.756E-03 | 8.908E-03 | 3.281E-02 | 9.570E-02 | 2.336E-01 |
| Ntorch-tot | *kgmole* | 1.000E+00 | 1.000E+00 | 1.001E+00 | 1.004E+00 | 1.016E+00 | 1.048E+00 | 1.117E+00 |
| MWt | *kg/kgmole* | 2.801E+01 | 2.801E+01 | 2.799E+01 | 2.789E+01 | 2.756E+01 | 2.673E+01 | 2.508E+01 |
| Ht2 | *kJ/kgprod* | 3.311E+03 | 3.978E+03 | 4.674E+03 | 5.471E+03 | 6.565E+03 | 8.350E+03 | 1.148E+04 |
| Ht2 | *kJ/kgN2* | 3.313E+03 | 3.980E+03 | 4.676E+03 | 5.474E+03 | 6.568E+03 | 8.354E+03 | 1.149E+04 |
| DHt | *kJ/kgN2* | 3.313E+03 | 3.980E+03 | 4.676E+03 | 5.474E+03 | 6.568E+03 | 8.354E+03 | 1.149E+04 |
| Mtorch | *kg N2/sec* | 1.509E-02 | 1.256E-02 | 1.069E-02 | 9.135E-03 | 7.612E-03 | 5.985E-03 | 4.353E-03 |
| | ***lb N2/hr*** | **119.79** | **99.71** | **84.86** | **72.50** | **60.42** | **47.50** | **34.55** |

**Ar torch**

| | | | | | | | | |
|---|---|---|---|---|---|---|---|---|
| Ht1 | *kJ/kgAr* | -9.85E-02 | -9.85E-02 | -9.85E-02 | -9.85E-02 | -9.85E-02 | -9.85E-02 | -9.85E-02 |
| Ar | *kgmole* | 1.000E+00 | 1.000E+00 | 1.000E+00 | 1.000E+00 | 1.000E+00 | 1.000E+00 | 1.000E+00 |
| Ntorch-tot | *kgmole* | 1.000E+00 | 1.000E+00 | 1.000E+00 | 1.000E+00 | 1.000E+00 | 1.000E+00 | 1.000E+00 |
| MWt | *kg/kgmole* | 3.994E+01 | 3.994E+01 | 3.994E+01 | 3.994E+01 | 3.994E+01 | 3.994E+01 | 3.994E+01 |
| Ht2 | *kJ/kgprod* | 1.467E+03 | 1.666E+03 | 1.926E+03 | 2.186E+03 | 2.447E+03 | 2.707E+03 | 2.967E+03 |
| Ht2 | *kJ/kgAr* | 1.467E+03 | 1.666E+03 | 1.926E+03 | 2.186E+03 | 2.447E+03 | 2.707E+03 | 2.967E+03 |
| DHt | *kJ/kgAr* | 1.467E+03 | 1.666E+03 | 1.926E+03 | 2.186E+03 | 2.447E+03 | 2.707E+03 | 2.967E+03 |
| Mtorch | *kg Ar/sec* | 3.408E-02 | 3.001E-02 | 2.596E-02 | 2.287E-02 | 2.043E-02 | 1.847E-02 | 1.685E-02 |
| | ***lb Ar/hr*** | **270.49** | **238.18** | **206.03** | **181.52** | **162.16** | **146.59** | **133.74** |

# 100 kW CASE

| Power | **100** | *kW* | | | | | | |
|---|---|---|---|---|---|---|---|---|
| **Ttorch** | ***K*** | **3007** | **3510** | **4000** | **4500** | **5000** | **5500** | **6000** |
| | *F* | 4952.6 | 5858 | 6740 | 7640 | 8540 | 9440 | 10340 |
| | | | | | | | | |
| **O2 torch** | | | | | | | | |
| Ht1 | *kJ/kgO2* | 0 | 0 | 0 | 0 | 0 | 0 | 0 |
| O2 | *kgmole* | 1.122E-01 | 4.756E-01 | 1.189E+00 | 1.736E+00 | 1.922E+00 | 1.974E+00 | 1.990E+00 |
| O | *kgmole* | 9.439E-01 | 7.622E-01 | 4.055E-01 | 1.321E-01 | 3.886E-02 | 1.309E-02 | 5.166E-03 |
| Ntorch-tot | *kgmole* | 1.056E+00 | 1.238E+00 | 1.594E+00 | 1.868E+00 | 1.961E+00 | 1.987E+00 | 1.995E+00 |
| MWt | *kg/kgmole* | 30.299 | 25.851 | 20.069 | 17.131 | 16.317 | 16.105 | 16.041 |
| Ht2 | *kJ/kgprod* | 3966 | 7519 | 13910 | 18970 | 21150 | 22250 | 23070 |
| Ht2 | *kJ/kgO2* | 3.966E+03 | 7.519E+03 | 1.391E+04 | 1.897E+04 | 2.115E+04 | 2.225E+04 | 2.307E+04 |
| DHt | *kJ/kgO2* | 3.966E+03 | 7.519E+03 | 1.391E+04 | 1.897E+04 | 2.115E+04 | 2.225E+04 | 2.307E+04 |
| Mtorch | *kg O2/sec* | 2.521E-02 | 1.330E-02 | 7.189E-03 | 5.272E-03 | 4.728E-03 | 4.494E-03 | 4.335E-03 |
| | ***lb O2/hr*** | **200.12** | **105.56** | **57.06** | **41.84** | **37.53** | **35.67** | **34.40** |
| | | | | | | | | |
| **H2O torch** | | | | | | | | |
| Ht1 | *kJ/kgH2O* | -15860 | -15860 | -15860 | -15860 | -15860 | -15860 | -15860 |
| H | *kgmole* | 6.767E-02 | 4.085E-01 | 1.183E+00 | 1.726E+00 | 1.910E+00 | 1.966E+00 | 1.985E+00 |
| HO | *kgmole* | 1.081E-01 | 2.405E-01 | 2.066E-01 | 8.189E-02 | 2.798E-02 | 1.066E-02 | 4.656E-03 |
| H2 | *kgmole* | 1.582E-01 | 2.995E-01 | 2.362E-01 | 8.997E-02 | 3.034E-02 | 1.147E-02 | 4.990E-03 |
| H2O | *kgmole* | 7.539E-01 | 3.760E-01 | 6.922E-02 | 5.895E-03 | 5.286E-04 | 6.552E-05 | 1.114E-05 |
| O | *kgmole* | 2.846E-02 | 1.923E-01 | 5.892E-01 | 8.681E-01 | 9.586E-01 | 9.849E-01 | 9.936E-01 |
| O2 | *kgmole* | 5.475E-02 | 9.561E-02 | 6.753E-02 | 2.208E-02 | 6.459E-03 | 2.176E-03 | 8.596E-04 |
| Ntorch-tot | *kgmole* | 1.171E+00 | 1.612E+00 | 2.351E+00 | 2.794E+00 | 2.934E+00 | 2.976E+00 | 2.989E+00 |
| MWt | *kg/kgmole* | 1.538E+01 | 1.117E+01 | 7.662E+00 | 6.447E+00 | 6.140E+00 | 6.055E+00 | 6.026E+00 |
| Ht2 | *kJ/kgprod* | -1.467E+03 | 1.239E+04 | 3.392E+04 | 4.729E+04 | 5.268E+04 | 5.552E+04 | 5.765E+04 |
| Ht2 | *kg/kgH2O* | -1.468E+03 | 1.240E+04 | 3.395E+04 | 4.733E+04 | 5.273E+04 | 5.557E+04 | 5.770E+04 |
| DHt | *kJ/kgH2O* | 1.439E+04 | 2.826E+04 | 4.981E+04 | 6.319E+04 | 6.859E+04 | 7.143E+04 | 7.356E+04 |
| Mtorch | *kg H2O/sec* | 6.948E-03 | 3.539E-03 | 2.008E-03 | 1.583E-03 | 1.458E-03 | 1.400E-03 | 1.359E-03 |
| | ***lb H2O/hr*** | **55.15** | **28.08** | **15.93** | **12.56** | **11.57** | **11.11** | **10.79** |
| | | | | | | | | |
| **AIR torch** | | | | | | | | |
| Ht1 | *kJ/kgAIR* | -0.137 | -0.137 | -0.137 | -0.137 | -0.137 | -0.137 | -0.137 |
| N | *kgmole* | 5.806E-05 | 9.460E-04 | 7.838E-03 | 4.052E-02 | 1.502E-01 | 4.371E-01 | 1.054E+00 |
| NO | *kgmole* | 2.071E-01 | 2.693E-01 | 2.349E-01 | 1.615E-01 | 1.077E-01 | 7.359E-02 | 5.071E-02 |
| NO2 | *kgmole* | 9.312E-05 | 6.645E-05 | 2.612E-05 | 7.449E-06 | 2.231E-06 | 7.604E-07 | 2.824E-07 |
| N2 | *kgmole* | 3.656E+00 | 3.625E+00 | 3.639E+00 | 3.659E+00 | 3.631E+00 | 3.505E+00 | 3.208E+00 |
| O | *kgmole* | 2.200E-01 | 7.699E-01 | 1.426E+00 | 1.750E+00 | 1.867E+00 | 1.918E+00 | 1.946E+00 |
| O2 | *kgmole* | 7.864E-01 | 4.803E-01 | 1.697E-01 | 4.433E-02 | 1.247E-02 | 4.137E-03 | 1.575E-03 |
| Ntorch-tot | *kgmole* | 4.870E+00 | 5.145E+00 | 5.477E+00 | 5.655E+00 | 5.769E+00 | 5.938E+00 | 6.260E+00 |
| MWt | *kg/kgmole* | 2.820E+01 | 2.669E+01 | 2.508E+01 | 2.428E+01 | 2.381E+01 | 2.313E+01 | 2.194E+01 |
| Ht2 | *kJ/kgprod* | 3.800E+03 | 5.530E+03 | 7.424E+03 | 8.771E+03 | 1.002E+04 | 1.181E+04 | 1.476E+04 |
| Ht2 | *kg/kgAIR* | 3.800E+03 | 5.530E+03 | 7.424E+03 | 8.771E+03 | 1.002E+04 | 1.181E+04 | 1.476E+04 |
| DHt | *kJ/kgAIR* | 3.800E+03 | 5.530E+03 | 7.424E+03 | 8.771E+03 | 1.002E+04 | 1.181E+04 | 1.476E+04 |
| Mtorch | *kg AIR/sec* | 2.632E-02 | 1.808E-02 | 1.347E-02 | 1.140E-02 | 9.980E-03 | 8.467E-03 | 6.775E-03 |
| | ***lb AIR/hr*** | **208.85** | **143.52** | **106.90** | **90.49** | **79.21** | **67.20** | **53.77** |

| Power | 100 | kW | | | | | | |
|---|---|---|---|---|---|---|---|---|
| **Ttorch** | *R* | **3000** | **3500** | **4000** | **4500** | **5000** | **5500** | **6000** |
| | *F* | 4940 | 5840 | 6740 | 7640 | 8540 | 9440 | 10340 |
| | | | | | | | | |
| **N2 torch** | | | | | | | | |
| Ht1 | *kJ/kgN2* | -1.36E-01 | -1.36E-01 | -1.36E-01 | -1.36E-01 | -1.36E-01 | -1.36E-01 | -1.36E-01 |
| N2 | *kgmole* | 1.000E+00 | 9.999E-01 | 9.991E-01 | 9.955E-01 | 9.836E-01 | 9.521E-01 | 8.832E-01 |
| N | *kgmole* | 1.376E-05 | 2.190E-04 | 1.756E-03 | 8.908E-03 | 3.281E-02 | 9.570E-02 | 2.336E-01 |
| Ntorch-tot | *kgmole* | 1.000E+00 | 1.000E+00 | 1.001E+00 | 1.004E+00 | 1.016E+00 | 1.048E+00 | 1.117E+00 |
| MWt | *kg/kgmole* | 2.801E+01 | 2.801E+01 | 2.799E+01 | 2.789E+01 | 2.756E+01 | 2.673E+01 | 2.508E+01 |
| Ht2 | *kJ/kgprod* | 3.311E+03 | 3.978E+03 | 4.674E+03 | 5.471E+03 | 6.565E+03 | 8.350E+03 | 1.148E+04 |
| Ht2 | *kJ/kgN2* | 3.313E+03 | 3.980E+03 | 4.676E+03 | 5.474E+03 | 6.568E+03 | 8.354E+03 | 1.149E+04 |
| DHt | *kJ/kgN2* | 3.313E+03 | 3.980E+03 | 4.676E+03 | 5.474E+03 | 6.568E+03 | 8.354E+03 | 1.149E+04 |
| Mtorch | *kg N2/sec* | 3.019E-02 | 2.513E-02 | 2.138E-02 | 1.827E-02 | 1.522E-02 | 1.197E-02 | 8.707E-03 |
| | ***lb N2/hr*** | **239.58** | **199.41** | **169.72** | **144.99** | **120.83** | **95.00** | **69.10** |
| | | | | | | | | |
| **Ar torch** | | | | | | | | |
| Ht1 | *kJ/kgAr* | -9.85E-02 | -9.85E-02 | -9.85E-02 | -9.85E-02 | -9.85E-02 | -9.85E-02 | -9.85E-02 |
| Ar | *kgmole* | 1.000E+00 | 1.000E+00 | 1.000E+00 | 1.000E+00 | 1.000E+00 | 1.000E+00 | 1.000E+00 |
| Ntorch-tot | *kgmole* | 1.000E+00 | 1.000E+00 | 1.000E+00 | 1.000E+00 | 1.000E+00 | 1.000E+00 | 1.000E+00 |
| MWt | *kg/kgmole* | 3.994E+01 | 3.994E+01 | 3.994E+01 | 3.994E+01 | 3.994E+01 | 3.994E+01 | 3.994E+01 |
| Ht2 | *kJ/kgprod* | 1.467E+03 | 1.666E+03 | 1.926E+03 | 2.186E+03 | 2.447E+03 | 2.707E+03 | 2.967E+03 |
| Ht2 | *kJ/kgAr* | 1.467E+03 | 1.666E+03 | 1.926E+03 | 2.186E+03 | 2.447E+03 | 2.707E+03 | 2.967E+03 |
| DHt | *kJ/kgAr* | 1.467E+03 | 1.666E+03 | 1.926E+03 | 2.186E+03 | 2.447E+03 | 2.707E+03 | 2.967E+03 |
| Mtorch | *kg Ar/sec* | 6.816E-02 | 6.002E-02 | 5.192E-02 | 4.574E-02 | 4.086E-02 | 3.694E-02 | 3.370E-02 |
| | ***lb Ar/hr*** | **540.97** | **476.36** | **412.06** | **363.05** | **324.33** | **293.18** | **267.49** |
| | | | | | | | | |
| | **enriched AIR torch** | | | | | | | |
| Ht1 | *kJ/kgAIR* | -0.137 | -0.137 | -0.137 | -0.137 | -0.137 | -0.137 | -0.137 |
| N | *kgmole* | 1.926E-05 | 3.186E-04 | 2.740E-03 | 1.459E-02 | 5.462E-02 | 1.581E-01 | 3.733E-01 |
| NO | *kgmole* | 1.107E-01 | 1.554E-01 | 1.529E-01 | 1.127E-01 | 7.653E-02 | 5.228E-02 | 3.573E-02 |
| NO2 | *kgmole* | 8.013E-05 | 6.566E-05 | 3.165E-05 | 1.007E-05 | 3.096E-06 | 1.061E-06 | 3.958E-07 |
| N2 | *kgmole* | 9.446E-01 | 9.221E-01 | 9.222E-01 | 9.363E-01 | 9.344E-01 | 8.948E-01 | 7.955E-01 |
| O | *kgmole* | 1.510E-01 | 5.879E-01 | 1.280E+00 | 1.719E+00 | 1.875E+00 | 1.931E+00 | 1.958E+00 |
| O2 | *kgmole* | 8.691E-01 | 6.283E-01 | 2.836E-01 | 8.435E-02 | 2.445E-02 | 8.179E-03 | 3.152E-03 |
| Ntorch-tot | *kgmole* | 2.075E+00 | 2.294E+00 | 2.641E+00 | 2.867E+00 | 2.965E+00 | 3.045E+00 | 3.166E+00 |
| MWt | *kg/kgmole* | 28.915 | 26.16 | 22.722 | 20.936 | 20.243 | 19.711 | 18.958 |
| Ht2 | *kJ/kgprod* | 3.992E+03 | 6.579E+03 | 1.022E+04 | 1.281E+04 | 1.442E+04 | 1.616E+04 | 1.872E+04 |
| Ht2 | *kg/kgAIR* | 3.993E+03 | 6.580E+03 | 1.022E+04 | 1.281E+04 | 1.442E+04 | 1.616E+04 | 1.872E+04 |
| DHt | *kJ/kgAIR* | 3.993E+03 | 6.581E+03 | 1.022E+04 | 1.281E+04 | 1.442E+04 | 1.616E+04 | 1.872E+04 |
| Mtorch | *kg AIR/sec* | 2.504E-02 | 1.520E-02 | 9.782E-03 | 7.804E-03 | 6.933E-03 | 6.187E-03 | 5.341E-03 |
| | ***lb AIR/hr*** | **198.77** | **120.61** | **77.64** | **61.94** | **55.03** | **49.10** | **42.39** |
| *Scfm* | **O2 torch** | 40.85 | 21.55 | 11.65 | 8.54 | 7.66 | 7.28 | 7.02 |
| *gal/min* | **H2O torch** | 0.11 | 0.06 | 0.03 | 0.03 | 0.02 | 0.02 | 0.02 |
| *Scfm* | **AIR torch** | 47.31 | 32.51 | 24.21 | 20.50 | 17.94 | 15.22 | 12.18 |
| *Scfm* | **N2 torch** | 55.89 | 46.52 | 39.59 | 33.83 | 28.19 | 22.16 | 16.12 |
| *Scfm* | **Ar torch** | 88.47 | 77.90 | 67.39 | 59.37 | 53.04 | 47.95 | 43.74 |
| *Scfm* | **enriched** | 43.28 | 26.26 | 16.91 | 13.49 | 11.98 | 10.69 | 9.23 |

# 150 kW CASE

| Power | 150 | *kW* | | | | | | |
|---|---|---|---|---|---|---|---|---|
| **Ttorch** | ***K*** | **3007** | **3510** | **4000** | **4500** | **5000** | **5500** | **6000** |
| | *F* | 4952.6 | 5858 | 6740 | 7640 | 8540 | 9440 | 10340 |
| | | | | | | | | |
| **O2 torch** | | | | | | | | |
| Ht1 | *kJ/kgO2* | 0 | 0 | 0 | 0 | 0 | 0 | 0 |
| O2 | *kgmole* | 1.122E-01 | 4.756E-01 | 1.189E+00 | 1.736E+00 | 1.922E+00 | 1.974E+00 | 1.990E+00 |
| O | *kgmole* | 9.439E-01 | 7.622E-01 | 4.055E-01 | 1.321E-01 | 3.886E-02 | 1.309E-02 | 5.166E-03 |
| Ntorch-tot | *kgmole* | 1.056E+00 | 1.238E+00 | 1.594E+00 | 1.868E+00 | 1.961E+00 | 1.987E+00 | 1.995E+00 |
| MWt | *kg/kgmole* | 30.299 | 25.851 | 20.069 | 17.131 | 16.317 | 16.105 | 16.041 |
| Ht2 | *kJ/kgprod* | 3966 | 7519 | 13910 | 18970 | 21150 | 22250 | 23070 |
| Ht2 | *kJ/kgO2* | 3.966E+03 | 7.519E+03 | 1.391E+04 | 1.897E+04 | 2.115E+04 | 2.225E+04 | 2.307E+04 |
| DHt | *kJ/kgO2* | 3.966E+03 | 7.519E+03 | 1.391E+04 | 1.897E+04 | 2.115E+04 | 2.225E+04 | 2.307E+04 |
| Mtorch | *kg O2/sec* | 3.782E-02 | 1.995E-02 | 1.078E-02 | 7.907E-03 | 7.092E-03 | 6.742E-03 | 6.502E-03 |
| | ***lb O2/hr*** | **300.18** | **158.34** | **85.59** | **62.76** | **56.29** | **53.51** | **51.60** |
| | | | | | | | | |
| **H2O torch** | | | | | | | | |
| Ht1 | *kJ/kgH2O* | -15860 | -15860 | -15860 | -15860 | -15860 | -15860 | -15860 |
| H | *kgmole* | 6.767E-02 | 4.085E-01 | 1.183E+00 | 1.726E+00 | 1.910E+00 | 1.966E+00 | 1.985E+00 |
| HO | *kgmole* | 1.081E-01 | 2.405E-01 | 2.066E-01 | 8.189E-02 | 2.798E-02 | 1.066E-02 | 4.656E-03 |
| H2 | *kgmole* | 1.582E-01 | 2.995E-01 | 2.362E-01 | 8.997E-02 | 3.034E-02 | 1.147E-02 | 4.990E-03 |
| H2O | *kgmole* | 7.539E-01 | 3.760E-01 | 6.922E-02 | 5.895E-03 | 5.286E-04 | 6.552E-05 | 1.114E-05 |
| O | *kgmole* | 2.846E-02 | 1.923E-01 | 5.892E-01 | 8.681E-01 | 9.586E-01 | 9.849E-01 | 9.936E-01 |
| O2 | *kgmole* | 5.475E-02 | 9.561E-02 | 6.753E-02 | 2.208E-02 | 6.459E-03 | 2.176E-03 | 8.596E-04 |
| Ntorch-tot | *kgmole* | 1.171E+00 | 1.612E+00 | 2.351E+00 | 2.794E+00 | 2.934E+00 | 2.976E+00 | 2.989E+00 |
| MWt | *kg/kgmole* | 1.538E+01 | 1.117E+01 | 7.662E+00 | 6.447E+00 | 6.140E+00 | 6.055E+00 | 6.026E+00 |
| Ht2 | *kJ/kgprod* | -1.467E+03 | 1.239E+04 | 3.392E+04 | 4.729E+04 | 5.268E+04 | 5.552E+04 | 5.765E+04 |
| Ht2 | *kg/kgH2O* | -1.468E+03 | 1.240E+04 | 3.395E+04 | 4.733E+04 | 5.273E+04 | 5.557E+04 | 5.770E+04 |
| DHt | *kJ/kgH2O* | 1.439E+04 | 2.826E+04 | 4.981E+04 | 6.319E+04 | 6.859E+04 | 7.143E+04 | 7.356E+04 |
| Mtorch | *kg H2O/sec* | 1.042E-02 | 5.308E-03 | 3.011E-03 | 2.374E-03 | 2.187E-03 | 2.100E-03 | 2.039E-03 |
| | ***lb H2O/hr*** | **82.72** | **42.13** | **23.90** | **18.84** | **17.36** | **16.67** | **16.18** |
| | | | | | | | | |
| **AIR torch** | | | | | | | | |
| Ht1 | *kJ/kgAIR* | -0.137 | -0.137 | -0.137 | -0.137 | -0.137 | -0.137 | -0.137 |
| N | *kgmole* | 5.806E-05 | 9.460E-04 | 7.838E-03 | 4.052E-02 | 1.502E-01 | 4.371E-01 | 1.054E+00 |
| NO | *kgmole* | 2.071E-01 | 2.693E-01 | 2.349E-01 | 1.615E-01 | 1.077E-01 | 7.359E-02 | 5.071E-02 |
| NO2 | *kgmole* | 9.312E-05 | 6.645E-05 | 2.612E-05 | 7.449E-06 | 2.231E-06 | 7.604E-07 | 2.824E-07 |
| N2 | *kgmole* | 3.656E+00 | 3.625E+00 | 3.639E+00 | 3.659E+00 | 3.631E+00 | 3.505E+00 | 3.208E+00 |
| O | *kgmole* | 2.200E-01 | 7.699E-01 | 1.426E+00 | 1.750E+00 | 1.867E+00 | 1.918E+00 | 1.946E+00 |
| O2 | *kgmole* | 7.864E-01 | 4.803E-01 | 1.697E-01 | 4.433E-02 | 1.247E-02 | 4.137E-03 | 1.575E-03 |
| Ntorch-tot | *kgmole* | 4.870E+00 | 5.145E+00 | 5.477E+00 | 5.655E+00 | 5.769E+00 | 5.938E+00 | 6.260E+00 |
| MWt | *kg/kgmole* | 2.820E+01 | 2.669E+01 | 2.508E+01 | 2.428E+01 | 2.381E+01 | 2.313E+01 | 2.194E+01 |
| Ht2 | *kJ/kgprod* | 3.800E+03 | 5.530E+03 | 7.424E+03 | 8.771E+03 | 1.002E+04 | 1.181E+04 | 1.476E+04 |
| Ht2 | *kg/kgAIR* | 3.800E+03 | 5.530E+03 | 7.424E+03 | 8.771E+03 | 1.002E+04 | 1.181E+04 | 1.476E+04 |
| DHt | *kJ/kgAIR* | 3.800E+03 | 5.530E+03 | 7.424E+03 | 8.771E+03 | 1.002E+04 | 1.181E+04 | 1.476E+04 |
| Mtorch | *kg AIR/sec* | 3.947E-02 | 2.712E-02 | 2.020E-02 | 1.710E-02 | 1.497E-02 | 1.270E-02 | 1.016E-02 |
| | ***lb AIR/hr*** | **313.28** | **215.27** | **160.36** | **135.73** | **118.81** | **100.80** | **80.66** |

| Power | **150** | *kW* | | | | | | |
|---|---|---|---|---|---|---|---|---|
| **Ttorch** | *R* | **3000** | **3500** | **4000** | **4500** | **5000** | **5500** | **6000** |
| | ***F*** | 4940 | 5840 | 6740 | 7640 | 8540 | 9440 | 10340 |

| **N2 torch** | | | | | | | | |
|---|---|---|---|---|---|---|---|---|
| Ht1 | *kJ/kgN2* | -1.36E-01 | -1.36E-01 | -1.36E-01 | -1.36E-01 | -1.36E-01 | -1.36E-01 | -1.36E-01 |
| N2 | *kgmole* | 1.000E+00 | 9.999E-01 | 9.991E-01 | 9.955E-01 | 9.836E-01 | 9.521E-01 | 8.832E-01 |
| N | *kgmole* | 1.376E-05 | 2.190E-04 | 1.756E-03 | 8.908E-03 | 3.281E-02 | 9.570E-02 | 2.336E-01 |
| Ntorch-tot | *kgmole* | 1.000E+00 | 1.000E+00 | 1.001E+00 | 1.004E+00 | 1.016E+00 | 1.048E+00 | 1.117E+00 |
| MWt | *kg/kgmole* | 2.801E+01 | 2.801E+01 | 2.799E+01 | 2.789E+01 | 2.756E+01 | 2.673E+01 | 2.508E+01 |
| Ht2 | *kJ/kgprod* | 3.311E+03 | 3.978E+03 | 4.674E+03 | 5.471E+03 | 6.565E+03 | 8.350E+03 | 1.148E+04 |
| Ht2 | *kJ/kgN2* | 3.313E+03 | 3.980E+03 | 4.676E+03 | 5.474E+03 | 6.568E+03 | 8.354E+03 | 1.149E+04 |
| DHt | *kJ/kgN2* | 3.313E+03 | 3.980E+03 | 4.676E+03 | 5.474E+03 | 6.568E+03 | 8.354E+03 | 1.149E+04 |
| Mtorch | *kg N2/sec* | 4.528E-02 | 3.769E-02 | 3.208E-02 | 2.740E-02 | 2.284E-02 | 1.796E-02 | 1.306E-02 |
| | ***lb N2/hr*** | **359.37** | **299.12** | **254.57** | **217.49** | **181.25** | **142.50** | **103.65** |

| **Ar torch** | | | | | | | | |
|---|---|---|---|---|---|---|---|---|
| Ht1 | *kJ/kgAr* | -9.85E-02 | -9.85E-02 | -9.85E-02 | -9.85E-02 | -9.85E-02 | -9.85E-02 | -9.85E-02 |
| Ar | *kgmole* | 1.000E+00 | 1.000E+00 | 1.000E+00 | 1.000E+00 | 1.000E+00 | 1.000E+00 | 1.000E+00 |
| Ntorch-tot | *kgmole* | 1.000E+00 | 1.000E+00 | 1.000E+00 | 1.000E+00 | 1.000E+00 | 1.000E+00 | 1.000E+00 |
| MWt | *kg/kgmole* | 3.994E+01 | 3.994E+01 | 3.994E+01 | 3.994E+01 | 3.994E+01 | 3.994E+01 | 3.994E+01 |
| Ht2 | *kJ/kgprod* | 1.467E+03 | 1.666E+03 | 1.926E+03 | 2.186E+03 | 2.447E+03 | 2.707E+03 | 2.967E+03 |
| Ht2 | *kJ/kgAr* | 1.467E+03 | 1.666E+03 | 1.926E+03 | 2.186E+03 | 2.447E+03 | 2.707E+03 | 2.967E+03 |
| DHt | *kJ/kgAr* | 1.467E+03 | 1.666E+03 | 1.926E+03 | 2.186E+03 | 2.447E+03 | 2.707E+03 | 2.967E+03 |
| Mtorch | *kg Ar/sec* | 1.022E-01 | 9.003E-02 | 7.788E-02 | 6.862E-02 | 6.130E-02 | 5.541E-02 | 5.055E-02 |
| | ***lb Ar/hr*** | **811.46** | **714.54** | **618.08** | **544.57** | **486.49** | **439.77** | **401.23** |

| | **enriched AIR torch** | | | | | | | |
|---|---|---|---|---|---|---|---|---|
| Ht1 | *kJ/kgAIR* | -0.137 | -0.137 | -0.137 | -0.137 | -0.137 | -0.137 | -0.137 |
| N | *kgmole* | 1.926E-05 | 3.186E-04 | 2.740E-03 | 1.459E-02 | 5.462E-02 | 1.581E-01 | 3.733E-01 |
| NO | *kgmole* | 1.107E-01 | 1.554E-01 | 1.529E-01 | 1.127E-01 | 7.653E-02 | 5.228E-02 | 3.573E-02 |
| NO2 | *kgmole* | 8.013E-05 | 6.566E-05 | 3.165E-05 | 1.007E-05 | 3.096E-06 | 1.061E-06 | 3.958E-07 |
| N2 | *kgmole* | 9.446E-01 | 9.221E-01 | 9.222E-01 | 9.363E-01 | 9.344E-01 | 8.948E-01 | 7.955E-01 |
| O | *kgmole* | 1.510E-01 | 5.879E-01 | 1.280E+00 | 1.719E+00 | 1.875E+00 | 1.931E+00 | 1.958E+00 |
| O2 | *kgmole* | 8.691E-01 | 6.283E-01 | 2.836E-01 | 8.435E-02 | 2.445E-02 | 8.179E-03 | 3.152E-03 |
| Ntorch-tot | *kgmole* | 2.075E+00 | 2.294E+00 | 2.641E+00 | 2.867E+00 | 2.965E+00 | 3.045E+00 | 3.166E+00 |
| MWt | *kg/kgmole* | 28.915 | 26.16 | 22.722 | 20.936 | 20.243 | 19.711 | 18.958 |
| Ht2 | *kJ/kgprod* | 3.992E+03 | 6.579E+03 | 1.022E+04 | 1.281E+04 | 1.442E+04 | 1.616E+04 | 1.872E+04 |
| Ht2 | *kg/kgAIR* | 3.993E+03 | 6.580E+03 | 1.022E+04 | 1.281E+04 | 1.442E+04 | 1.616E+04 | 1.872E+04 |
| DHt | *kJ/kgAIR* | 3.993E+03 | 6.581E+03 | 1.022E+04 | 1.281E+04 | 1.442E+04 | 1.616E+04 | 1.872E+04 |
| Mtorch | *kg AIR/sec* | 3.757E-02 | 2.279E-02 | 1.467E-02 | 1.171E-02 | 1.040E-02 | 9.280E-03 | 8.011E-03 |
| | ***lb AIR/hr*** | **298.15** | **180.91** | **116.46** | **92.91** | **82.54** | **73.65** | **63.58** |
| *scfm* | **O2 torch** | 61.28 | 32.32 | 17.47 | 12.81 | 11.49 | 10.92 | 10.53 |
| *gal/min* | **H2O torch** | 0.17 | 0.08 | 0.05 | 0.04 | 0.03 | 0.03 | 0.03 |
| *scfm* | **AIR torch** | 70.96 | 48.76 | 36.32 | 30.74 | 26.91 | 22.83 | 18.27 |
| *scfm* | **N2 torch** | 83.84 | 69.78 | 59.39 | 50.74 | 42.29 | 33.25 | 24.18 |
| *scfm* | **Ar torch** | 132.70 | 116.85 | 101.08 | 89.06 | 79.56 | 71.92 | 65.62 |
| *scfm* | **enriched** | 64.92 | 39.39 | 25.36 | 20.23 | 17.97 | 16.04 | 13.84 |

# 200 kW CASE

| Power | 200 | *kW* | | | | | | |
|---|---|---|---|---|---|---|---|---|
| **Ttorch** | ***K*** | **3007** | **3510** | **4000** | **4500** | **5000** | **5500** | **6000** |
| | *F* | 4952.6 | 5858 | 6740 | 7640 | 8540 | 9440 | 10340 |
| | | | | | | | | |
| **O2 torch** | | | | | | | | |
| Ht1 | *kJ/kgO2* | 0 | 0 | 0 | 0 | 0 | 0 | 0 |
| O2 | *kgmole* | 1.122E-01 | 4.756E-01 | 1.189E+00 | 1.736E+00 | 1.922E+00 | 1.974E+00 | 1.990E+00 |
| O | *kgmole* | 9.439E-01 | 7.622E-01 | 4.055E-01 | 1.321E-01 | 3.886E-02 | 1.309E-02 | 5.166E-03 |
| Ntorch-tot | *kgmole* | 1.056E+00 | 1.238E+00 | 1.594E+00 | 1.868E+00 | 1.961E+00 | 1.987E+00 | 1.995E+00 |
| MWt | *kg/kgmole* | 30.299 | 25.851 | 20.069 | 17.131 | 16.317 | 16.105 | 16.041 |
| Ht2 | *kJ/kgprod* | 3966 | 7519 | 13910 | 18970 | 21150 | 22250 | 23070 |
| Ht2 | *kJ/kgO2* | 3.966E+03 | 7.519E+03 | 1.391E+04 | 1.897E+04 | 2.115E+04 | 2.225E+04 | 2.307E+04 |
| DHt | *kJ/kgO2* | 3.966E+03 | 7.519E+03 | 1.391E+04 | 1.897E+04 | 2.115E+04 | 2.225E+04 | 2.307E+04 |
| Mtorch | *kg O2/sec* | 5.043E-02 | 2.660E-02 | 1.438E-02 | 1.054E-02 | 9.456E-03 | 8.989E-03 | 8.669E-03 |
| | ***lb O2/hr*** | **400.24** | **211.11** | **114.12** | **83.68** | **75.05** | **71.34** | **68.81** |
| | | | | | | | | |
| **H2O torch** | | | | | | | | |
| Ht1 | *kJ/kgH2O* | -15860 | -15860 | -15860 | -15860 | -15860 | -15860 | -15860 |
| H | *kgmole* | 6.767E-02 | 4.085E-01 | 1.183E+00 | 1.726E+00 | 1.910E+00 | 1.966E+00 | 1.985E+00 |
| HO | *kgmole* | 1.081E-01 | 2.405E-01 | 2.066E-01 | 8.189E-02 | 2.798E-02 | 1.066E-02 | 4.656E-03 |
| H2 | *kgmole* | 1.582E-01 | 2.995E-01 | 2.362E-01 | 8.997E-02 | 3.034E-02 | 1.147E-02 | 4.990E-03 |
| H2O | *kgmole* | 7.539E-01 | 3.760E-01 | 6.922E-02 | 5.895E-03 | 5.286E-04 | 6.552E-05 | 1.114E-05 |
| O | *kgmole* | 2.846E-02 | 1.923E-01 | 5.892E-01 | 8.681E-01 | 9.586E-01 | 9.849E-01 | 9.936E-01 |
| O2 | *kgmole* | 5.475E-02 | 9.561E-02 | 6.753E-02 | 2.208E-02 | 6.459E-03 | 2.176E-03 | 8.596E-04 |
| Ntorch-tot | *kgmole* | 1.171E+00 | 1.612E+00 | 2.351E+00 | 2.794E+00 | 2.934E+00 | 2.976E+00 | 2.989E+00 |
| MWt | *kg/kgmole* | 1.538E+01 | 1.117E+01 | 7.662E+00 | 6.447E+00 | 6.140E+00 | 6.055E+00 | 6.026E+00 |
| Ht2 | *kJ/kgprod* | - 1.467E+03 | 1.239E+04 | 3.392E+04 | 4.729E+04 | 5.268E+04 | 5.552E+04 | 5.765E+04 |
| Ht2 | *kg/kgH2O* | - 1.468E+03 | 1.240E+04 | 3.395E+04 | 4.733E+04 | 5.273E+04 | 5.557E+04 | 5.770E+04 |
| DHt | *kJ/kgH2O* | 1.439E+04 | 2.826E+04 | 4.981E+04 | 6.319E+04 | 6.859E+04 | 7.143E+04 | 7.356E+04 |
| Mtorch | *kg H2O/sec* | 1.390E-02 | 7.077E-03 | 4.015E-03 | 3.165E-03 | 2.916E-03 | 2.800E-03 | 2.719E-03 |
| | ***lb H2O/hr*** | **110.29** | **56.17** | **31.87** | **25.12** | **23.14** | **22.22** | **21.58** |
| | | | | | | | | |
| **AIR torch** | | | | | | | | |
| Ht1 | *kJ/kgAIR* | -0.137 | -0.137 | -0.137 | -0.137 | -0.137 | -0.137 | -0.137 |
| N | *kgmole* | 5.806E-05 | 9.460E-04 | 7.838E-03 | 4.052E-02 | 1.502E-01 | 4.371E-01 | 1.054E+00 |
| NO | *kgmole* | 2.071E-01 | 2.693E-01 | 2.349E-01 | 1.615E-01 | 1.077E-01 | 7.359E-02 | 5.071E-02 |
| NO2 | *kgmole* | 9.312E-05 | 6.645E-05 | 2.612E-05 | 7.449E-06 | 2.231E-06 | 7.604E-07 | 2.824E-07 |
| N2 | *kgmole* | 3.656E+00 | 3.625E+00 | 3.639E+00 | 3.659E+00 | 3.631E+00 | 3.505E+00 | 3.208E+00 |
| O | *kgmole* | 2.200E-01 | 7.699E-01 | 1.426E+00 | 1.750E+00 | 1.867E+00 | 1.918E+00 | 1.946E+00 |
| O2 | *kgmole* | 7.864E-01 | 4.803E-01 | 1.697E-01 | 4.433E-02 | 1.247E-02 | 4.137E-03 | 1.575E-03 |
| Ntorch-tot | *kgmole* | 4.870E+00 | 5.145E+00 | 5.477E+00 | 5.655E+00 | 5.769E+00 | 5.938E+00 | 6.260E+00 |
| MWt | *kg/kgmole* | 2.820E+01 | 2.669E+01 | 2.508E+01 | 2.428E+01 | 2.381E+01 | 2.313E+01 | 2.194E+01 |
| Ht2 | *kJ/kgprod* | 3.800E+03 | 5.530E+03 | 7.424E+03 | 8.771E+03 | 1.002E+04 | 1.181E+04 | 1.476E+04 |
| Ht2 | *kg/kgAIR* | 3.800E+03 | 5.530E+03 | 7.424E+03 | 8.771E+03 | 1.002E+04 | 1.181E+04 | 1.476E+04 |
| DHt | *kJ/kgAIR* | 3.800E+03 | 5.530E+03 | 7.424E+03 | 8.771E+03 | 1.002E+04 | 1.181E+04 | 1.476E+04 |
| Mtorch | *kg AIR/sec* | 5.263E-02 | 3.617E-02 | 2.694E-02 | 2.280E-02 | 1.996E-02 | 1.693E-02 | 1.355E-02 |
| | ***lb AIR/hr*** | **417.71** | **287.03** | **213.81** | **180.97** | **158.41** | **134.40** | **107.54** |

| Power | 200 | *kW* | | | | | | |
|---|---|---|---|---|---|---|---|---|
| **Ttorch** | *R* | **3000** | **3500** | **4000** | **4500** | **5000** | **5500** | **6000** |
| | *F* | 4940 | 5840 | 6740 | 7640 | 8540 | 9440 | 10340 |
| **N2 torch** | | | | | | | | |
| Ht1 | *kJ/kgN2* | -1.36E-01 | -1.36E-01 | -1.36E-01 | -1.36E-01 | -1.36E-01 | -1.36E-01 | -1.36E-01 |
| N2 | *kgmole* | 1.000E+00 | 9.999E-01 | 9.991E-01 | 9.955E-01 | 9.836E-01 | 9.521E-01 | 8.832E-01 |
| N | *kgmole* | 1.376E-05 | 2.190E-04 | 1.756E-03 | 8.908E-03 | 3.281E-02 | 9.570E-02 | 2.336E-01 |
| Ntorch-tot | *kgmole* | 1.000E+00 | 1.000E+00 | 1.001E+00 | 1.004E+00 | 1.016E+00 | 1.048E+00 | 1.117E+00 |
| MWt | *kg/kgmole* | 2.801E+01 | 2.801E+01 | 2.799E+01 | 2.789E+01 | 2.756E+01 | 2.673E+01 | 2.508E+01 |
| Ht2 | *kJ/kgprod* | 3.311E+03 | 3.978E+03 | 4.674E+03 | 5.471E+03 | 6.565E+03 | 8.350E+03 | 1.148E+04 |
| Ht2 | *kJ/kgN2* | 3.313E+03 | 3.980E+03 | 4.676E+03 | 5.474E+03 | 6.568E+03 | 8.354E+03 | 1.149E+04 |
| DHt | *kJ/kgN2* | 3.313E+03 | 3.980E+03 | 4.676E+03 | 5.474E+03 | 6.568E+03 | 8.354E+03 | 1.149E+04 |
| Mtorch | *kg N2/sec* | 6.037E-02 | 5.025E-02 | 4.277E-02 | 3.654E-02 | 3.045E-02 | 2.394E-02 | 1.741E-02 |
| | ***lb N2/hr*** | **479.16** | **398.83** | **339.43** | **289.99** | **241.67** | **190.00** | **138.20** |
| **Ar torch** | | | | | | | | |
| Ht1 | *kJ/kgAr* | -9.85E-02 | -9.85E-02 | -9.85E-02 | -9.85E-02 | -9.85E-02 | -9.85E-02 | -9.85E-02 |
| Ar | *kgmole* | 1.000E+00 | 1.000E+00 | 1.000E+00 | 1.000E+00 | 1.000E+00 | 1.000E+00 | 1.000E+00 |
| Ntorch-tot | *kgmole* | 1.000E+00 | 1.000E+00 | 1.000E+00 | 1.000E+00 | 1.000E+00 | 1.000E+00 | 1.000E+00 |
| MWt | *kg/kgmole* | 3.994E+01 | 3.994E+01 | 3.994E+01 | 3.994E+01 | 3.994E+01 | 3.994E+01 | 3.994E+01 |
| Ht2 | *kJ/kgprod* | 1.467E+03 | 1.666E+03 | 1.926E+03 | 2.186E+03 | 2.447E+03 | 2.707E+03 | 2.967E+03 |
| Ht2 | *kJ/kgAr* | 1.467E+03 | 1.666E+03 | 1.926E+03 | 2.186E+03 | 2.447E+03 | 2.707E+03 | 2.967E+03 |
| DHt | *kJ/kgAr* | 1.467E+03 | 1.666E+03 | 1.926E+03 | 2.186E+03 | 2.447E+03 | 2.707E+03 | 2.967E+03 |
| Mtorch | *kg Ar/sec* | 1.363E-01 | 1.200E-01 | 1.038E-01 | 9.149E-02 | 8.173E-02 | 7.388E-02 | 6.741E-02 |
| | ***lb Ar/hr*** | **1081.95** | **952.72** | **824.11** | **726.10** | **648.65** | **586.35** | **534.97** |
| | **enriched AIR torch** | | | | | | | |
| Ht1 | *kJ/kgAIR* | -0.137 | -0.137 | -0.137 | -0.137 | -0.137 | -0.137 | -0.137 |
| N | *kgmole* | 1.926E-05 | 3.186E-04 | 2.740E-03 | 1.459E-02 | 5.462E-02 | 1.581E-01 | 3.733E-01 |
| NO | *kgmole* | 1.107E-01 | 1.554E-01 | 1.529E-01 | 1.127E-01 | 7.653E-02 | 5.228E-02 | 3.573E-02 |
| NO2 | *kgmole* | 8.013E-05 | 6.566E-05 | 3.165E-05 | 1.007E-05 | 3.096E-06 | 1.061E-06 | 3.958E-07 |
| N2 | *kgmole* | 9.446E-01 | 9.221E-01 | 9.222E-01 | 9.363E-01 | 9.344E-01 | 8.948E-01 | 7.955E-01 |
| O | *kgmole* | 1.510E-01 | 5.879E-01 | 1.280E+00 | 1.719E+00 | 1.875E+00 | 1.931E+00 | 1.958E+00 |
| O2 | *kgmole* | 8.691E-01 | 6.283E-01 | 2.836E-01 | 8.435E-02 | 2.445E-02 | 8.179E-03 | 3.152E-03 |
| Ntorch-tot | *kgmole* | 2.075E+00 | 2.294E+00 | 2.641E+00 | 2.867E+00 | 2.965E+00 | 3.045E+00 | 3.166E+00 |
| MWt | *kg/kgmole* | 28.915 | 26.16 | 22.722 | 20.936 | 20.243 | 19.711 | 18.958 |
| Ht2 | *kJ/kgprod* | 3.992E+03 | 6.579E+03 | 1.022E+04 | 1.281E+04 | 1.442E+04 | 1.616E+04 | 1.872E+04 |
| Ht2 | *kg/kgAIR* | 3.993E+03 | 6.580E+03 | 1.022E+04 | 1.281E+04 | 1.442E+04 | 1.616E+04 | 1.872E+04 |
| DHt | *kJ/kgAIR* | 3.993E+03 | 6.581E+03 | 1.022E+04 | 1.281E+04 | 1.442E+04 | 1.616E+04 | 1.872E+04 |
| Mtorch | *kg AIR/sec* | 5.009E-02 | 3.039E-02 | 1.956E-02 | 1.561E-02 | 1.387E-02 | 1.237E-02 | 1.068E-02 |
| | ***lb AIR/hr*** | **397.53** | **241.21** | **155.28** | **123.88** | **110.05** | **98.20** | **84.77** |
| *scfm* | **O2 torch** | 81.70 | 43.10 | 23.30 | 17.08 | 15.32 | 14.56 | 14.05 |
| *gal/min* | **H2O torch** | 0.22 | 0.11 | 0.06 | 0.05 | 0.05 | 0.04 | 0.04 |
| *scfm* | **AIR torch** | 94.61 | 65.01 | 48.43 | 40.99 | 35.88 | 30.44 | 24.36 |
| *scfm* | **N2 torch** | 111.79 | 93.05 | 79.19 | 67.65 | 56.38 | 44.33 | 32.24 |
| *scfm* | **Ar torch** | 176.94 | 155.81 | 134.77 | 118.74 | 106.08 | 95.89 | 87.49 |
| *scfm* | **enriched** | 86.56 | 52.52 | 33.81 | 26.97 | 23.96 | 21.38 | 18.46 |

# 250 kW CASE

| Power | **250** | *kW* | | | | | | |
|---|---|---|---|---|---|---|---|---|
| **Ttorch** | ***K*** | **3007** | **3510** | **4000** | **4500** | **5000** | **5500** | **6000** |
| | *F* | 4952.6 | 5858 | 6740 | 7640 | 8540 | 9440 | 10340 |
| | | | | | | | | |
| **O2 torch** | | | | | | | | |
| Ht1 | *kJ/kgO2* | 0 | 0 | 0 | 0 | 0 | 0 | 0 |
| O2 | *kgmole* | 1.122E-01 | 4.756E-01 | 1.189E+00 | 1.736E+00 | 1.922E+00 | 1.974E+00 | 1.990E+00 |
| O | *kgmole* | 9.439E-01 | 7.622E-01 | 4.055E-01 | 1.321E-01 | 3.886E-02 | 1.309E-02 | 5.166E-03 |
| Ntorch-tot | *kgmole* | 1.056E+00 | 1.238E+00 | 1.594E+00 | 1.868E+00 | 1.961E+00 | 1.987E+00 | 1.995E+00 |
| MWt | *kg/kgmole* | 30.299 | 25.851 | 20.069 | 17.131 | 16.317 | 16.105 | 16.041 |
| Ht2 | *kJ/kgprod* | 3966 | 7519 | 13910 | 18970 | 21150 | 22250 | 23070 |
| Ht2 | *kJ/kgO2* | 3.966E+03 | 7.519E+03 | 1.391E+04 | 1.897E+04 | 2.115E+04 | 2.225E+04 | 2.307E+04 |
| DHt | *kJ/kgO2* | 3.966E+03 | 7.519E+03 | 1.391E+04 | 1.897E+04 | 2.115E+04 | 2.225E+04 | 2.307E+04 |
| Mtorch | *kg O2/sec* | 6.304E-02 | 3.325E-02 | 1.797E-02 | 1.318E-02 | 1.182E-02 | 1.124E-02 | 1.084E-02 |
| | ***lb O2/hr*** | **500.30** | **263.89** | **142.64** | **104.60** | **93.81** | **89.18** | **86.01** |
| | | | | | | | | |
| **H2O torch** | | | | | | | | |
| Ht1 | *kJ/kgH2O* | -15860 | -15860 | -15860 | -15860 | -15860 | -15860 | -15860 |
| H | *kgmole* | 6.767E-02 | 4.085E-01 | 1.183E+00 | 1.726E+00 | 1.910E+00 | 1.966E+00 | 1.985E+00 |
| HO | *kgmole* | 1.081E-01 | 2.405E-01 | 2.066E-01 | 8.189E-02 | 2.798E-02 | 1.066E-02 | 4.656E-03 |
| H2 | *kgmole* | 1.582E-01 | 2.995E-01 | 2.362E-01 | 8.997E-02 | 3.034E-02 | 1.147E-02 | 4.990E-03 |
| H2O | *kgmole* | 7.539E-01 | 3.760E-01 | 6.922E-02 | 5.895E-03 | 5.286E-04 | 6.552E-05 | 1.114E-05 |
| O | *kgmole* | 2.846E-02 | 1.923E-01 | 5.892E-01 | 8.681E-01 | 9.586E-01 | 9.849E-01 | 9.936E-01 |
| O2 | *kgmole* | 5.475E-02 | 9.561E-02 | 6.753E-02 | 2.208E-02 | 6.459E-03 | 2.176E-03 | 8.596E-04 |
| Ntorch-tot | *kgmole* | 1.171E+00 | 1.612E+00 | 2.351E+00 | 2.794E+00 | 2.934E+00 | 2.976E+00 | 2.989E+00 |
| MWt | *kg/kgmole* | 1.538E+01 | 1.117E+01 | 7.662E+00 | 6.447E+00 | 6.140E+00 | 6.055E+00 | 6.026E+00 |
| Ht2 | *kJ/kgprod* | -1.467E+03 | 1.239E+04 | 3.392E+04 | 4.729E+04 | 5.268E+04 | 5.552E+04 | 5.765E+04 |
| Ht2 | *kg/kgH2O* | -1.468E+03 | 1.240E+04 | 3.395E+04 | 4.733E+04 | 5.273E+04 | 5.557E+04 | 5.770E+04 |
| DHt | *kJ/kgH2O* | 1.439E+04 | 2.826E+04 | 4.981E+04 | 6.319E+04 | 6.859E+04 | 7.143E+04 | 7.356E+04 |
| Mtorch | *kg H2O/sec* | 1.737E-02 | 8.846E-03 | 5.019E-03 | 3.956E-03 | 3.645E-03 | 3.500E-03 | 3.399E-03 |
| | ***lb H2O/hr*** | **137.87** | **70.21** | **39.83** | **31.40** | **28.93** | **27.78** | **26.97** |
| | | | | | | | | |
| **AIR torch** | | | | | | | | |
| Ht1 | *kJ/kgAIR* | -0.137 | -0.137 | -0.137 | -0.137 | -0.137 | -0.137 | -0.137 |
| N | *kgmole* | 5.806E-05 | 9.460E-04 | 7.838E-03 | 4.052E-02 | 1.502E-01 | 4.371E-01 | 1.054E+00 |
| NO | *kgmole* | 2.071E-01 | 2.693E-01 | 2.349E-01 | 1.615E-01 | 1.077E-01 | 7.359E-02 | 5.071E-02 |
| NO2 | *kgmole* | 9.312E-05 | 6.645E-05 | 2.612E-05 | 7.449E-06 | 2.231E-06 | 7.604E-07 | 2.824E-07 |
| N2 | *kgmole* | 3.656E+00 | 3.625E+00 | 3.639E+00 | 3.659E+00 | 3.631E+00 | 3.505E+00 | 3.208E+00 |
| O | *kgmole* | 2.200E-01 | 7.699E-01 | 1.426E+00 | 1.750E+00 | 1.867E+00 | 1.918E+00 | 1.946E+00 |
| O2 | *kgmole* | 7.864E-01 | 4.803E-01 | 1.697E-01 | 4.433E-02 | 1.247E-02 | 4.137E-03 | 1.575E-03 |
| Ntorch-tot | *kgmole* | 4.870E+00 | 5.145E+00 | 5.477E+00 | 5.655E+00 | 5.769E+00 | 5.938E+00 | 6.260E+00 |
| MWt | *kg/kgmole* | 2.820E+01 | 2.669E+01 | 2.508E+01 | 2.428E+01 | 2.381E+01 | 2.313E+01 | 2.194E+01 |
| Ht2 | *kJ/kgprod* | 3.800E+03 | 5.530E+03 | 7.424E+03 | 8.771E+03 | 1.002E+04 | 1.181E+04 | 1.476E+04 |
| Ht2 | *kg/kgAIR* | 3.800E+03 | 5.530E+03 | 7.424E+03 | 8.771E+03 | 1.002E+04 | 1.181E+04 | 1.476E+04 |
| DHt | *kJ/kgAIR* | 3.800E+03 | 5.530E+03 | 7.424E+03 | 8.771E+03 | 1.002E+04 | 1.181E+04 | 1.476E+04 |
| Mtorch | *kg AIR/sec* | 6.579E-02 | 4.521E-02 | 3.367E-02 | 2.850E-02 | 2.495E-02 | 2.117E-02 | 1.694E-02 |
| | ***lb AIR/hr*** | **522.14** | **358.79** | **267.26** | **226.21** | **198.02** | **168.00** | **134.43** |

| Power | **250** | *kW* | | | | | | |
|---|---|---|---|---|---|---|---|---|
| **Ttorch** | *R* | **3000** | **3500** | **4000** | **4500** | **5000** | **5500** | **6000** |
| | ***F*** | 4940 | 5840 | 6740 | 7640 | 8540 | 9440 | 10340 |
| | | | | | | | | |
| **N2 torch** | | | | | | | | |
| Ht1 | *kJ/kgN2* | -1.36E-01 | -1.36E-01 | -1.36E-01 | -1.36E-01 | -1.36E-01 | -1.36E-01 | -1.36E-01 |
| N2 | *kgmole* | 1.000E+00 | 9.999E-01 | 9.991E-01 | 9.955E-01 | 9.836E-01 | 9.521E-01 | 8.832E-01 |
| N | *kgmole* | 1.376E-05 | 2.190E-04 | 1.756E-03 | 8.908E-03 | 3.281E-02 | 9.570E-02 | 2.336E-01 |
| Ntorch-tot | *kgmole* | 1.000E+00 | 1.000E+00 | 1.001E+00 | 1.004E+00 | 1.016E+00 | 1.048E+00 | 1.117E+00 |
| MWt | *kg/kgmole* | 2.801E+01 | 2.801E+01 | 2.799E+01 | 2.789E+01 | 2.756E+01 | 2.673E+01 | 2.508E+01 |
| Ht2 | *kJ/kgprod* | 3.311E+03 | 3.978E+03 | 4.674E+03 | 5.471E+03 | 6.565E+03 | 8.350E+03 | 1.148E+04 |
| Ht2 | *kJ/kgN2* | 3.313E+03 | 3.980E+03 | 4.676E+03 | 5.474E+03 | 6.568E+03 | 8.354E+03 | 1.149E+04 |
| DHt | *kJ/kgN2* | 3.313E+03 | 3.980E+03 | 4.676E+03 | 5.474E+03 | 6.568E+03 | 8.354E+03 | 1.149E+04 |
| Mtorch | *kg N2/sec* | 7.547E-02 | 6.281E-02 | 5.346E-02 | 4.567E-02 | 3.806E-02 | 2.993E-02 | 2.177E-02 |
| | ***lb N2/hr*** | **598.95** | **498.53** | **424.29** | **362.49** | **302.08** | **237.51** | **172.75** |
| | | | | | | | | |
| **Ar torch** | | | | | | | | |
| Ht1 | *kJ/kgAr* | -9.85E-02 | -9.85E-02 | -9.85E-02 | -9.85E-02 | -9.85E-02 | -9.85E-02 | -9.85E-02 |
| Ar | *kgmole* | 1.000E+00 | 1.000E+00 | 1.000E+00 | 1.000E+00 | 1.000E+00 | 1.000E+00 | 1.000E+00 |
| Ntorch-tot | *kgmole* | 1.000E+00 | 1.000E+00 | 1.000E+00 | 1.000E+00 | 1.000E+00 | 1.000E+00 | 1.000E+00 |
| MWt | *kg/kgmole* | 3.994E+01 | 3.994E+01 | 3.994E+01 | 3.994E+01 | 3.994E+01 | 3.994E+01 | 3.994E+01 |
| Ht2 | *kJ/kgprod* | 1.467E+03 | 1.666E+03 | 1.926E+03 | 2.186E+03 | 2.447E+03 | 2.707E+03 | 2.967E+03 |
| Ht2 | *kJ/kgAr* | 1.467E+03 | 1.666E+03 | 1.926E+03 | 2.186E+03 | 2.447E+03 | 2.707E+03 | 2.967E+03 |
| DHt | *kJ/kgAr* | 1.467E+03 | 1.666E+03 | 1.926E+03 | 2.186E+03 | 2.447E+03 | 2.707E+03 | 2.967E+03 |
| Mtorch | *kg Ar/sec* | 1.704E-01 | 1.501E-01 | 1.298E-01 | 1.144E-01 | 1.022E-01 | 9.235E-02 | 8.426E-02 |
| | ***lb Ar/hr*** | **1352.43** | **1190.90** | **1030.14** | **907.62** | **810.82** | **732.94** | **668.72** |
| | | | | | | | | |
| | **enriched AIR torch** | | | | | | | |
| Ht1 | *kJ/kgAIR* | -0.137 | -0.137 | -0.137 | -0.137 | -0.137 | -0.137 | -0.137 |
| N | *kgmole* | 1.926E-05 | 3.186E-04 | 2.740E-03 | 1.459E-02 | 5.462E-02 | 1.581E-01 | 3.733E-01 |
| NO | *kgmole* | 1.107E-01 | 1.554E-01 | 1.529E-01 | 1.127E-01 | 7.653E-02 | 5.228E-02 | 3.573E-02 |
| NO2 | *kgmole* | 8.013E-05 | 6.566E-05 | 3.165E-05 | 1.007E-05 | 3.096E-06 | 1.061E-06 | 3.958E-07 |
| N2 | *kgmole* | 9.446E-01 | 9.221E-01 | 9.222E-01 | 9.363E-01 | 9.344E-01 | 8.948E-01 | 7.955E-01 |
| O | *kgmole* | 1.510E-01 | 5.879E-01 | 1.280E+00 | 1.719E+00 | 1.875E+00 | 1.931E+00 | 1.958E+00 |
| O2 | *kgmole* | 8.691E-01 | 6.283E-01 | 2.836E-01 | 8.435E-02 | 2.445E-02 | 8.179E-03 | 3.152E-03 |
| Ntorch-tot | *kgmole* | 2.075E+00 | 2.294E+00 | 2.641E+00 | 2.867E+00 | 2.965E+00 | 3.045E+00 | 3.166E+00 |
| MWt | *kg/kgmole* | 28.915 | 26.16 | 22.722 | 20.936 | 20.243 | 19.711 | 18.958 |
| Ht2 | *kJ/kgprod* | 3.992E+03 | 6.579E+03 | 1.022E+04 | 1.281E+04 | 1.442E+04 | 1.616E+04 | 1.872E+04 |
| Ht2 | *kg/kgAIR* | 3.993E+03 | 6.580E+03 | 1.022E+04 | 1.281E+04 | 1.442E+04 | 1.616E+04 | 1.872E+04 |
| DHt | *kJ/kgAIR* | 3.993E+03 | 6.581E+03 | 1.022E+04 | 1.281E+04 | 1.442E+04 | 1.616E+04 | 1.872E+04 |
| Mtorch | *kg AIR/sec* | 6.261E-02 | 3.799E-02 | 2.446E-02 | 1.951E-02 | 1.733E-02 | 1.547E-02 | 1.335E-02 |
| | ***lb AIR/hr*** | **496.92** | **301.52** | **194.10** | **154.85** | **137.57** | **122.75** | **105.96** |
| *scfm* | **O2 torch** | 102.13 | 53.87 | 29.12 | 21.35 | 19.15 | 18.20 | 17.56 |
| *gal/min* | **H2O torch** | 0.28 | 0.14 | 0.08 | 0.06 | 0.06 | 0.06 | 0.05 |
| *scfm* | **AIR torch** | 118.27 | 81.27 | 60.54 | 51.24 | 44.85 | 38.05 | 30.45 |
| *scfm* | **N2 torch** | 139.74 | 116.31 | 98.99 | 84.57 | 70.48 | 55.41 | 40.30 |
| *scfm* | **Ar torch** | 221.17 | 194.76 | 168.47 | 148.43 | 132.60 | 119.86 | 109.36 |
| *scfm* | **enriched** | 108.20 | 65.65 | 42.26 | 33.72 | 29.95 | 26.73 | 23.07 |

# 300 kW CASE

| Power | **300** | *kW* | | | | | | |
|---|---|---|---|---|---|---|---|---|
| **Ttorch** | ***K*** | **3007** | **3510** | **4000** | **4500** | **5000** | **5500** | **6000** |
| | *F* | 4952.6 | 5858 | 6740 | 7640 | 8540 | 9440 | 10340 |
| | | | | | | | | |
| **O2 torch** | | | | | | | | |
| Ht1 | *kJ/kgO2* | 0 | 0 | 0 | 0 | 0 | 0 | 0 |
| O2 | *kgmole* | 1.122E-01 | 4.756E-01 | 1.189E+00 | 1.736E+00 | 1.922E+00 | 1.974E+00 | 1.990E+00 |
| O | *kgmole* | 9.439E-01 | 7.622E-01 | 4.055E-01 | 1.321E-01 | 3.886E-02 | 1.309E-02 | 5.166E-03 |
| Ntorch-tot | *kgmole* | 1.056E+00 | 1.238E+00 | 1.594E+00 | 1.868E+00 | 1.961E+00 | 1.987E+00 | 1.995E+00 |
| MWt | *kg/kgmole* | 30.299 | 25.851 | 20.069 | 17.131 | 16.317 | 16.105 | 16.041 |
| Ht2 | *kJ/kgprod* | 3966 | 7519 | 13910 | 18970 | 21150 | 22250 | 23070 |
| Ht2 | *kJ/kgO2* | 3.966E+03 | 7.519E+03 | 1.391E+04 | 1.897E+04 | 2.115E+04 | 2.225E+04 | 2.307E+04 |
| DHt | *kJ/kgO2* | 3.966E+03 | 7.519E+03 | 1.391E+04 | 1.897E+04 | 2.115E+04 | 2.225E+04 | 2.307E+04 |
| Mtorch | *kg O2/sec* | 7.564E-02 | 3.990E-02 | 2.157E-02 | 1.581E-02 | 1.418E-02 | 1.348E-02 | 1.300E-02 |
| | ***lb O2/hr*** | **600.36** | **316.67** | **171.17** | **125.51** | **112.58** | **107.01** | **103.21** |
| | | | | | | | | |
| **H2O torch** | | | | | | | | |
| Ht1 | *kJ/kgH2O* | -15860 | -15860 | -15860 | -15860 | -15860 | -15860 | -15860 |
| H | *kgmole* | 6.767E-02 | 4.085E-01 | 1.183E+00 | 1.726E+00 | 1.910E+00 | 1.966E+00 | 1.985E+00 |
| HO | *kgmole* | 1.081E-01 | 2.405E-01 | 2.066E-01 | 8.189E-02 | 2.798E-02 | 1.066E-02 | 4.656E-03 |
| H2 | *kgmole* | 1.582E-01 | 2.995E-01 | 2.362E-01 | 8.997E-02 | 3.034E-02 | 1.147E-02 | 4.990E-03 |
| H2O | *kgmole* | 7.539E-01 | 3.760E-01 | 6.922E-02 | 5.895E-03 | 5.286E-04 | 6.552E-05 | 1.114E-05 |
| O | *kgmole* | 2.846E-02 | 1.923E-01 | 5.892E-01 | 8.681E-01 | 9.586E-01 | 9.849E-01 | 9.936E-01 |
| O2 | *kgmole* | 5.475E-02 | 9.561E-02 | 6.753E-02 | 2.208E-02 | 6.459E-03 | 2.176E-03 | 8.596E-04 |
| Ntorch-tot | *kgmole* | 1.171E+00 | 1.612E+00 | 2.351E+00 | 2.794E+00 | 2.934E+00 | 2.976E+00 | 2.989E+00 |
| MWt | *kg/kgmole* | 1.538E+01 | 1.117E+01 | 7.662E+00 | 6.447E+00 | 6.140E+00 | 6.055E+00 | 6.026E+00 |
| Ht2 | *kJ/kgprod* | -1.467E+03 | 1.239E+04 | 3.392E+04 | 4.729E+04 | 5.268E+04 | 5.552E+04 | 5.765E+04 |
| Ht2 | *kg/kgH2O* | -1.468E+03 | 1.240E+04 | 3.395E+04 | 4.733E+04 | 5.273E+04 | 5.557E+04 | 5.770E+04 |
| DHt | *kJ/kgH2O* | 1.439E+04 | 2.826E+04 | 4.981E+04 | 6.319E+04 | 6.859E+04 | 7.143E+04 | 7.356E+04 |
| Mtorch | *kg H2O/sec* | 2.085E-02 | 1.062E-02 | 6.023E-03 | 4.748E-03 | 4.374E-03 | 4.200E-03 | 4.078E-03 |
| | ***lb H2O/hr*** | **165.44** | **84.25** | **47.80** | **37.68** | **34.72** | **33.33** | **32.37** |
| | | | | | | | | |
| **AIR torch** | | | | | | | | |
| Ht1 | *kJ/kgAIR* | -0.137 | -0.137 | -0.137 | -0.137 | -0.137 | -0.137 | -0.137 |
| N | *kgmole* | 5.806E-05 | 9.460E-04 | 7.838E-03 | 4.052E-02 | 1.502E-01 | 4.371E-01 | 1.054E+00 |
| NO | *kgmole* | 2.071E-01 | 2.693E-01 | 2.349E-01 | 1.615E-01 | 1.077E-01 | 7.359E-02 | 5.071E-02 |
| NO2 | *kgmole* | 9.312E-05 | 6.645E-05 | 2.612E-05 | 7.449E-06 | 2.231E-06 | 7.604E-07 | 2.824E-07 |
| N2 | *kgmole* | 3.656E+00 | 3.625E+00 | 3.639E+00 | 3.659E+00 | 3.631E+00 | 3.505E+00 | 3.208E+00 |
| O | *kgmole* | 2.200E-01 | 7.699E-01 | 1.426E+00 | 1.750E+00 | 1.867E+00 | 1.918E+00 | 1.946E+00 |
| O2 | *kgmole* | 7.864E-01 | 4.803E-01 | 1.697E-01 | 4.433E-02 | 1.247E-02 | 4.137E-03 | 1.575E-03 |
| Ntorch-tot | *kgmole* | 4.870E+00 | 5.145E+00 | 5.477E+00 | 5.655E+00 | 5.769E+00 | 5.938E+00 | 6.260E+00 |
| MWt | *kg/kgmole* | 2.820E+01 | 2.669E+01 | 2.508E+01 | 2.428E+01 | 2.381E+01 | 2.313E+01 | 2.194E+01 |
| Ht2 | *kJ/kgprod* | 3.800E+03 | 5.530E+03 | 7.424E+03 | 8.771E+03 | 1.002E+04 | 1.181E+04 | 1.476E+04 |
| Ht2 | *kg/kgAIR* | 3.800E+03 | 5.530E+03 | 7.424E+03 | 8.771E+03 | 1.002E+04 | 1.181E+04 | 1.476E+04 |
| DHt | *kJ/kgAIR* | 3.800E+03 | 5.530E+03 | 7.424E+03 | 8.771E+03 | 1.002E+04 | 1.181E+04 | 1.476E+04 |
| Mtorch | *kg AIR/sec* | 7.895E-02 | 5.425E-02 | 4.041E-02 | 3.420E-02 | 2.994E-02 | 2.540E-02 | 2.033E-02 |
| | ***lb AIR/hr*** | **626.56** | **430.55** | **320.71** | **271.46** | **237.62** | **201.60** | **161.31** |

| Power | 300 | *kW* | | | | | | |
|---|---|---|---|---|---|---|---|---|
| **Ttorch** | *R* | **3000** | **3500** | **4000** | **4500** | **5000** | **5500** | **6000** |
| | ***F*** | 4940 | 5840 | 6740 | 7640 | 8540 | 9440 | 10340 |
| **N2 torch** | | | | | | | | |
| Ht1 | *kJ/kgN2* | -1.36E-01 | -1.36E-01 | -1.36E-01 | -1.36E-01 | -1.36E-01 | -1.36E-01 | -1.36E-01 |
| N2 | *kgmole* | 1.000E+00 | 9.999E-01 | 9.991E-01 | 9.955E-01 | 9.836E-01 | 9.521E-01 | 8.832E-01 |
| N | *kgmole* | 1.376E-05 | 2.190E-04 | 1.756E-03 | 8.908E-03 | 3.281E-02 | 9.570E-02 | 2.336E-01 |
| Ntorch-tot | *kgmole* | 1.000E+00 | 1.000E+00 | 1.001E+00 | 1.004E+00 | 1.016E+00 | 1.048E+00 | 1.117E+00 |
| MWt | *kg/kgmole* | 2.801E+01 | 2.801E+01 | 2.799E+01 | 2.789E+01 | 2.756E+01 | 2.673E+01 | 2.508E+01 |
| Ht2 | *kJ/kgprod* | 3.311E+03 | 3.978E+03 | 4.674E+03 | 5.471E+03 | 6.565E+03 | 8.350E+03 | 1.148E+04 |
| Ht2 | *kJ/kgN2* | 3.313E+03 | 3.980E+03 | 4.676E+03 | 5.474E+03 | 6.568E+03 | 8.354E+03 | 1.149E+04 |
| DHt | *kJ/kgN2* | 3.313E+03 | 3.980E+03 | 4.676E+03 | 5.474E+03 | 6.568E+03 | 8.354E+03 | 1.149E+04 |
| Mtorch | *kg N2/sec* | 9.056E-02 | 7.538E-02 | 6.415E-02 | 5.481E-02 | 4.567E-02 | 3.591E-02 | 2.612E-02 |
| | ***lb N2/hr*** | **718.74** | **598.24** | **509.15** | **434.98** | **362.50** | **285.01** | **207.30** |
| **Ar torch** | | | | | | | | |
| Ht1 | *kJ/kgAr* | -9.85E-02 | -9.85E-02 | -9.85E-02 | -9.85E-02 | -9.85E-02 | -9.85E-02 | -9.85E-02 |
| Ar | *kgmole* | 1.000E+00 | 1.000E+00 | 1.000E+00 | 1.000E+00 | 1.000E+00 | 1.000E+00 | 1.000E+00 |
| Ntorch-tot | *kgmole* | 1.000E+00 | 1.000E+00 | 1.000E+00 | 1.000E+00 | 1.000E+00 | 1.000E+00 | 1.000E+00 |
| MWt | *kg/kgmole* | 3.994E+01 | 3.994E+01 | 3.994E+01 | 3.994E+01 | 3.994E+01 | 3.994E+01 | 3.994E+01 |
| Ht2 | *kJ/kgprod* | 1.467E+03 | 1.666E+03 | 1.926E+03 | 2.186E+03 | 2.447E+03 | 2.707E+03 | 2.967E+03 |
| Ht2 | *kJ/kgAr* | 1.467E+03 | 1.666E+03 | 1.926E+03 | 2.186E+03 | 2.447E+03 | 2.707E+03 | 2.967E+03 |
| DHt | *kJ/kgAr* | 1.467E+03 | 1.666E+03 | 1.926E+03 | 2.186E+03 | 2.447E+03 | 2.707E+03 | 2.967E+03 |
| Mtorch | *kg Ar/sec* | 2.045E-01 | 1.801E-01 | 1.558E-01 | 1.372E-01 | 1.226E-01 | 1.108E-01 | 1.011E-01 |
| | ***lb Ar/hr*** | **1622.92** | **1429.08** | **1236.17** | **1089.15** | **972.98** | **879.53** | **802.46** |
| | **enriched AIR torch** | | | | | | | |
| Ht1 | *kJ/kgAIR* | -0.137 | -0.137 | -0.137 | -0.137 | -0.137 | -0.137 | -0.137 |
| N | *kgmole* | 1.926E-05 | 3.186E-04 | 2.740E-03 | 1.459E-02 | 5.462E-02 | 1.581E-01 | 3.733E-01 |
| NO | *kgmole* | 1.107E-01 | 1.554E-01 | 1.529E-01 | 1.127E-01 | 7.653E-02 | 5.228E-02 | 3.573E-02 |
| NO2 | *kgmole* | 8.013E-05 | 6.566E-05 | 3.165E-05 | 1.007E-05 | 3.096E-06 | 1.061E-06 | 3.958E-07 |
| N2 | *kgmole* | 9.446E-01 | 9.221E-01 | 9.222E-01 | 9.363E-01 | 9.344E-01 | 8.948E-01 | 7.955E-01 |
| O | *kgmole* | 1.510E-01 | 5.879E-01 | 1.280E+00 | 1.719E+00 | 1.875E+00 | 1.931E+00 | 1.958E+00 |
| O2 | *kgmole* | 8.691E-01 | 6.283E-01 | 2.836E-01 | 8.435E-02 | 2.445E-02 | 8.179E-03 | 3.152E-03 |
| Ntorch-tot | *kgmole* | 2.075E+00 | 2.294E+00 | 2.641E+00 | 2.867E+00 | 2.965E+00 | 3.045E+00 | 3.166E+00 |
| MWt | *kg/kgmole* | 28.915 | 26.16 | 22.722 | 20.936 | 20.243 | 19.711 | 18.958 |
| Ht2 | *kJ/kgprod* | 3.992E+03 | 6.579E+03 | 1.022E+04 | 1.281E+04 | 1.442E+04 | 1.616E+04 | 1.872E+04 |
| Ht2 | *kg/kgAIR* | 3.993E+03 | 6.580E+03 | 1.022E+04 | 1.281E+04 | 1.442E+04 | 1.616E+04 | 1.872E+04 |
| DHt | *kJ/kgAIR* | 3.993E+03 | 6.581E+03 | 1.022E+04 | 1.281E+04 | 1.442E+04 | 1.616E+04 | 1.872E+04 |
| Mtorch | *kg AIR/sec* | 7.513E-02 | 4.559E-02 | 2.935E-02 | 2.341E-02 | 2.080E-02 | 1.856E-02 | 1.602E-02 |
| | ***lb AIR/hr*** | **596.30** | **361.82** | **232.91** | **185.82** | **165.08** | **147.30** | **127.16** |
| *scfm* | **O2 torch** | 122.56 | 64.64 | 34.94 | 25.62 | 22.98 | 21.85 | 21.07 |
| *gal/min* | **H2O torch** | 0.33 | 0.17 | 0.10 | 0.08 | 0.07 | 0.07 | 0.06 |
| *scfm* | **AIR torch** | 141.92 | 97.52 | 72.64 | 61.49 | 53.82 | 45.66 | 36.54 |
| *scfm* | **N2 torch** | 167.68 | 139.57 | 118.78 | 101.48 | 84.57 | 66.49 | 48.36 |
| *scfm* | **Ar torch** | 265.41 | 233.71 | 202.16 | 178.12 | 159.12 | 143.84 | 131.23 |
| *scfm* | **enriched** | 129.84 | 78.78 | 50.72 | 40.46 | 35.95 | 32.07 | 27.69 |

# 350 kW CASE

| Power | 350 | *kW* | | | | | | |
|---|---|---|---|---|---|---|---|---|
| **Ttorch** | ***K*** | **3007** | **3510** | **4000** | **4500** | **5000** | **5500** | **6000** |
| | *F* | 4952.6 | 5858 | 6740 | 7640 | 8540 | 9440 | 10340 |
| **O2 torch** | | | | | | | | |
| Ht1 | *kJ/kgO2* | 0 | 0 | 0 | 0 | 0 | 0 | 0 |
| O2 | *kgmole* | 1.122E-01 | 4.756E-01 | 1.189E+00 | 1.736E+00 | 1.922E+00 | 1.974E+00 | 1.990E+00 |
| O | *kgmole* | 9.439E-01 | 7.622E-01 | 4.055E-01 | 1.321E-01 | 3.886E-02 | 1.309E-02 | 5.166E-03 |
| Ntorch-tot | *kgmole* | 1.056E+00 | 1.238E+00 | 1.594E+00 | 1.868E+00 | 1.961E+00 | 1.987E+00 | 1.995E+00 |
| MWt | *kg/kgmole* | 30.299 | 25.851 | 20.069 | 17.131 | 16.317 | 16.105 | 16.041 |
| Ht2 | *kJ/kgprod* | 3966 | 7519 | 13910 | 18970 | 21150 | 22250 | 23070 |
| Ht2 | *kJ/kgO2* | 3.966E+03 | 7.519E+03 | 1.391E+04 | 1.897E+04 | 2.115E+04 | 2.225E+04 | 2.307E+04 |
| DHt | *kJ/kgO2* | 3.966E+03 | 7.519E+03 | 1.391E+04 | 1.897E+04 | 2.115E+04 | 2.225E+04 | 2.307E+04 |
| Mtorch | *kg O2/sec* | 8.825E-02 | 4.655E-02 | 2.516E-02 | 1.845E-02 | 1.655E-02 | 1.573E-02 | 1.517E-02 |
| | ***lb O2/hr*** | **700.42** | **369.45** | **199.70** | **146.43** | **131.34** | **124.85** | **120.41** |
| **H2O torch** | | | | | | | | |
| Ht1 | *kJ/kgH2O* | -15860 | -15860 | -15860 | -15860 | -15860 | -15860 | -15860 |
| H | *kgmole* | 6.767E-02 | 4.085E-01 | 1.183E+00 | 1.726E+00 | 1.910E+00 | 1.966E+00 | 1.985E+00 |
| HO | *kgmole* | 1.081E-01 | 2.405E-01 | 2.066E-01 | 8.189E-02 | 2.798E-02 | 1.066E-02 | 4.656E-03 |
| H2 | *kgmole* | 1.582E-01 | 2.995E-01 | 2.362E-01 | 8.997E-02 | 3.034E-02 | 1.147E-02 | 4.990E-03 |
| H2O | *kgmole* | 7.539E-01 | 3.760E-01 | 6.922E-02 | 5.895E-03 | 5.286E-04 | 6.552E-05 | 1.114E-05 |
| O | *kgmole* | 2.846E-02 | 1.923E-01 | 5.892E-01 | 8.681E-01 | 9.586E-01 | 9.849E-01 | 9.936E-01 |
| O2 | *kgmole* | 5.475E-02 | 9.561E-02 | 6.753E-02 | 2.208E-02 | 6.459E-03 | 2.176E-03 | 8.596E-04 |
| Ntorch-tot | *kgmole* | 1.171E+00 | 1.612E+00 | 2.351E+00 | 2.794E+00 | 2.934E+00 | 2.976E+00 | 2.989E+00 |
| MWt | *kg/kgmole* | 1.538E+01 | 1.117E+01 | 7.662E+00 | 6.447E+00 | 6.140E+00 | 6.055E+00 | 6.026E+00 |
| Ht2 | *kJ/kgprod* | -1.467E+03 | 1.239E+04 | 3.392E+04 | 4.729E+04 | 5.268E+04 | 5.552E+04 | 5.765E+04 |
| Ht2 | *kg/kgH2O* | -1.468E+03 | 1.240E+04 | 3.395E+04 | 4.733E+04 | 5.273E+04 | 5.557E+04 | 5.770E+04 |
| DHt | *kJ/kgH2O* | 1.439E+04 | 2.826E+04 | 4.981E+04 | 6.319E+04 | 6.859E+04 | 7.143E+04 | 7.356E+04 |
| Mtorch | *kg H2O/sec* | 2.432E-02 | 1.238E-02 | 7.027E-03 | 5.539E-03 | 5.103E-03 | 4.900E-03 | 4.758E-03 |
| | ***lb H2O/hr*** | **193.02** | **98.29** | **55.77** | **43.96** | **40.50** | **38.89** | **37.76** |
| **AIR torch** | | | | | | | | |
| Ht1 | *kJ/kgAIR* | -0.137 | -0.137 | -0.137 | -0.137 | -0.137 | -0.137 | -0.137 |
| N | *kgmole* | 5.806E-05 | 9.460E-04 | 7.838E-03 | 4.052E-02 | 1.502E-01 | 4.371E-01 | 1.054E+00 |
| NO | *kgmole* | 2.071E-01 | 2.693E-01 | 2.349E-01 | 1.615E-01 | 1.077E-01 | 7.359E-02 | 5.071E-02 |
| NO2 | *kgmole* | 9.312E-05 | 6.645E-05 | 2.612E-05 | 7.449E-06 | 2.231E-06 | 7.604E-07 | 2.824E-07 |
| N2 | *kgmole* | 3.656E+00 | 3.625E+00 | 3.639E+00 | 3.659E+00 | 3.631E+00 | 3.505E+00 | 3.208E+00 |
| O | *kgmole* | 2.200E-01 | 7.699E-01 | 1.426E+00 | 1.750E+00 | 1.867E+00 | 1.918E+00 | 1.946E+00 |
| O2 | *kgmole* | 7.864E-01 | 4.803E-01 | 1.697E-01 | 4.433E-02 | 1.247E-02 | 4.137E-03 | 1.575E-03 |
| Ntorch-tot | *kgmole* | 4.870E+00 | 5.145E+00 | 5.477E+00 | 5.655E+00 | 5.769E+00 | 5.938E+00 | 6.260E+00 |
| MWt | *kg/kgmole* | 2.820E+01 | 2.669E+01 | 2.508E+01 | 2.428E+01 | 2.381E+01 | 2.313E+01 | 2.194E+01 |
| Ht2 | *kJ/kgprod* | 3.800E+03 | 5.530E+03 | 7.424E+03 | 8.771E+03 | 1.002E+04 | 1.181E+04 | 1.476E+04 |
| Ht2 | *kg/kgAIR* | 3.800E+03 | 5.530E+03 | 7.424E+03 | 8.771E+03 | 1.002E+04 | 1.181E+04 | 1.476E+04 |
| DHt | *kJ/kgAIR* | 3.800E+03 | 5.530E+03 | 7.424E+03 | 8.771E+03 | 1.002E+04 | 1.181E+04 | 1.476E+04 |
| Mtorch | *kg AIR/sec* | 9.210E-02 | 6.329E-02 | 4.714E-02 | 3.990E-02 | 3.493E-02 | 2.964E-02 | 2.371E-02 |
| | ***lb AIR/hr*** | **730.99** | **502.31** | **374.17** | **316.70** | **277.22** | **235.21** | **188.20** |

| Power | **350** | *kW* | | | | | | |
|---|---|---|---|---|---|---|---|---|
| **Ttorch** | *R* | **3000** | **3500** | **4000** | **4500** | **5000** | **5500** | **6000** |
| | ***F*** | 4940 | 5840 | 6740 | 7640 | 8540 | 9440 | 10340 |
| **N2 torch** | | | | | | | | |
| Ht1 | *kJ/kgN2* | -1.36E-01 | -1.36E-01 | -1.36E-01 | -1.36E-01 | -1.36E-01 | -1.36E-01 | -1.36E-01 |
| N2 | *kgmole* | 1.000E+00 | 9.999E-01 | 9.991E-01 | 9.955E-01 | 9.836E-01 | 9.521E-01 | 8.832E-01 |
| N | *kgmole* | 1.376E-05 | 2.190E-04 | 1.756E-03 | 8.908E-03 | 3.281E-02 | 9.570E-02 | 2.336E-01 |
| Ntorch-tot | *kgmole* | 1.000E+00 | 1.000E+00 | 1.001E+00 | 1.004E+00 | 1.016E+00 | 1.048E+00 | 1.117E+00 |
| MWt | *kg/kgmole* | 2.801E+01 | 2.801E+01 | 2.799E+01 | 2.789E+01 | 2.756E+01 | 2.673E+01 | 2.508E+01 |
| Ht2 | *kJ/kgprod* | 3.311E+03 | 3.978E+03 | 4.674E+03 | 5.471E+03 | 6.565E+03 | 8.350E+03 | 1.148E+04 |
| Ht2 | *kJ/kgN2* | 3.313E+03 | 3.980E+03 | 4.676E+03 | 5.474E+03 | 6.568E+03 | 8.354E+03 | 1.149E+04 |
| DHt | *kJ/kgN2* | 3.313E+03 | 3.980E+03 | 4.676E+03 | 5.474E+03 | 6.568E+03 | 8.354E+03 | 1.149E+04 |
| Mtorch | *kg N2/sec* | 1.057E-01 | 8.794E-02 | 7.484E-02 | 6.394E-02 | 5.329E-02 | 4.190E-02 | 3.047E-02 |
| | ***lb N2/hr*** | **838.53** | **697.94** | **594.01** | **507.48** | **422.92** | **332.51** | **241.85** |
| **Ar torch** | | | | | | | | |
| Ht1 | *kJ/kgAr* | -9.85E-02 | -9.85E-02 | -9.85E-02 | -9.85E-02 | -9.85E-02 | -9.85E-02 | -9.85E-02 |
| Ar | *kgmole* | 1.000E+00 | 1.000E+00 | 1.000E+00 | 1.000E+00 | 1.000E+00 | 1.000E+00 | 1.000E+00 |
| Ntorch-tot | *kgmole* | 1.000E+00 | 1.000E+00 | 1.000E+00 | 1.000E+00 | 1.000E+00 | 1.000E+00 | 1.000E+00 |
| MWt | *kg/kgmole* | 3.994E+01 | 3.994E+01 | 3.994E+01 | 3.994E+01 | 3.994E+01 | 3.994E+01 | 3.994E+01 |
| Ht2 | *kJ/kgprod* | 1.467E+03 | 1.666E+03 | 1.926E+03 | 2.186E+03 | 2.447E+03 | 2.707E+03 | 2.967E+03 |
| Ht2 | *kJ/kgAr* | 1.467E+03 | 1.666E+03 | 1.926E+03 | 2.186E+03 | 2.447E+03 | 2.707E+03 | 2.967E+03 |
| DHt | *kJ/kgAr* | 1.467E+03 | 1.666E+03 | 1.926E+03 | 2.186E+03 | 2.447E+03 | 2.707E+03 | 2.967E+03 |
| Mtorch | *kg Ar/sec* | 2.386E-01 | 2.101E-01 | 1.817E-01 | 1.601E-01 | 1.430E-01 | 1.293E-01 | 1.180E-01 |
| | ***lb Ar/hr*** | **1893.40** | **1667.25** | **1442.20** | **1270.67** | **1135.14** | **1026.12** | **936.20** |
| | **enriched AIR torch** | | | | | | | |
| Ht1 | *kJ/kgAIR* | -0.137 | -0.137 | -0.137 | -0.137 | -0.137 | -0.137 | -0.137 |
| N | *kgmole* | 1.926E-05 | 3.186E-04 | 2.740E-03 | 1.459E-02 | 5.462E-02 | 1.581E-01 | 3.733E-01 |
| NO | *kgmole* | 1.107E-01 | 1.554E-01 | 1.529E-01 | 1.127E-01 | 7.653E-02 | 5.228E-02 | 3.573E-02 |
| NO2 | *kgmole* | 8.013E-05 | 6.566E-05 | 3.165E-05 | 1.007E-05 | 3.096E-06 | 1.061E-06 | 3.958E-07 |
| N2 | *kgmole* | 9.446E-01 | 9.221E-01 | 9.222E-01 | 9.363E-01 | 9.344E-01 | 8.948E-01 | 7.955E-01 |
| O | *kgmole* | 1.510E-01 | 5.879E-01 | 1.280E+00 | 1.719E+00 | 1.875E+00 | 1.931E+00 | 1.958E+00 |
| O2 | *kgmole* | 8.691E-01 | 6.283E-01 | 2.836E-01 | 8.435E-02 | 2.445E-02 | 8.179E-03 | 3.152E-03 |
| Ntorch-tot | *kgmole* | 2.075E+00 | 2.294E+00 | 2.641E+00 | 2.867E+00 | 2.965E+00 | 3.045E+00 | 3.166E+00 |
| MWt | *kg/kgmole* | 28.915 | 26.16 | 22.722 | 20.936 | 20.243 | 19.711 | 18.958 |
| Ht2 | *kJ/kgprod* | 3.992E+03 | 6.579E+03 | 1.022E+04 | 1.281E+04 | 1.442E+04 | 1.616E+04 | 1.872E+04 |
| Ht2 | *kg/kgAIR* | 3.993E+03 | 6.580E+03 | 1.022E+04 | 1.281E+04 | 1.442E+04 | 1.616E+04 | 1.872E+04 |
| DHt | *kJ/kgAIR* | 3.993E+03 | 6.581E+03 | 1.022E+04 | 1.281E+04 | 1.442E+04 | 1.616E+04 | 1.872E+04 |
| Mtorch | *kg AIR/sec* | 8.766E-02 | 5.319E-02 | 3.424E-02 | 2.732E-02 | 2.427E-02 | 2.165E-02 | 1.869E-02 |
| | ***lb AIR/hr*** | **695.68** | **422.12** | **271.73** | **216.79** | **192.59** | **171.85** | **148.35** |
| *scfm* | **O2 torch** | 142.98 | 75.42 | 40.77 | 29.89 | 26.81 | 25.49 | 24.58 |
| *gal/min* | **H2O torch** | 0.39 | 0.20 | 0.11 | 0.09 | 0.08 | 0.08 | 0.08 |
| *scfm* | **AIR torch** | 165.57 | 113.77 | 84.75 | 71.73 | 62.79 | 53.28 | 42.63 |
| *scfm* | **N2 torch** | 195.63 | 162.83 | 138.58 | 118.40 | 98.67 | 77.57 | 56.42 |
| *scfm* | **Ar torch** | 309.64 | 272.66 | 235.85 | 207.80 | 185.64 | 167.81 | 153.11 |
| *scfm* | **enriched** | 151.48 | 91.92 | 59.17 | 47.21 | 41.94 | 37.42 | 32.30 |

# 400 kW CASE

| Power | **400** | *kW* | | | | | | |
|---|---|---|---|---|---|---|---|---|
| **Ttorch** | ***K*** | **3007** | **3510** | **4000** | **4500** | **5000** | **5500** | **6000** |
| | *F* | 4952.6 | 5858 | 6740 | 7640 | 8540 | 9440 | 10340 |

| **O2 torch** | | | | | | | | |
|---|---|---|---|---|---|---|---|---|
| Ht1 | *kJ/kgO2* | 0 | 0 | 0 | 0 | 0 | 0 | 0 |
| O2 | *kgmole* | 1.122E-01 | 4.756E-01 | 1.189E+00 | 1.736E+00 | 1.922E+00 | 1.974E+00 | 1.990E+00 |
| O | *kgmole* | 9.439E-01 | 7.622E-01 | 4.055E-01 | 1.321E-01 | 3.886E-02 | 1.309E-02 | 5.166E-03 |
| Ntorch-tot | *kgmole* | 1.056E+00 | 1.238E+00 | 1.594E+00 | 1.868E+00 | 1.961E+00 | 1.987E+00 | 1.995E+00 |
| MWt | *kg/kgmole* | 30.299 | 25.851 | 20.069 | 17.131 | 16.317 | 16.105 | 16.041 |
| Ht2 | *kJ/kgprod* | 3966 | 7519 | 13910 | 18970 | 21150 | 22250 | 23070 |
| Ht2 | *kJ/kgO2* | 3.966E+03 | 7.519E+03 | 1.391E+04 | 1.897E+04 | 2.115E+04 | 2.225E+04 | 2.307E+04 |
| DHt | *kJ/kgO2* | 3.966E+03 | 7.519E+03 | 1.391E+04 | 1.897E+04 | 2.115E+04 | 2.225E+04 | 2.307E+04 |
| Mtorch | *kg O2/sec* | 1.009E-01 | 5.320E-02 | 2.876E-02 | 2.109E-02 | 1.891E-02 | 1.798E-02 | 1.734E-02 |
| | ***lb O2/hr*** | **800.48** | **422.23** | **228.23** | **167.35** | **150.10** | **142.68** | **137.61** |

| **H2O torch** | | | | | | | | |
|---|---|---|---|---|---|---|---|---|
| Ht1 | *kJ/kgH2O* | -15860 | -15860 | -15860 | -15860 | -15860 | -15860 | -15860 |
| H | *kgmole* | 6.767E-02 | 4.085E-01 | 1.183E+00 | 1.726E+00 | 1.910E+00 | 1.966E+00 | 1.985E+00 |
| HO | *kgmole* | 1.081E-01 | 2.405E-01 | 2.066E-01 | 8.189E-02 | 2.798E-02 | 1.066E-02 | 4.656E-03 |
| H2 | *kgmole* | 1.582E-01 | 2.995E-01 | 2.362E-01 | 8.997E-02 | 3.034E-02 | 1.147E-02 | 4.990E-03 |
| H2O | *kgmole* | 7.539E-01 | 3.760E-01 | 6.922E-02 | 5.895E-03 | 5.286E-04 | 6.552E-05 | 1.114E-05 |
| O | *kgmole* | 2.846E-02 | 1.923E-01 | 5.892E-01 | 8.681E-01 | 9.586E-01 | 9.849E-01 | 9.936E-01 |
| O2 | *kgmole* | 5.475E-02 | 9.561E-02 | 6.753E-02 | 2.208E-02 | 6.459E-03 | 2.176E-03 | 8.596E-04 |
| Ntorch-tot | *kgmole* | 1.171E+00 | 1.612E+00 | 2.351E+00 | 2.794E+00 | 2.934E+00 | 2.976E+00 | 2.989E+00 |
| MWt | *kg/kgmole* | 1.538E+01 | 1.117E+01 | 7.662E+00 | 6.447E+00 | 6.140E+00 | 6.055E+00 | 6.026E+00 |
| Ht2 | *kJ/kgprod* | -1.467E+03 | 1.239E+04 | 3.392E+04 | 4.729E+04 | 5.268E+04 | 5.552E+04 | 5.765E+04 |
| Ht2 | *kg/kgH2O* | -1.468E+03 | 1.240E+04 | 3.395E+04 | 4.733E+04 | 5.273E+04 | 5.557E+04 | 5.770E+04 |
| DHt | *kJ/kgH2O* | 1.439E+04 | 2.826E+04 | 4.981E+04 | 6.319E+04 | 6.859E+04 | 7.143E+04 | 7.356E+04 |
| Mtorch | *kg H2O/sec* | 2.779E-02 | 1.415E-02 | 8.031E-03 | 6.330E-03 | 5.832E-03 | 5.600E-03 | 5.438E-03 |
| | ***lb H2O/hr*** | **220.59** | **112.34** | **63.74** | **50.24** | **46.29** | **44.44** | **43.16** |

| **AIR torch** | | | | | | | | |
|---|---|---|---|---|---|---|---|---|
| Ht1 | *kJ/kgAIR* | -0.137 | -0.137 | -0.137 | -0.137 | -0.137 | -0.137 | -0.137 |
| N | *kgmole* | 5.806E-05 | 9.460E-04 | 7.838E-03 | 4.052E-02 | 1.502E-01 | 4.371E-01 | 1.054E+00 |
| NO | *kgmole* | 2.071E-01 | 2.693E-01 | 2.349E-01 | 1.615E-01 | 1.077E-01 | 7.359E-02 | 5.071E-02 |
| NO2 | *kgmole* | 9.312E-05 | 6.645E-05 | 2.612E-05 | 7.449E-06 | 2.231E-06 | 7.604E-07 | 2.824E-07 |
| N2 | *kgmole* | 3.656E+00 | 3.625E+00 | 3.639E+00 | 3.659E+00 | 3.631E+00 | 3.505E+00 | 3.208E+00 |
| O | *kgmole* | 2.200E-01 | 7.699E-01 | 1.426E+00 | 1.750E+00 | 1.867E+00 | 1.918E+00 | 1.946E+00 |
| O2 | *kgmole* | 7.864E-01 | 4.803E-01 | 1.697E-01 | 4.433E-02 | 1.247E-02 | 4.137E-03 | 1.575E-03 |
| Ntorch-tot | *kgmole* | 4.870E+00 | 5.145E+00 | 5.477E+00 | 5.655E+00 | 5.769E+00 | 5.938E+00 | 6.260E+00 |
| MWt | *kg/kgmole* | 2.820E+01 | 2.669E+01 | 2.508E+01 | 2.428E+01 | 2.381E+01 | 2.313E+01 | 2.194E+01 |
| Ht2 | *kJ/kgprod* | 3.800E+03 | 5.530E+03 | 7.424E+03 | 8.771E+03 | 1.002E+04 | 1.181E+04 | 1.476E+04 |
| Ht2 | *kg/kgAIR* | 3.800E+03 | 5.530E+03 | 7.424E+03 | 8.771E+03 | 1.002E+04 | 1.181E+04 | 1.476E+04 |
| DHt | *kJ/kgAIR* | 3.800E+03 | 5.530E+03 | 7.424E+03 | 8.771E+03 | 1.002E+04 | 1.181E+04 | 1.476E+04 |
| Mtorch | *kg AIR/sec* | 1.053E-01 | 7.233E-02 | 5.388E-02 | 4.560E-02 | 3.992E-02 | 3.387E-02 | 2.710E-02 |
| | ***lb AIR/hr*** | **835.42** | **574.07** | **427.62** | **361.94** | **316.83** | **268.81** | **215.08** |

| Power | 400 | *kW* | | | | | | |
|---|---|---|---|---|---|---|---|---|
| **Ttorch** | *R* | **3000** | **3500** | **4000** | **4500** | **5000** | **5500** | **6000** |
| | ***F*** | 4940 | 5840 | 6740 | 7640 | 8540 | 9440 | 10340 |
| | | | | | | | | |
| **N2 torch** | | | | | | | | |
| Ht1 | *kJ/kgN2* | -1.36E-01 | -1.36E-01 | -1.36E-01 | -1.36E-01 | -1.36E-01 | -1.36E-01 | -1.36E-01 |
| N2 | *kgmole* | 1.000E+00 | 9.999E-01 | 9.991E-01 | 9.955E-01 | 9.836E-01 | 9.521E-01 | 8.832E-01 |
| N | *kgmole* | 1.376E-05 | 2.190E-04 | 1.756E-03 | 8.908E-03 | 3.281E-02 | 9.570E-02 | 2.336E-01 |
| Ntorch-tot | *kgmole* | 1.000E+00 | 1.000E+00 | 1.001E+00 | 1.004E+00 | 1.016E+00 | 1.048E+00 | 1.117E+00 |
| MWt | *kg/kgmole* | 2.801E+01 | 2.801E+01 | 2.799E+01 | 2.789E+01 | 2.756E+01 | 2.673E+01 | 2.508E+01 |
| Ht2 | *kJ/kgprod* | 3.311E+03 | 3.978E+03 | 4.674E+03 | 5.471E+03 | 6.565E+03 | 8.350E+03 | 1.148E+04 |
| Ht2 | *kJ/kgN2* | 3.313E+03 | 3.980E+03 | 4.676E+03 | 5.474E+03 | 6.568E+03 | 8.354E+03 | 1.149E+04 |
| DHt | *kJ/kgN2* | 3.313E+03 | 3.980E+03 | 4.676E+03 | 5.474E+03 | 6.568E+03 | 8.354E+03 | 1.149E+04 |
| Mtorch | *kg N2/sec* | 1.207E-01 | 1.005E-01 | 8.554E-02 | 7.308E-02 | 6.090E-02 | 4.788E-02 | 3.483E-02 |
| | ***lb N2/hr*** | **958.33** | **797.65** | **678.86** | **579.98** | **483.33** | **380.01** | **276.40** |
| | | | | | | | | |
| **Ar torch** | | | | | | | | |
| Ht1 | *kJ/kgAr* | -9.85E-02 | -9.85E-02 | -9.85E-02 | -9.85E-02 | -9.85E-02 | -9.85E-02 | -9.85E-02 |
| Ar | *kgmole* | 1.000E+00 | 1.000E+00 | 1.000E+00 | 1.000E+00 | 1.000E+00 | 1.000E+00 | 1.000E+00 |
| Ntorch-tot | *kgmole* | 1.000E+00 | 1.000E+00 | 1.000E+00 | 1.000E+00 | 1.000E+00 | 1.000E+00 | 1.000E+00 |
| MWt | *kg/kgmole* | 3.994E+01 | 3.994E+01 | 3.994E+01 | 3.994E+01 | 3.994E+01 | 3.994E+01 | 3.994E+01 |
| Ht2 | *kJ/kgprod* | 1.467E+03 | 1.666E+03 | 1.926E+03 | 2.186E+03 | 2.447E+03 | 2.707E+03 | 2.967E+03 |
| Ht2 | *kJ/kgAr* | 1.467E+03 | 1.666E+03 | 1.926E+03 | 2.186E+03 | 2.447E+03 | 2.707E+03 | 2.967E+03 |
| DHt | *kJ/kgAr* | 1.467E+03 | 1.666E+03 | 1.926E+03 | 2.186E+03 | 2.447E+03 | 2.707E+03 | 2.967E+03 |
| Mtorch | *kg Ar/sec* | 2.726E-01 | 2.401E-01 | 2.077E-01 | 1.830E-01 | 1.635E-01 | 1.478E-01 | 1.348E-01 |
| | ***lb Ar/hr*** | **2163.89** | **1905.43** | **1648.22** | **1452.19** | **1297.31** | **1172.71** | **1069.95** |
| | | | | | | | | |
| | **enriched AIR torch** | | | | | | | |
| Ht1 | *kJ/kgAIR* | -0.137 | -0.137 | -0.137 | -0.137 | -0.137 | -0.137 | -0.137 |
| N | *kgmole* | 1.926E-05 | 3.186E-04 | 2.740E-03 | 1.459E-02 | 5.462E-02 | 1.581E-01 | 3.733E-01 |
| NO | *kgmole* | 1.107E-01 | 1.554E-01 | 1.529E-01 | 1.127E-01 | 7.653E-02 | 5.228E-02 | 3.573E-02 |
| NO2 | *kgmole* | 8.013E-05 | 6.566E-05 | 3.165E-05 | 1.007E-05 | 3.096E-06 | 1.061E-06 | 3.958E-07 |
| N2 | *kgmole* | 9.446E-01 | 9.221E-01 | 9.222E-01 | 9.363E-01 | 9.344E-01 | 8.948E-01 | 7.955E-01 |
| O | *kgmole* | 1.510E-01 | 5.879E-01 | 1.280E+00 | 1.719E+00 | 1.875E+00 | 1.931E+00 | 1.958E+00 |
| O2 | *kgmole* | 8.691E-01 | 6.283E-01 | 2.836E-01 | 8.435E-02 | 2.445E-02 | 8.179E-03 | 3.152E-03 |
| Ntorch-tot | *kgmole* | 2.075E+00 | 2.294E+00 | 2.641E+00 | 2.867E+00 | 2.965E+00 | 3.045E+00 | 3.166E+00 |
| MWt | *kg/kgmole* | 28.915 | 26.16 | 22.722 | 20.936 | 20.243 | 19.711 | 18.958 |
| Ht2 | *kJ/kgprod* | 3.992E+03 | 6.579E+03 | 1.022E+04 | 1.281E+04 | 1.442E+04 | 1.616E+04 | 1.872E+04 |
| Ht2 | *kg/kgAIR* | 3.993E+03 | 6.580E+03 | 1.022E+04 | 1.281E+04 | 1.442E+04 | 1.616E+04 | 1.872E+04 |
| DHt | *kJ/kgAIR* | 3.993E+03 | 6.581E+03 | 1.022E+04 | 1.281E+04 | 1.442E+04 | 1.616E+04 | 1.872E+04 |
| Mtorch | *kg AIR/sec* | 1.002E-01 | 6.078E-02 | 3.913E-02 | 3.122E-02 | 2.773E-02 | 2.475E-02 | 2.136E-02 |
| | ***lb AIR/hr*** | **795.07** | **482.43** | **310.55** | **247.76** | **220.11** | **196.40** | **169.54** |
| *scfm* | **O2 torch** | 163.41 | 86.19 | 46.59 | 34.16 | 30.64 | 29.13 | 28.09 |
| *gal/min* | **H2O torch** | 0.44 | 0.22 | 0.13 | 0.10 | 0.09 | 0.09 | 0.09 |
| *scfm* | **AIR torch** | 189.23 | 130.03 | 96.86 | 81.98 | 71.76 | 60.89 | 48.72 |
| *scfm* | **N2 torch** | 223.58 | 186.09 | 158.38 | 135.31 | 112.76 | 88.66 | 64.48 |
| *scfm* | **Ar torch** | 353.88 | 311.61 | 269.55 | 237.49 | 212.16 | 191.78 | 174.98 |
| *scfm* | **enriched** | 173.12 | 105.05 | 67.62 | 53.95 | 47.93 | 42.77 | 36.92 |

# 450 kW CASE

| Power | 450 | *kW* | | | | | | |
|---|---|---|---|---|---|---|---|---|
| **Ttorch** | ***K*** | **3007** | **3510** | **4000** | **4500** | **5000** | **5500** | **6000** |
| | *F* | 4952.6 | 5858 | 6740 | 7640 | 8540 | 9440 | 10340 |
| | | | | | | | | |
| **O2 torch** | | | | | | | | |
| Ht1 | *kJ/kgO2* | 0 | 0 | 0 | 0 | 0 | 0 | 0 |
| O2 | *kgmole* | 1.122E-01 | 4.756E-01 | 1.189E+00 | 1.736E+00 | 1.922E+00 | 1.974E+00 | 1.990E+00 |
| O | *kgmole* | 9.439E-01 | 7.622E-01 | 4.055E-01 | 1.321E-01 | 3.886E-02 | 1.309E-02 | 5.166E-03 |
| Ntorch-tot | *kgmole* | 1.056E+00 | 1.238E+00 | 1.594E+00 | 1.868E+00 | 1.961E+00 | 1.987E+00 | 1.995E+00 |
| MWt | *kg/kgmole* | 30.299 | 25.851 | 20.069 | 17.131 | 16.317 | 16.105 | 16.041 |
| Ht2 | *kJ/kgprod* | 3966 | 7519 | 13910 | 18970 | 21150 | 22250 | 23070 |
| Ht2 | *kJ/kgO2* | 3.966E+03 | 7.519E+03 | 1.391E+04 | 1.897E+04 | 2.115E+04 | 2.225E+04 | 2.307E+04 |
| DHt | *kJ/kgO2* | 3.966E+03 | 7.519E+03 | 1.391E+04 | 1.897E+04 | 2.115E+04 | 2.225E+04 | 2.307E+04 |
| Mtorch | *kg O2/sec* | 1.135E-01 | 5.985E-02 | 3.235E-02 | 2.372E-02 | 2.128E-02 | 2.023E-02 | 1.951E-02 |
| | ***lb O2/hr*** | **900.54** | **475.01** | **256.76** | **188.27** | **168.86** | **160.52** | **154.81** |
| | | | | | | | | |
| **H2O torch** | | | | | | | | |
| Ht1 | *kJ/kgH2O* | -15860 | -15860 | -15860 | -15860 | -15860 | -15860 | -15860 |
| H | *kgmole* | 6.767E-02 | 4.085E-01 | 1.183E+00 | 1.726E+00 | 1.910E+00 | 1.966E+00 | 1.985E+00 |
| HO | *kgmole* | 1.081E-01 | 2.405E-01 | 2.066E-01 | 8.189E-02 | 2.798E-02 | 1.066E-02 | 4.656E-03 |
| H2 | *kgmole* | 1.582E-01 | 2.995E-01 | 2.362E-01 | 8.997E-02 | 3.034E-02 | 1.147E-02 | 4.990E-03 |
| H2O | *kgmole* | 7.539E-01 | 3.760E-01 | 6.922E-02 | 5.895E-03 | 5.286E-04 | 6.552E-05 | 1.114E-05 |
| O | *kgmole* | 2.846E-02 | 1.923E-01 | 5.892E-01 | 8.681E-01 | 9.586E-01 | 9.849E-01 | 9.936E-01 |
| O2 | *kgmole* | 5.475E-02 | 9.561E-02 | 6.753E-02 | 2.208E-02 | 6.459E-03 | 2.176E-03 | 8.596E-04 |
| Ntorch-tot | *kgmole* | 1.171E+00 | 1.612E+00 | 2.351E+00 | 2.794E+00 | 2.934E+00 | 2.976E+00 | 2.989E+00 |
| MWt | *kg/kgmole* | 1.538E+01 | 1.117E+01 | 7.662E+00 | 6.447E+00 | 6.140E+00 | 6.055E+00 | 6.026E+00 |
| Ht2 | *kJ/kgprod* | - 1.467E+03 | 1.239E+04 | 3.392E+04 | 4.729E+04 | 5.268E+04 | 5.552E+04 | 5.765E+04 |
| Ht2 | *kg/kgH2O* | - 1.468E+03 | 1.240E+04 | 3.395E+04 | 4.733E+04 | 5.273E+04 | 5.557E+04 | 5.770E+04 |
| DHt | *kJ/kgH2O* | 1.439E+04 | 2.826E+04 | 4.981E+04 | 6.319E+04 | 6.859E+04 | 7.143E+04 | 7.356E+04 |
| Mtorch | *kg H2O/sec* | 3.127E-02 | 1.592E-02 | 9.034E-03 | 7.122E-03 | 6.561E-03 | 6.300E-03 | 6.118E-03 |
| | ***lb H2O/hr*** | **248.16** | **126.38** | **71.70** | **56.52** | **52.07** | **50.00** | **48.55** |
| | | | | | | | | |
| **AIR torch** | | | | | | | | |
| Ht1 | *kJ/kgAIR* | -0.137 | -0.137 | -0.137 | -0.137 | -0.137 | -0.137 | -0.137 |
| N | *kgmole* | 5.806E-05 | 9.460E-04 | 7.838E-03 | 4.052E-02 | 1.502E-01 | 4.371E-01 | 1.054E+00 |
| NO | *kgmole* | 2.071E-01 | 2.693E-01 | 2.349E-01 | 1.615E-01 | 1.077E-01 | 7.359E-02 | 5.071E-02 |
| NO2 | *kgmole* | 9.312E-05 | 6.645E-05 | 2.612E-05 | 7.449E-06 | 2.231E-06 | 7.604E-07 | 2.824E-07 |
| N2 | *kgmole* | 3.656E+00 | 3.625E+00 | 3.639E+00 | 3.659E+00 | 3.631E+00 | 3.505E+00 | 3.208E+00 |
| O | *kgmole* | 2.200E-01 | 7.699E-01 | 1.426E+00 | 1.750E+00 | 1.867E+00 | 1.918E+00 | 1.946E+00 |
| O2 | *kgmole* | 7.864E-01 | 4.803E-01 | 1.697E-01 | 4.433E-02 | 1.247E-02 | 4.137E-03 | 1.575E-03 |
| Ntorch-tot | *kgmole* | 4.870E+00 | 5.145E+00 | 5.477E+00 | 5.655E+00 | 5.769E+00 | 5.938E+00 | 6.260E+00 |
| MWt | *kg/kgmole* | 2.820E+01 | 2.669E+01 | 2.508E+01 | 2.428E+01 | 2.381E+01 | 2.313E+01 | 2.194E+01 |
| Ht2 | *kJ/kgprod* | 3.800E+03 | 5.530E+03 | 7.424E+03 | 8.771E+03 | 1.002E+04 | 1.181E+04 | 1.476E+04 |
| Ht2 | *kg/kgAIR* | 3.800E+03 | 5.530E+03 | 7.424E+03 | 8.771E+03 | 1.002E+04 | 1.181E+04 | 1.476E+04 |
| DHt | *kJ/kgAIR* | 3.800E+03 | 5.530E+03 | 7.424E+03 | 8.771E+03 | 1.002E+04 | 1.181E+04 | 1.476E+04 |
| Mtorch | *kg AIR/sec* | 1.184E-01 | 8.137E-02 | 6.061E-02 | 5.130E-02 | 4.491E-02 | 3.810E-02 | 3.049E-02 |
| | ***lb AIR/hr*** | **939.84** | **645.82** | **481.07** | **407.19** | **356.43** | **302.41** | **241.97** |

| Power | **450** | *kW* | | | | | | |
|---|---|---|---|---|---|---|---|---|
| **Ttorch** | *R* | **3000** | **3500** | **4000** | **4500** | **5000** | **5500** | **6000** |
| | ***F*** | 4940 | 5840 | 6740 | 7640 | 8540 | 9440 | 10340 |
| **N2 torch** | | | | | | | | |
| Ht1 | *kJ/kgN2* | -1.36E-01 | -1.36E-01 | -1.36E-01 | -1.36E-01 | -1.36E-01 | -1.36E-01 | -1.36E-01 |
| N2 | *kgmole* | 1.000E+00 | 9.999E-01 | 9.991E-01 | 9.955E-01 | 9.836E-01 | 9.521E-01 | 8.832E-01 |
| N | *kgmole* | 1.376E-05 | 2.190E-04 | 1.756E-03 | 8.908E-03 | 3.281E-02 | 9.570E-02 | 2.336E-01 |
| Ntorch-tot | *kgmole* | 1.000E+00 | 1.000E+00 | 1.001E+00 | 1.004E+00 | 1.016E+00 | 1.048E+00 | 1.117E+00 |
| MWt | *kg/kgmole* | 2.801E+01 | 2.801E+01 | 2.799E+01 | 2.789E+01 | 2.756E+01 | 2.673E+01 | 2.508E+01 |
| Ht2 | *kJ/kgprod* | 3.311E+03 | 3.978E+03 | 4.674E+03 | 5.471E+03 | 6.565E+03 | 8.350E+03 | 1.148E+04 |
| Ht2 | *kJ/kgN2* | 3.313E+03 | 3.980E+03 | 4.676E+03 | 5.474E+03 | 6.568E+03 | 8.354E+03 | 1.149E+04 |
| DHt | *kJ/kgN2* | 3.313E+03 | 3.980E+03 | 4.676E+03 | 5.474E+03 | 6.568E+03 | 8.354E+03 | 1.149E+04 |
| Mtorch | *kg N2/sec* | 1.358E-01 | 1.131E-01 | 9.623E-02 | 8.221E-02 | 6.851E-02 | 5.387E-02 | 3.918E-02 |
| | ***lb N2/hr*** | **1078.12** | **897.36** | **763.72** | **652.48** | **543.75** | **427.51** | **310.95** |
| **Ar torch** | | | | | | | | |
| Ht1 | *kJ/kgAr* | -9.85E-02 | -9.85E-02 | -9.85E-02 | -9.85E-02 | -9.85E-02 | -9.85E-02 | -9.85E-02 |
| Ar | *kgmole* | 1.000E+00 | 1.000E+00 | 1.000E+00 | 1.000E+00 | 1.000E+00 | 1.000E+00 | 1.000E+00 |
| Ntorch-tot | *kgmole* | 1.000E+00 | 1.000E+00 | 1.000E+00 | 1.000E+00 | 1.000E+00 | 1.000E+00 | 1.000E+00 |
| MWt | *kg/kgmole* | 3.994E+01 | 3.994E+01 | 3.994E+01 | 3.994E+01 | 3.994E+01 | 3.994E+01 | 3.994E+01 |
| Ht2 | *kJ/kgprod* | 1.467E+03 | 1.666E+03 | 1.926E+03 | 2.186E+03 | 2.447E+03 | 2.707E+03 | 2.967E+03 |
| Ht2 | *kJ/kgAr* | 1.467E+03 | 1.666E+03 | 1.926E+03 | 2.186E+03 | 2.447E+03 | 2.707E+03 | 2.967E+03 |
| DHt | *kJ/kgAr* | 1.467E+03 | 1.666E+03 | 1.926E+03 | 2.186E+03 | 2.447E+03 | 2.707E+03 | 2.967E+03 |
| Mtorch | *kg Ar/sec* | 3.067E-01 | 2.701E-01 | 2.336E-01 | 2.058E-01 | 1.839E-01 | 1.662E-01 | 1.517E-01 |
| | ***lb Ar/hr*** | **2434.38** | **2143.61** | **1854.25** | **1633.72** | **1459.47** | **1319.30** | **1203.69** |
| | **enriched AIR torch** | | | | | | | |
| Ht1 | *kJ/kgAIR* | -0.137 | -0.137 | -0.137 | -0.137 | -0.137 | -0.137 | -0.137 |
| N | *kgmole* | 1.926E-05 | 3.186E-04 | 2.740E-03 | 1.459E-02 | 5.462E-02 | 1.581E-01 | 3.733E-01 |
| NO | *kgmole* | 1.107E-01 | 1.554E-01 | 1.529E-01 | 1.127E-01 | 7.653E-02 | 5.228E-02 | 3.573E-02 |
| NO2 | *kgmole* | 8.013E-05 | 6.566E-05 | 3.165E-05 | 1.007E-05 | 3.096E-06 | 1.061E-06 | 3.958E-07 |
| N2 | *kgmole* | 9.446E-01 | 9.221E-01 | 9.222E-01 | 9.363E-01 | 9.344E-01 | 8.948E-01 | 7.955E-01 |
| O | *kgmole* | 1.510E-01 | 5.879E-01 | 1.280E+00 | 1.719E+00 | 1.875E+00 | 1.931E+00 | 1.958E+00 |
| O2 | *kgmole* | 8.691E-01 | 6.283E-01 | 2.836E-01 | 8.435E-02 | 2.445E-02 | 8.179E-03 | 3.152E-03 |
| Ntorch-tot | *kgmole* | 2.075E+00 | 2.294E+00 | 2.641E+00 | 2.867E+00 | 2.965E+00 | 3.045E+00 | 3.166E+00 |
| MWt | *kg/kgmole* | 28.915 | 26.16 | 22.722 | 20.936 | 20.243 | 19.711 | 18.958 |
| Ht2 | *kJ/kgprod* | 3.992E+03 | 6.579E+03 | 1.022E+04 | 1.281E+04 | 1.442E+04 | 1.616E+04 | 1.872E+04 |
| Ht2 | *kg/kgAIR* | 3.993E+03 | 6.580E+03 | 1.022E+04 | 1.281E+04 | 1.442E+04 | 1.616E+04 | 1.872E+04 |
| DHt | *kJ/kgAIR* | 3.993E+03 | 6.581E+03 | 1.022E+04 | 1.281E+04 | 1.442E+04 | 1.616E+04 | 1.872E+04 |
| Mtorch | *kg AIR/sec* | 1.127E-01 | 6.838E-02 | 4.402E-02 | 3.512E-02 | 3.120E-02 | 2.784E-02 | 2.403E-02 |
| | ***lb AIR/hr*** | **894.45** | **542.73** | **349.37** | **278.73** | **247.62** | **220.95** | **190.74** |
| *scfm* | **O2 torch** | 183.83 | 96.97 | 52.41 | 38.43 | 34.47 | 32.77 | 31.60 |
| *gal/min* | **H2O torch** | 0.50 | 0.25 | 0.14 | 0.11 | 0.10 | 0.10 | 0.10 |
| *scfm* | **AIR torch** | 212.88 | 146.28 | 108.96 | 92.23 | 80.73 | 68.50 | 54.81 |
| *scfm* | **N2 torch** | 251.52 | 209.35 | 178.18 | 152.22 | 126.86 | 99.74 | 72.55 |
| *scfm* | **Ar torch** | 398.11 | 350.56 | 303.24 | 267.18 | 238.68 | 215.76 | 196.85 |

# APPENDIX B
# HOT TUBE TEST DATA

Data for the five experiments conducted to test the hot tube are presented graphically below in Figures B.1 through B.34. A brief summary of the experimental test objectives is presented prior to each set of figures. An explanation of data points is provided in Section 8.0.

Experiment One – Figures B.1 through B.6. Experiment 1 was a proof of principle test.

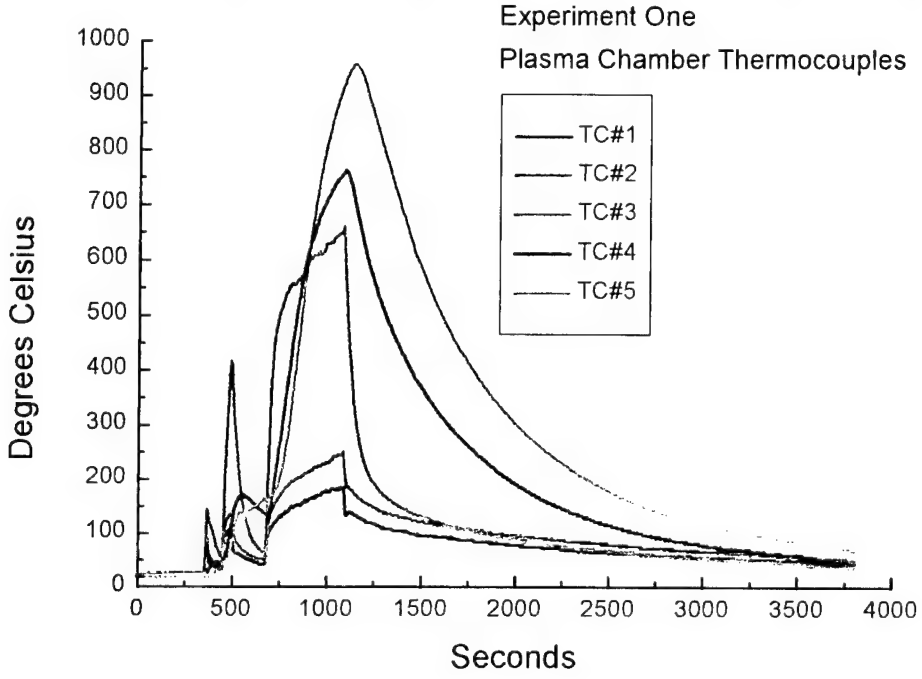


**Figure B.1 – Experiment One: Plasma Chamber Thermocouples**

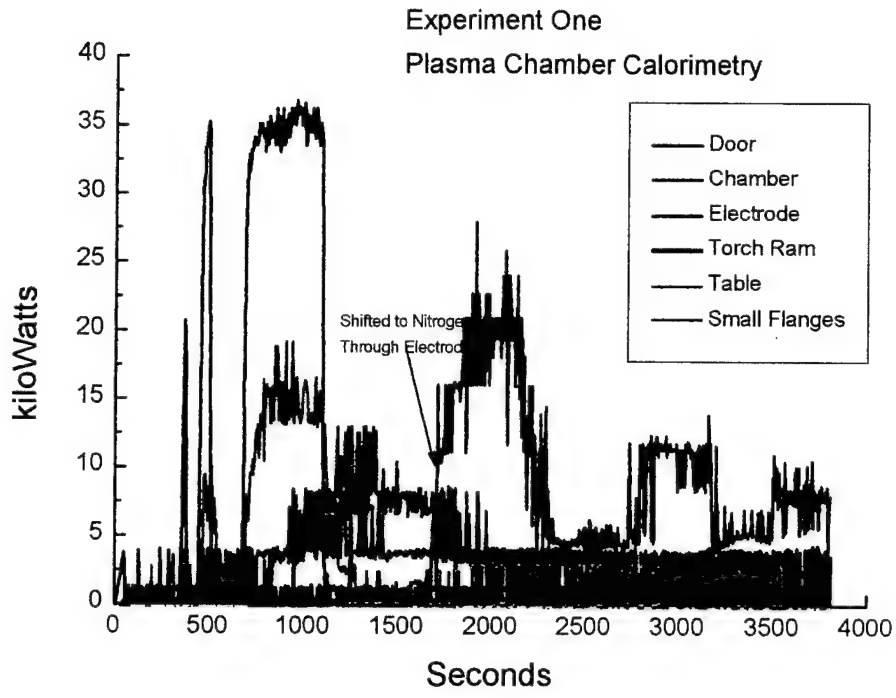


**Figure B.2 - Experiment One: Plasma Chamber Calorimetry**

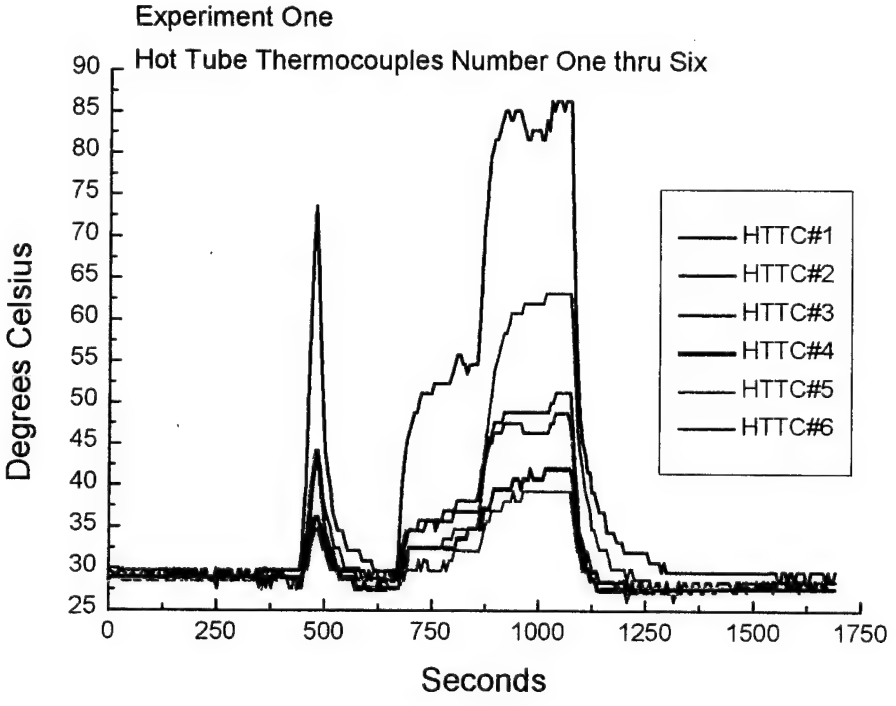


**Figure B.3 - Experiment One: Hot Tube Thermocouples One thru Six**

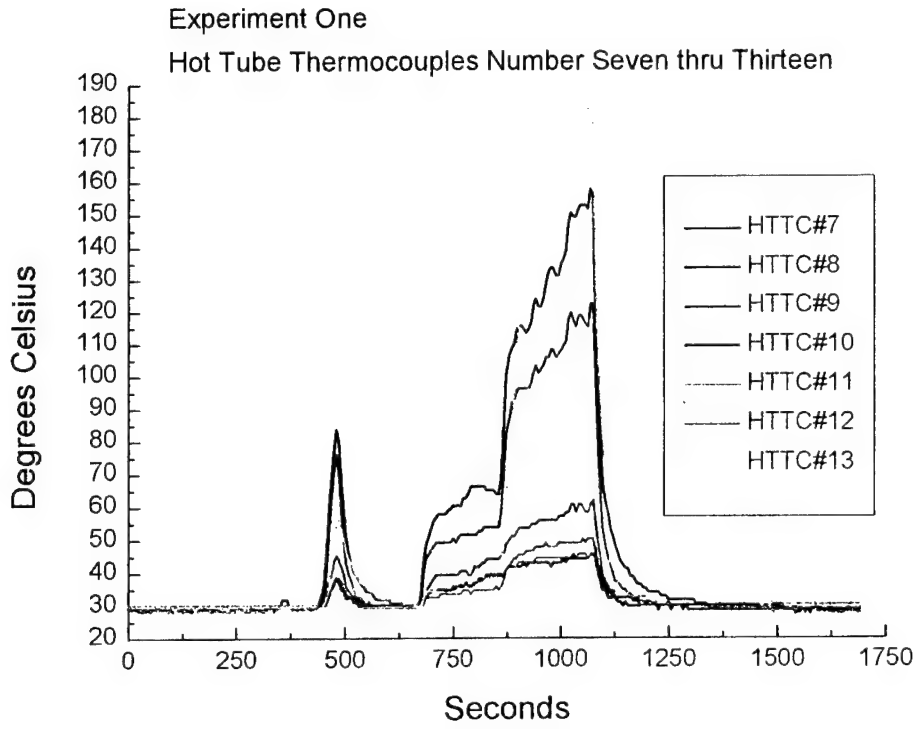


**Figure B.4 - Experiment One: Hot Tube Thermocouples Number Seven thru Thirteen**

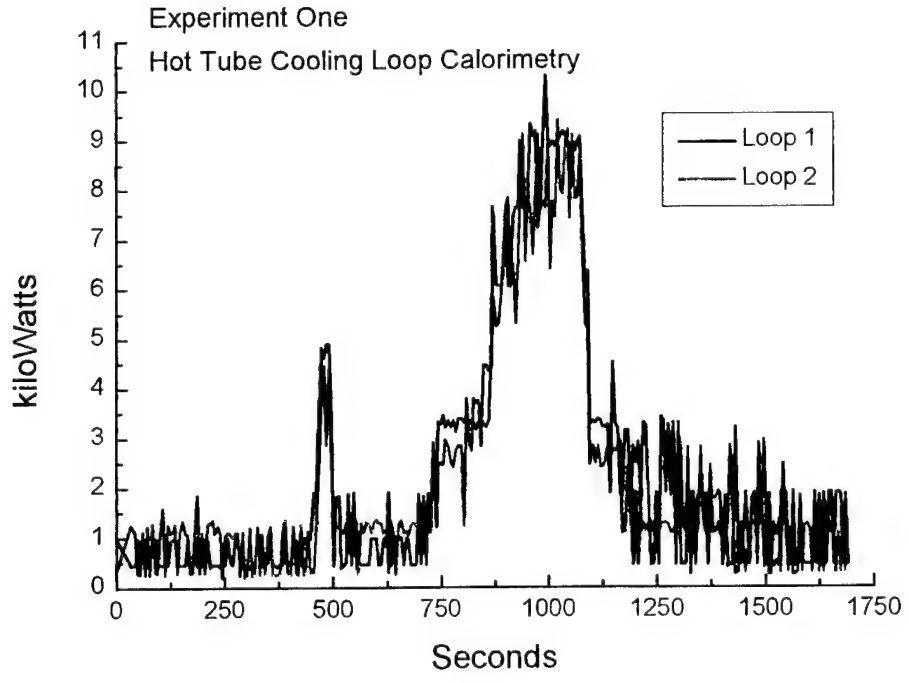


**Figure B.5 - Experiment One: Hot Tube Cooling Loops Calorimetry**

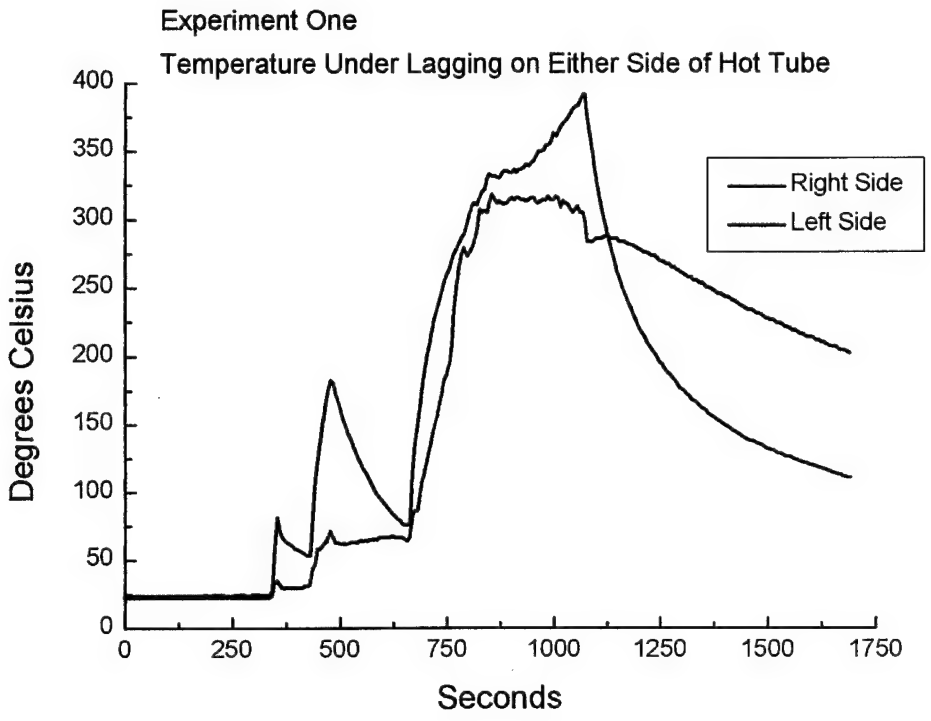


**Figure B.6 - Experiment One: Temperature Under Lagging on Either Side of Hot Tube**

Experiment Two – Figures B.7 through B.12. In this experiment the torch position was fixed as the center of the Hot Tube and the torch was operated for ten minutes.

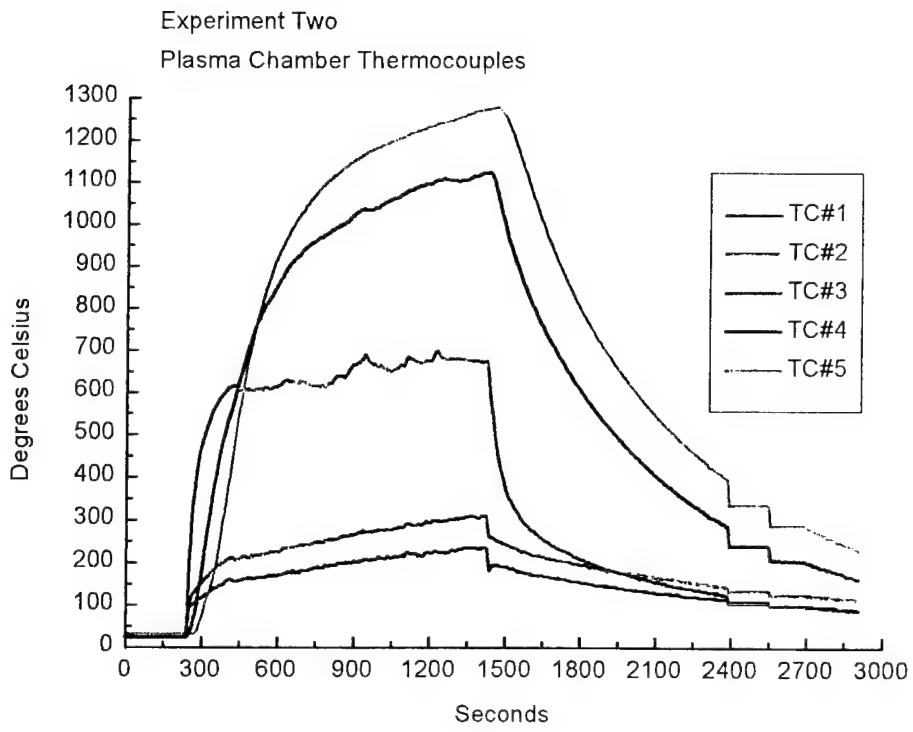


**Figure B.7 - Experiment Two: Plasma Chamber Thermocouples**

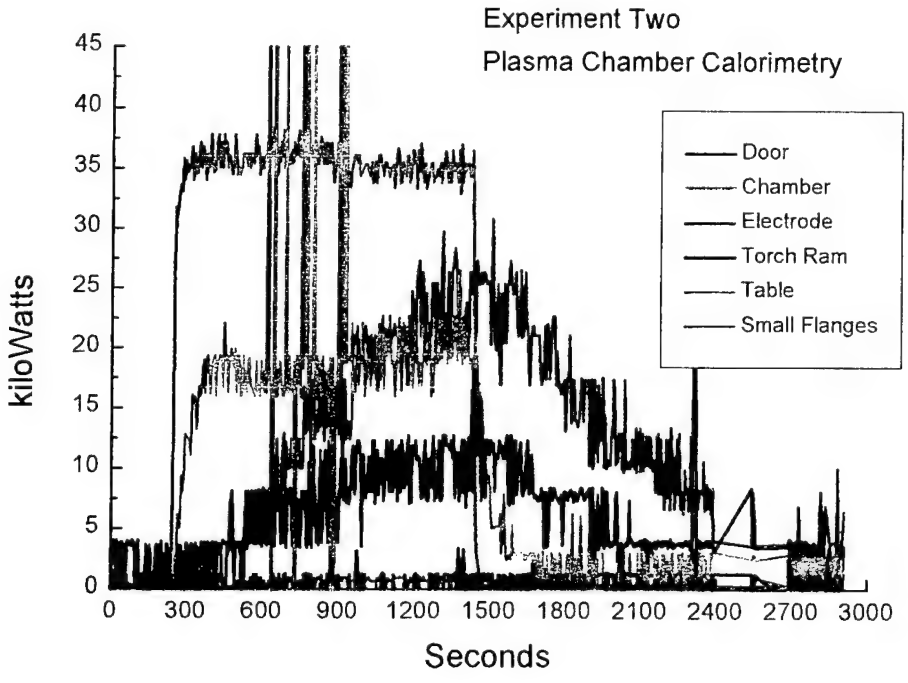


**Figure B.8 - Experiment Two: Plasma Chamber Calorimetry**

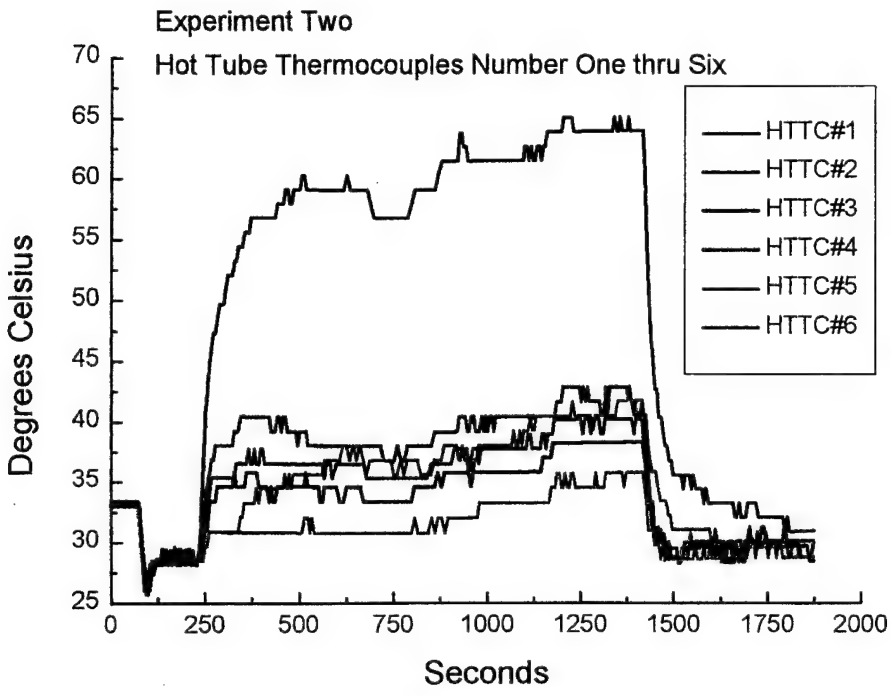


**Figure B.9 - Experiment Two: Hot Tube Thermocouples One thru Six**

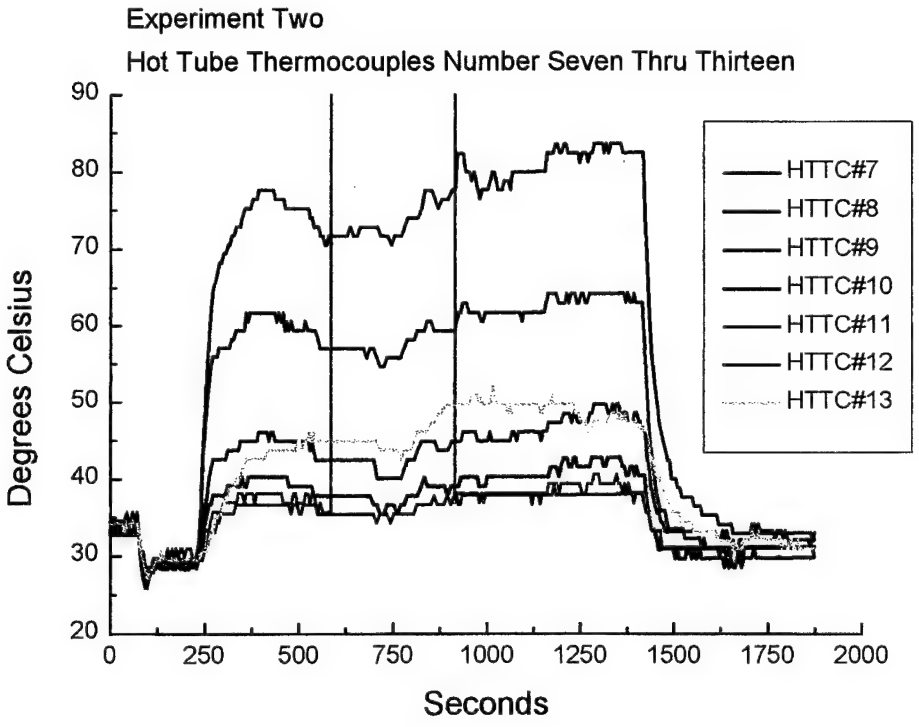


**Figure B.10 - Experiment Two: Hot Tube Thermocouples Seven thru Thirteen**

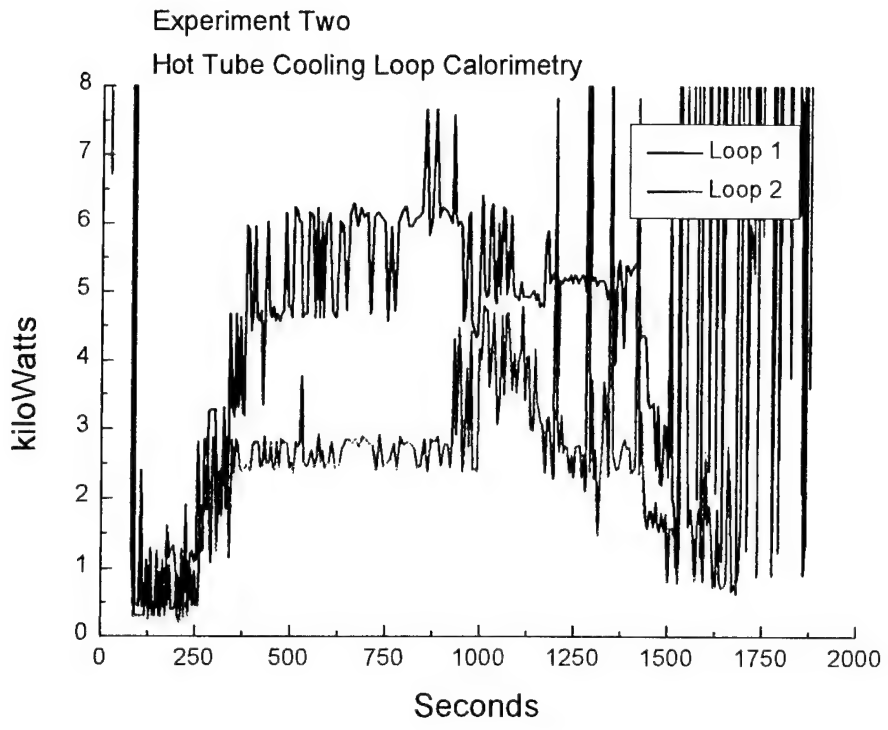


**Figure B.11 - Experiment Two: Hot Tube Cooling Loops Calorimetry**

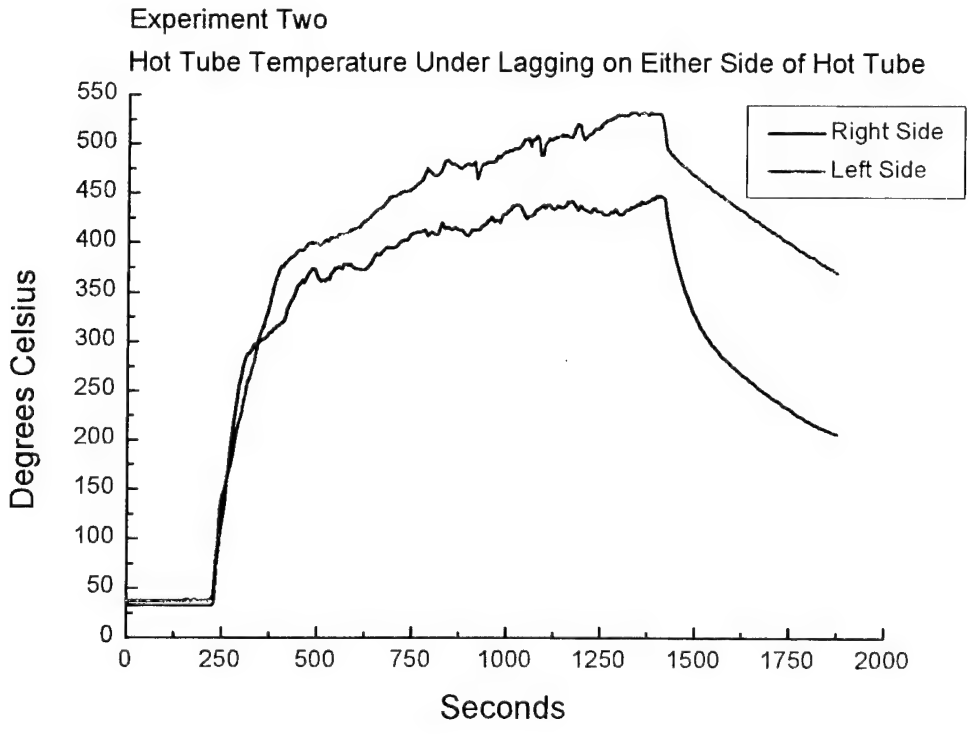


**Figure B.12 - Hot Tube Temperature Under Lagging on Either Side of Hot Tube**

Experiment Three – Figures B.13 through B.19. . In this experiment thermocouple number thirteen was moved next to the wall at the bottom of the Hot Tube. The torch was operated for twelve minutes.

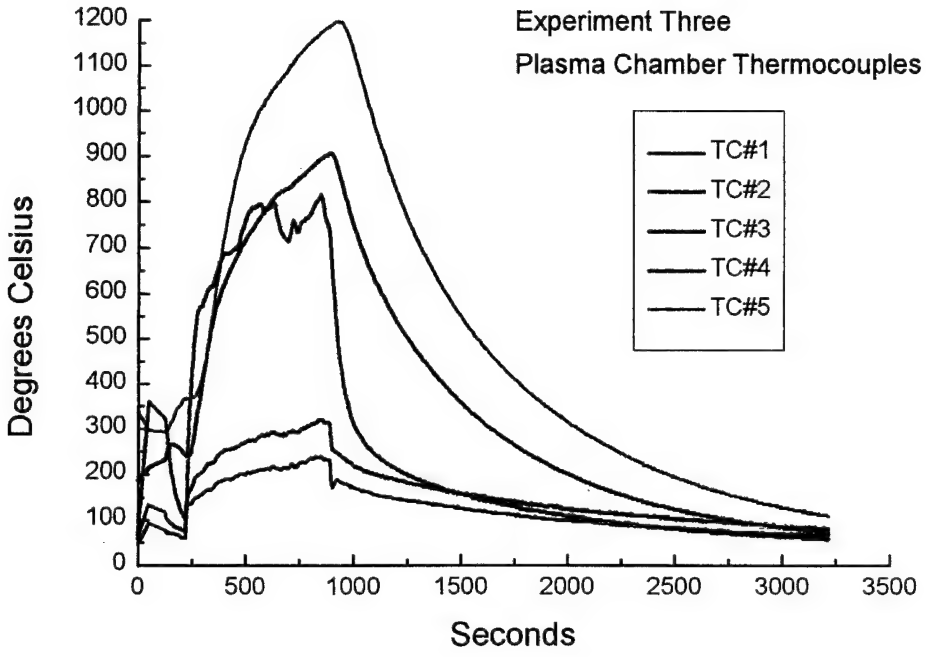


**Figure B.13 - Experiment Three: Plasma Chamber Thermocouples**

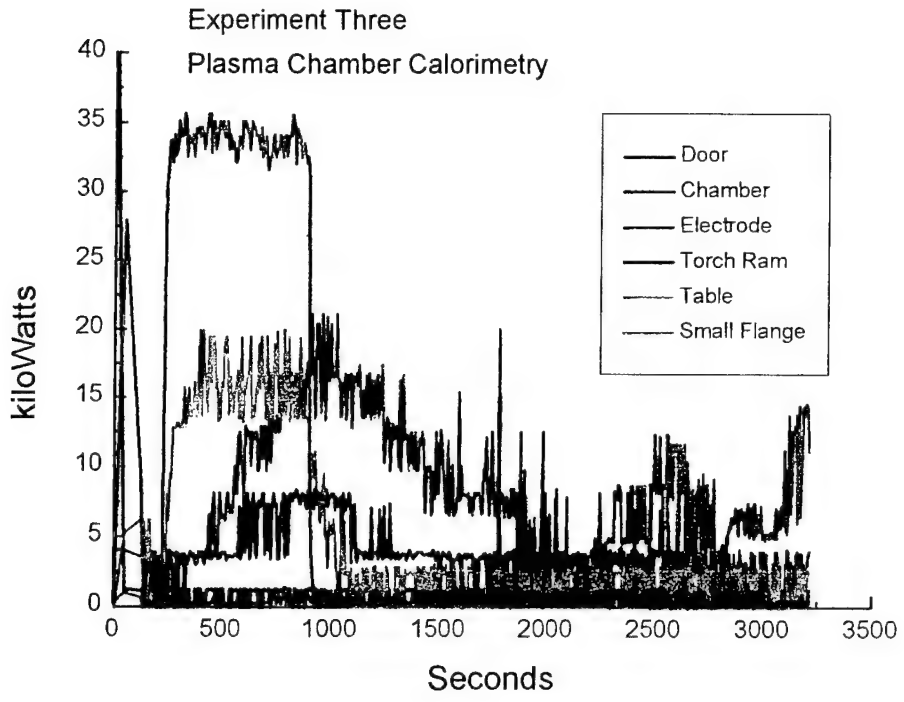


**Figure B.14 - Experiment Three: Plasma Chamber Calorimetry**

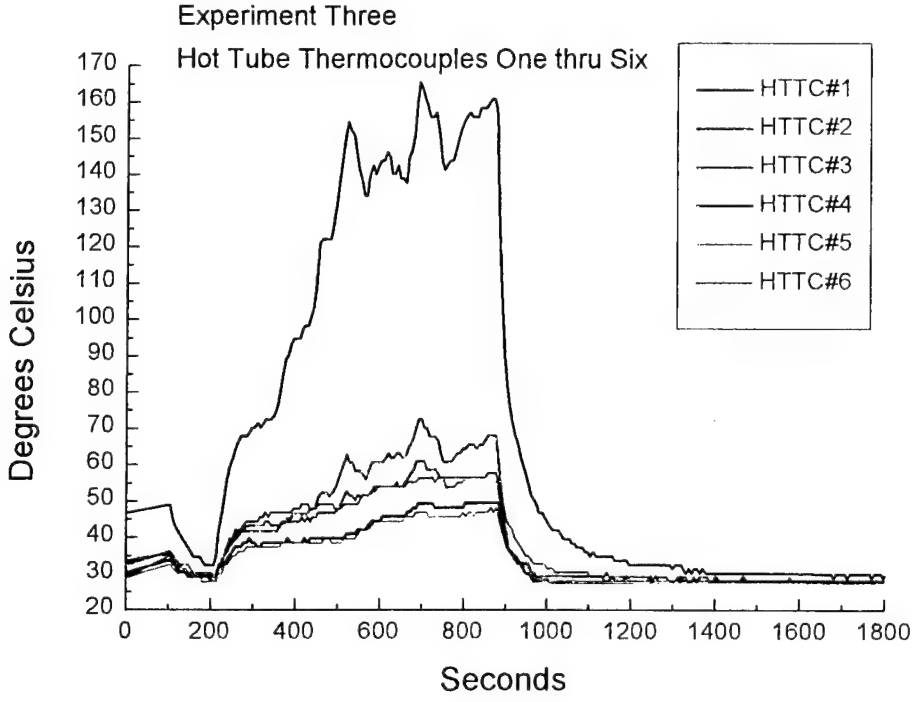


**Figure B.15 - Experiment Three: Hot Tube Thermocouples One thru Six**

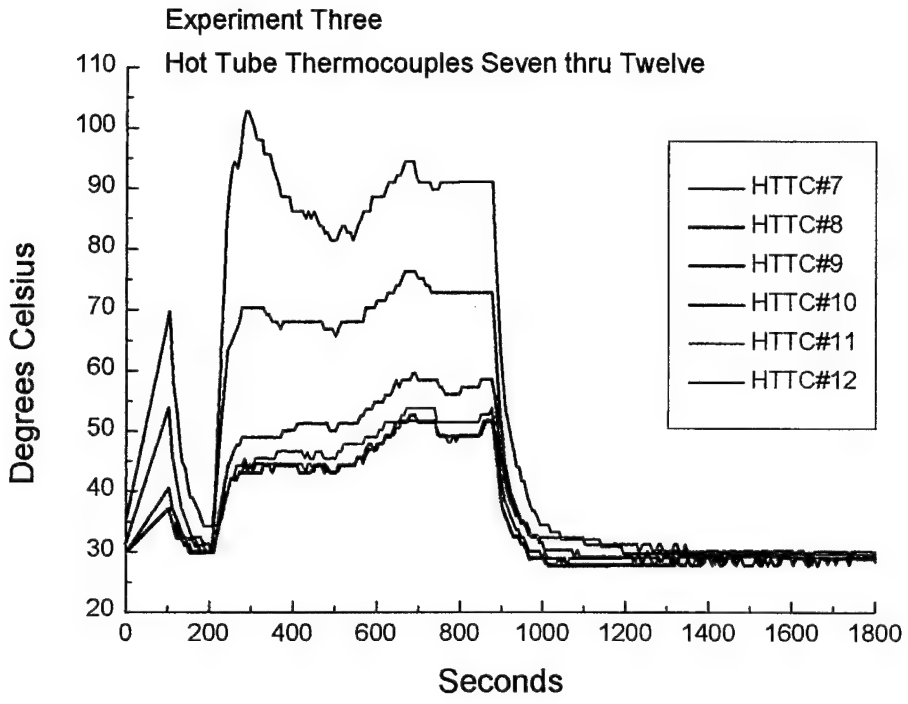


**Figure B.16 - Experiment Three: Hot Tube Thermocouples Seven thru Twelve**

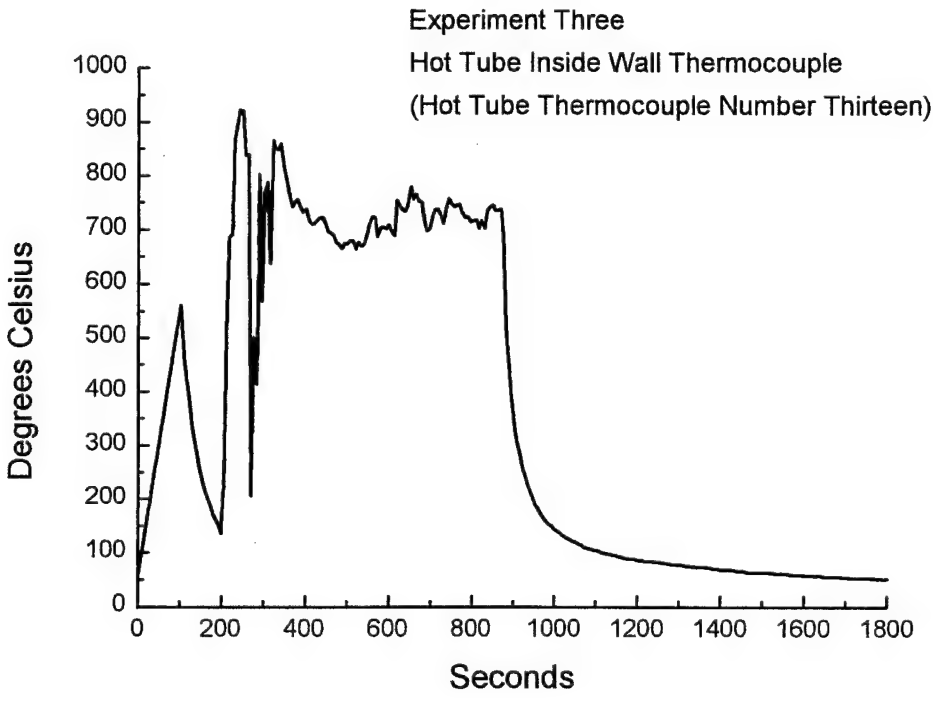


**Figure B.17 - Experiment Three: Hot Tube Inside Wall Temperature, (Old Hot Tube Thermocouple Number Thirteen)**

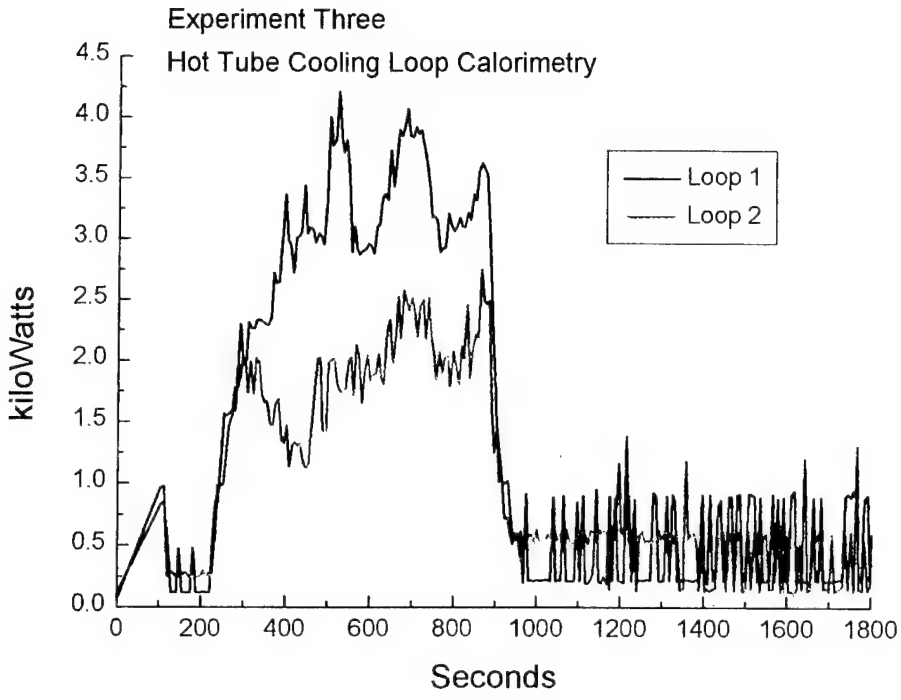


**Figure B.18 - Experiment Three: Hot Tube Cooling Loop Calorimetry**

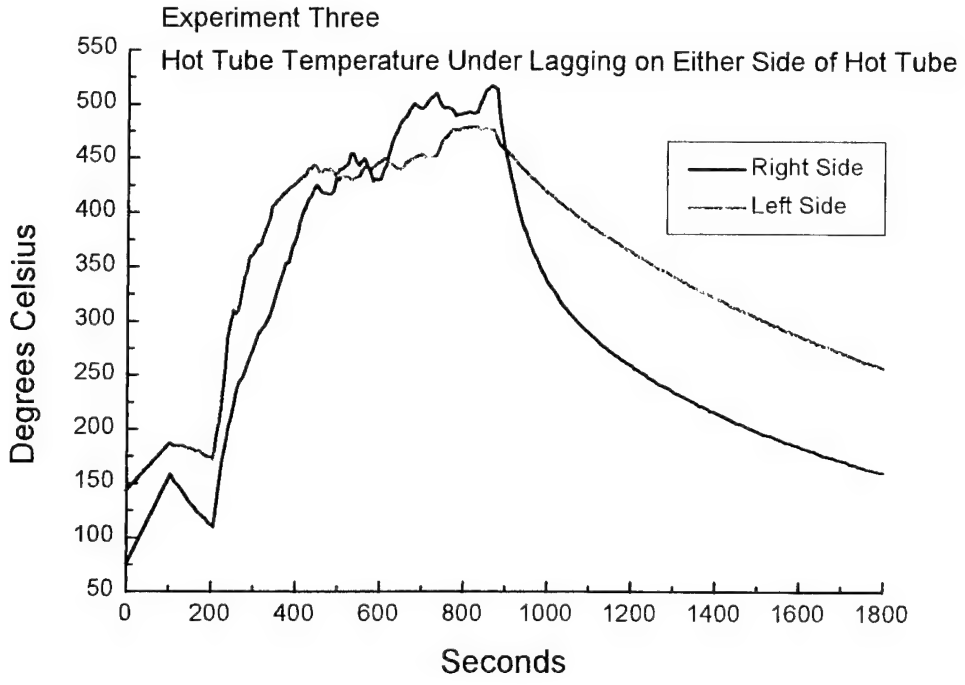


**Figure B.19 - Experiment Three: Hot Tube Temperature under Lagging on Either Side of Hot Tube**

Experiment Four – Figures B.20 through B.26. . In this experiment the end of the plasma torch was placed approximately at the center of the Hot Tube and the water flow through the Hot Tube cooling loop was decreased in an attempt to increase the wall temperature. The torch was operated for sixteen minutes.

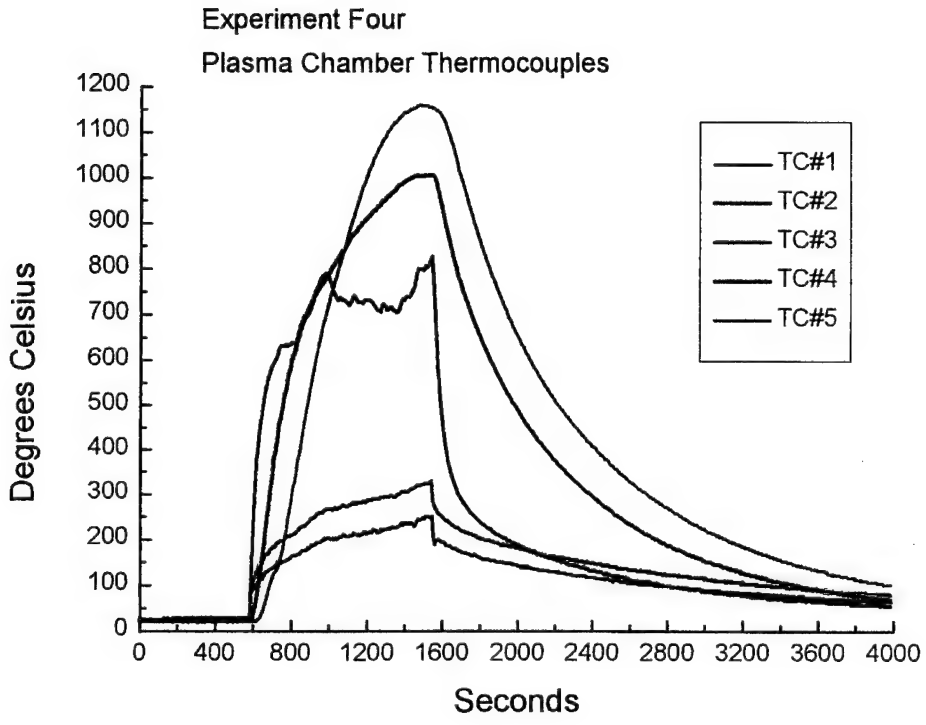


**Figure B.20 - Experiment Four: Plasma Chamber Thermocouples**

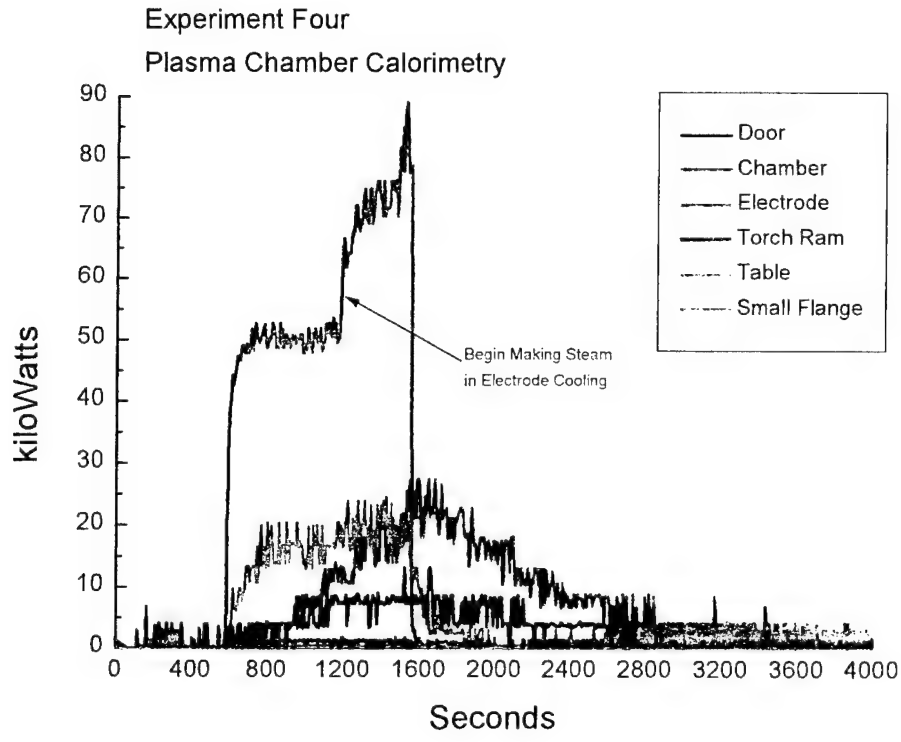


**Figure B.21 - Experiment Four: Plasma Chamber Calorimetry**

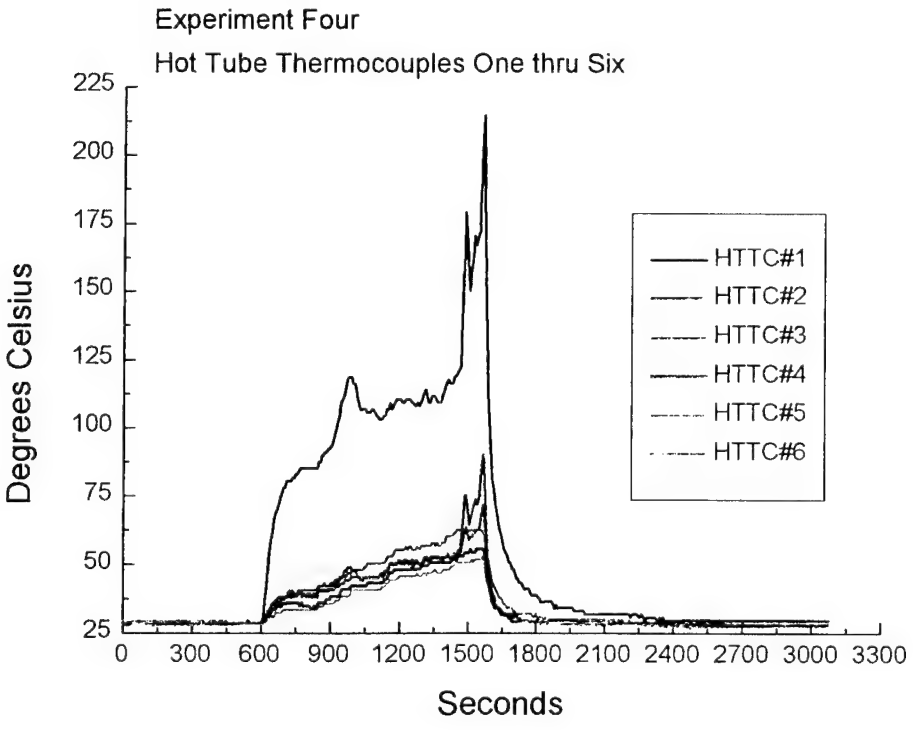


**Figure B.22 - Experiment Four: Hot Tube Thermocouples One thru Six**

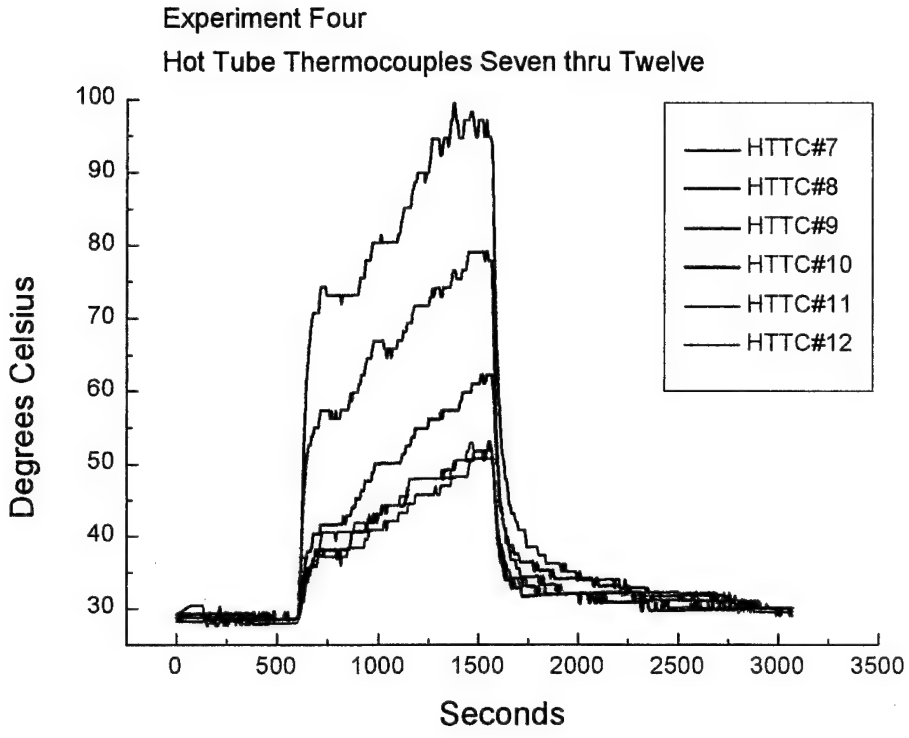


**Figure B.23 - Experiment Four: Hot Tube Thermocouples Seven thru Twelve**

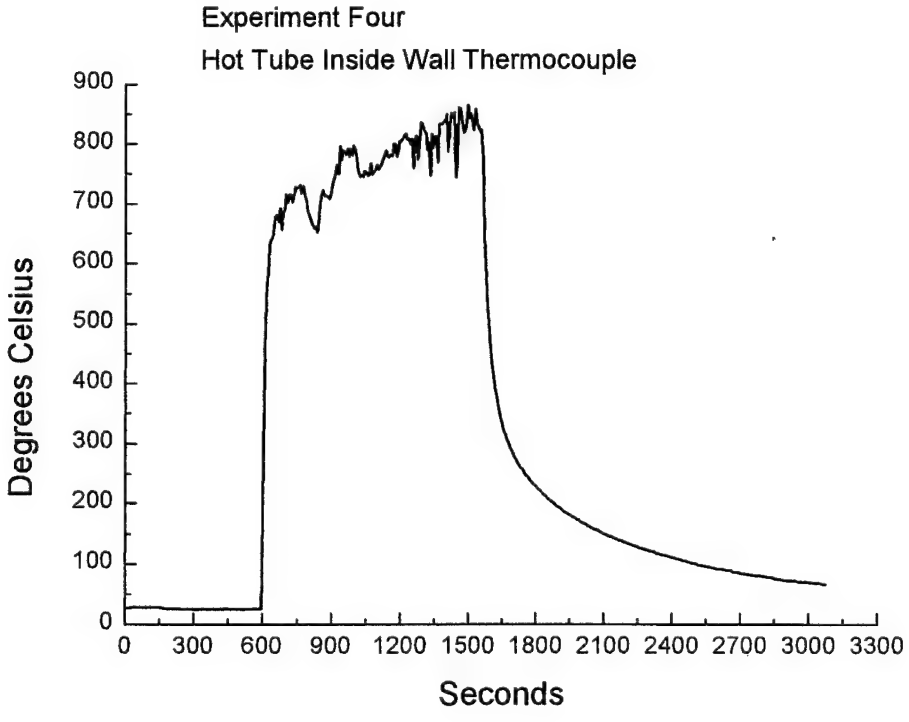


**Figure B.24 - Experiment Four: Hot Tube Inside Wall Thermocouple**

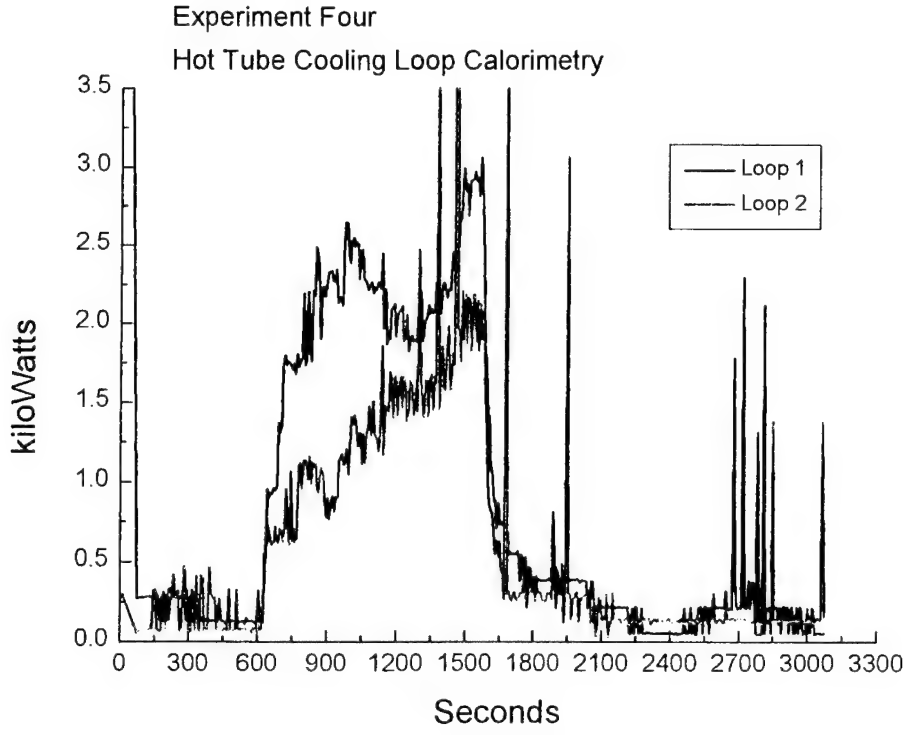


**Figure B.25 - Experiment Four: Hot Tube Cooling Loop Calorimetry**

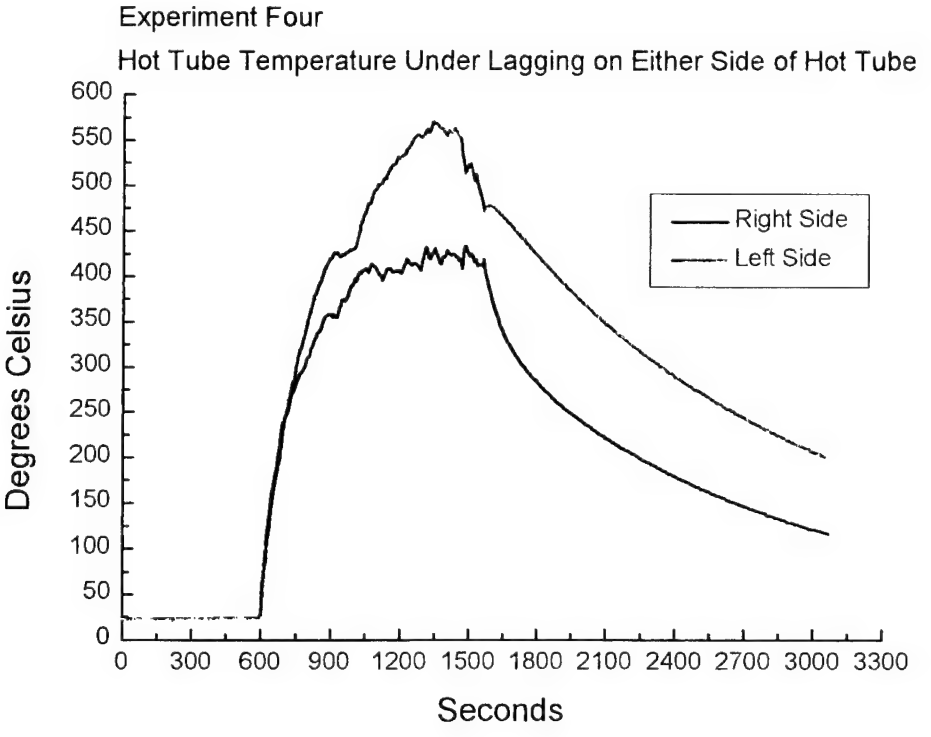


**Figure B.26 - Experiment Four: Hot Tube Temperature under Lagging on Either Side of Hot Tube**

Experiment Five – Figures B.27 through B.34 . In this experiment the end of the plasma torch was fully retracted, maximizing the exposure of the Hot Tube to the plasma plume. The water flow through the Hot Tube cooling loop was decreased in order to increase the wall temperature. The torch was operated for fifteen minutes.

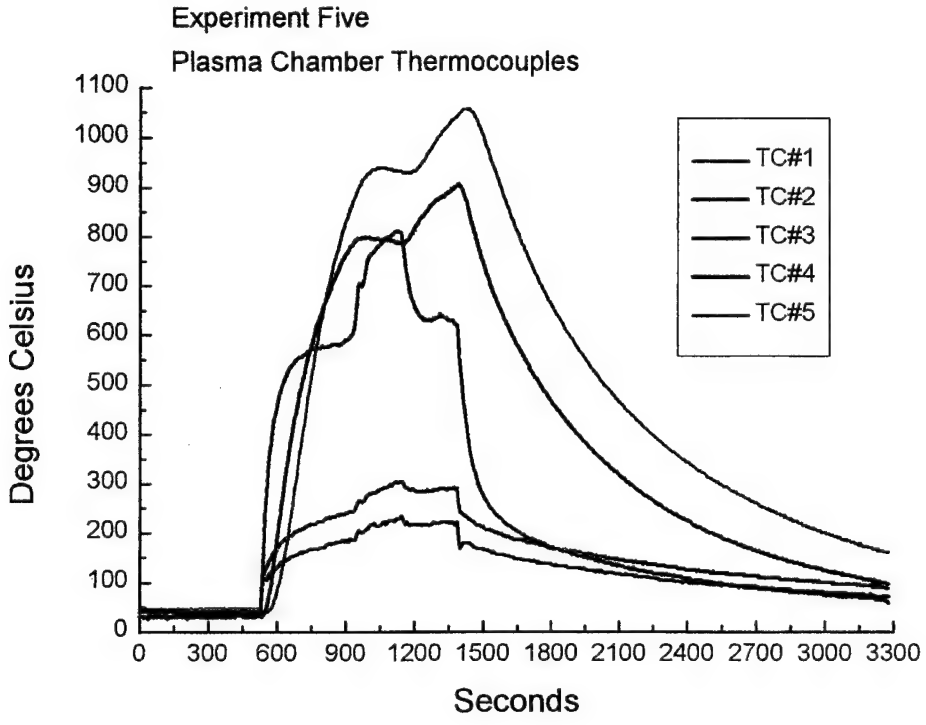


**Figure B.27 - Experiment Five - Plasma Chamber Thermocouples**

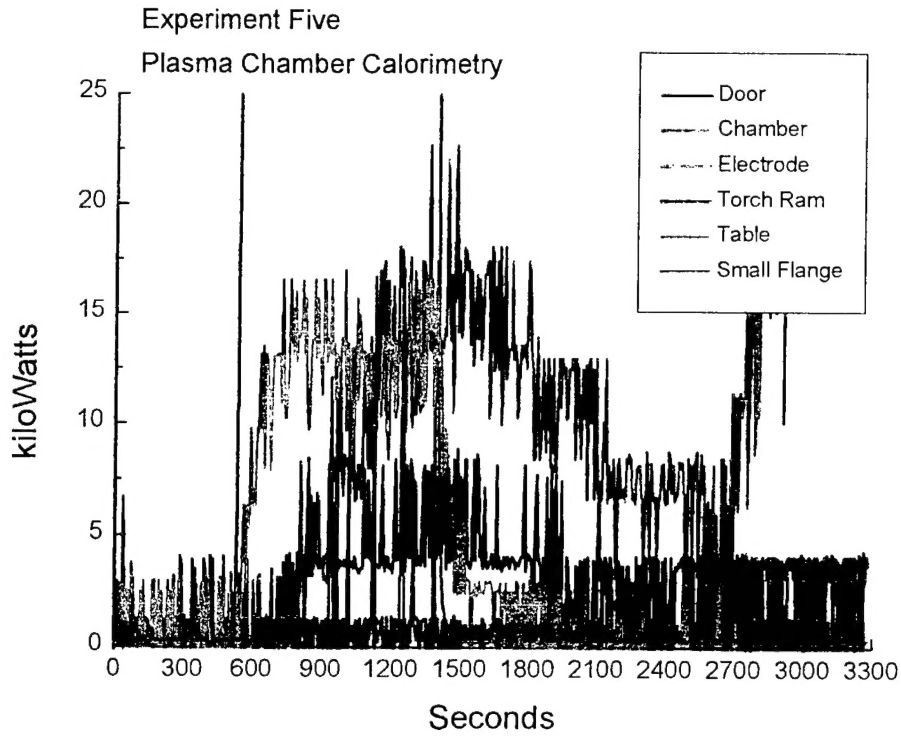


**Figure B.28 - Experiment Five: Plasma Chamber Calorimetry**

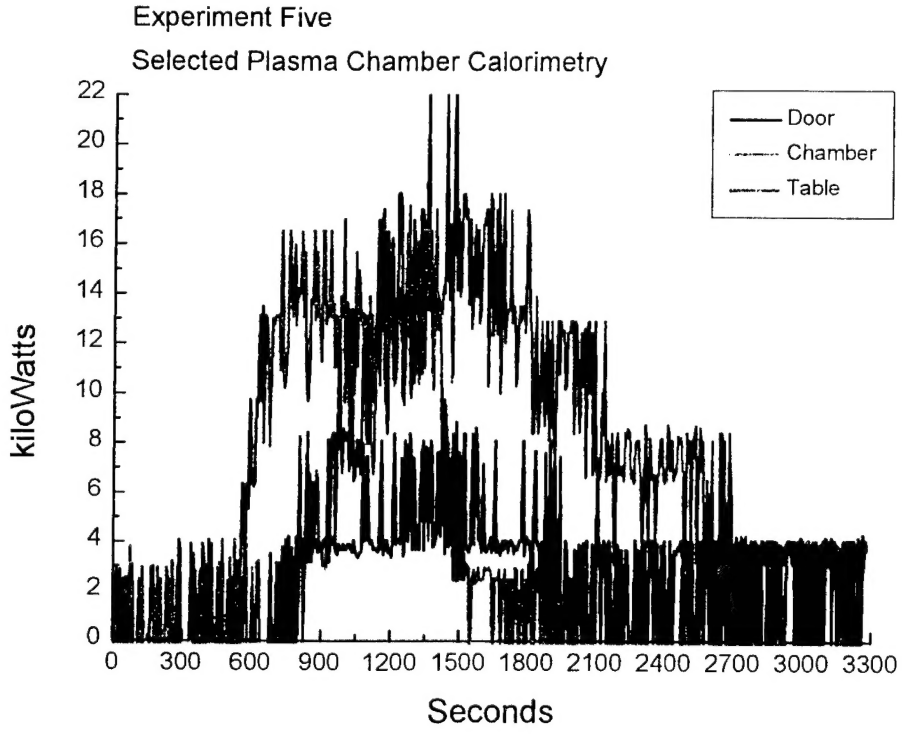


**Figure B.29 - Experiment Five: Selected Plasma Chamber Calorimetry**

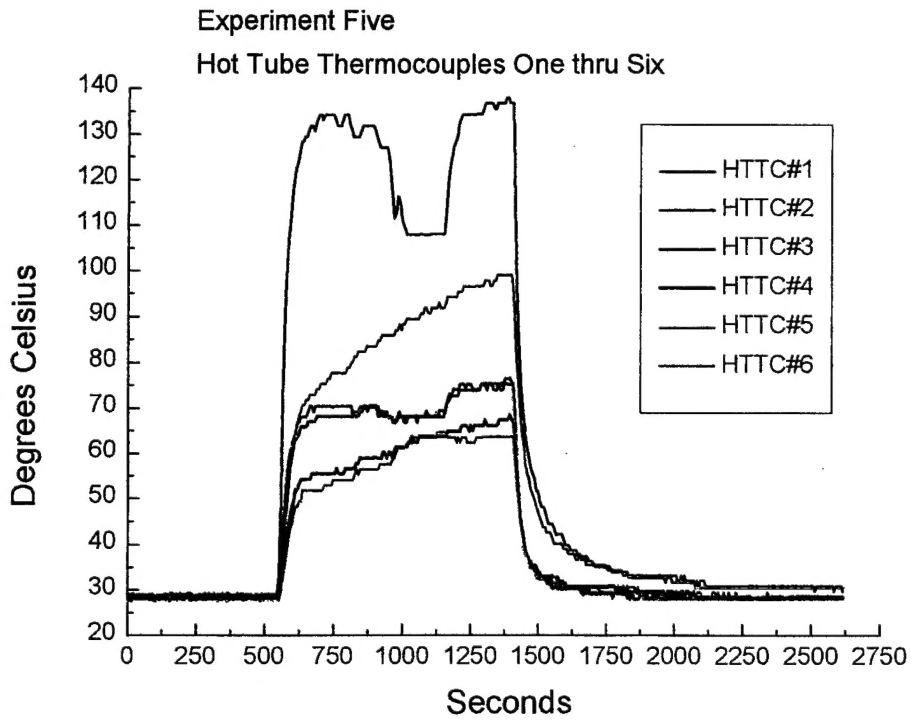


**Figure B.30 - Experiment Five: Hot Tube Thermocouples One thru Six**

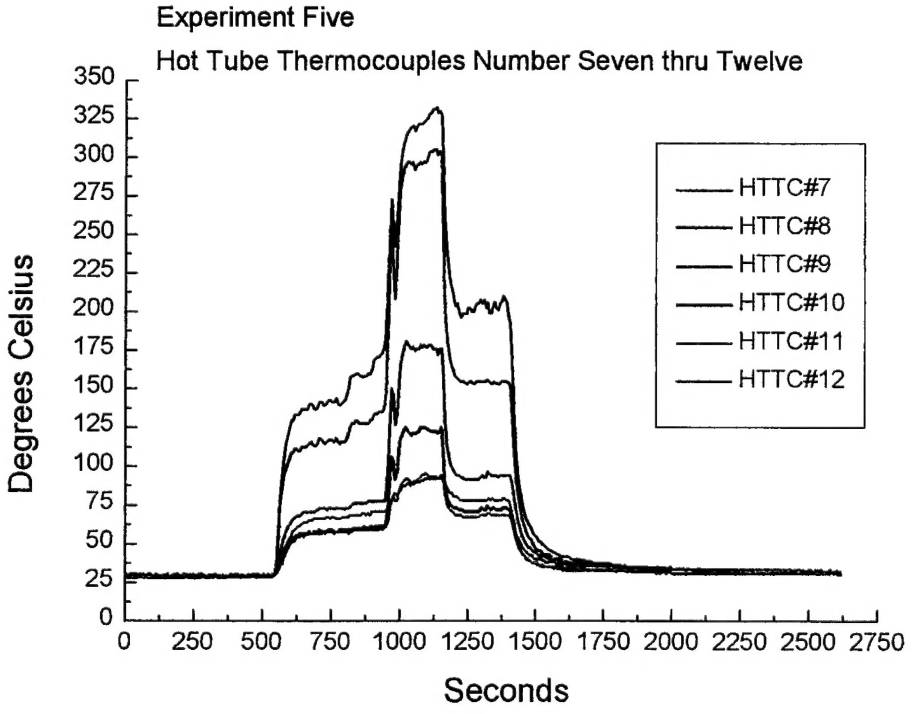


**Figure B.31 - Experiment Five: Hot Tube Thermocouples Seven thru Twelve**

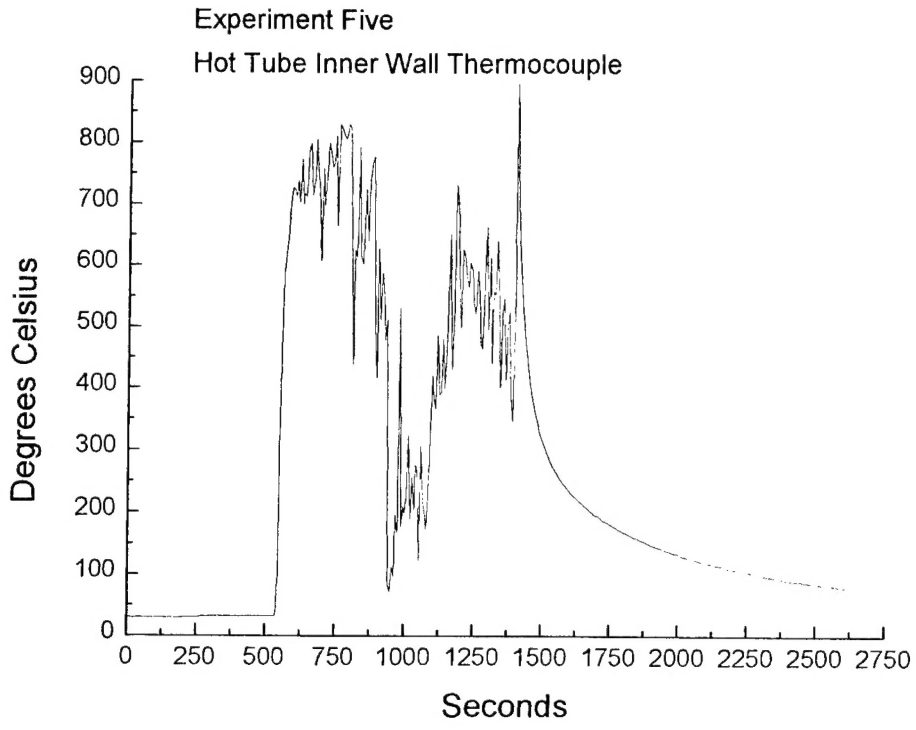


**Figure B.32 - Experiment Five: Hot Tube Inner Wall Thermocouple**

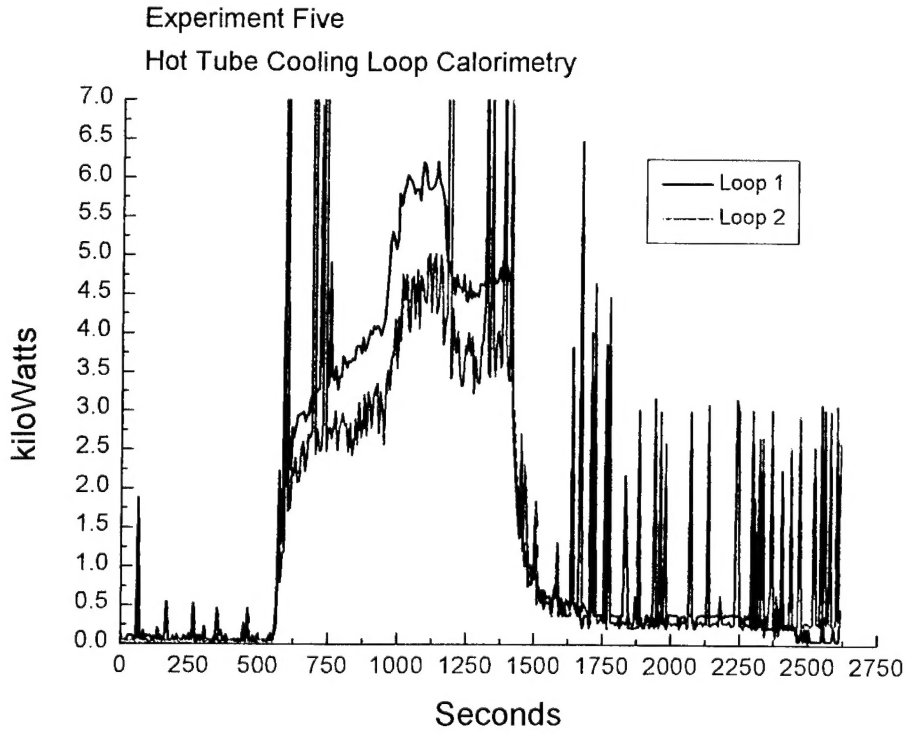


**Figure B.33 - Experiment Five: Hot Tube Cooling Loop Calorimetry**

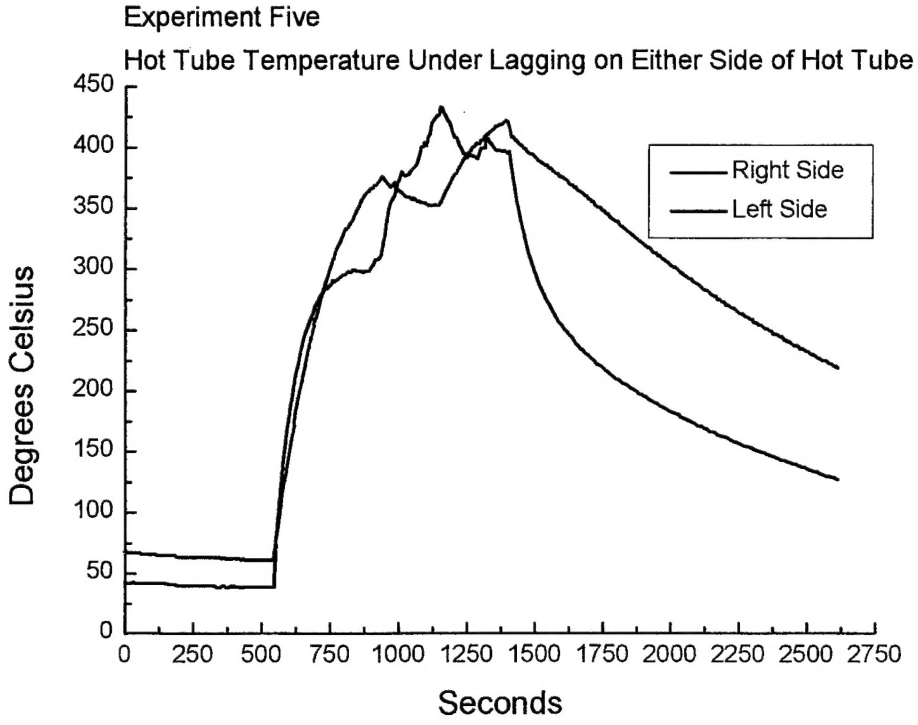


**Figure A.2.34 - Experiment Five: Hot Tube Temperature Under Lagging on Either Side of Hot Tube**